CERTIFICATO DI FIRMA DIGITALE

Si certifica che questo documento informatico

PhD-thesis_Anichini-Gabriele.pdf

composto da n217 pagine

È stato firmato digitalmente in data odierna con Firma Elettronica Qualificata (FEQ), avente l'efficacia e gli effetti giuridici equivalenti a quelli di una firma autografa, ai sensi dell'art. 2702 del Codice Civile e dell'art. 25 del Regolamento UE n. 910/2014 eIDAS (electronic IDentification Authentication and Signature).

PROCESSI INFORMATICI COMPLETATI

- **Apposizione di Firma Elettronica Qualificata Remota** emessa da Intesi Group S.p.A. in qualità di prestatore di servizi fiduciari qualificati autorizzato da AgID, per garantire con certezza l'autenticità, l'integrità, il non ripudio e l'immodificabilità del documento informatico e la sua riconducibilità in maniera manifesta e inequivoca all'autore, ai sensi dell'art. 20 comma 2 del CAD - D.lgs 82/2005.

- **Apposizione di Marca Temporale Qualificata** emessa da Intesi Group S.p.A. in qualità di prestatore di servizi fiduciari qualificati autorizzato da AgID, per attribuire una data e un orario opponibile a terzi, ai sensi dell'art. 20 comma 3 del CAD - D.lgs 82/2005 e per far sì che la Firma Elettronica Qualificata apposta su questo documento informatico, risulti comunque valida per i prossimi 20 anni a partire dalla data odierna, anche nel caso in cui il relativo certificato risultasse scaduto, sospeso o revocato.

- **Apposizione di Contrassegno Elettronico**, l'unica soluzione tecnologica che permette di prorogare la validità giuridica di un documento informatico sottoscritto con firma digitale e/o marcato temporalmente, rendendolo inalterabile, certo e non falsificabile, una volta stampato su supporto cartaceo, ai sensi dell'art. 23 del CAD - D.lgs 82/2005.

  Per risalire all'originale informatico è necessario scansionare il Contrassegno Elettronico, utilizzando l'applicazione HONOS, disponibile per dispositivi Android e iOS.

DEPARTMENT OF MEDICAL BIOTECHNOLOGIES

PhD Program in Medical Biotechnologies

Section of Microbiology and Vaccines

XXXIV Cycle

Immune response analysis to Measles virus in subjects vaccinated with MMR vaccine and naturally infected subjects.

Supervisor:

Chiar.ma Prof.ssa Maria Grazia Cusi

Candidate:

Gabriele Anichini

Academic Year 2020-2021

Acknowledgments

Vorrei ringraziare in modo veramente sincero la Prof.ssa Maria Grazia Cusi, per la capacità di saper trasmettere la passione e la cura che mette quotidianamente in tutto ciò che fa, per la determinazione con cui porta avanti le proprie idee e, non per ultimo, per la fiducia che mi ha sempre fatto sentire. Durante questo percorso, numerose sono state le volte in cui mi sono sentito oltremodo gratificato per quanto fatto. Grazie di cuore.

Un ringraziamento speciale va ai miei supervisori, che con il passare del tempo ho percepito sempre più come colleghi, confidenti ed amici: Gianni Gori Savellini, Claudia Gandolfo, Chiara Terrosi e Shibily Prathyumnan. In questo percorso di crescita professionale ed umana c'è tanto di ognuno di voi.

Grazie a babbo a mamma per avermi tolto tanti pensieri dalla testa, così che potessi dedicarmi al meglio a ciò che mi stimola ed appassiona. Grazie a Matilde, sempre vicina al cuore, nonostante i chilometri. Grazie a chi non c'è più e a coloro per cui non ci sono quanto meriterebbero.

Se la mia vita fosse una tesi, non ne sarei altro che la copertina, per cui grazie a chiunque abbia lasciato anche soltanto una parola, un commento o una revisione.

Foreword

This thesis is divided in eight sections: abstract; introduction; aim of PhD project; materials and methods; results; conclusions; bibliography and annexes.

The annexes include the paper that has been published in relation to the thesis work and other fifteen papers published during the PhD period, but not related to this work.

Index

Abstract

Measles virus belongs to the *Morbillivirus* genus, *Paramixoviridae* family.

It is the causative agent of a highly contagious acute infective disease, typical of infancy, characterized by fever, skin rash, cough and conjunctivitis, and a generalized immune suppression (Griffin, 2013). The virus is transmitted through the respiratory tract, multiplicates in its upper part and in regional lymph nodes, thus resulting in lymphatic and hematic dissemination with appearance of first clinical signs after 9-19 days (de Vries et al., 2015). In 30% of the cases, complications in the lower respiratory tract or the central nervous system (CNS) can occur. The first sign of infection is represented by an early immune depression, due to the loss of B and T immune memory cells (Mina et al., 2015), resulting in an increased susceptibility to opportunistic infections and to life-threatening complications such as pneumonia and/or gastro-intestinal disease (de Vries et al., 2015). However, this type of disease is paradoxically associated with the induction of a strong and specific immune response to the virus, which is usually permanent (Laksono et al., 2016).

There is no specific treatment against measles, and this is the reason why vaccination is considered the best strategy against the virus. Furthermore, the monotypic nature of the virus and the lack of an animal reservoir, make measles a considerable candidate for eradication (Rota et al., 2016).

Although a combined vaccine, called MMR (measles, mumps and rubella) is used in routinely vaccination schedule, measles remains a significative cause of morbidity and mortality, particularly during infancy (Moss & Griffin, 2012; Wolfson et al., 2009; Nandy et al., 2003). MMR live attenuated vaccine is very efficacious in protecting people against measles, mumps, and rubella, and preventing the complications caused by these diseases. The measles virus contained in the vaccine is represented by the live attenuated Edmoston B strain. The World Health Organization recommends two doses of vaccine for all children and adults; the first dose should be given at 13-15 months of age. The second dose is often done at 5 - 6 years, in Italy.

About 3 out of 100 people who get two doses of MMR vaccine will get measles if exposed to the virus. However, they are more likely to have a milder illness, and are also less likely to spread the disease to other people (Centers for Disease Control and Prevention, 2018).

Epidemiologic studies have shown that the level of neutralizing antibodies at the time of exposure to wild type (WT) virus in the community is a good indicator of protection from infection, with higher titers necessary to prevent infection than to prevent disease (rash) (Chen et al., 1990). High avidity antibodies are required to neutralize CD150-mediated WT MeV infection of lymphoid cells (Polack et al., 2003). However, levels of circulating anti-measles neutralizing antibody tend to reduce or even to fade during lifetime, especially among vaccinated subjects (Kennedy et al., 2019;

Davidkin et al., 2008; Carryn et al., 2019; Seagle et al., 2018; Gonçalves et al., 2015; Le Baron et al., 2007). Because CD4$^+$ T cell help is required for isotype and affinity maturation of antibody-secreting cells, B cell memory and maturation of CD8$^+$ T cell memory, cellular immune response is also important for the induction of protective immunity (Laksono et al., 2018).

All these things highlight the necessity to invest on studies focused on the correlates of protection against Measles virus. Recent evaluation systems for vaccines point towards the measurement of T-cell quality with regards to cytokine secretion as a protective correlate in addition to antibody titers in serum during the course of an immune response. Although the generation of immune memory supports the concept of vaccine efficacy, direct assessment of immune memory cells and their precursors has not yet been established as a correlate of protection. With the growing knowledge on the phenotype, function and localization of the immune memory cells in the body, researchers think that these cells may provide a novel correlate of protection for evaluation of more efficacious vaccines.

Finally, transcriptome-level characterization (mRNA-Seq data) of responses to measles virus stimulation in antibody responders (either vaccinated or naturally infected) and those who have not responded to the vaccine, could help to identify plausible regulators (genes/pathways) that drive the observed differences among these subjects.

Such study may help to develop a panel of biomarkers to monitor, besides the antibody response, the immune response to measles vaccine with the aim to protect, in case of outbreaks, not only the fragile subjects, but also the vaccinated subjects who eventually become seronegative along the time, with a booster composed of specific, immunogenic MeV proteins.

Chapter 1

Measles virus: an overview

1.1 *Paramyxoviridae*

The *Paramixoviridae* family, within the order *Mononegavirales*, consists of large enveloped, non-fragmented ssRNA viruses with negative polarity. This family comprises eight genera, which include a wide number of both human (Measles, MeV; Mumps, MuV; Respiratory Syncytial virus, RSV; Parainfluenza viruses, PIV 1-4), animal (Vescicular Stomatitis virus, VSV; Newcastle disease virus, NDV; Canine Distemper virus) and zoonotic (Nipah, Hendra and Rabies virus) pathogens (Figure 1).

Virions are 150-500 nm in diameter, pleomorphic, but mostly spherical. They consist of a nucleocapsid surrounded by a lipid envelope, which is directly derived from the host cell plasma membrane by budding and contains two transmembrane glycoproteins. These proteins are present as homo-oligomers and form spike-like projections, with a length of 8–12 nm, spaced 7–10 nm apart (depending on virus genus). In addition, depending on the genus, one or two additional transmembrane proteins may be present. A non-glycosylated membrane or matrix protein is associated with the inner face of the envelope. The virus nucleocapsid, which consists of negative-sense virus genome RNA and the nucleocapsid protein (N), has a helical symmetry and is approximately 18 nm in diameter with a 7 nm pitch, with a length up to 1,000 nm in viruses of some genera. The ribonucleoprotein (RNP) complex consists of the nucleocapsid together with the polymerase-associated or phosphoprotein (P) and the L protein (including RNA-directed RNA polymerase, capping and cap methylation activities) (Lamb & Parks, 2007). The RNA genome ranges from 14.3 to 20.1 kb. The genomes of all viruses in the *Paramyxoviridae* family are multiples of 6 nucleotides, a requirement for efficient replication (Calain & Roux, 1993). Intracellularly, or in virions, genome-length RNA is found exclusively encapsidated in ribonucleocapsids (RNPs). The genome RNA does not contain a 5′-cap, nor a covalently linked protein. The genome 3′-end is not polyadenylated.
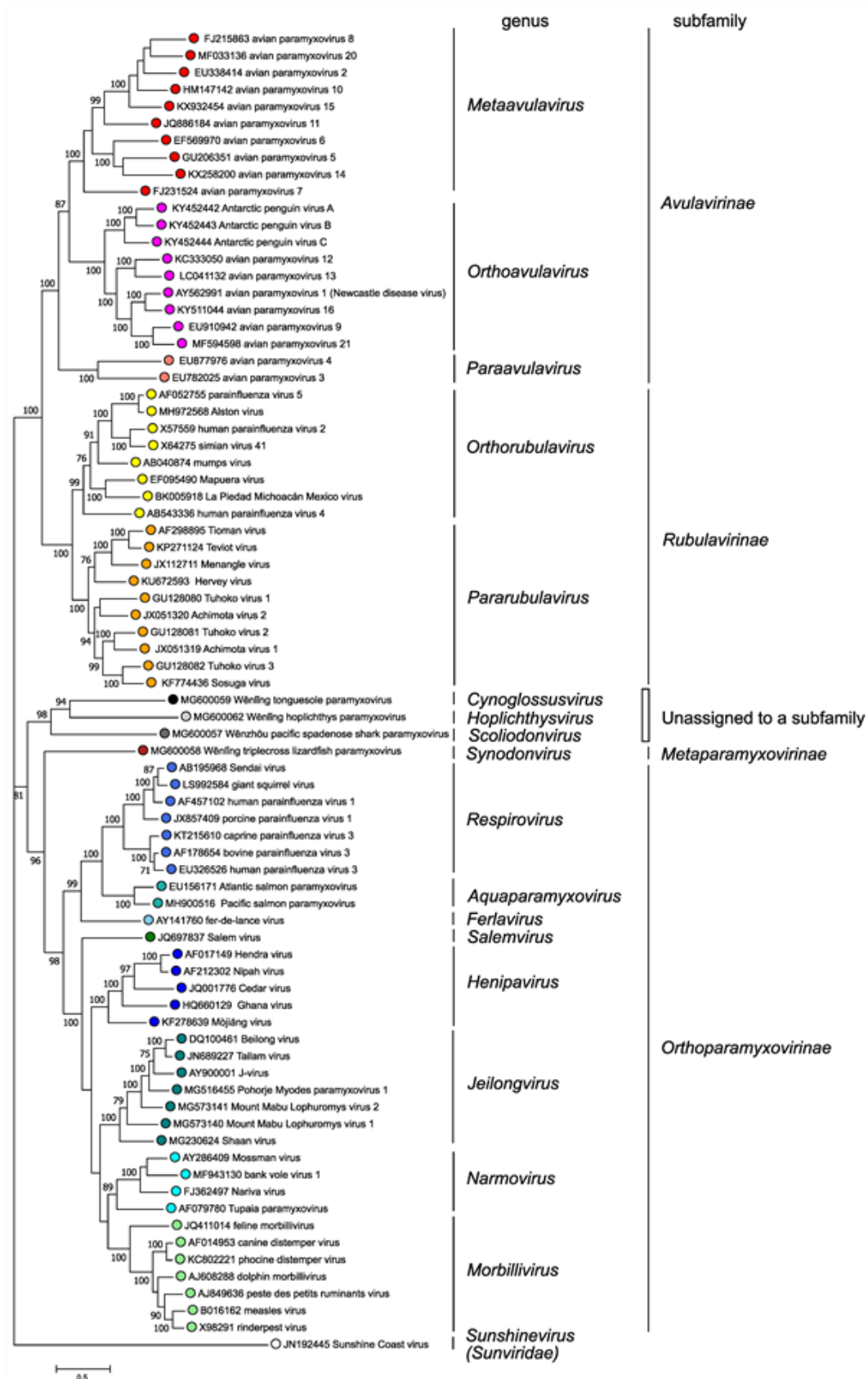
Figure 1: Phylogenetic analysis of complete L protein amino acid sequences of members of the family *Paramyxoviridae*. Credit: ICTV Virus Taxonomy Profile: Paramyxoviridae

Members of the *Paramyxoviridae* family encode 6–10 proteins (5–250 kDa) (Figure 2) of which several may be derived either from gene editing events in the P locus and an overlapping ORF in the P gene itself. Virion proteins common to all genera include: three nucleocapsid-associated proteins, i.e., an RNA-binding nucleocapsid protein (N), a polymerase-associated phosphoprotein (P) and a large protein (L), including an RNA-directed RNA polymerase (RdRP), mRNA guanylyl- and methyltransferases, methylation functions required for the capping of mRNAs and three membrane-associated proteins: an unglycosylated inner membrane or matrix protein (M) and two glycosylated envelope proteins, comprising a fusion protein (F) and an attachment or receptor-binding protein (RBP; designated variably as HN, haemagglutinin-neuraminidase protein; H, haemagglutinin or G, glycoprotein). The F protein is synthesized within infected cells as a precursor (F_0) which is further activated upon cleavage by cellular proteases to produce the virion disulfide-linked F_1 and F_2 subunits (order: N-F_2-S-S-F_1-C). Some viruses also encode putative non-structural proteins (C), a cysteine-rich protein that binds Zn^{2+} (V) that can be structural or non-structural depending on the virus, a small integral membrane protein (SH) and transmembrane proteins (tM). Some virus genomes, such as the Fer-de-Lance virus (FDLV), contain transcription units encoding proteins with unidentified functions (gene 'U') (Kurath et al., 2004). Virion enzyme activities include the RNA-directed RNA polymerase and mRNA guanylyl-and methyltransferases functionally encoded in the L protein. Variously represented among the genera are neuraminidases associated with the RBP.

After attachment to cell receptors, virion entry is achieved by fusion of the virion envelope with the cell membrane surface, which can occur at neutral pH. Virus replication takes place in the cytoplasm and is thought to be independent of host nuclear functions. The genome is transcribed processively from the 3′-end by the virion-associated RdRP into 6–8 separate positive-sense mRNAs. Transcription is guided by short (10–13 nt) conserved gene start (GS) and gene end (GE) signals flanking the intergenic sequence. The mRNAs are capped by the guanylyl- and methyltransferase activities of the L protein and possess 3′-poly(A) tracts synthesized by reiterative copying of U tracts in GE sequence. Intergenic regions are highly conserved in length (3 nt) and sequence (CUU with few exceptions) in the Orthoparamyxoviruses and Metaparamyxoviruses. Neither the length or sequence of the intergenic sequences is conserved in Avulavirus or Rubulavirus genomes. RNA replication occurs through an intermediate, the antigenome, which is an exact positive-sense copy of the genome.

Ribonucleoprotein assembly occurs in the cytoplasm and is tightly linked to RNA synthesis. RNPs are enveloped by budding at the cell surface plasma membrane at sites containing virion envelope proteins. Orthoparamyxovirus genomes contain 6–8 transcriptional elements (Figure 2) that encode

7–11 proteins. Each element encodes a single mRNA with the exception of the P/V element. This element is transcribed into an exact copy mRNA (P or V mRNA, depending on genus) and into alternative versions in which the RNA transcriptase 'stutters' on the template at an editing motif midway down the element. This stuttering results in the insertion of one or more pseudo-templated G nucleotides ("RNA editing") and shifts the reading frame to access alternative ORFs. The exact copy and edited mRNAs synthesize two alternative proteins, P and V, which have identical amino-terminal domains but due to the insertions of G residues have different carboxy-terminal domains. Other truncated, or chimeric, proteins (called I, W, or D, depending on the virus) can be produced by shifting into the third reading frame. The C ORF present in henipavirus, morbillivirus, narmovirus, jeilongvirus, aquaparamyxovirus and respirovirus genomes overlaps the P ORF and can initiate synthesis at an AUG codon that is accessed by ribosomal choice or at alternative start codons in the same ORF.
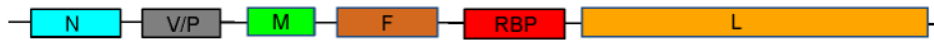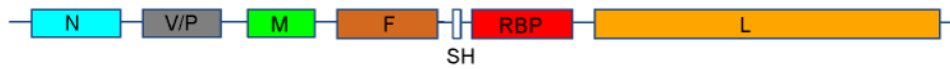
Figure 2: Genome organization (3′-to-5′) of representative viruses in the family *Paramyxoviridae*. Each box represents a separately encoded coding sequence; slashes indicate where multiple distinct ORFs are present within mRNA transcripts. The lengths of the boxes are approximately to scale although the non-coding sequences (NCS) are not to scale. Credit: ICTV Virus Taxonomy Profile: Paramyxoviridae

Paramyxoviruses have been conclusively identified only in vertebrates and primarily in mammals and birds (Table 1), although recently they have also been detected in reptiles and fish, including boneless fishes. Most viruses have a limited host range in nature but can infect a broader range of cultured cells. Infection of cultured cells is generally lytic, but temperate or persistent *in vitro* and *in vivo* infections are common among the viruses of this family. Other features of infection include the formation of inclusion bodies and syncytia. Host cell surface receptor molecules for the attachment for members of the family can vary (Thibault et al., 2017). Respiroviruses, some rubulaviruses and all avulaviruses use sialoglycoproteins and glycolipids as receptors. The cell surface proteins signaling lymphocytic activation molecule family member 1 (SLAMF1, aka CD150) and nectin cell adhesion molecule 4 (nectin 4) are major receptors for measles virus and other morbilliviruses. Henipaviruses use ephrin B2 (EFNB2) and B3 (EFNB3) proteins as cellular entry receptors.

Transmission of paramyxoviruses occurs horizontally, primarily through airborne and direct contact routes; no vectors are known. Paramyxovirus infection typically begins in the respiratory tract and may remain at that site (e.g., human parainfluenza virus 1 [HPIV-1]) or spread to secondary tissues (e.g. lymphoid and endothelial tissues for measles virus) (Rima et al., 2019; Griffin, 2007), the parotid gland, CNS and endothelial tissues for mumps virus (MuV) (Rima et al., 2019; Carbone & Rubin, 2007) or lung and CNS for Hendra virus (HeV) and Nipah virus (NiV) (Rima et al., 2019; Eaton et al., 2007). In general, paramyxovirus infections are limited, and eliminated, by host immunity. However, this virus can sometimes be spread in healthy and, especially, in immunocompromised individuals for weeks or months. Latent infection is unknown. However, long-term persistent infection is known for several morbilliviruses such as MV in subacute sclerosing panencephalitis, a rare complication that involves persistence of a defective measles virus in the CNS for a mean period of 8 years. Old dog distemper can involve persistence of defective or fully infectious canine distemper virus for weeks or months in healthy and, especially, immunocompromised animals. Feline morbillivirus has been shown to be shed for long periods from the kidneys of cats. The recurrence of neurological manifestations has also been noted in NiV patients more than 4 years after recovery from acute encephalitis (Rima et al., 2019; Eaton et al., 2007). The RBP and F proteins are of primary importance in inducing virus-neutralizing antibodies and immunity against reinfection. Antibodies to N and, variably, to other virus proteins are also induced by infection. Following processing into small peptides the virus proteins also stimulate cell-mediated immune responses.

1.2 Measles virus

Measles virus (MeV) is a non-segmented, negative-sense RNA virus, which belongs to the *Morbillivirus* genus, within the Paramyxoviridae family. It has been isolated for the first time in 1954 in 13-year-old David Edmonston's blood, during a measles outbreak in Boston, Massachussets (Griffin, 2013).

Closely related to the recently eradicated cattle virus rinderpest, (de Swart et al., 2012) measles virus (MeV) probably evolved from an ancestral virus and emerged as a zoonotic infection in communities in which cattle and humans lived in close proximity (Barrett et al., 1999). Although historical evidence is lacking, epidemiolocal evidence suggests that measles became a common human pathogen around 5,000 years ago, when human populations achieved sufficient size in Middle Eastern agrarian civilizations to maintain virus transmission (Weiss et al., 2001; Black, 1966; Keeling & Grenfell, 1997).

Before the introduction of vaccine in 1963, 30 million cases of measles were estimated to occur every year, with an estimated number of deaths of just under two million. As for other diseases, measles incidence and mortality underwent a robust decline, especially in Europe, due to the improvement of the hygiene conditions, nutrition status and progresses in healthcare. Further steps were made after the introduction of antibiotics, able to counteract measles-associated bacterial infections (i.e. pneumonia) (Mina et al., 2015).

However, the best results in the campaign against measles were obtained after the introduction of the first dose of MCV1 (measles-containing vaccine) in the first year of life. The introduction of a two-dose formulation paved the way to the complete eradication of this disease, thanks also to the lack of an animal reservoir (Rota et al., 2016).

1.2.1 Epidemiology

Measles is an airborne pathogen which can be transmitted through inhalation of respiratory droplets and smaller aerosols which can remain suspended for several minutes or hours. (Chen et al., 1989; Bloch et al., 1985). This virus can also be transmitted through direct contact with infected secretions, but does not survive for a long time on fomites. Moreover, it can be inactivated by heat and UV exposure within a few hours. (Measles, Rota, 2016).

For these reasons, MeV is one of the most highly contagious infectious agents known, with a R0 value between 13.7 and 18 (which represents, on average, the number of people that a single infected person can be expected to transmit that disease). Therefore, outbreaks can occur even in populations in which <10% of individuals are susceptible to measles (Chen et al., 1989; Sutcliffe & Rea, 1996).

MeV transmission generally occurs among susceptible individuals in closed contact settings, including households, schools and health care facilities.

The high infectivity of MeV implies that a high level of protection is required among population in order to interrupt virus transmission. However, interruption of MeV transmission does not require the achievement of immunity in all the individuals within a population. The probability of a susceptible individual to be exposed to an infectious one decreases below the threshold required to support transmission only when a sufficient proportion (which varies for different infectious agents) of the population acquires protective immunity. The estimated level of population immunity that is necessary to stop MeV transmission (and so to establish a herd immunity) is between 89 and 94%. This herd immunity threshold does not include only the level of measles vaccination coverage but the overall proportion of the population protected against measles (including both vaccinated and naturally infected subjects). However, a single dose of measles-containing vaccine (MCV1), delivered to children at 9 months of age, will not achieve this level of population immunity. For this reason, the WHO recommends to provide a second dose (MCV2) of vaccine and target ≥95% two-dose coverage for achieving and maintaining measles elimination. (Rota, 2016).

During the 2000–2016 period, the number of reported measles cases worldwide had an 84% decrease, from 853,479 (2000) to 132,490 (2016). From 2000 to 2016, annual measles incidence decreased 88%, from 145 cases per million (2000) to 18 (2016). This goal was achieved thanks to the global increase in MCV first dose (MCV1) coverage from 72% to 84% (Figure 3). However, a global resurgence during 2017–2019 occurred, with an increased incidence of 567% to 120 cases per million (2019) (Dixon et al., 2021). In particular, Europe has experienced a major resurgence of measles due to the suboptimal vaccination coverage below 95% in many countries (Figure 4), even among healthcare workers (Anichini et al., 2020), despite the global increase up to 86%. This raise was strictly linked with general negative attitudes and behaviors toward vaccinations, a phenomenon called "vaccine hesitancy". (Tabacchi et al., 2016; Genovese et al., 2019). For this reason, in 2019 measles vaccination among newborns became mandatory in many European countries. Measles incidence had an apparent decline in 2020 during the COVID-19 pandemic. Despite this decline, millions of children were susceptible to measles at the end of 2020 more than in 2019. MCV1 coverage decreased globally and in all but one region (Western pacific) in 2020. Among 194 WHO member states, only 75 (39%) achieved ≥90% MCV1 coverage in 2020, a 13% decrease respect to the 86 (45%) countries reported in 2000, and a 37% decrease from the 119 (61%) countries reported in 2019. This lowering of coverage is mainly due to the fact that, in 2020, 22.3 million infants did not receive MCV1 through routine immunization services, an increase of three million (16%) respect to 2019 (Figure 3, Figure 5) (Dixon et al., 2021). These data show that,

despite the presence of an extremely effective vaccine, we are still far from the eradication of the disease.
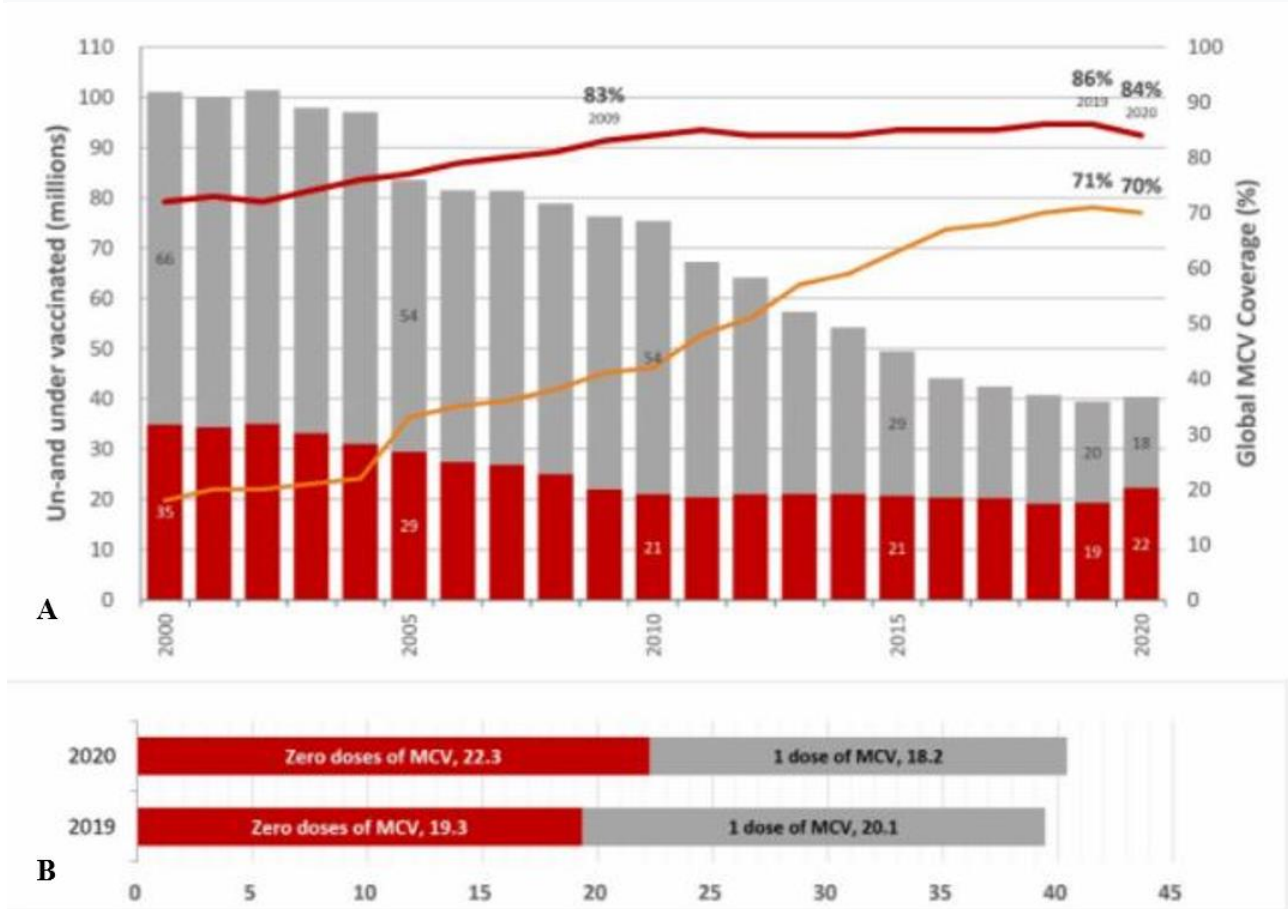
Figure 3: A: Global MCV coverage (%) in the 2000-2020 period. The red bar reports the number (millions) of unvaccinated children for that specific year, while the grey bar reports the number of children who received an uncomplete vaccination (only one dose of MCV). The red line represents the worldwide vaccination coverage for MCV-1, while the orange one represents the vaccination coverage for MCV-2.
B: Enlargment of the 2019-2020 period reflecting the lowering in MCV-1 vaccination coverage from 86% to 84%, leaving 3 million more children unvaccinated in 2020 respect to 2019. Credit: WHO, 2022.
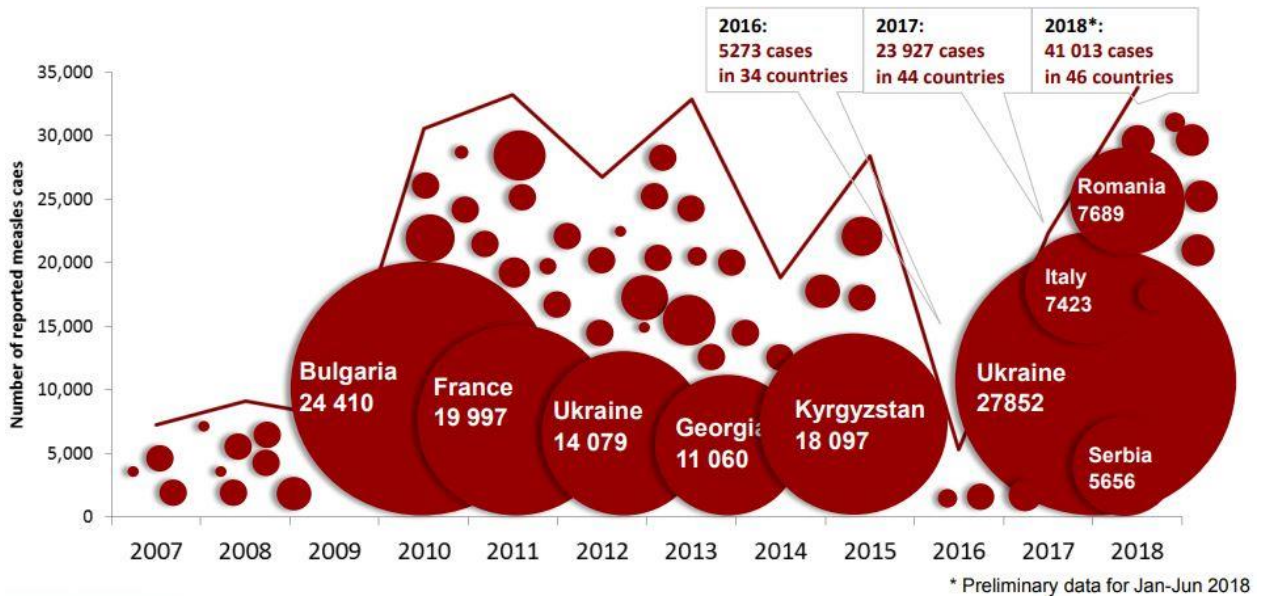
Figure 4: Number of measles-reported cases in the WHO European Region from 2007 to 2018. The graph shows the resurgence of measles outbreaks among european countries between 2017 and 2018. Credit: CISID, extracted 1 August 2018.
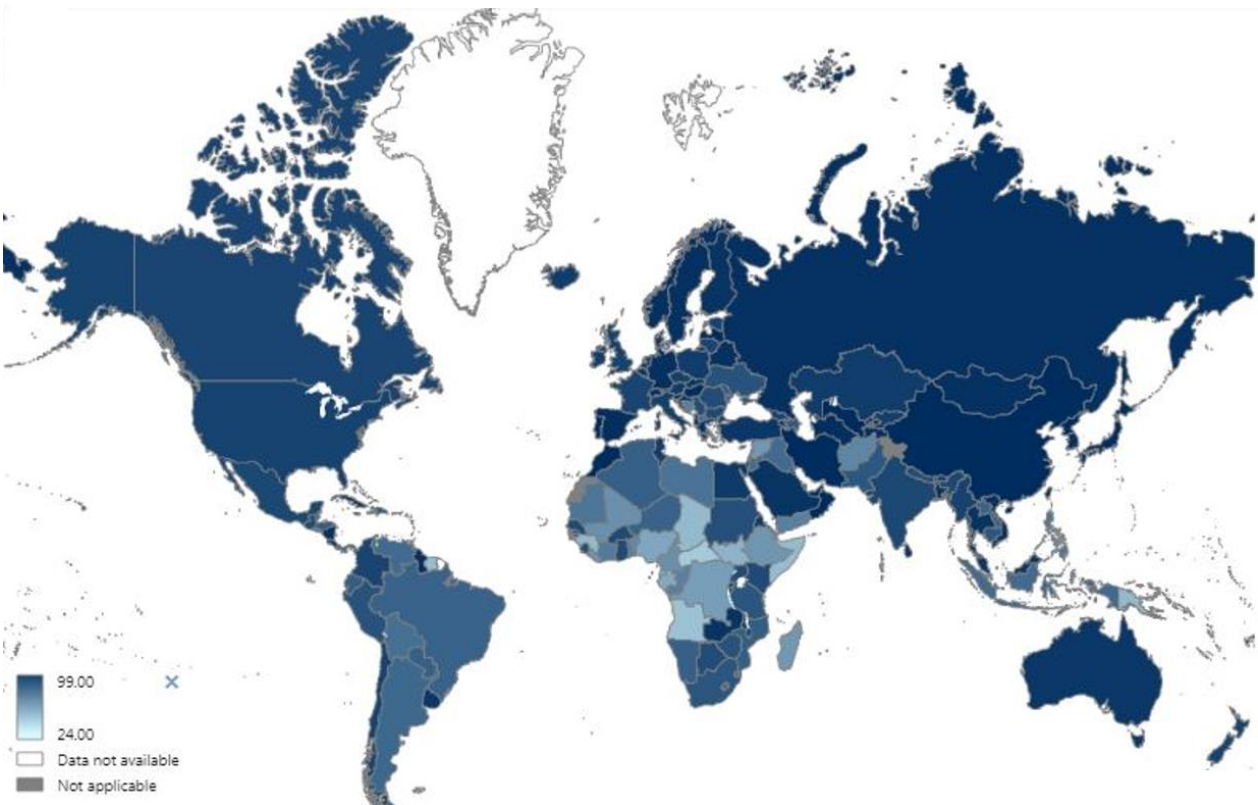
Figure 5: Worldwide immunization coverage with MCV1 among 1-year-old infants**.** Credit: WHO,2022.

1.2.2 MeV genome and lifecycle

MeV has a non-segmented, negative-sense, single-stranded RNA genome of approximately 16,000 nucleotides in length. The genome consists of six genes, each encoding a single structural protein: the nucleocapsid (N) protein, phosphoprotein (P), matrix (M) protein, fusion (F) protein, haemagglutinin (H) protein and large (L) protein. The P gene encodes two additional, non-structural proteins: V and C proteins (Griffin, 2013) (Figure 6a, 6b).

Both the H and the F transmembrane glycoproteins are exposed at the virus surface. Binding of the H protein to a host receptor triggers conformational changes in the F protein, which induces fusion of the viral envelope with the plasma membrane and the release of ribonucleoprotein (RNP) complexes in the cytoplasm of target cells. Once replication and transcription of the viral genome in the cytoplasm occur, the H protein and the F protein, expressed on the cell surface of MeV-infected cells, induce fusion between those cells and the adjacent ones, thus producing multinucleated giant cells or syncytia. During these processes, the virus assembles and is released from the infected cells (Figure 6c). Although progeny virions are assembled at and bud from the plasma membrane, the budding of MeV is inefficient and a large amount of the infectious progeny viruses remains associated with the cell (Udem, 1984). Virus dissemination within the host is primarily mediated by direct cell-to-cell transmission of the virus via infectious synapses.
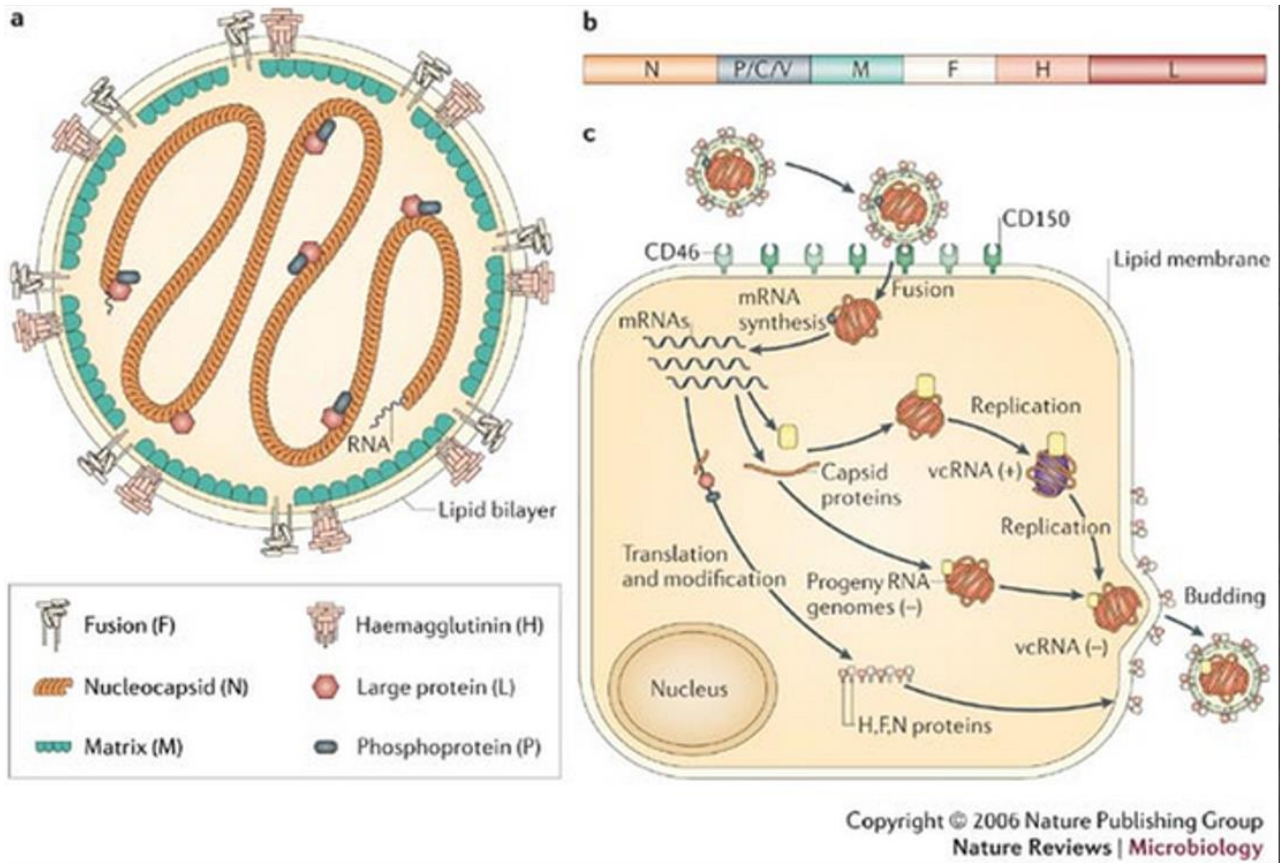
Figure 6: Structure of measles virus (3a, 3b): The RNA genome of MeV is encapsulated by the nucleoprotein (N), associated with viral RNA-dependent RNA polymerase (L protein) and polymerase cofactor (P) forming a helical ribonucleoprotein (RNP). On its lipid envelope, which is derived from the host cell membrane, MeV displays two different transmembrane glycoproteins, the hemagglutinin (H) the fusion (F) protein, The first one is responsible for receptor binding with the host cell, while the second one mediates membrane fusion. The M protein interacts with both the RNP complex and the cytoplasmic tails of the glycoprotein spikes, thus promoting virion assembly. The non-structural V protein and C protein are involved in the evasion of host innate immune responses in infected cells.

MeV lifecycle (3c): After the binding of the H protein to the host receptor, membrane fusion occurs, and the viral RNA is released into the host cytoplasm. Replication and transcription of the viral genome takes place into the cytoplasm. RNA polymerase transcribes the viral RNA genome into mRNA, which then undergoes translation in order to manufacture viral proteins. These viral proteins function to formulate new helical capsids for the replication of the virus, which eventually leaves the host cell through the process of budding.

1.2.3 Host receptors

Signaling lymphocyte activation molecule (SLAM; also known as SLAMF1 and CD150) has been identified as a major cellular receptor for MeV (Tatsuo et al., 2000). This receptor is expressed on thymocytes, macrophages, mature dendritic cells (DCs), Langerhans cells (LCs), lymphocytes and platelets and its expression further increases following immune activation (van der Vlist et al., 2011; Cannons et al., 2011). Nectin 4 (also known as PVRL4), which is expressed at adherens junctions of epithelia, was identified as a second major cellular receptor for MeV (Noyce et al., 2011; Muhlebach et al., 2011). Additionally, DC-specific intercellular adhesion molecule 3-grabbing non-integrin 1 (DC-SIGN; also known as CD209) and C-type lectin domain family 4 member K (also known as Langerin) promote MeV-mediated infection of DCs and LCs, respectively, possibly contributing to the high transmissibility of MeV (van der Vlist et al., 2011; de Witte et al., 2006). Although MeV shows neurovirulence, no cellular receptor for MeV has yet been identified in neural cells. However, studies have suggested that the substance P receptor supports transsynaptic transmission of MeV by interacting with the F protein. Vaccine strains and certain laboratory strains of MeV also use human membrane cofactor protein (MCP; also known as CD46) (Dorig et al., 1993) via specific amino acid substitutions in the H protein (N481Y or S546G) (Yanagi et al., 2009). The ability to use CD46 as a receptor is essential for haemagglutination by MeV.

1.2.4 MeV infection

The main targets of MeV *in vivo* are the SLAM-expressing lymphocytes and dendritic cells (DCs) (de Swart et al., 2007; de Vries & de Swart, 2014; de Vries et al., 2010). In addition, tissue-resident DCs in the respiratory tract are putative initial targets of MeV (Figure 7a). The infection of immune cells with MeV is mediated by SLAM, but the attachment of MeV to DCs is also supported by DC-SIGN, promoting SLAM-mediated MeV infection and the transmission of MeV to T lymphocytes (de Witte et al., 2008). MeV can also directly infect alveolar macrophages in the lungs, which express SLAM as well (de Vries et al., 2010; de Witte et al., 2008). Epithelial cells are unlikely to be the initial targets of infection because MeV antigens are not detected in epithelial tissues early after infection and nectin 4 is not expressed on the apical surface of these cells. MeV infection is amplified in draining lymphoid tissues and subsequently causes viraemia through circulating MeV-infected lymphocytes (Lemon et al., 2011). Analyses in non-human primates using recombinant MeVs lacking SLAM-binding or nectin 4-binding ability (SLAM-blind MeV and nectin 4-blind MeV, respectively) further clarified the individual roles of SLAM and nectin 4 (Leonard et al., 2010; Leonard et al., 2008). Nectin 4-blind MeV efficiently infected non-human

primates, causing a systemic infection and replicating in immune cells as wild-type MeV, even when administered intranasally (Leonard et al., 2008). Conversely, infection by SLAM-blind MeV was highly attenuated and this virus induced strong adaptive immune responses and hardly caused viraemia in non-human primate models (Leonard et al., 2010), suggesting that SLAM is primarily important for MeV pathogenesis.

MeV-infected lymphocytes and DCs can migrate into subepithelial cell layers of the respiratory tract where they can transmit MeV to epithelial cells using nectin 4 as a receptor (Figure 7b) (Ludlow et al., 2010; Frenzke et al., 2013). Experiments using polarized airway epithelial cells *in vitro* demonstrated that MeV can enter cells from the basolateral side and buds exclusively from the apical membrane (Leonard et al., 2008), replicating directional entry and budding of MeV *in vivo*. The virus is efficiently transmitted between epithelial cells through intercellular membrane pores (Baxby et al., 1997; Singh et al., 2016a; Singh et al., 2016b). Other mechanisms of transmission have also been proposed. For example, damage to the epithelium of lymphoid tissues in the upper respiratory tract may allow shedding of the virus produced by MeV-infected immune cells or epithelial cell debris by coughing and sneezing (de Vries et al., 2012).
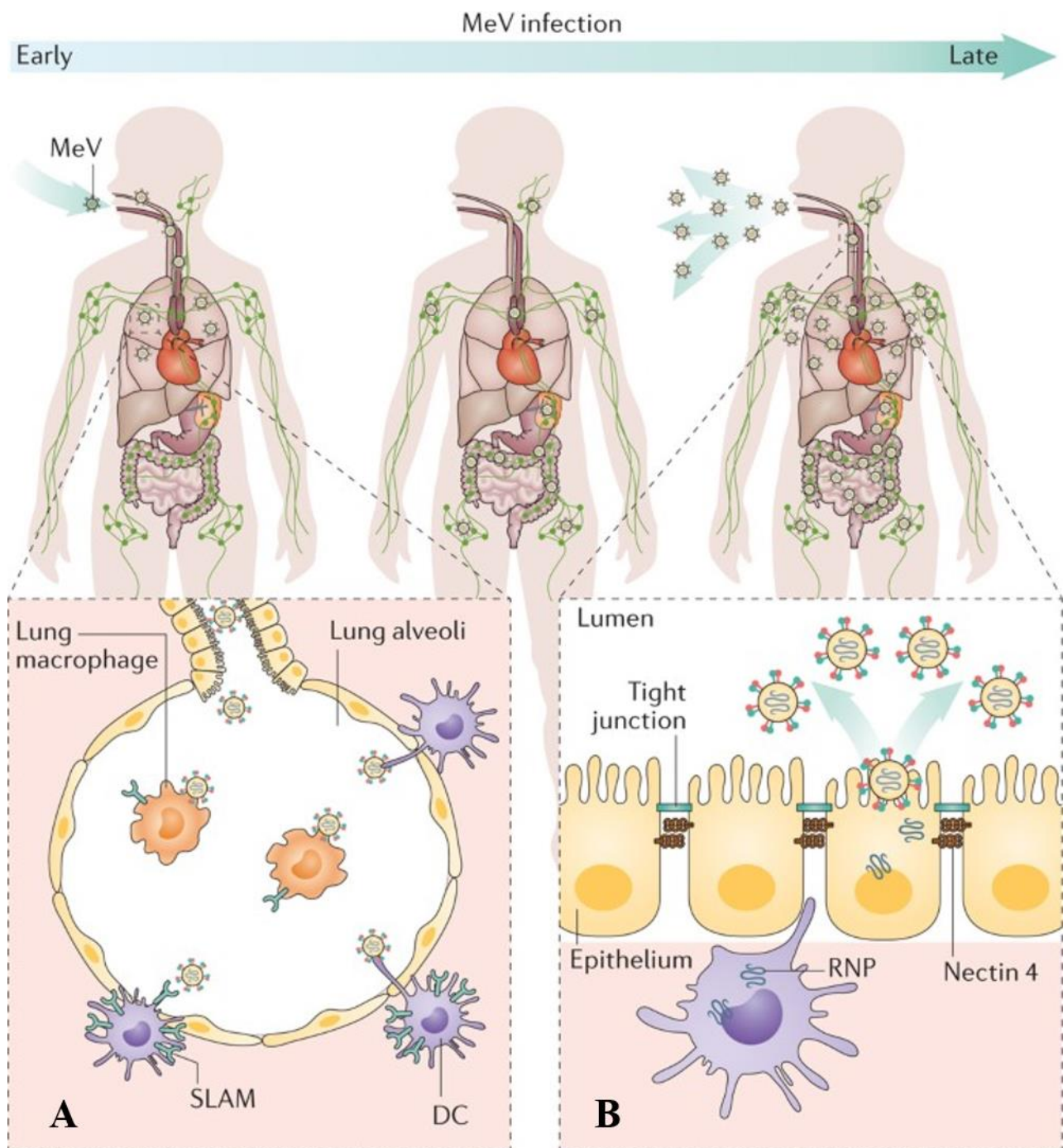
Figure 7: Measles virus (MeV) infection of alveolar macrophages or dendritic cells (DCs) in the respiratory tract mediated by signalling lymphocytic activation molecule (SLAM; also known as CD150) receptor **(A)**. Infected lymphocytes and DCs migrate into the subepithelial cell layer and **(B)** transmit MeV to epithelial cells of various organs or tissues (where is in turn amplified and released) using nectin 4 as a receptor. Credit: Rota, 2016.

1.2.5 Genetic and antigenic variability

Although MeV is considered as an antigenically monotypic virus, genetic and antigenic variation has been described among wild-type viruses. Although sequencing studies have demonstrated that the genome of MeV is quite stable, considering it as a monotypic virus, genomes with insertions and deletions have been detected (Bankamp et al., 2014). These mutations have been used to assign wild-type MeV into one of 24 genotypes (A, B1–B3, C1–C2, D1–D11, E, F, G1–G3 and H1–H2) (World Health Organization, 2012; Rota et al., 2014). However, only eight of these genotypes have been detected in recent years (B3, D3, D4, D6, D8, D9, G3, and H1), while five genotypes (B1, D1, E, F, and G1) are considered inactive since they have not been detected for more than 25 years (Rota et al., 2003; World Health Organization, 2016). Antigenic differences between different wild-type strains have also been detected based on the binding of monoclonal antibodies to viral proteins (especially the H protein) and neutralization assays with polyclonal antiserum (Shi et al., 2011; Santibanez et al., 2005; Finsterbusch et al., 2009; Kuhne et al., Kuhne et al., 2006). These findings suggest that antibodies induced by vaccination might not recognize all wild-type strains. However, some of the epitopes recognized by vaccine-induced neutralizing antibodies target-conserved regions of the H protein, including the regions involved in receptor binding or in the interaction between the H protein and the F protein, thus limiting the possibility for antigenic variation (Tahara et al., 2013a; Tahara et al., 2013b; Beaty & Lee, 2016). In support of this observation, sequencing studies have not produced evidence for the action of selective pressure on the H protein of MeV (Zhang et al., 2014). This is also proved by the high vaccine efficacy against MeV in all countries regardless of the predominant endemic genotype.

1.2.6 Signs and symptoms

Measles-associated signs and symptoms start to appear after an incubation period of around 8 to 12 days (range 7–21 days) after the exposure to the virus. The illness typically begins with nonspecific prodromal symptoms of fever, malaise, dry cough, coryza, and conjunctivitis. The patient may also have a sore throat. One day before rash onset, small white spots with bluish-white centers on a red background (Koplik spots), may be seen on the buccal mucosa and can persist for several days, generally fading before resolution of the skin rash. (Tanaka et al., 2019; Lefebvre et al., 2010).

This characteristic appearance of Koplik spots is sometimes referred to as "grains of salt on a red background" and this sign is considered as pathognomic for the diagnosis of measles disease.

Occasionally, they may also appear in other areas such as the soft palate, conjunctival fold, and vaginal or intestinal mucosa (Suringa et al., 1970).

After 2 to 4 days of intensifying prodromal symptoms, the characteristic erythematous maculopapular rash appears. The rash starts on the face and neck and progresses down the arms and

trunk to the distal extremities. Meanwhile, fever rises rapidly, often as high as 40°C–41°C. The rash lasts for 3 to 7 days and then fades in the order of appearance (Figure 8). Persons with measles are considered infectious from 4 days before until 4 days after onset of rash. Measles in immunocompromised persons can be more severe with longer duration of rash and visceral dissemination of measles virus; however, some immunocompromised patients might not develop a rash. Measles in vaccinated persons may be milder and modified and may not meet the clinical case definition. Atypical measles, an illness that was characterized by high fever, an atypical (vesicular, petechial, or purpuric) rash that was most prominent on the extremities, and a high rate of pneumonitis, occurred in children who received inactivated measles vaccine that was in limited use in the United States from 1963 to 1968 (Fulginiti et al., 1967; Brodsky et al., 1972).
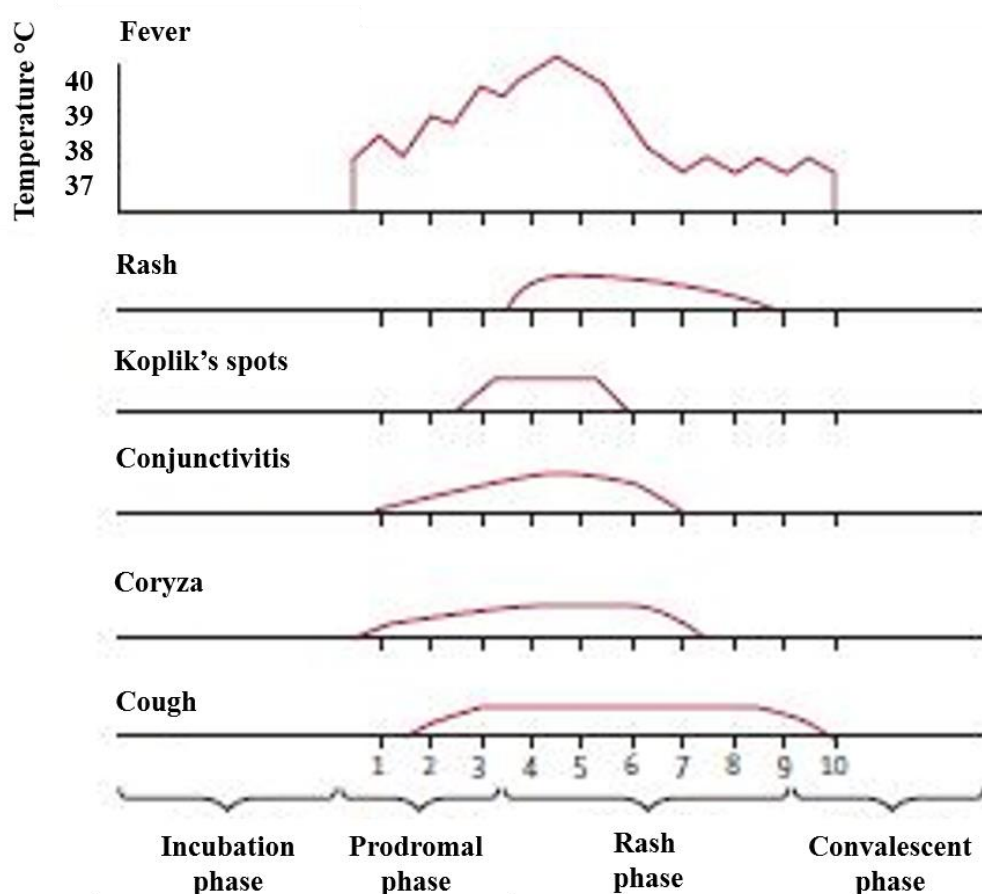

Figure 8: Graphic representation of measles disease course and symptoms throughout the different stages of infection. Credit: Moss, 2017.

1.2.7 Complications

Measles can be serious in all age groups. In fact, those who contract measles generally have a 30-40% chance of developing at least one complication (Moss & Griffin, 2012). However, there are several groups, mostly depending on age or health status, that are more prone to develop complications, such as children younger than 5 years of age, adults older than 20 years of age, pregnant women and people with compromised immune systems, such as those with leukemia or HIV infection (Moss & Griffin, 2012). These can include pulmonary complications, otitis that can lead to hearing loss, and complications in the gastrointestinal tract with stomatitis and diarrhea (Moss & Griffin, 2012). Optically, MeV-associated keratoconjunctivitis can occur, which can lead to blindness. In pregnant women, premature miscarriage may occur or, if close to delivery, the virus may be transmitted to the unborn child with possible adverse consequences (White et al., 2012). MeV can also lead to devastating complications in the central nervous system (CNS) (Buchanan & Bonthius, 2012). Primary viral encephalitis has a prognosis of approximately 10/15% mortality while neurological damage is present in 25% of cases. Other additional neurologic sequelae associated with measles are infectious encephalomyelitis, a demyelinating disease that can lead to severe CNS damage, and subacute sclerosing panencephalitis, a neurodegenerative disease that causes sudden personality changes, cognitive decline, and motor dysfunction. Subacute sclerosing panencephalitis is fatal with a life expectancy of 1 to 2 years (Buchanan & Bonthius, 2012). However, one of the most interesting and studied complications is immunosuppression at the expense of the adaptive immune system.

Immunosuppression is characterized by: lymphopenia, long-term cytokine imbalance and peripheral lymphocyte silencing. This consequence is related to the fact that measles affects CD150$^+$ cells, including dendritic cells, modulating their activation and damaging their functioning. The damage caused to DCs will then actively interfere with the activation of T lymphocytes. The effects produced by these mechanisms are: lymphopenia, which lasts for a few days (Ryon et al., 2012), suppression of prolonged cell-mediated immunity (Th2-biased) (Griffin & Ward, 1993) and inability to activate lymphocytes, which will not be able to perform clonal expansion in response to the viral antigen (Avota et al., 2010; Schneider-Schaulies et al., 2002).

Lymphopenia is mainly evident in the acute phase of the disease and is characterized by a decrease in B and T lymphocytes, both CD4$^+$ and CD8$^+$ (Ryon et al., 2012). This decrease in circulating lymphocytes is primarily caused by the cytopathic effect of MeV but it is possible that it is also caused by the suppression of hematopoiesis caused by infection (Ryon et al., 2012). While lymphopenia ends with the acute phase, cytokine imbalance may last for months or even years and contributes to long-term immunosuppression.

Despite this immunosuppression, the organism that has come in contact with MeV develops an extremely strong and effective permanent immunity, this process is commonly known as the "measles paradox" (Rota et al., 2016).

1.2.8 Molecular diagnosis

Although the diagnosis of this disease is mainly based on the clinical picture, it can be confirmed in laboratory by serological, culture and polymerase chain reaction (PCR) tests on saliva or blood samples. The serological test is the most frequently performed one, as the detection of IgM antibodies against MeV by enzyme immunoassays (EIA) is considered the standard method for the diagnosis of acute measles (Bellini & Helfand, 2003; Sampedro et al., 2013). Moreover, rising IgG from the acute to the convalescent phase can be detected using IgG-specific EIA, hemagglutinin inhibition, complement fixation or virus neutralization assays (Moss & Griffin, 2012). MeV can also be isolated and grown in tissue culture from white blood cells, nasopharyngeal swabs, conjunctival swabs, urine or respiratory secretions. For even greater accuracy, PCR tests can be performed to identify the presence of viral RNA from patient's blood, urine and nasal secretions. These tests have a specificity of around 100% and are also excellent for defining the viral genotype. For the containment of infected subjects, precautional methods such as isolation from other patients or the use of negative pressure rooms should be taken (Bester, 2016).

1.2.9 Treatment

There is no specific treatment for measles infection. However, there are some measures which can be considered, especially for the protection of vulnerable individuals who have been exposed to the virus. Nonimmunized people, including infants, may receive measles vaccination within 72 hours of exposure to acquire protection against the disease. However, measles could still develop, but the illness has usually milder symptoms and lasts for a shorter time. Moreover, pregnant women, infants and people with weakened immune systems who are exposed to the virus may receive an injection of immune serum globulin, preferably within six days from the virus exposure, in order to prevent measles or make symptoms less severe.

The major components of case management include provision of vitamin A, prompt treatment of secondary bacterial infections and nutritional support.

Vitamin A has been widely distributed through polio and measles supplemental immunization activities as well as through routine child health services. The WHO recommends administration of two daily doses of 200,000 IU to all children aged 12 months or older or 100,000 IU for those with less than 12 months of age, resulting in a 64% reduction in the risk of mortality (D'Souza & D'Souza, 2002).

Secondary bacterial infections are a major cause of morbidity and mortality following measles (Moss et al., 2009). In particular, *Streptococcus pneumoniae* and *Haemophilus influenza* type b are the most common causes of bacterial pneumonia following measles, and antibiotic therapy should be directed against these pathogens. However, the use of prophylactic antibiotics, especially in hospitalized children, remains controversial, as it may reduce the incidence of pneumonia but not mortality (Moss et al., 2009). For this reason, the potential benefits of antibiotic prophylaxis must be weighed against the risks of accelerating antibiotic resistance.

A measles anti-viral drug could be very helpful by stopping the virus from spreading far in outbreaks, either among the unvaccinated, or when the vaccine has failed. However, although the broad antiviral agent ribavirin has been used to treat immunocompromised persons or persons with *Subacute Sclerosing Panencephalitis (*SSPE), alone or in combination with IFN-α or intravenous immunoglobulin (Moss et al., 2009), no specific antiviral drug is used routinely or has been approved to treat measles virus infection. Recently, an orally bioavailable small-molecule polymerase inhibitor has shown to prevent measles disease in squirrel monkeys (*Saimiri sciureus*) (Wittwer et al., 2021), thus making it a promising clinical candidate for post-exposure treatment of MeV.

Chapter 2

Antiviral host immunity and prevention

2.1 The immune response in measles

After introduction of MeV into the respiratory tract, immature pulmonary dendritic cells (DCs) or alveolar macrophages capture and transport MeV to other lymphoid tissues and to endothelial and epithelial cells in multiple organs including skin, liver and conjunctiva. Here, the immune response takes place, virus is amplified and the spread of infection facilitated (Ludlow et al., 2013; Mesman et al., 2012).

After that, infected immune cells (B cells, CD4+ and CD8+ memory T cells, monocytes) enter the circulation system and facilitate the spread of the virus to multiple lymphoid (spleen, thymus, lymphnodes) and non-lymphoid (skin, conjunctivae, kidney, lung, liver) tissues where it replicates in endothelial and epithelial cells, lymphocytes and macrophages (de Vries et al., 2012; McChesney et al., 1997; Esolen et al., 1995).

The immune response plays an essential role in the different stages of MeV infection and disease. Initially, after viral infection, the host immune system is triggered by the detection of pathogen-associated molecular patterns (PAMPs), such as the presence of cytoplasmic ssRNA bearing 5'-triphosphate or dsRNA. These structures are recognized by host pathogen recognition receptors (PRRs), which are highly sensible intracellular receptors such as RIG-I (retinoic acid-inducible gene I protein), MDA5 (melanoma differentiation protein) and LGP2 (laboratory of genetics and physiology 2). With regard to measles, the most engaged receptors are RIG-I and, to a less extent, MDA5 (Ikegame et al., 2010; Plumet et al., 2007; Yoneyama et al., 2015).

2.1.1 Innate immune response

The initial phase of the innate immune response, which occurs during the prodromal phase of the illness, is limited due the production of interferons (IFN) which allow extensive virus replication and spread during a silent latent period of 10–14 days.

Typically, the innate response to RNA virus infection is characterized by the production of types I and III IFNs by the infected cells. The induction of these early-released cytokines occurs through recognition of alerting viral antigens or replication components by host pattern-recognizing toll-like receptors (TLRs) or by cytoplasmic RNA helicases that trigger the activation of cytoplasmic transcription factors IFN regulatory factor (IRF)-3 and nuclear factor kappa-light-chain-enhancer of activated B cells (NF-kB). Wild-type (but not vaccine strain) MeV H protein has been shown to activate TLR2, which leads to the induction of pro-inflammatory cytokines such as IL-6 in in macrophages (Bieback et al., 2002). Translocation of IRF-3 and NF-kB to the nucleus, triggered by phosphorylation, induces transcription of the mRNAs for early response proteins such as Normal T Cell Expressed and Secreted/Chemokine (C-C motif) ligand 5 (RANTES/CCL5), IRF-7 and IFN-gamma with subsequent induction of IFN-stimulated genes (ISGs) with antiviral activity including

myxovirus resistance (Mx), adenosine deaminase acting on RNA 1 (ADAR1), ISG15, ISG56 and IFN-stimulated genes that can act to suppress virus replication (Randall et al., 2008; Yoneyama et al., 2010).

However, in absence of defective interfering RNAs both induction of and signaling by IFN-gamma are effectively inhibited through the combined activities of the MeV P, C and V proteins (Davis et al., 2014; Li et al., 2012; Schuhmann et al., 2011; Childs et al., 2009; Shivakoti et al., 2013) with little or no evidence of IFN production *in vivo* during the acute response to MeV infection (Shivakoti et al., 2015; Yu et al., 2008).

In fact, MeV possesses useful mechanisms for evading the host immune system. Protein V primarily binds MDA5 and LGP2 leading to the inhibition of IFN synthesis (Parisien et al., 2009). In addition, C protein can also interfere with the interferon mechanism at the transcriptional level or by modulating viral RNA synthesis (Sparrer et al., 2012). In fact, viruses defective for C protein will undergo immoderate RNA production that is easier for the host cell to detect (Sparrer et al., 2012; Nakatsu et al., 2008; Devaux et al., 2008). Regarding the mechanism of IFNs, V also carries inhibition at the level of JAK-STAT signaling by interacting with STAT1 and STAT2 (Caignard et al., 2009). C and V are proteins that have been shown to be critical in giving MeV high virulence *in vivo*. Indeed, IFN is not produced to suppress virus replication after infection, resulting in a prolonged latent period during which there is systemic virus replication and dissemination without signs or symptoms of infection. The virus also exhibits a system that induces suppression of the adaptive immune system, thus making opportunistic infections possible (Devaux et al., 2008).

However, there is evidence for engagement of stress-response proteins and inflammasome activation by MeV infection. In antigen presenting cells (APCs), interaction between MeV and DC-specific intercellular adhesion molecule-3 grabbing non-integrin (DC-SIGN) suppresses RNA helicase activation so that infection increases expression of stress-induced genes without inducing IFN (Shivakoti et al., 2013; Shivakoti et al., 2015; Yu et al., 2008; Mesman et al., 2014).

In vitro studies showed that MeV infection of myeloid cells stimulates assembly of the NACHT, LRR and PYD domains-containing protein (NLRP3) inflammasome in a mitofusin 2-dependent process with activation of caspase-1 followed by cleavage and secretion of mature interleukin (IL)-1 and IL-18 (Ichinohe et al., 2013; Komune et al., 2011). Transcriptional analysis of peripheral blood mononuclear cells (PBMCs) during MeV infection shows up-regulated expression of NLRP3 and IL-1 mRNAs necessary for inflammasome activation (Komune et al., 2011). As further *in vivo* evidence of the innate response during measles, plasma levels of NF_B-induced proteins IL-6 and IL-8/CXCL8 (Zilliox et al., 2007) and inflammasome products IL-1 and IL-18 are increased (Zilliox et al., 2007; Phillips et al., 2004; Okada et al., 2001).

Therefore, the innate response does not include IRF-3-mediated induction of type I or III IFNs, but does include induction of a subset of NF-kB- and inflammasome-associated cytokines and chemokines that are important for initiating the adaptive immune response.

However, clearance of viral RNA from blood and tissues is much slower than clearance of infectious virus and proceeds over weeks to months (Figure 9).
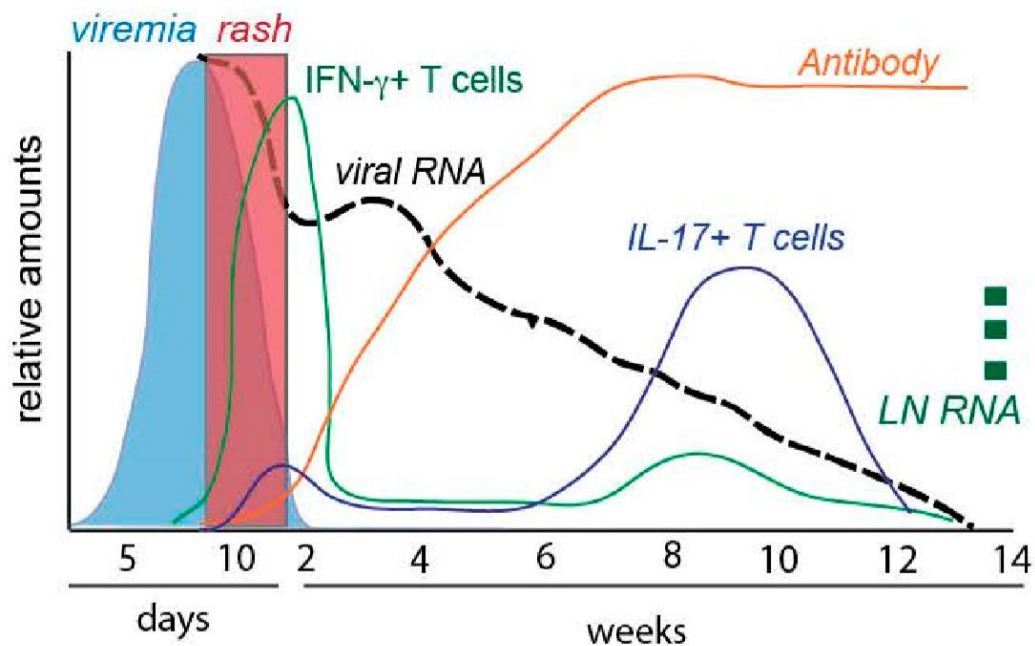
Figure 9: Schematic diagram of measles virus (MeV) clearance and immune response in rhesus macaques. While viremia is generally resolved within two weeks after infection, viral RNA clearance occurs only after 12-14 weeks from infection. Rash is generally related to the appearance of IFN-γ-producing T cells which rapidly decline after viremia is cleared. After two weeks, antibodies start to being produced and increase in amount and avidity. However, there is a prolonged phase of slow viral RNA clearance from peripheral blood mononuclear cells (PBMCs) with persistence of viral RNA in lymph nodes (LN RNA). Waves of MeV-specific T cells continue to appear in circulation with a shift from IFN-γ production to interleukin 17 (IL-17) production. Credit: Griffin, 2016

2.1.2 Adaptive immune response

Cellular immune responses are considered the most important elements for clearance of MeV, strengthened by the fact that infected children with agammaglobulinemia recover, while those with defects in cellular immunity may develop progressive disease (Permar et al., 2006).

The maculopapular rash that appears between 10 and 14 days after infection is a manifestation of the adaptive response to infection (Figure 9), and it is caused by lymphocyte infiltration into sites of viral replication in skin epithelial cells (Griffin, 2021).

CD4$^+$ and CD8$^+$ T cell epitopes are present in many viral proteins (Jaye et al., 2003; Ota et al., 2007; Schellens et al., 2015). The initial cellular immune response, which is crucial for the control and clearance of infection is characterized by the presence of MeV-specific cytotoxic CD8+ T lymphocytes, IFN-γ-producing CD4$^+$ and CD8$^+$ T cells, along with soluble indicators of T cell activation (e.g., 2 microglobulin, cytokines and soluble CD4, CD8 and Fas) (Griffin et al., 1992; Griffin et al., 1990; Griffin et al., 1989; Nelson et al., 2017). Depletion of CD8$^+$ T cells from experimentally infected macaques results in higher and more prolonged viremias (Permar et al., 2003); moreover, CD8$^+$ T cells can control virus spread *in vitro* (de Vries et al., 2010). As CD4$^+$ and CD8$^+$ T cells infiltrate sites of virus replication (Polack et al., 1999), infectious virus decreases rapidly to undetectable levels, the rash fades and the fever resolves.

However, the effector T cell response present in blood during the rash is transient, perhaps due to rapid induction of regulatory T cells as the rash is cleared, and does not result in clearance of viral RNA (Permar et al., 2001; Riddell et al., 2007). Studies regarding monkeys experimentally infected with a WT strain of MeV showed persistence of MeV RNA in PBMCs for months after resolution of the rash (Figure 9) (Lin et al., 2012; Nelson et al., 2020). Quantitation of the MeV RNA present showed that clearance from PBMCs occurs in three to four phases (Figure 9).

After an initial peak at 7–10 days (during the viremia when infectious virus can be recovered), there is a period of rapid decline coincident with clearance of infectious virus (10–14 days), followed by a rebound with up to a 10-fold increase in RNA levels (14–24 days) and then a slow decline (24–60 days) to an undetectable level. At this time lymphnodes, and potentially other tissues, still harbour MeV RNA that can transiently reappear in PBMCs at later times (Lin et al., 2012; Pan et al., 2005; Pan et al., 2010).

Detailed quantitative studies of RNA clearance and the immune responses in individual macaques combined with mathematical modeling indicate that T cell responses (as indicated by IFN-γ-producing cells) correlate with clearance of infectious virus from blood, but that both antibody and T cells are required to explain the decline in viral RNA (Lin et al., 2012).

2.1.3 Maturation of the immune response

Continued presence of MeV RNA and proteins in lymphoid tissue after the acute phase of infection may explain suppressed immune responses to new infections, but is also an aid in maturation of the immune response to MeV and may be required to establish life-long protective immunity.

Dendritic cells play a central role as they contribute to both the innate and adaptive immune responses and bridge these processes through the production of pro-inflammatory cytokines as well as their ability to function as efficient antigen-presenting cells (APCs). These cells are present at mucosal surfaces (Lyakh et al., 2008), such as the lung, and can become infected with pathogens such as measles virus through direct infection or by phagocytizing infected cells in the airways. Infection of dendritic cells promotes their maturation, leading to increased expression of MHC class II molecules (Zhou & Tedder, 1996).

Peptides of measles virus are presented to naïve T cells to induce differentiation and expansion into effector T cell subsets (Banchereau & Steinman, 1998; Mellman & Steinman, 2001)

The inflammatory environment established by innate immune cells allows for the expansion and differentiation of antigen-specific effector T cells that encompasses a large portion of the adaptive immune response.

Immune activation and lymphocyte proliferation, particularly of CD4$^+$ T cells, are evident in the acute phase and then for months after resolution of the rash (de Vries et al., 2012; Ryon et al., 2002). During this period, there is a shift in cytokine production from type 1 T cell cytokines (e.g., IFN-γ) to type 2 cytokines (e.g., IL-4, IL-10, IL-13) and appearance of IL-17-producing cells (Moss et al., 2002; Griffin & Ward, 1993) (Figure 9). This shift is likely to promote B cell maturation and contribute to the continued production of antibody-secreting cells (Nair et al., 2009). Ongoing improvement in antibody quality, as evidenced by increasing avidity, suggests continued activity of T follicular helper (TFh) cells and B cell selection in the germinal centers of lymphoid tissue (Figure 9). Development of long-lived plasma cells is necessary to sustain plasma antibody levels for life.

2.1.4 Protective immunity

Epidemiologic studies have shown that the level of neutralizing antibodies at the time of exposure to WT virus in the community is a good correlate of protection from infection with higher titers needed to prevent infection than to prevent disease (Chen et al., 1990). High avidity antibodies are required to neutralize CD150-mediated WT MeV infection of lymphoid cells (Polack et al., 2003).

The mechanism involved in the maintenance of high levels of neutralizing antibodies is still not well understood, but the persistence of MeV RNA in lymphoid tissues, triggering a continuous development of germinal centers, could be a determinant factor (Nelson et al., 2020). However,

since CD4$^+$ T cell help is required for isotype and affinity maturation of antibody-secreting cells, B cell memory and maturation of CD8$^+$ T cell memory, a cellular immune response is also important for the induction of immunological memory against MeV and therefore protective immunity.

T cell immunity has been implicated also as directly protective in individuals with low levels of antibody. The antiviral effects of T cells can be mediated both by secretion of cytokines that suppress virus replication (e.g., IFN-γ) and by cytotoxic elimination of infected cells. Because T cells do not directly block infection but rather react to control or eliminate virus-infected cells once infection has occurred, the contribution of T cells to protection is generally considered minor in comparison to neutralizing antibodies. Furthermore, studies in macaques have shown that T cell immunity alone cannot protect from MeV infection or disease, but does facilitate RNA clearance and generation of a robust T cell and antibody response after challenge infection (Lin et al., 2014). Therefore, generation of both immune-mediated clearance and long-lived protection requires development of effective and durable MeV-specific antibody and CD4$^+$ and CD8$^+$ T cell responses.

2.1.5 Immune suppression following MeV infection

Another clinical feature related to measles virus infection is the immune suppression induced by the virus, causing a high susceptibility to other pathogens even for a long time after recovery (Mina et al., 2015; Behrens et al., 2020). In fact, most of measles death are due to other infection or co-infections (Beckford et al., 1985). There are several factors that contribute to this period of immunosuppression still not completely understood. Following measles virus infection, little, if any, type I interferon is produced (Griffin, 2010; Moss et al., 2004). Apoptosis and impaired proliferation lead to abnormalities in the number and function of lymphocytes. (Moss et al., 2004; Laksono et al., 2018). Furthermore, impaired maturation and antigen presentation by dendritic cells may lead to decreased T cell activation (Griffin, 2010; Moss et al., 2004).

The interaction of measles virus H protein with its receptor, CD150, results in the inhibition of IL-12 production by dendritic cells (Hahm et al., 2007). Additionally, cross-linking the CD46 receptor decreases the production of IL-12 by monocytes (Moss et al., 2006). The suppression of the IL-12 response could lead to a decrease in induction of Th1 cells (Moss et al., 2004; Hahm et al., 2007). Moreover, IFN-γ, which is produced by Th1 cells inhibits the proliferation of the Th2 subset, and conversely IL-4 and IL-10, produced by Th2 cells, inhibit Th1 cytokine production (Fiorentino et al., 1989; Fiorentino et al., 1991).

The shift from a Th1 to a Th2 response early after infection suppresses activation of macrophages and proliferation of T cells, and may prevent the host from mounting an effective Th1 response upon subsequent exposure to new pathogens, leaving the host more vulnerable to these exposures (Moss et al., 2004).

Furthermore, a prolonged presence of IL-10 and regulatory T cells could play a role in immune suppression as well, as Tregs can pave the way to opportunistic infections, and also can suppress T cell responses that clear viral infections (Mills, 2004; Laksono et al., 2018).

A measles outbreak among the Dutch Orthodox Protestant community in 2013, provided a unique opportunity to study the pathogenesis of measles immune suppression in unvaccinated children. In peripheral blood mononuclear cells (PBMC) of prodromal measles patients, MV-infected memory CD4$^+$ and CD8$^+$ T cells and naive and memory B cells were detected at similar levels as those observed in non-human primates (Laksono et al., 2018). Moreover, in paired PBMC collected before and after measles, a reduced frequency of circulating memory B cells and increased frequencies of regulatory T cells and transitional B cells after measles were observed, supporting the hypothesis of immune amnesia and explaining the long-term effects of measles on host resistance (Laksono et al., 2018).

2.2 Measles vaccine

In 1954, John F. Enders and Dr. Thomas C. Peebles collected blood samples from several ill students during a measles outbreak in Boston with the aim to isolate the measles virus from their blood and thus to create a measles vaccine. They succeeded in isolating measles in 13-year-old David Edmonston's blood. In 1963, John Enders and colleagues transformed their Edmonston-B strain of measles virus into a vaccine and licensed it in the United States. In 1968, a live-attenuated measles vaccine, developed by Maurice Hilleman and colleagues, began to be distributed. This vaccine was produced starting from the wild-type (WT) Edmonston strain virus after being passed on different cultures to modify its characteristics and attenuate its virulence. In addition to the live attenuated vaccine strains, a formalin-inactivated Edmonston vaccine was in use during 1963–1967; however, use of this vaccine was discontinued because vaccinated individuals were at risk for developing atypical measles after wild-type measles virus infection.

For this reason, the Edmonston-Enders (formerly "Moraten") strain has been the only measles vaccine used in the United States since 1968. Thus, the development of current vaccines, (Edmonston Zagreb®, Schwarz®, AIK-C®, Moraten®, Attenuvax® and Rubeovax®), all made with live-inactivated virus, has always had a common starting point, that is the use of the Edmonston strain, although being passaged in different cultures: chicken embryonic, chicken embryonic fibroblasts, sheep kidney, dog kidney and human somatic cells.

In fact, vaccines consisting of attenuated viruses are an excellent method of immunization as they infect the individual but do not cause the classical symptomatology of the disease. Attenuated viruses have the possibility to replicate in humans and this is a great advantage because very small doses are sufficient to bring immunization as the immune system will recognize and eliminate the virus in its classic modus operandi, all this without having an obvious clinical manifestation. These vaccines, however, have some disadvantages, mainly related to the fact that there may be a random reversion to virulence, thus starting the real disease especially in immunocompromised subjects. This defect is very rare, but it can be avoided in case there is an inactivated vaccine available (as was the case for polio with Sabin and Salk) which is less immunizing. Another problem with attenuated vaccines is the difficulty of storage, as it is important not to interrupt the cold chain (a problem usually present during vaccinations in territories with inadequate health facilities).

Worldwide, measles vaccine is licensed in monovalent or combination formulations for measles-rubella (MR), measles-mumps-rubella (MMR), and measles-mumps-rubella-varicella (MMRV, ProQuad, Merck and Co., Inc) vaccines. Two doses of measles vaccine are recommended for children and national schedules vary throughout the world with the first dose most commonly recommended at 9 or 12 months of age.

Vaccine administration before that age is not recommended because of immunologic immaturity and the interference of transplacentally acquired maternal antibodies with replication of vaccine virus (Moss et al., 2009). For children in the United States, the first measles vaccine dose is recommended at 12 to 15 months of age and the second dose at 4 to 6 years. Recommendations may differ during outbreaks and before international travel.

The vaccine is generally administered subcutaneously starting with freeze-dried and frozen doses then reconstituted with distilled water or sterile saline. 0.5 ml of vaccine is then administered, which contains 1000 $TCID_{50}$ (tissue culture infectious doses) of attenuated virus.

However, there is an alternative method of administration, such as aerosol administration that appears to be equally effective (Naim, 2015).

Measles vaccine effectiveness is 93% following 1 dose administered at the age of 12 months or greater and 97% for 2 doses (McLean et al., 2013; Fiebelkorn et al., 2016). Therefore, despite its great effectiveness, about 3 out of 100 people who get two doses of MMR vaccine will get measles if exposed to the virus. However, they are more likely to have a milder illness, and are also less likely to spread the disease to other people (Centers for Disease Control and Prevention, 2018).

Although antibody levels decline over time, they remain above protective levels for most vaccinated persons and there is no consistent evidence that protection from measles declines along with age (LeBaron et al., 2007; Anichini et al., 2020). On the contrary, protection against MeV seems to be more correlated with the immunization schedule which, since the introduction of MeV vaccine, has been changed several times over the years. Moreover, since vaccination was only recommended, in most of the cases the schedule was not followed within the suggested timeframe (Anichini et al., 2020).

For this reason, continued monitoring of duration of immunity and protection could of major importance.

2.2.1 Safety profile

The safety of MCVs, including measles-only, measles-rubella (MR), measles-mumps-rubella (MMR), and MMR-varicella (MMRV) vaccines is well-established. MCVs have similar safety profiles and are well tolerated, and common reactions after vaccination are mild (McLean et al., 2013; World Health Organization, 2009). Common adverse events after MMR vaccination depend on components of the vaccine and include fever (5%−15%), rashes (5%), and lymphadenopathy (5%−20%), as well as parotitis and transient arthralgias/arthritis (Macartney et al., 2015; McLean et al., 2013; Naim, 2015).

These adverse events occur approximately 6−12 days after vaccination, the time period of peak vaccine virus replication.

Compared with the first dose of vaccine, adverse events are less common after the second dose of vaccine, because most children are immune at the time they receive the second vaccination, and therefore, less viral replication occurs. Thrombocytopenia can occur after natural measles infection, but is generally mild and resolved within 7 days, on average. Anaphylaxis and other immediate hypersensitivity reactions can occur after MMR vaccination, and are likely related to allergies to the gelatin or neomycin components of the vaccine.

Immunocompromised patients should also not receive the MMR vaccine. Potential fatal adverse events in immunocompromised hosts include measles pneumonia, Measles inclusion body encephalitis (MIBE), and disseminated measles infection (Portais et al., 2021, Permar et al., 2006; Monafo et al., 1994; Stokke et al., 2021). This recommendation is inclusive of persons with human immunodeficiency virus (HIV) infection who are severely immunocompromised. MMR vaccine is contraindicated in pregnancy owing to theoretical concerns of fetal harm including congenital rubella syndrome (McLean et al., 2013).

The highly favorable safety profile of MCV has been an essential component of the global measles eradication strategy.

2.2.2 Measles vaccination in Italy

In Italy, the single-antigen vaccine was introduced in 1976 and, since 1979, one dose was recommended to be administered at 15 months of age. The introduction of the trivalent vaccine MMR (measles, mumps, rubella) occurred in the '90s, while the administration of a second dose has been recommended only since 2003. However, misleading knowledge and perceptions on the MMR vaccine, and general negative attitudes and behaviors toward vaccinations (enclosed under the definition of 'vaccine hesitancy'), were significantly associated with lower MMR vaccination uptake rates since 2012. This hesitancy resulted in a robust increase of measles cases and outbreaks in 2017 in 15 of the 53 countries in the WHO European Region, with the highest numbers of affected people reported in Romania (5562), Italy (5006) and Ukraine (4767). (World Health Organization, 2018; Tabacchi et al., 2016; Odone et al., 2018; Bonanni et al., 2015).

As a result of this epidemic, due to the low vaccination coverage (<90%, especially among youth and adolescents but also among healthcare workers) (Genovese et al., 2019; Anichini et al., 2020) the administration of a two-dose schedule (at 13-15 months and 6 years of age) of the MMR vaccine in Italy has been made mandatory through a specific law (Italian Ministry of Health, 2017a,b). As a consequence of this law, vaccination coverage for the first dose of measles-containing vaccine raised up to 94.49% among infants in 2019. In 2020, only 103 measles cases (1.69 per million population) have been notified in Italy, with no cases detected from April to

December (Istituto Superiore di Sanità, 2021), below the European average (2106 cases, 4.24 per million).

2.2.3 Impact of Covid-19 pandemic on measles vaccination routine

Recently, the emergency state due to the Covid-19 pandemics has disrupted vaccine coverage in many countries worldwide and may lead to a further increase in cases and deaths from measles and other vaccine preventable diseases (Tanne et al., 2020). As of October 2020, (World Health Organization, 2020) had either fully or partially postponed measles-related vaccine campaigns during the COVID-19 pandemic to help avert further spread of the virus. Together, more than 117 million children in 37 countries, many of whom live in regions with ongoing measles outbreaks, could be impacted by the suspension of scheduled immunization activities. (UNICEF, 2020; World Health Organization, 2021; World Bank, 2021; Rana et al., 2021).

This staggering number does not include the number of infants that may not be vaccinated because of the effect of COVID-19 on routine immunization services. Children younger than 12-months of age are more likely to die from measles complications, and if the circulation of measles virus is not arrested, their risk of exposure to measles will increase daily.

These data show that we are still far from the eradication of the disease, which is considered possible thanks to some peculiarities such as the low capacity of virus mutation, the lack of animal reservoir and especially thanks to the presence of an extremely efficacious vaccine.

Chapter 3

Aim of the project

Aim of the study is to evaluate the differences in the humoral and cellular immune response against identified measles antigens, among subjects vaccinated with MMR, subjects who had natural infection, unvaccinated subjects who have never had the infection and subjects who did not respond immunologically after a two-dose MMR vaccination, although responding to mumps and rubella.

First of all, levels of functional neutralizing antibodies, which is considered a good correlate of protection from infection during measles outbreaks, were investigated among either vaccinees or naturally infected subjects. In fact, according to literature, levels of anti-measles antibodies tend to decline over the life course, as demonstrated by measuring the level of measles neutralizing antibodies in the subjects' sera at different times after vaccination (Kennedy et al., 2019; Davidkin et al., 2008; Carryn et al., 2019; Seagle et al., 2018). Moreover, this phenomenon appears to occur faster following vaccination rather than after naturally infection (Gonçalves et al., 2015; Le Baron et al., 2007). Since many of the vaccinated subjects who received a two-dose vaccination were seronegative at the time of screening, it was important to understand which variables could influence the vaccine-induced antibody response and which parameters might influence the risk of vaccine failure.

Since it has been shown that long lasting humoral response is mainly addressed to measles virus N, P and L proteins, we wanted to analyze whether this feature corresponded to a higher number of circulating T cells, especially memory subsets, either in vaccinees or in naturally infected individuals.

To this aim, peripheral blood mononuclear cells (PBMC) drawn from the four categories of subjects were analyzed via flow cytometry before and after *in vitro* stimulation with inactivated measles virus. Naïve, memory and effector T cells were studied. Data obtained were used to evaluate the effectiveness of MMR vaccination and to understand whether those subjects lacking of specific antibodies, several years after vaccination, were no more protected because of waning humoral response or could still have and maintain an immune memory response against measles. Finally, transcriptome-level characterization (mRNA-Seq data) of responses to measles virus stimulation in antibody responders (either vaccinated or naturally infected) and those who had not responded to the vaccine is in progress, with the aim to identify define plausible regulators (genes/pathways) that drive the observed differences among these subjects.

Such study may help to explain what are the specific markers of adaptive (or innate) immune response which distinguish the natural from the induced immunity and to develop a panel of biomarkers to monitor, besides the antibody response, the immune response to measles vaccine with the aim to protect the subjects who eventually become seronegative along the time, with a booster composed of immunogenic and protective viral proteins.

Chapter 4

Materials and Methods

4.1 Study population

The participants in this observational study were students, postgraduates, medical doctors and health care workers subjected to routine analysis for the biological risk assessment at the Center of Preventive Medicine and Health Surveillance of the University Hospital 'Santa Maria alle Scotte' in Siena between January 2018 and May 2019. Among the participants, some subjects presented their history of vaccination against measles, some had never been vaccinated and others had a history of measles infection.

A total of 1092 subjects, 361 males and 731 females, (mean age 27.1 years; CI 95% 26.6–27.6) were screened for the presence of both anti-measles IgG and IgM. All subjects born before 1977 (before the introduction of measles vaccine in Italy) declared to have contracted measles infection; the others, born later, were distinguished into three groups, according to their vaccination records: vaccinated with one or two doses and nonvaccinated.

Lastly, among those born after 1977, 110 sera of subjects (mean age 24.9 years; CI 95% 24.1–25.7) vaccinated with two doses of measles vaccine, either monovalent (Moraten, Istituto sieroterapico e vaccinogeno svizzero, Berna, Switzerland) or trivalent (measles, mumps and rubella; MMR) Priorix (GlaxoSmithKline, Verona, Italy) were analyzed for the titer of specific neutralizing antibodies. These titers were compared with 100 samples of subjects (mean age 48.6 years; CI 95% 46.2–51.1), who had been naturally infected during childhood.

Furthermore, from 24 patients, of whom ten vaccinated, ten with natural infection, two non-reponders and two non-vaccinated and uninfected controls, blood was collected in order to analyze the cell-mediated immune response after *in vitro* stimulation of isolated PBMC with UV-inactivated measles virus. Finally, transcriptomic analysis of the T cell response upon stimulation in PBMC from 12 subjects randomly selected from the study group, equally distributed between vaccinated, naturally infected and non-responders, has been performed.

This research was carried out according to the principles of Helsinki declaration. Ethical approval was obtained from the local Ethical Committee for clinical trials (approval n◦ 11466_2017) (Comitato Etico Regione Toscana-Area Vasta Sud Est) in terms of General Data Protection and Regulation (GDPR) upon written informed consent signed by all subjects prior to participating in this study.

	Study Group (1022)					
	IgG positive (769)			IgG negative (253)		
N°of doses received	Males	Females	Total	Males	Females	Total
0	36	84	120	15	25	40
1	166	342	508	49	112	161
2	7	6	13	1	3	4
>2	47	81	128	18	30	48
Total	256	513	**769**	83	170	**253**

Table 1: Schematic representation of the study subjects divided by gender, seroprevalence and number of doses of measles vaccine received (either monovalent or trivalent). Regarding nonvaccinated subjects (n° of doses = 0), the IgG positives concern those who had been naturally infected, all during their childhood, while those IgG negative those who have never been exposed to measles virus (nonvaccinated and noninfected).

4.2 Cells and viruses

Vero cells (ATCC CCL-81) were grown as a monolayer in Dulbecco's modified Eagle's medium (DMEM) (Euroclone, Milan, Italy) supplemented with 100 U/mL penicillin/streptomycin (Euroclone, Milan, Itay) and 5% heat-inactivated fetal calf serum (FCS) (Euroclone, Milan, Italy) at 37 °C in a humidified 5% CO2 atmosphere. Then, PBMC were isolated from blood of the selected donors, upon written informed consent, by Ficoll-Hypaque gradient separation and cultured in Roswell Park Memorial Institute (DMEM) (Euroclone, Milan, Italy) supplemented with 100 U/mL penicillin/streptomycin (Euroclone, Milan, Italy) and 10% heat-inactivated fetal calf serum (FCS) (Euroclone, Milan, Italy) at 37 °C in a humidified 5% CO2 atmosphere. Measles virus Edmonston B strain (ATCC VR-24) was propagated on Vero (ATCC CCL-81) cells.

4.3 Measles IgM/IgG antibody detection

Sera obtained from subjects were analyzed for the presence of measles specific IgM/IgG antibodies to the recombinant MV nucleoprotein, by LIAISON XL (Liaison Measles IgG/IgM, DiaSorin, Saluggia, Italy), a chemiluminescence analyzer using paramagnetic solid phase microparticles. Threshold IgG values regarded as positive immune status were >16.5 AU (Arbitrary Unit)/mL, with detection limit of 13.5 AU/mL; while IgM threshold for the presence of measles infection was >1.1 AU/mL, with detection limit at 0.9 AU/mL.

4.4 Measles virus titration

Briefly, the supernatant of infected Vero cells (ATCC-CCL-81) was ten-fold diluted. Therefore, 50µl of each dilution was added in quadruplicate to a 96 well-plate together with an equal volume (50µl) containing $2x10^5$ cells. After four days, the presence of cytopathic effect (CPE) was observed under microscope (Olympus IX51; Olympus, Tokyo, Japan) and the 50% end point titer was calculated using the Reed and Muench method (Reed & Muench, 1938).

4.5 Measles microneutralization assay

The measles virus neutralization assay was carried out on Vero cells in a 96-well microplate. Twenty-five microliters of 2-fold serial dilutions (1:8 to 1:1024) of vaccinated or naturally infected people sera were added to an equal volume of the Edmonston B strain MV containing 250 TCID50 and incubated for 90 min at 37 ∘C. Finally, 50 µL of Vero cells uspension (2×10^5 cells/mL) prepared in a complete DMEM (Euroclone) medium were added to each well. Five days after incubation at 37 ∘C, the cultures were microscopically examined for the presence of CPE. The 50% end point titer of the serum neutralizing titer was calculated using the Reed and Muench method (Reed & Muench, 1938). Serum samples with neutralizing titers of less than eight were considered

negative (Anichini et al., 2020). A positive and negative control serum (Liaison Measles IgG Ctr) were included in each assay (Anichini et al., 2020).

4.6 UV-inactivation of measles virus

Measles virus (Edmonston B strain) was UV-inactivated at a dose of about 1.5×10^2 pW/mm (van Binnendijk et al., 1992). The protein concentration of measles virus and Vero cells as determined by the Bradford assay. To confirm the complete viral inactivation, the UV-treated virus was titrated on Vero cells, showing no cytopathic effect after one week by microscopical examination.

4.7 Peripheral blood mononuclear cells isolation and stimulation

For the evaluation of the T-cell response after stimulation with UV-inactivated measles virus, 24 subjects, of whom ten vaccinated, ten naturally infected, two unvaccinated and uninfected negative controls and two non-responders after receiving a complete vaccination, were selected. Then, peripheral blood mononuclear cells (PBMCs) were isolated from whole blood of those subjects using Lympholyte® Cell Separation Media (Cedarlane, Burlington, Canada). Afterwards, PBMCs were washed with RBC (Red Blood Cell) lysis buffer and seeded in quadruplicate at a density of 1×10^6 cells in 500 µl in 24-well plates with RPMI-1640 medium (Euroclone, Milan, Italy), supplemented with 10% heat-inactivated human serum (Euroclone, Milan, Italy). After 6 hours, UV-inactivated measles virus was added in one well from each subject at a concentration of 1 MOI, while the other well was kept as the unstimulated control. T-cell populations were analyzed 48 hours after antigen stimulation. After that, cells were harvested and analyzed by flow cytometry.

4.8 Multiparameter flow cytometry analysis

After stimulation, PBMCs of selected subjects were harvested and washed, using PBS supplemented with 3% FCS, then stained with a fixable viability dye (LIVE/DEAD™ Fixable Aqua Dead Cell Stain Kit, Thermo Fisher Scientific, Waltham, MA, USA) for 20 min at 4°C. Surface staining with antibodies binding to CD3 (clone SK7), CD4 (clone SK3), CD8 (clone RPA-T8), CCR7 (clone 150503), CD45RA (clone HI100), CD38 (clone HIT2), HLA-DR (clone G46-6), CXCR3 (clone 1C6), and CCR6 (clone 11A9) for the analysis of T-helper was performed, according to manufacturer's instructions. All antibodies were supplied from BD Biosciences (New York, NY, USA). After fixation with PBS + 2% paraformaldehyde for 20 min at 4°C, cells were washed and resuspended in PBS, supplemented with 0,5 mM EDTA before being acquired with SO LSRFortessa X20 flow cytometer (BD Biosciences, New York, NY USA). Data analysis was performed using FlowJo v10 (TreeStar, Ashland, OR, USA).

4.9 RNA extraction and library preparation protocol

After stimulation, $1x10^6$ PBMCs (either stimulated and non) from each subject were harvested and their RNA was extracted using Single Cell RNA Purification Kit (Norgen Biotek Corp., Thorold, ON, USA). Then, RNA concentration was evaluated with Qubit™ RNA high sensitivity (HS) Assay Kit (Thermo Fisher Scientific, Waltham, MA, USA) using a Qubit 3 fluorometer.

Therefore, DNA library was prepared using NEBNext® Ultra™ II DNA Library Prep Kit for Illumina® (New England Biolabs, Ipswich, MA, USA), according to manufacturer's instructions. Purification steps were performed using Next Generation Sequencing (NGS), DNA/RNA Clean Up Mag-Bind® TotalPure (Omega Bio-tek, Inc. Norcross, GA, USA)**.** Libraries were barcoded using NexNext® Multiple Oligos for Illumina® (New England Biolabs, Ipswich, MA, USA), in order to sequence twenty-four samples on the same chip. Then, barcoded libraries were purified using Next Generation Sequencing (NGS), DNA/RNA Clean Up Mag-Bind® TotalPure (Omega Bio-tek, Inc. Norcross, GA, USA). The quantity of each library was evaluated on a 2100 Bioanalyser Instrument (Agilent, Santa Clara, CA, USA) using a High Sensitivity DNA Kit (Agilent, Santa Clara, CA, USA).

Libraries were initially diluted to a concentration of 4nM and pooled all together, then denatured and diluted at a final concentration of 1,8pM together with PhiX control v3, according to manufacturer's instruction (Illumina Inc., San Diego, CA, USA). Finally, 1,3 ml of the pooled 1,8pM library was loaded on a NextSeq™ 500/550 High Output Reagent Cartridge v3 (75 cycles), and the run performed using a NextSeq 550 Sequencer (Illumina, San Diego, CA, USA) according to manufacturer's protocol.

4.10 Statistical Analysis

Seroprevalence was calculated as the ratio between the number of positive test results and the number of performed tests. Geometric mean titers (GMTs), obtained by the neutralization assay, were calculated as log-transformed reciprocal titers and reported as back-transformed for each subclass. Differences between vaccination status, sex, time elapsed between dose one and two of the vaccine and time elapsed since the second dose of vaccine, and the last serological measles investigation, were evaluated. Furthermore, statistical significances were assessed with the two-tailed chi-squared test. Results were considered statistically significant at $p < 0.05$. When appropriate, 95% confidence interval (CI 95%) was calculated and reported. Spearman's rank correlation coefficient was used to assess correlations of log-transformed continuous variables by the group. All analyses were performed by using Graph Pad Prism software (v.7.0). To represent data and to perform results comparisons, each single cell population analyzed by cytofluorimetry

was normalized to the amounts of cells of interest for the specific subset of cells population. For each cell population, differences upon stimulation were reported as the increase in the population percentage compared to the unstimulated control.

Chapter 5

Results

Part I

Differences in humoral immune response among vaccinated and naturally infected subjects

5.1.1 Study group

For this study, we enrolled 1092 subjects, who were screened for the presence of specific anti-measles IgG and IgM. None of the subjects was found to be IgM positive at the time of screening. Regarding IgG, 843 subjects (77.2%) were seropositive and 249 (22.8%) seronegative to MeV, far from the percentages required to achieve herd immunity (Table 1). The mean age of vaccinated subjects was 24.9 years (CI 95% CI 24.1–25.7). Among the nonvaccinated subjects, seropositives (naturally infected) and seronegatives (never exposed to the virus) had, respectively, a mean age of 39.0 years (95% CI 37.1–40.9) and 26.1 years (95% CI 24.6–27.4) ($p < 0.00001$). Vaccination coverage with one or two doses of vaccine, either monovalent or trivalent, of this population sample was estimated 77.1% (842/1092), lower than the 90%–95% threshold required for achieving herd immunity. The enrolled people were lately divided according to their vaccination history (one or two doses) or non-vaccinated (including naturally infected or non-exposed to the virus) (Table 1). Surprisingly, among those who received two doses of vaccine (as recommended by the Italian Ministry of Health since 2003), 161 out of 682 subjects (23.6%) were seronegative after vaccination. Except for one subject, who had not responded to the trivalent MMR vaccine, all the others were seropositive to mumps and rubella viruses, indicating that these individuals, although not having antibodies against measles, had nonetheless responded to vaccination. Surprisingly, this percentage was similar to that observed for subjects who received only one dose (40/160, 25%) (Table 1). No significant differences in the seroprevalence rates were found in all the groups with respect to gender ($p > 0.05$).

5.1.2 Age-specific IgG prevalence

In order to analyze the IgG prevalence trend, the enrolled subjects have also been divided into groups according to their age, regardless of their vaccination status (Figure 10). There was no significant difference in the percentage of seronegatives ($p > 0.05$) among the groups aged 19–42 (Figure 10).

On the contrary, a consistent increase of seropositives, up to almost 100%, was observed in subjects over 43 years old, therefore born before the introduction of measles vaccine in Italy. As far as seronegativity rates are concerned, some differences among the age groups are also worthy of being mentioned. All negative subjects in the 37–42 age group had never been exposed to the virus; most of the subjects aged 31–36 had been vaccinated with just one dose, while the majority of the 19–24 age group had been vaccinated with two doses. Regarding the group aged 25–30, the percentage of seronegatives was equally distributed between those vaccinated with one or two doses of vaccine.
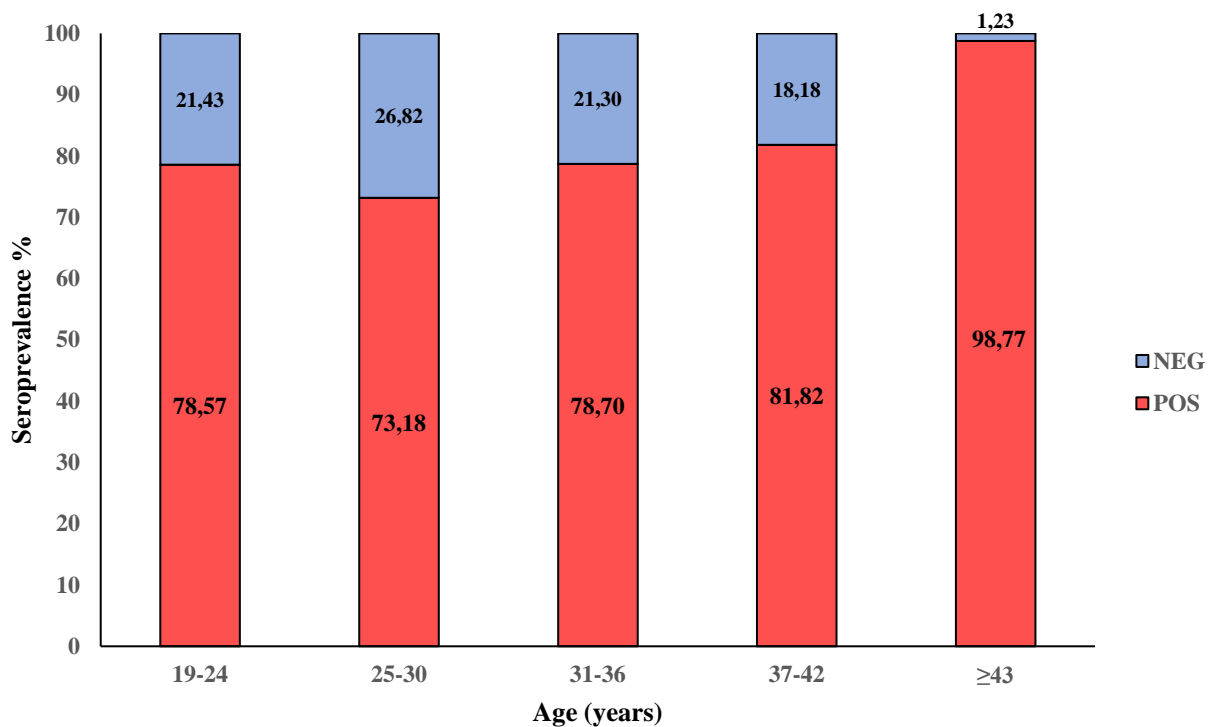

Figure 10: Age-specific measles IgG prevalence categorized into different age groups. Subjects over 43 years old were included into the same group, since all of them were born before the introduction of measles vaccine in Italy.

5.1.3 Decline of humoral response to measles after vaccination

Figure 11 reports the seroprevalence analyzed during the period of 8–18 years after receiving the second dose of vaccine in 562 subjects within the same range of age (mean age 24.4 years; CI 95% 24.2–24.6). Although the number of tested subjects decreased over time, it was evident that an increasing number of vaccinees became seronegative in parallel with the increase of time post-vaccination. We noticed a higher percentage of seronegative subjects between 13 and 16 years after vaccination, suggesting that the decrease of the humoral response could be due to a measles-specific antibody titer after vaccination lower than after natural infection. However, this hypothesis could not be endorsed since the antibody titers after vaccine administration were not available. Extending the monitoring time, the trend was similar, although the serological profile appeared variable, probably due to the limited number of tested samples.
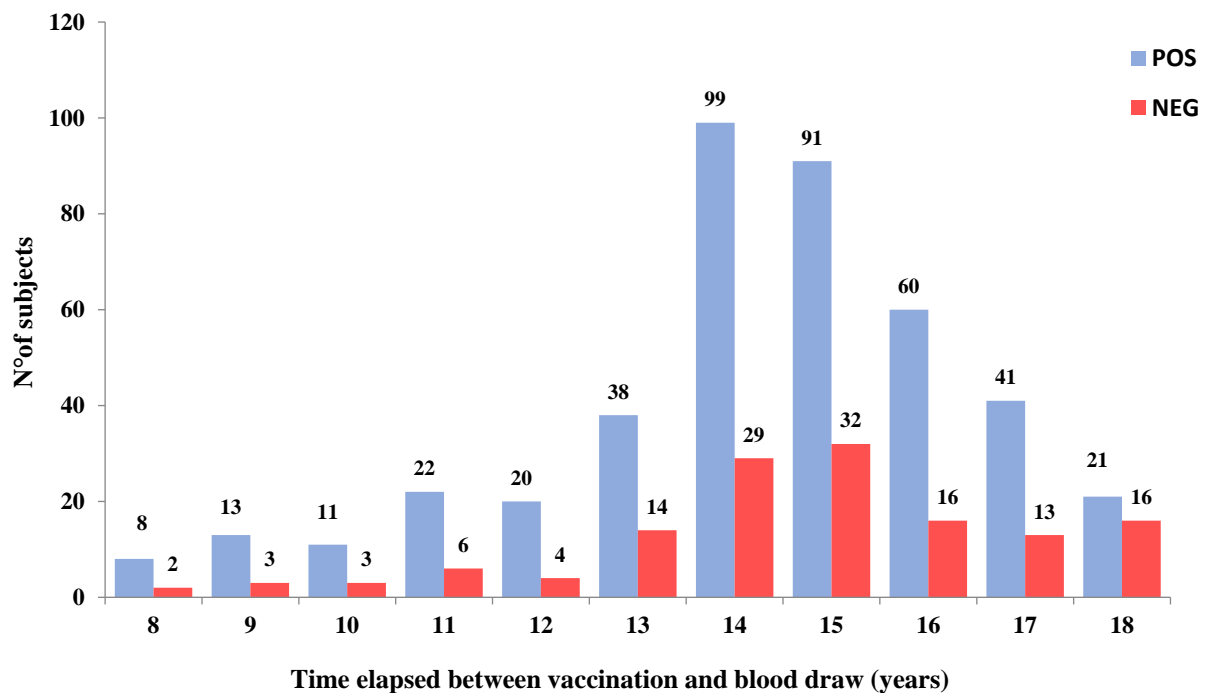

Figure 11: Seroprevalence of measles antibodies after vaccination over-time. Antibody response in vaccinees was analyzed 8–18 years after complete vaccination. The number of seropositive and seronegative subjects was plotted.

5.1.4 Evaluation of neutralizing antibody titers

One hundred and ten sera of seropositive subjects who had received two doses of the measles vaccine and 100 sera of randomly selected subjects who had contracted a natural infection were tested for the presence of neutralizing antibodies against the virus. With regard to naturally infected subjects, the GMT of the tested samples was 570.6 and no substantial differences were found between males and females ($p = 0.46$). Among those vaccinated with two doses of measles vaccine, the GMT was 172.1, which was considerably lower than that recorded in naturally infected subjects ($p < 0.00001$). Moreover, no gender related significant differences in GMT were found during this analysis ($p = 0.38$) (Figure 12).
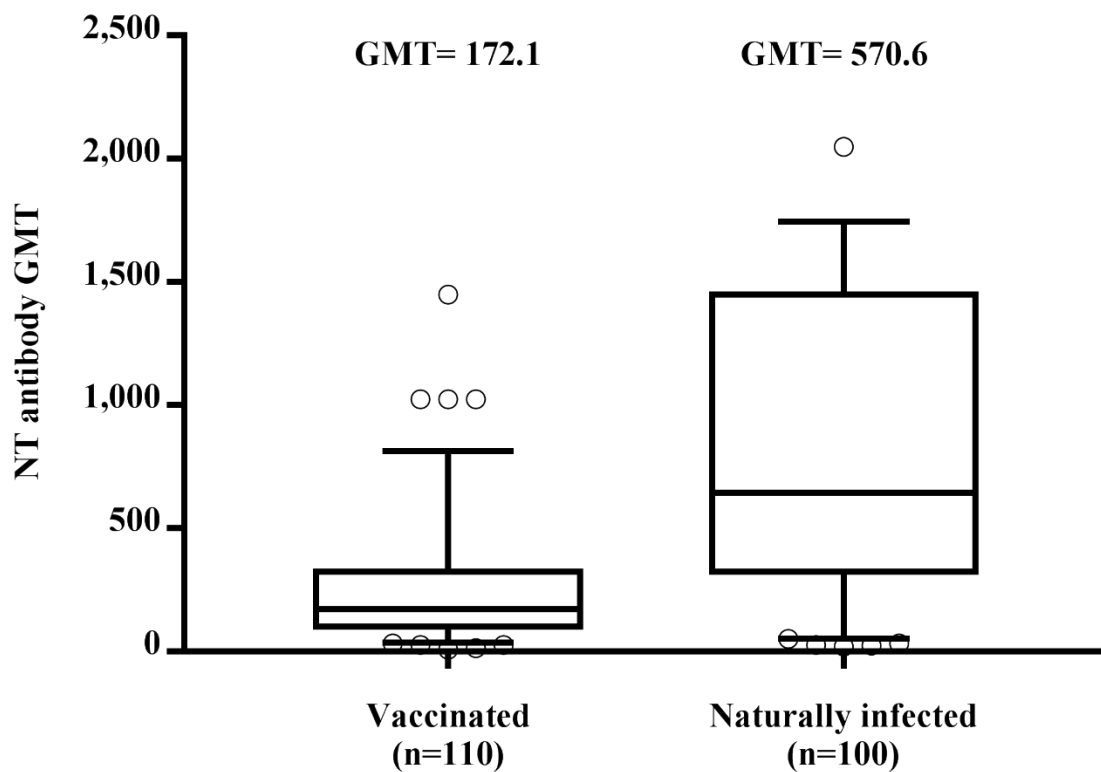

Figure 12: Differences in neutralizing antibody titers between subjects vaccinated with two doses of measles vaccine and naturally infected subjects are shown. The whiskers represent the values from the 5th to the 95th percentiles; the median, the 25th and 75th percentiles are depicted by the horizontal lines in the boxes. Individual data points are shown; outlier values are shown as black circles or squares. GMTs are shown above the population columns. *p*-value of the GMT between the two groups is ≤0.00001.

5.1.5 Decline of neutralizing antibody titers

Since many studies reported that the measles protective antibody titer was decreasing over time after the administration of the second dose of MMR vaccine (Kennedy et al., 2019; Carryn et al., 2019; Davidkin et al., 2008; Seagle et al., 2018; Gonçalves et al., 2015), our aim was to evaluate this phenomenon in our cohort. The vaccinated subjects were divided into three groups, on the basis of the time elapsed since the administration of the second dose of vaccine: eleven years (35 subjects), 12–14 years (39 subjects) and ≥15 years (36 subjects). Results showed a significant decrease in GMT between the groups tested at 1–11 and 12–14 years after vaccination (232.4 vs. 147.4; $p < 0.05$) (Figure 13), thus confirming a possible decline of the protective antibody response against measles during their lifetime. No further difference was evidenced after ≥15 years since vaccination.
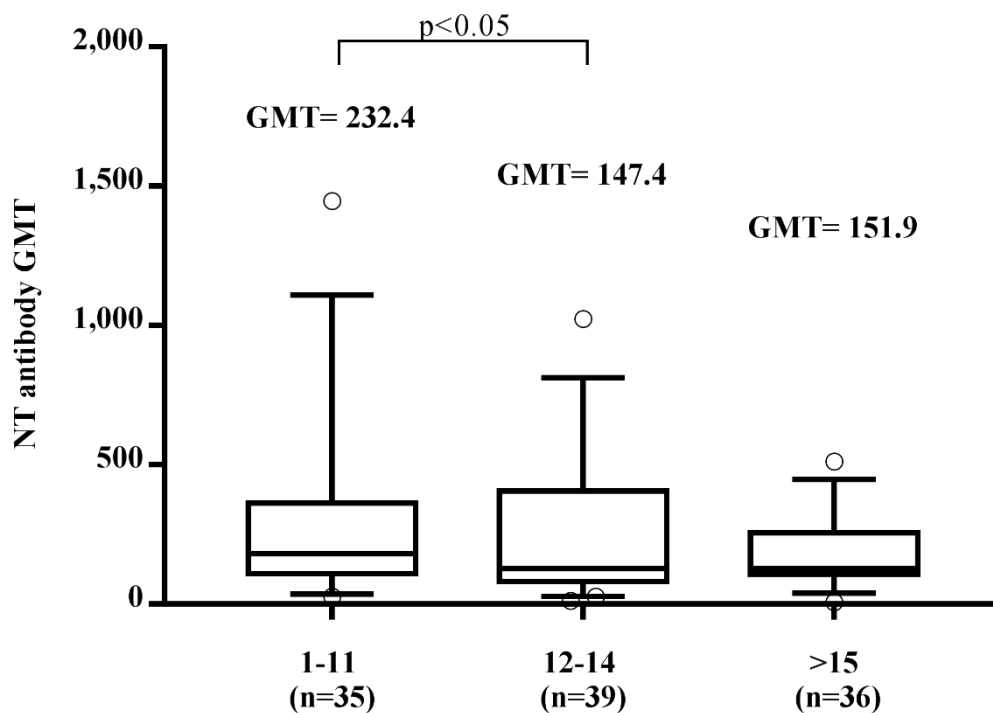
Figure 13: Time elapsed between the second dose of vaccine and the serological test (years). Effects of negative correlation based on the time elapsed between the second dose of measles vaccine and the last measles investigation test on neutralizing antibody response. The whiskers represent the values from the 5th to the 95th percentiles; the median, the 25th and 75th percentiles are depicted by the horizontal lines in the boxes. Individual data points are shown; outlier

values are shown as black circles. GMTs are shown above the population columns. *P*-value of the GMT between the first (1-11) and second (12–14) group is <0.05.

Subjects vaccinated with two doses were further studied on the basis of the time elapsed between the first and second dose of vaccine: 1–6 y (49 subjects), 7–10 y (34 subjects), and ≥11y (27 subjects). Spearman's rank correlation analysis showed a statistically significant ($p = 0.004$) inverse correlation (r = −0.270), between neutralization titers of subject sera and time elapsed between the two-dose vaccination. Indeed, the GMT comparison among the three groups evidenced a decrease of neutralizing GMTs, 215.5 in the 1–6 y, 165.6 in the 7–10 y, and 120.1 in the ≥11 y groups ($p <$ 0.05) (Figure 14), particularly relevant in subjects receiving the second dose of vaccine over 10–11 years since the first vaccination ($p < 0.05$). No significant differences related to the gender were found in this analysis either.
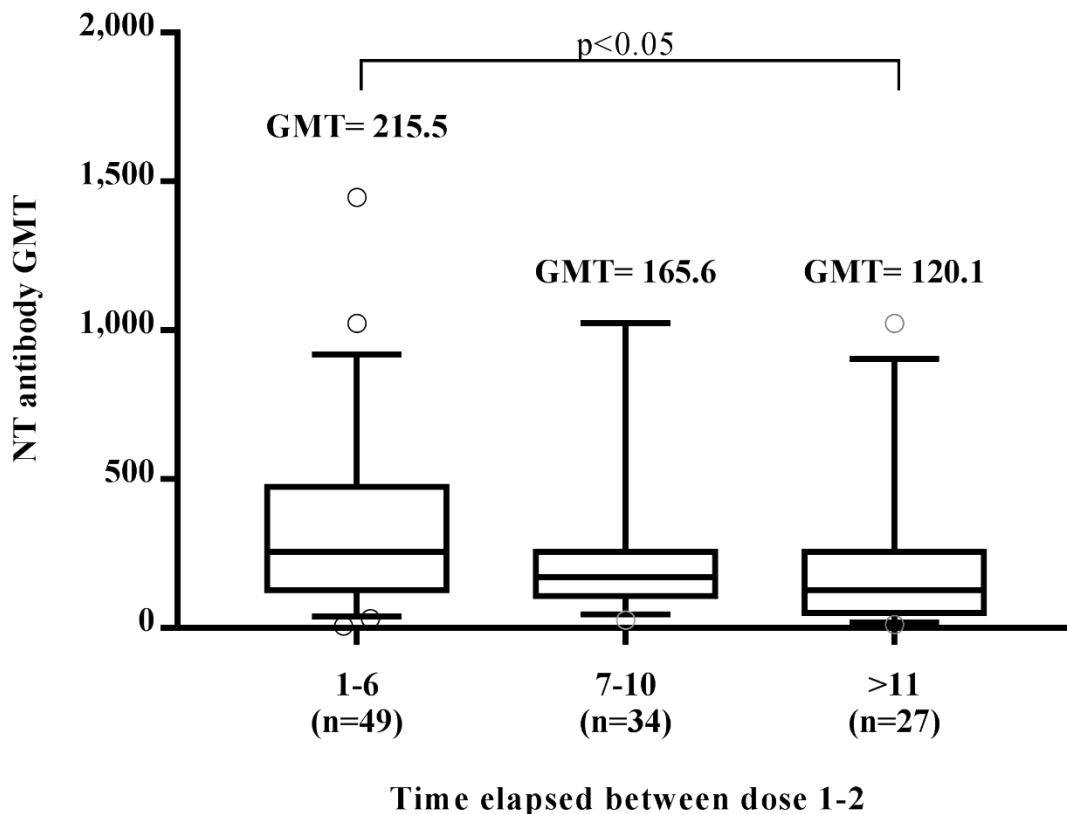

Figure 14: Effect of time elapsed between the two doses of measles vaccine on the neutralizing antibody response. The whiskers represent the values from the 5th to the 95th percentiles; the median, the 25th and 75th percentiles are depicted by the horizontal lines in the boxes. Individual data points are shown; outlier values are shown as black circles or squares. GMTs are shown above the population columns. The difference in GMTs between the first (1–6) and the third (≥11) group is statistically significant ($p \leq 0.05$).

5.1.6 Neutralizing Antibody GMT in Natural Infected Subjects

No differences in GMT were found in serum samples of naturally infected subjects during their childhood, either in those born before (GMT 571.7; mean age 54.8) or after (GMT 552.9; mean age 31.0) the introduction of measles vaccine (Figure 15). These data confirmed a more pronounced tendency of the protective immune response to wane in vaccinated people than in naturally infected people.
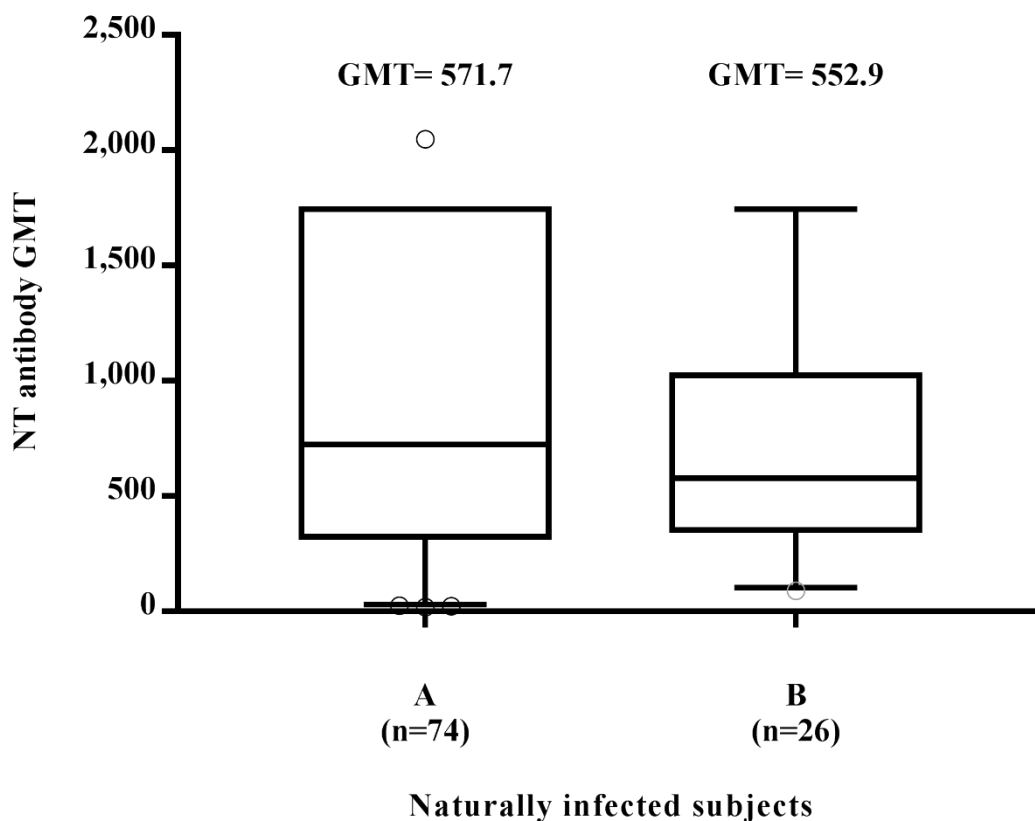

Figure 15: Differences in neutralizing antibody titers in naturally infected subjects born before (A) and after (B) 1977 (one year after the introduction of measles vaccine in Italy). The whiskers represent the values from the 5th to the 95th percentiles; the median, the 25th and 75th percentiles are depicted by the horizontal lines in the boxes. Individual data points are shown; outlier values are shown as black circles or squares. GMTs are shown above the population columns. Difference in GMT between the two groups is not significant (p>0.05).

Part II

Cell-mediated immune response to measles virus after PBMC *in vitro* stimulation.

5.2.1 Study group

Among the overall population, T cell immune response was evaluated in 24 randomly-selected subjects. Ten of them (five males, five females) were vaccinated with two doses of MMR vaccine (mean age 34.1 years, time elapsed from vaccination 11.9 years, time elapsed between the two-dose administration 5.9 years), ten (five males, five females) were naturally infected (mean age 46.5 years, all infected during childhood). Moreover, four negative controls represented by two (one male, one female) subjects who had neither been infected nor vaccinated (mean age 37,4 years) and two (one male, one female) who were non-responders, as they were seronegative after receiving a complete vaccination cycle (mean age 31.7 years), were included.

We assessed the variation of the percentage of specific T-cell ($CD3^+$) populations after *in vitro* stimulation of subject's PBMC with the UV-inactivated measles virus respect to the unstimulated control samples (as described in 'Mat. &Met'), in order to mimic a real-life event of re-exposure to the virus.

Then, we analyzed $CD4^+$ and $CD8^+$ Naïve ($CD45RA^+$ $CCR7^+$), Central Memory (CM; $CD45RA^-$ $CCR7^+$), Effector Memory (EM; $CD45RA^-$ $CCR7^-$) and Effector Memory cells re-expressing CD45RA (TEMRA $CD45RA^+$ $CCR7^-$). Moreover, $CD4^+$ Th17 ($CXCR3^-$ $CCR6^+$) together with Th1 ($CXCR3^+$ $CCR6^-$) and Th2 ($CXCR3^-$ $CCR6^-$) helper cells were also analyzed (Table 2).

Subset	Definition
T cells	CD3$^+$
CD4$^+$ T cells	CD3$^+$ CD4$^+$ CD8$^-$
<u>Naive cells</u>	CD3$^+$ CD4$^+$ CD8$^-$ CD45RA$^+$ CCR7$^+$
<u>Memory cells</u>	
T$_{CM}$	CD3$^+$ CD4$^+$ CD8$^-$ CD45RA$^-$ CCR7$^+$
T$_{EM}$	CD3$^+$ CD4$^+$ CD8$^-$ CD45RA$^-$ CCR7$^-$
T$_{EMRA}$	CD3$^+$ CD4$^+$ CD8$^-$ CD45RA$^+$ CCR7$^-$
<u>Helper cells</u>	
T$_H$1	CD3$^+$ CD4$^+$ CD8$^-$ CD45RA$^-$ CCR6$^-$ CXCR3$^+$
T$_H$2	CD3$^+$ CD4$^+$ CD8$^-$ CD45RA$^-$ CCR6$^-$ CXCR3$^-$
T$_H$17	CD3$^+$ CD4$^+$ CD8$^-$ CD45RA$^-$ CCR6$^+$ CXCR3$^-$
<u>Treg</u>	CD3$^+$ CD4$^+$ CD8$^-$ CD45RA$^-$ CD25^{high} CD127$^{-/low}$
CD8$^+$ T cells	CD3$^+$ CD4$^-$ CD8$^+$
<u>Naive cells</u>	CD3$^+$ CD4$^-$ CD8$^+$ CD45RA$^+$ CCR7$^+$
<u>Memory cells</u>	
T$_{CM}$	CD3$^+$ CD4$^-$ CD8$^+$ CD45RA$^-$ CCR7$^+$
T$_{EM}$	CD3$^+$ CD4$^-$ CD8$^+$ CD45RA$^-$ CCR7$^-$
T$_{EMRA}$	CD3$^+$CD4$^-$ CD8$^+$ CD45RA$^+$ CCR7$^-$

Table 2: Definition of peripheral blood T lymphocyte subsets.

5.2.2 Variations in T cell populations after stimulation

First of all, a significant difference in the overall percentage of CD3+ T cell population was observed after *in vitro* stimulation between the vaccinated and the naturally infected groups (p=0.01) (Figure 16). On one hand, all the naturally infected subjects showed an increased percentage of CD3$^+$ cells compared to the unstimulated controls (p=0.003). On the other hand, although an average increase (even if not significant) was observed among vaccinees, a more heterogeneous picture was observed respect to subjects with a past history of natural infection.

Regarding CD4 and CD8 T cell subsets, few or no differences were observed after stimulation in the group of vaccinated subjects. Among those who had natural infection, an average decrease in CD4$^+$ cell population was observed, while, a heterogeneous response was observed for the CD8$^+$ subset. However, in both cases no significant differences respect to the unstimulated controls were found, probably due to the low number of subjects examined for each group (Figure 16).
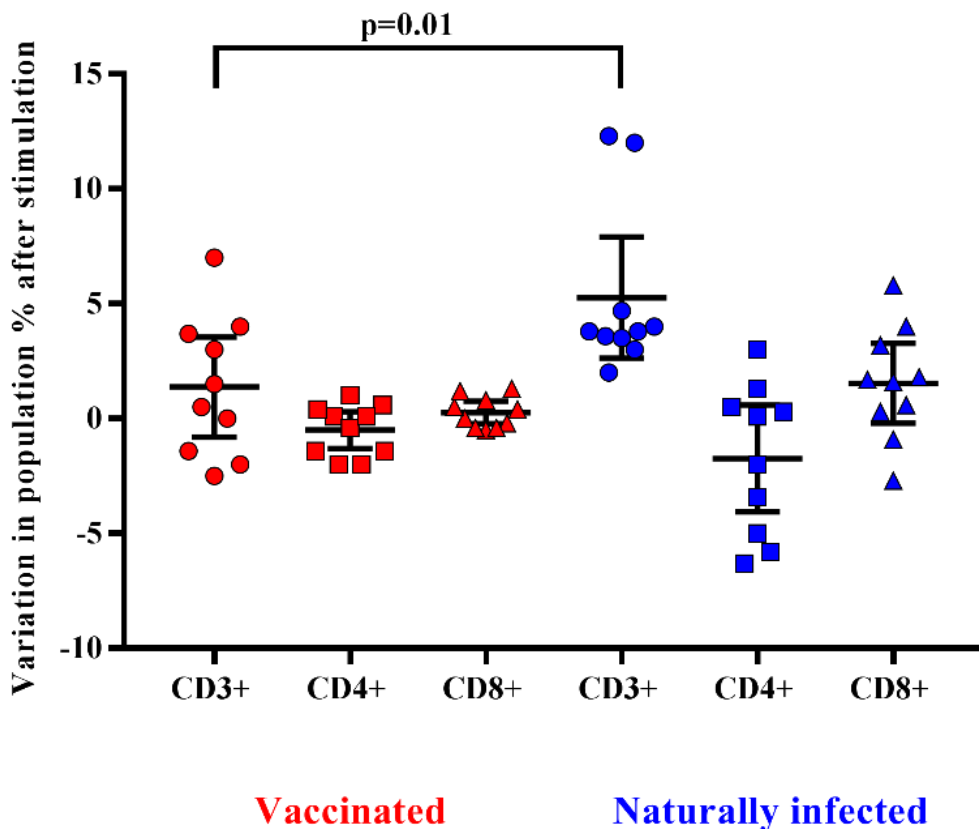

Figure 16: Representation of relative variations compared to the unstimulated controls in CD3$^+$ T cells and their CD4$^+$ and CD8$^+$ subpopulations after stimulation in vaccinated (red circle) and naturally infected (blue square) subjects. Results are reported in horizontal lines as mean values and upper and lower 95% CI. Individual data points are shown. *P*-value of the differences in CD3$^+$ among the two groups is reported. The mean percent changes in the three populations obtained following stimulation of negative controls were subtracted from each value obtained, so as to normalize the data. P value of the difference between the CD4$^+$ and CD8$^+$ populations was not reported as it was >0.05.

Thereafter, we analyzed CD4$^+$ and CD8$^+$ T cell subsets in order to investigate the potential role of T cell memory in a setting of virus re-exposure. Specifically, Naïve, Central Memory (CM), Effector Memory (EM) and Effector Memory cells re-expressing CD45RA (TEMRA). Moreover, CD4$^+$ T helper cell subsets (Th1, Th2, Th17) were also analyzed (Figure 17).

With regard to the Th17 population, no differences in the population percentages were observed in both groups after stimulation. On the other hand, differences in both Th1 and Th2 response induction were found in both groups, although not statistically significative (even in this case due to the low number of subjects analyzed for each group). In fact, all but one vaccinated subject showed an induction of the Th1 response and, as a consequence, a repression of the Th2 response after stimulation. This statement is confirmed by the strong inverse correlation between the Th1 and Th2 response after stimulation among all the subjects analyzed (r =-0.79). Among naturally infected subjects, Th1 and Th2 responses were extremely variable, with an average value close to zero. As we can clearly see in Figure 17, focusing on the single samples, half of naturally infected subjects showed an increase in Th1/Th2 population percentage after *in vitro* stimulation, while the other subjects had a completely opposite pattern of response, so as to make the average change almost zero. Considering that all naturally infected subjects contracted the disease during their childhood, so as to make the time elapsed since the infection negligible, this behavior was not seen to be correlated neither with the age not with the sex of the selected subjects, thus making an in-depth study necessary.
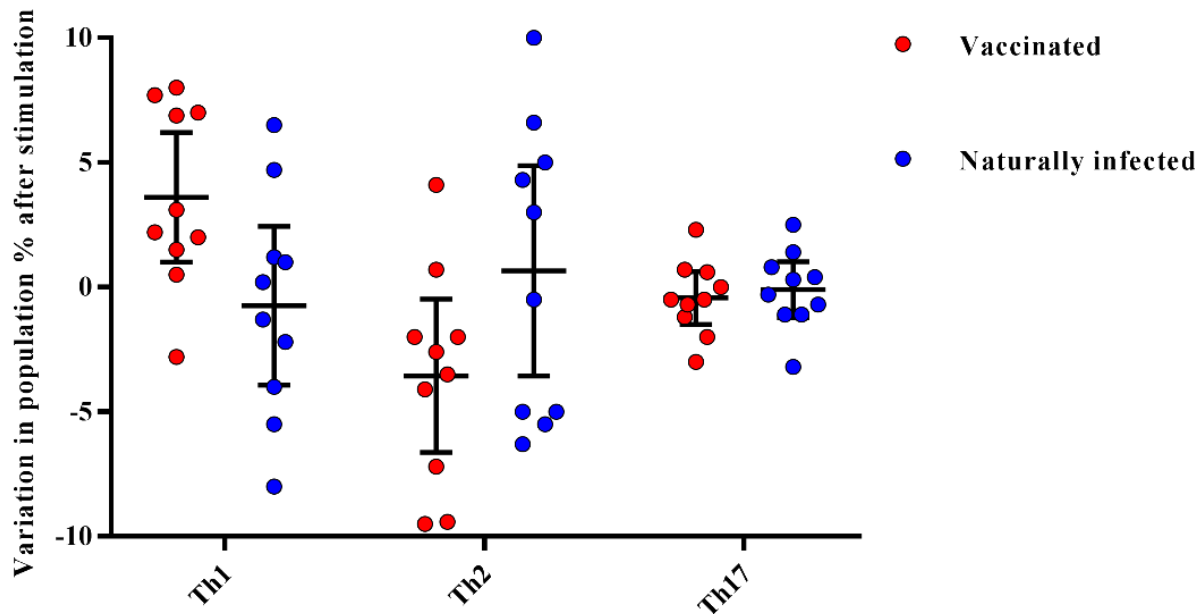
Figure 17: Representation of relative variations compared to the unstimulated controls in T helper cells (Th1, Th2 and Th17) after stimulation in vaccinated (red circles) and naturally infected (blue circles) subjects. Results are reported in horizontal lines as mean values and upper and lower 95% CI. Individual data points are shown. The mean percent changes in the three populations obtained following stimulation of negative controls were subtracted from each value obtained, so as to normalize the data. *P* values of the differences in Th1, Th2 and Th17 between the two groups was not reported as it was >0.05

No significant differences with the unstimulated controls after stimulation were observed for Naïve, Central Memory, Effector Memory and TEMRA, so the data were not reported.

Finally, Treg population was also analyzed but, since only few subjects (3 naturally infected and only one vaccinated) showed an activation of this population after stimulation, it was difficult to evaluate concrete differences within the two groups.

To confirm the reported results, transcriptome-level characterization (mRNA-Seq data) of responses to measles virus stimulation in vaccinated, naturally infected and subjects who had not responded to measles virus after receiving a complete schedule for the second time, was performed with the aim to identify define plausible regulators (genes/pathways) that could drive the differences observed by FACS analysis and to find immune signatures which could be related to failure of the response after vaccination among non-responders. However, at the present time, data analysis is still ongoing.

Chapter 6

Conclusions

Measles morbidity and mortality have been reduced since the implementation of enhanced vaccination strategies (Rota et al., 2016), even though many countries, especially in Europe, had experienced a major resurgence of measles due to the suboptimal vaccination coverage below 95% (Dixon et al., 2021; Genovese et al., 2019) during the 2017-2019 period .

For this reason, in 2019 measles vaccination among newborns became mandatory in many European countries, including France and Italy (Vaz et al., 2020; D'Ancona et al., 2019). These programs aimed at preventing widespread measles transmission, by inducing a specific humoral response in the community, which is a good indicator of protection from infection.

However, because of COVID-19 pandemic (World Health Organization), many countries had either fully or partially postponed measles-related vaccine campaigns to limit further spread of SARS-CoV-2 virus. Together, more than 117 million children in 37 countries, many of whom live in regions with ongoing measles outbreaks, could be impacted by the suspension of scheduled immunization activities. (UNICEF, 2020; World Health Organization, 2021; World Bank, 2021; Rana et al., 2021). Therefore, although having a highly effective vaccine and the lack of an animal reservoir, measles disease continues to be difficult to eradicate.

For the above reasons, monitoring measles immunization levels among the population will be critical to protect susceptible individuals from possible resurgence of outbreaks. Finally, it will be also critical to monitor vaccinated individuals who have become seronegative, to see their degree of susceptibility to infection, as well as the few individuals for whom vaccination has failed.

In this study, we evaluated the immunization status and the seroprevalence of measles antibodies among a healthy adult population. Afterwards, we investigated the persistence of anti-measles IgG among vaccinated and naturally infected people. Collected data showed that, out of the 1092 enrolled subjects, 682 (62.45%) had received two doses of measles vaccine (monovalent and/or MMR) and among these, only 24 subjects received as first dose the monovalent vaccine, since this was replaced in the early 1990s by the combined measles–mumps–rubella (MMR).We noted that 23% of the subjects who received two doses of measles vaccine did not show IgG response, similarly to those receiving only one dose of vaccine (25%) (Table 2). This percentage appeared higher than that reported by other authors (Kennedy et al., 2019; Seagle et al., 2018; Kim et al., 2021; Friedrich et al., 2021) thus, it is advisable to monitor the immune status of vaccinees 10–15 years after vaccination, in order to evaluate the immune protection against measles and, eventually, implement a possible prophylactic measure. On the other hand, a long-term high rate of seropositivity persist after natural infection; indeed, subjects enrolled in this study who reported measles infection history were all seropositive. Therefore, we evaluated the presence of the neutralizing antibody response to the virus in naturally infected subjects and in those vaccinated

with two doses.   The geometric mean titer to measles was high (GMT 552.9) in naturally infected people, versus a GMT of 172.1 in vaccinees of the same age cohort, indicating that the antibody titer decline was more evident in the vaccinated people, probably because the starting antibody titer after vaccination was lower than that induced after natural infection.

Indeed, in this study, the neutralizing antibody titer inversely correlated with the time elapsed between the second dose of vaccine and the blood drawn. This trend was confirmed by a gradual decrease of GMT titers (Figure 13), concomitant with the increase of years spent since vaccination, particularly over 12–14 years (GMT 232.4 vs. 147.4). Finally, a new interesting factor considered in this analysis was that most of the subjects had been vaccinated at different lifetimes with two doses, either because of the change in the national vaccination program in Italy in 2003 or because, since the administration was recommended and not mandatory, in many cases the timing of immunization was not respected.

Therefore, this parameter was analyzed to understand whether the interval of time elapsed between the two vaccine administrations could influence the immune response. It is known that schedules which have longer intervals between vaccine doses usually lead to higher immune responses (Rumke et al., 2011; Middleman et al., 2001; Sabidò et al., 2007). On the contrary, our results, obtained by the neutralization assay on serum samples of subjects vaccinated with two doses (Figure 14), showed a different picture. An inverse correlation between neutralizing titer and time elapsed between the two vaccinations was evidenced with a significant decline of the GMT when the interval was ≥11 years in comparison to that observed within the 1−6 years interval (p = 0.02). The result could be very useful for the formulation of the vaccination schedule, because this finding is not valid for all vaccinations and represents a further variable factor to be considered when new vaccinations are requested. We did not find the gender factor as a variable for the immune response to measles vaccination, since no significant difference was recorded.

Subsequently, considering the differences that we observed in the humoral immune response between vaccinated and naturally infected subjects, our aim was to evaluate differences also in the cellular immune response, especially within T cells.

In fact, considering the decline of antibody titers in vaccinated subjects, even in those who received two doses, and considering the high number of vaccinated subjects who turned seronegative years after vaccination, our interest was to see if these differences could be correlated to a different cell-mediated response in case of re-exposure to the viral antigen.

To this aim, peripheral blood mononuclear cells (PBMC) drawn from the four categories of subjects were analyzed via flow cytometry before and after *in vitro* stimulation with UV-inactivated measles virus.

Data showed a significant increase in the percentage of CD3$^+$ T cells among naturally infected subjects in comparison with the correspondent unstimulated samples (p=0.003). This increase was significant also respect to the vaccinated cohort (p=0.01), thus meaning a stronger T cell induction after antigen exposure in naturally infected subjects rather than in vaccinees. Subsequently, the same differences were evaluated among the CD4$^+$ and CD8$^+$ T cell subsets. While the average response among vaccinated subjects was almost unvaried, naturally infected subjects showed a heterogeneous response of both CD4$^+$ (showing an average decrease, although non significative) and CD8$^+$ cells, confirming that the induction of T cells among naturally infected subjects brought to a differentiation of T cells subsets, while an unvaried response was shown among vaccinated subjects.

Finally, CD4$^+$ helper population (Th1, Th2, Th17) were analyzed. While an unvaried Th17 response was observed in both groups, differences were observed regarding the Th1/Th2 responses. In fact, while in all-but one vaccinated subject a preferential induction of the Th1 response was observed (and, as a consequence, a decrease of the Th2 response), a highly heterogeneous response was observed among naturally infected subjects. For this reason, further experiments will be needed to confirm this behavior, and ultimately to identify possible factors related to that. Since supernatants were stocked at the time of PBMC collection, it might also be of great support to measure specific cytokines related to the Th1 (IL-1β, IL-2, IL-12, TNF-α, and IFN-γ) or Th2 (IL-4, IL-5 and IL-10) response.

We also tried to investigate the role of CD4$^+$ and CD8$^+$ naïve, memory and effector subsets. However, no differences were observed after stimulation in both groups.

For this reason, and in order to confirm the previous findings regarding the T cell subsets, transcriptome-level characterization (mRNA-Seq data) of responses to measles virus stimulation in antibody responders (either vaccinated or naturally infected) and those who had not responded to measles virus after receiving a complete schedule for the second time, was performed with the aim to identify plausible regulators (genes/pathways) that drive the observed differences among vaccinated and naturally infected subjects. Moreover, the study is still ongoing to find the immune signatures which could drive the 'non-response' to the vaccine among the four non-responders. At the moment, the complex transcriptome data are under analysis and very preliminary (data not shown).

Such study might be very helpful to develop a panel of biomarkers to easily monitor, besides the antibody response, the immune response to measles vaccine, even several years away from it, with the aim to identify and protect the subjects, who eventually become seronegative along the time, with a booster composed of immunogenic and protective viral proteins.

Chapter 7

Bibliography

Anderson RM, May RM. Directly transmitted infections diseases: control by vaccination. *Science*. 1982;215(4536):1053-1060. doi:10.1126/science.7063839

Anichini G, Gandolfo C, Fabrizi S, et al. Seroprevalence to Measles Virus after Vaccination or Natural Infection in an Adult Population, in Italy. *Vaccines (Basel)*. 2020;8(1):66. Published 2020 Feb 3. doi:10.3390/vaccines8010066

Avota E, Gassert E, Schneider-Schaulies S. Measles virus-induced immunosuppression: from effectors to mechanisms. *Med Microbiol Immunol*. 2010;199(3):227-237. doi:10.1007/s00430-010-0152-3

Banchereau J, Steinman RM. Dendritic cells and the control of immunity. *Nature*. 1998;392(6673):245-252. doi:10.1038/32588

Bankamp B, Liu C, Rivailler P, et al. Wild-type measles viruses with non-standard genome lengths. *PLoS One*. 2014;9(4):e95470. Published 2014 Apr 18. doi:10.1371/journal.pone.0095470

Barrett T. Morbillivirus infections, with special emphasis on morbilliviruses of carnivores. *Vet Microbiol*. 1999;69(1-2):3-13. doi:10.1016/s0378-1135(99)00080-2

Baxby D. The diagnosis of the invasion of measles from a study of the exanthema as it appears on the buccal mucous membraneBy Henry Koplik, M.D. Reproduced from Arch. Paed. 13, 918-922 (1886). *Rev Med Virol*. 1997;7(2):71-74. doi:10.1002/(sici)1099-1654(199707)7:2<71:aid-rmv185>3.0.co;2-s

Beaty SM, Lee B. Constraints on the Genetic and Antigenic Variability of Measles Virus. *Viruses*. 2016;8(4):109. Published 2016 Apr 21. doi:10.3390/v8040109 doi:10.1128/JVI.02033-12

Beckford AP, Kaschula RO, Stephen C. Factors associated with fatal cases of measles. A retrospective autopsy study. *S Afr Med J*. 1985;68(12):858-863.

Behrens L, Cherry JD, Heininger U; Swiss Measles Immune Amnesia Study Group. The Susceptibility to Other Infectious Diseases Following Measles During a Three Year Observation Period in Switzerland. *Pediatr Infect Dis J*. 2020;39(6):478-482. doi:10.1097/INF.0000000000002599

Bellini WJ, Helfand RF. The challenges and strategies for laboratory diagnosis of measles in an international setting. *J Infect Dis*. 2003;187 Suppl 1:S283-S290. doi:10.1086/368040

Bellini WJ, Rota PA. Biological feasibility of measles eradication. *Virus Res*. 2011;162(1-2):72-79. doi:10.1016/j.virusres.2011.09.023

Bester JC. Measles and Measles Vaccination: A Review. *JAMA Pediatr*. 2016;170(12):1209-1215. doi:10.1001/jamapediatrics.2016.1787

Bieback K, Lien E, Klagge IM, et al. Hemagglutinin protein of wild-type measles virus activates toll-like receptor 2 signaling. *J Virol*. 2002;76(17):8729-8736. doi:10.1128/jvi.76.17.8729-8736.2002

Black FL. Measles endemicity in insular populations: critical community size and its evolutionary implication. *J Theor Biol*. 1966;11(2):207-211. doi:10.1016/0022-5193(66)90161-5

Bloch AB, Orenstein WA, Ewing WM, et al. Measles outbreak in a pediatric practice: airborne transmission in an office setting. *Pediatrics*. 1985;75(4):676-683.

Bonanni P, Ferro A, Guerra R, et al. Vaccine coverage in Italy and assessment of the 2012-2014 National Immunization Prevention Plan. *Epidemiol Prev*. 2015;39(4 Suppl 1):146-158.

Brodsky AL. Atypical measles. Severe illness in recipients of killed measles virus vaccine upon exposure to natural infection. *JAMA*. 1972;222(11):1415-1416. doi:10.1001/jama.222.11.1415

Buchanan R, Bonthius DJ. Measles virus and associated central nervous system sequelae. *Semin Pediatr Neurol*. 2012;19(3):107-114. doi:10.1016/j.spen.2012.02.003

Caignard G, Bouraï M, Jacob Y; Infection-MAPping project I-MAP, Tangy F, Vidalain PO. Inhibition of IFN-alpha/beta signaling by two discrete peptides within measles virus V protein that specifically bind STAT1 and STAT2. *Virology*. 2009;383(1):112-120. doi:10.1016/j.virol.2008.10.014

Calain P, Roux L. Functional characterisation of the genomic and antigenomic promoters of Sendai virus. *Virology*. 1995;212(1):163-173. doi:10.1006/viro.1995.1464.

Cannons JL, Tangye SG, Schwartzberg PL. SLAM family receptors and SAP adaptors in immunity. *Annu Rev Immunol*. 2011;29:665-705. doi:10.1146/annurev-immunol-030409-101302

Carbone, K. M. & Rubin, S. A. Mumps virus. In *Fields Virology 5th edition*, 2007;1527–1550. Edited by D. M. Knipe & P. M. Howley. Philadelphia, PA: Lippincott Williams and Wilkins.

Chen RT, Goldbaum GM, Wassilak SG, Markowitz LE, Orenstein WA. An explosive point-source measles outbreak in a highly vaccinated population. Modes of transmission and risk factors for disease. *Am J Epidemiol*. 1989;129(1):173-182. doi:10.1093/oxfordjournals.aje.a115106

Chen RT, Markowitz LE, Albrecht P, et al. Measles antibody: reevaluation of protective titers. *J Infect Dis*. 1990;162(5):1036-1042. doi:10.1093/infdis/162.5.1036

Childs KS, Andrejeva J, Randall RE, Goodbourn S. Mechanism of mda-5 Inhibition by paramyxovirus V proteins. *J Virol*. 2009;83(3):1465-1473. doi:10.1128/JVI.01768-08

Davis ME, Wang MK, Rennick LJ, et al. Antagonism of the phosphatase PP1 by the measles virus V protein is required for innate immune escape of MDA5. *Cell Host Microbe*. 2014;16(1):19-30. doi:10.1016/j.chom.2014.06.007

de Swart RL, Duprex WP, Osterhaus AD. Rinderpest eradication: lessons for measles eradication?. *Curr Opin Virol*. 2012;2(3):330-334. doi:10.1016/j.coviro.2012.02.010

de Swart RL, Ludlow M, de Witte L, et al. Predominant infection of CD150+ lymphocytes and dendritic cells during measles virus infection of macaques [published correction appears in PLoS Pathog. 2008 Dec;4(12). doi.org//10.1371/annotation/df340d50-1f94-4d8b-a252-1a82a7fa5cc7]. *PLoS Pathog*. 2007;3(11):e178. doi:10.1371/journal.ppat.0030178

de Vries RD, de Swart RL. Measles immune suppression: functional impairment or numbers game?. *PLoS Pathog*. 2014;10(12):e1004482. Published 2014 Dec 18. doi:10.1371/journal.ppat.1004482

de Vries RD, Lemon K, Ludlow M, et al. In vivo tropism of attenuated and pathogenic measles virus expressing green fluorescent protein in macaques. *J Virol*. 2010;84(9):4714-4724. doi:10.1128/JVI.02633-09

de Vries RD, McQuaid S, van Amerongen G, et al. Measles immune suppression: lessons from the macaque model. *PLoS Pathog*. 2012;8(8):e1002885. doi:10.1371/journal.ppat.1002885

de Vries RD, Mesman AW, Geijtenbeek TB, Duprex WP, de Swart RL. The pathogenesis of measles. *Curr Opin Virol*. 2012;2(3):248-255. doi:10.1016/j.coviro.2012.03.005

de Vries RD, Yüksel S, Osterhaus AD, de Swart RL. Specific CD8(+) T-lymphocytes control dissemination of measles virus. *Eur J Immunol*. 2010;40(2):388-395. doi:10.1002/eji.200939949

de Witte L, Abt M, Schneider-Schaulies S, van Kooyk Y, Geijtenbeek TB. Measles virus targets DC-SIGN to enhance dendritic cell infection. *J Virol*. 2006;80(7):3477-3486. doi:10.1128/JVI.80.7.3477-3486.2006

de Witte L, de Vries RD, van der Vlist M, et al. DC-SIGN and CD150 have distinct roles in transmission of measles virus from dendritic cells to T-lymphocytes. *PLoS Pathog*. 2008;4(4):e1000049. Published 2008 Apr 18. doi:10.1371/journal.ppat.1000049

Devaux P, Hodge G, McChesney MB, Cattaneo R. Attenuation of V- or C-defective measles viruses: infection control by the inflammatory and interferon responses of rhesus monkeys. *J Virol*. 2008;82(11):5359-5367. doi:10.1128/JVI.00169-08

Dixon MG, Ferrari M, Antoni S, et al. Progress Toward Regional Measles Elimination – Worldwide, 2000-2020. MMWR Morb Mortal Wkly Rep 2021;70:1563-1569. doi: 10.15585/mmwr.mm7045alexternal icon

Dörig RE, Marcil A, Chopra A, Richardson CD. The human CD46 molecule is a receptor for measles virus (Edmonston strain). *Cell*. 1993;75(2):295-305. doi:10.1016/0092-8674(93)80071-l

D'Souza RM, D'Souza R. Vitamin A for the treatment of children with measles--a systematic review. *J Trop Pediatr*. 2002;48(6):323-327. doi:10.1093/tropej/48.6.323

Duke T, Mgone CS. Measles: not just another viral exanthem. *Lancet*. 2003;361(9359):763-773. doi:10.1016/S0140-6736(03)12661-X

Eaton, B. T., Mackenzie, J. S., **Wang, L.** Henipaviruses. In *Fields Virology, 5th edition*, 2007;1587–1600. Edited by D. M. Knipe & P. M. Howley. Philadelphia, PA: Lippincott Williams and Wilkins.

Esolen LM, Takahashi K, Johnson RT, et al. Brain endothelial cell infection in children with acute fatal measles. *J Clin Invest*. 1995;96(5):2478-2481. doi:10.1172/JCI118306

Fiebelkorn AP, Coleman LA, Belongia EA, et al. Measles Virus Neutralizing Antibody Response, Cell-Mediated Immunity, and Immunoglobulin G Antibody Avidity Before and After Receipt of a Third Dose of Measles, Mumps, and Rubella Vaccine in Young Adults. *J Infect Dis*. 2016;213(7):1115-1123. doi:10.1093/infdis/jiv555

Finsterbusch T, Wolbert A, Deitemeier I, et al. Measles viruses of genotype H1 evade recognition by vaccine-induced neutralizing antibodies targeting the linear haemagglutinin noose epitope. *J Gen Virol*. 2009;90(Pt 11):2739-2745. doi:10.1099/vir.0.013524-0

Fiorentino DF, Bond MW, Mosmann TR. Two types of mouse T helper cell. IV. Th2 clones secrete a factor that inhibits cytokine production by Th1 clones. *J Exp Med*. 1989;170(6):2081-2095. doi:10.1084/jem.170.6.2081

Fiorentino DF, Zlotnik A, Vieira P, et al. IL-10 acts on the antigen-presenting cell to inhibit cytokine production by Th1 cells. *J Immunol*. 1991;146(10):3444-3451.

Forni AL, Schluger NW, Roberts RB. Severe measles pneumonitis in adults: evaluation of clinical characteristics and therapy with intravenous ribavirin. *Clin Infect Dis*. 1994;19(3):454-462. doi:10.1093/clinids/19.3.454

Frenzke M, Sawatsky B, Wong XX, et al. Nectin-4-dependent measles virus spread to the cynomolgus monkey tracheal epithelium: role of infected immune cells infiltrating the lamina propria. *J Virol*. 2013;87(5):2526-2534. doi:10.1128/JVI.03037-12

Friedrich N, Poethko-Müller C, Kuhnert R, et al. Seroprevalence of Measles-, Mumps-, and Rubella-specific antibodies in the German adult population - cross-sectional analysis of the German Health Interview and Examination Survey for Adults (DEGS1). *Lancet Reg Health Eur*. 2021;7:100128. Published 2021 Jun 5. doi:10.1016/j.lanepe.2021.100128

Fulginiti VA, Eller JJ, Downie AW, Kempe CH. Altered reactivity to measles virus. Atypical measles in children previously immunized with inactivated measles virus vaccines. *JAMA*. 1967;202(12):1075-1080. doi:10.1001/jama.202.12.1075

Gans HA, Arvin AM, Galinus J, Logan L, DeHovitz R, Maldonado Y. Deficiency of the humoral immune response to measles vaccine in infants immunized at age 6 months. *JAMA*. 1998;280(6):527-532. doi:10.1001/jama.280.6.527

Gastañaduy PA, Goodson JL, Panagiotakopoulos L, Rota PA, Orenstein WA, Patel M. Measles in the 21st Century: Progress Toward Achieving and Sustaining Elimination. *J Infect Dis*. 2021;224(Supplement_4):S420-S428. doi:10.1093/infdis/jiaa793

Genovese C, Picerno IAM, Trimarchi G, et al. Vaccination coverage in healthcare workers: a multicenter cross-sectional study in Italy. *J Prev Med Hyg*. 2019;60(1):E12-E17. Published 2019 Mar 29. doi:10.15167/2421-4248/jpmh2019.60.1.1097

Graves M, Griffin DE, Johnson RT, et al. Development of antibody to measles virus polypeptides during complicated and uncomplicated measles virus infections. *J Virol*. 1984;49(2):409-412. doi:10.1128/JVI.49.2.409-412.1984

Griffin DE, Ward BJ, Jauregui E, Johnson RT, Vaisberg A. Immune activation during measles: interferon-gamma and neopterin in plasma and cerebrospinal fluid in complicated and uncomplicated disease. *J Infect Dis*. 1990;161(3):449-453. doi:10.1093/infdis/161.3.449

Griffin DE, Ward BJ, Jauregui E, Johnson RT, Vaisberg A. Immune activation in measles. *N Engl J Med*. 1989;320(25):1667-1672. doi:10.1056/NEJM198906223202506

Griffin DE, Ward BJ, Juaregui E, Johnson RT, Vaisberg A. Immune activation during measles: beta 2-microglobulin in plasma and cerebrospinal fluid in complicated and uncomplicated disease. *J Infect Dis*. 1992;166(5):1170-1173. doi:10.1093/infdis/166.5.1170

Griffin DE, Ward BJ. Differential CD4 T cell activation in measles. *J Infect Dis*. 1993;168(2):275-281. doi:10.1093/infdis/168.2.275

Griffin DE. Measles immunity and immunosuppression. *Curr Opin Virol*. 2021;46:9-14. doi:10.1016/j.coviro.2020.08.002

Griffin, D. E. (2007). Measles virus. In *Fields Virology, 5th edition*, pp. 1551-1585. Edited by D. M. Knipe & P. M. Howley. Philadelphia, PA: Lippincott Williams and Wilkins.

Griffin, D. E. in *Fields Virology* (eds Fields, B. N., Howley, P. M., Cohen, J. I. & Knipe, D. M.) 1042–1069 (Wolters Kluver/Lippincott Williams & Wilkins, 2013).

Hahm B, Cho JH, Oldstone MB. Measles virus-dendritic cell interaction via SLAM inhibits innate immunity: selective signaling through TLR4 but not other TLRs mediates suppression of IL-12 synthesis. *Virology*. 2007;358(2):251-257. doi:10.1016/j.virol.2006.10.004

https://www.euro.who.int/en/media-centre/sections/press-releases/2018/europe-observes-a-4-fold-increase-in-measles-cases-in-2017-compared-to-previous-year

Ichinohe T, Yamazaki T, Koshiba T, Yanagi Y. Mitochondrial protein mitofusin 2 is required for NLRP3 inflammasome activation after RNA virus infection. *Proc Natl Acad Sci U S A*. 2013;110(44):17963-17968. doi:10.1073/pnas.1312571110

Ikegame S, Takeda M, Ohno S, Nakatsu Y, Nakanishi Y, Yanagi Y. Both RIG-I and MDA5 RNA helicases contribute to the induction of alpha/beta interferon in measles virus-infected human cells. J Virol. 2010;84(1):372-379.

Istituto Superiore di Sanità, Morbillo & Rosolia News, Rapporto n°63 – Gennaio 2021

Italian Ministry of Health. Decree Law 7 June 2017, n. 73, Urgent Provisions on Vaccination Prevention, as Amended by the Conversion Law. http://www.trovanorme.salute.gov.it/norme/dettaglioAtto?id=59548. 7 June 2017.

Jaye A, Herberts CA, Jallow S, et al. Vigorous but short-term gamma interferon T-cell responses against a dominant HLA-A*02-restricted measles virus epitope in patients with measles. *J Virol*. 2003;77(8):5014-5016. doi:10.1128/jvi.77.8.5014-5016.2003

Keeling MJ, Grenfell BT. Disease extinction and community size: modeling the persistence of measles. *Science*. 1997;275(5296):65-67. doi:10.1126/science.275.5296.65

Kim CJ, Bae JY, Jun KI, et al. Risk of Absence of Measles Antibody in Healthcare Personnel and Efficacy of Booster Vaccination. *Vaccines (Basel)*. 2021;9(5):501. Published 2021 May 12. doi:10.3390/vaccines9050501

Komune N, Ichinohe T, Ito M, Yanagi Y. Measles virus V protein inhibits NLRP3 inflammasome-mediated interleukin-1β secretion. *J Virol*. 2011;85(24):13019-13026. doi:10.1128/JVI.05942-11

Kühne M, Brown DW, Jin L. Genetic variability of measles virus in acute and persistent infections. *Infect Genet Evol*. 2006;6(4):269-276. doi:10.1016/j.meegid.2005.08.003

Kurath G, Batts WN, Ahne W, Winton JR. Complete genome sequence of Fer-de-Lance virus reveals a novel gene in reptilian paramyxoviruses. *J Virol*. 2004;78(4):2045-2056. doi:10.1128/jvi.78.4.2045-2056.2004

Lamb, R. A. & Parks, G. D. (2007). *Paramyxoviridae*: the viruses and their replication. In *Fields Virology, 5th edition*, pp. 1449-1496. Edited by D. M. Knipe & P. M. Howley. Philadelphia, PA: Lippincott Williams and Wilkins.

Law Decree 22 December 2017, No. 219, published in the Official Gazette No. 12 of 16 January 2018. Available online: https://www.gazzettaufficiale.it/eli/gu/2018/01/16/12/sg/pdf Accessed August 2, 2020.

LeBaron CW, Beeler J, Sullivan BJ, et al. Persistence of measles antibodies after 2 doses of measles vaccine in a postelimination environment. *Arch Pediatr Adolesc Med*. 2007;161(3):294-301. doi:10.1001/archpedi.161.3.294

Lefebvre N, Camuset G, Bui E, Christmann D, Hansmann Y. Koplik spots: a clinical sign with epidemiological implications for measles control. *Dermatology*. 2010;220(3):280-281. doi:10.1159/000277122

Lemon K, de Vries RD, Mesman AW, et al. Early target cells of measles virus after aerosol infection of non-human primates. *PLoS Pathog*. 2011;7(1):e1001263. Published 2011 Jan 27. doi:10.1371/journal.ppat.1001263

Leonard VH, Hodge G, Reyes-Del Valle J, McChesney MB, Cattaneo R. Measles virus selectively blind to signaling lymphocytic activation molecule (SLAM; CD150) is attenuated and induces strong adaptive immune responses in rhesus monkeys. *J Virol*. 2010;84(7):3413-3420. doi:10.1128/JVI.02304-09

Leonard VH, Sinn PL, Hodge G, et al. Measles virus blind to its epithelial cell receptor remains virulent in rhesus monkeys but cannot cross the airway epithelium and is not shed. *J Clin Invest*. 2008;118(7):2448-2458. doi:10.1172/JCI35454

Li Z, Okonski KM, Samuel CE. Adenosine deaminase acting on RNA 1 (ADAR1) suppresses the induction of interferon by measles virus. *J Virol*. 2012;86(7):3787-3794. doi:10.1128/JVI.06307-11

Lin WH, Kouyos RD, Adams RJ, Grenfell BT, Griffin DE. Prolonged persistence of measles virus RNA is characteristic of primary infection dynamics. *Proc Natl Acad Sci U S A*. 2012;109(37):14989-14994. doi:10.1073/pnas.1211138109

Lin WH, Pan CH, Adams RJ, Laube BL, Griffin DE. Vaccine-induced measles virus-specific T cells do not prevent infection or disease but facilitate subsequent clearance of viral RNA. *mBio*. 2014;5(2):e01047. Published 2014 Apr 15. doi:10.1128/mBio.01047-14

Ludlow M, Lemon K, de Vries RD, et al. Measles virus infection of epithelial cells in the macaque upper respiratory tract is mediated by subepithelial immune cells. *J Virol*. 2013;87(7):4033-4042. doi:10.1128/JVI.03258-12

Ludlow M, Rennick LJ, Sarlang S, et al. Wild-type measles virus infection of primary epithelial cells occurs via the basolateral surface without syncytium formation or release of infectious virus. *J Gen Virol*. 2010;91(Pt 4):971-979. doi:10.1099/vir.0.016428-0

Lyakh L, Trinchieri G, Provezza L, Carra G, Gerosa F. Regulation of interleukin-12/interleukin-23 production and the T-helper 17 response in humans. *Immunol Rev*. 2008;226:112-131. doi:10.1111/j.1600-065X.2008.00700.x

Macartney KK, Gidding HF, Trinh L, et al. Febrile seizures following measles and varicella vaccines in young children in Australia. *Vaccine*. 2015;33(11):1412-1417. doi:10.1016/j.vaccine.2014.10.071

McChesney MB, Miller CJ, Rota PA, et al. Experimental measles. I. Pathogenesis in the normal and the immunized host. *Virology*. 1997;233(1):74-84. doi:10.1006/viro.1997.8576

McLean HQ, Fiebelkorn AP, Temte JL, Wallace GS; Centers for Disease Control and Prevention. Prevention of measles, rubella, congenital rubella syndrome, and mumps, 2013: summary recommendations of the Advisory

Committee on Immunization Practices (ACIP) [published correction appears in MMWR Recomm Rep. 2015 Mar 13;64(9):259]. *MMWR Recomm Rep*. 2013;62(RR-04):1-34.

Measles vaccines: WHO position paper. *Wkly Epidemiol Rec*. 2009;84(35):349-360.

Mellman I, Steinman RM. Dendritic cells: specialized and regulated antigen processing machines. *Cell*. 2001;106(3):255-258. doi:10.1016/s0092-8674(01)00449-4

Mesman AW, de Vries RD, McQuaid S, Duprex WP, de Swart RL, Geijtenbeek TB. A prominent role for DC-SIGN+ dendritic cells in initiation and dissemination of measles virus infection in non-human primates. *PLoS One*. 2012;7(12):e49573. doi:10.1371/journal.pone.0049573

Mesman AW, Zijlstra-Willems EM, Kaptein TM, et al. Measles virus suppresses RIG-I-like receptor activation in dendritic cells via DC-SIGN-mediated inhibition of PP1 phosphatases. *Cell Host Microbe*. 2014;16(1):31-42. doi:10.1016/j.chom.2014.06.008

Middleman AB, Kozinetz CA, Robertson LM, DuRant RH, Emans SJ. The effect of late doses on the achievement of seroprotection and antibody titer levels with hepatitis b immunization among adolescents. *Pediatrics*. 2001;107(5):1065-1069. doi:10.1542/peds.107.5.1065

Mills KH. Regulatory T cells: friend or foe in immunity to infection?. *Nat Rev Immunol*. 2004;4(11):841-855. doi:10.1038/nri1485

Mina MJ, Metcalf CJ, de Swart RL, Osterhaus AD, Grenfell BT. Long-term measles-induced immunomodulation increases overall childhood infectious disease mortality. *Science*. 2015;348(6235):694-699. doi:10.1126/science.aaa3662

Monafo WJ, Haslam DB, Roberts RL, Zaki SR, Bellini WJ, Coffin CM. Disseminated measles infection after vaccination in a child with a congenital immunodeficiency. *J Pediatr*. 1994;124(2):273-276. doi:10.1016/s0022-3476(94)70318-3

Moss WJ, Griffin DE. Measles. *Lancet*. 2012;379(9811):153-164. doi:10.1016/S0140-6736(10)62352-5

Moss WJ, Ota MO, Griffin DE. Measles: immune suppression and immune responses. *Int J Biochem Cell Biol*. 2004;36(8):1380-1385. doi:10.1016/j.biocel.2004.01.019

Moss WJ, Ryon JJ, Monze M, Griffin DE. Differential regulation of interleukin (IL)-4, IL-5, and IL-10 during measles in Zambian children. *J Infect Dis*. 2002;186(7):879-887. doi:10.1086/344230

Mühlebach MD, Mateo M, Sinn PL, et al. Adherens junction protein nectin-4 is the epithelial receptor for measles virus. *Nature*. 2011;480(7378):530-533. Published 2011 Nov 2. doi:10.1038/nature10639

Naim HY. Measles virus. *Hum Vaccin Immunother*. 2015;11(1):21-26. doi:10.4161/hv.34298

Nair N, Moss WJ, Scott S, et al. HIV-1 infection in Zambian children impairs the development and avidity maturation of measles virus-specific immunoglobulin G after vaccination and infection. *J Infect Dis*. 2009;200(7):1031-1038. doi:10.1086/605648

Nakatsu Y, Takeda M, Ohno S, Shirogane Y, Iwasaki M, Yanagi Y. Measles virus circumvents the host interferon response by different actions of the C and V proteins. *J Virol*. 2008;82(17):8296-8306. doi:10.1128/JVI.00108-08

Nelson AN, Lin WW, Shivakoti R, et al. Association of persistent wild-type measles virus RNA with long-term humoral immunity in rhesus macaques. *JCI Insight*. 2020;5(3):e134992. Published 2020 Feb 13. doi:10.1172/jci.insight.134992

Nelson AN, Putnam N, Hauer D, Baxter VK, Adams RJ, Griffin DE. Evolution of T Cell Responses during Measles Virus Infection and RNA Clearance. *Sci Rep*. 2017;7(1):11474. Published 2017 Sep 13. doi:10.1038/s41598-017-10965-z

Noyce RS, Bondre DG, Ha MN, et al. Tumor cell marker PVRL4 (nectin 4) is an epithelial cell receptor for measles virus. *PLoS Pathog*. 2011;7(8):e1002240. doi:10.1371/journal.ppat.1002240

Odone A, Tramutola V, Morgado M, Signorelli C. Immunization and media coverage in Italy: an eleven-year analysis (2007-17). *Hum Vaccin Immunother*. 2018;14(10):2533-2536. doi:10.1080/21645515.2018.1486156

Okada H, Sato TA, Katayama A, et al. Comparative analysis of host responses related to immunosuppression between measles patients and vaccine recipients with live attenuated measles vaccines. *Arch Virol*. 2001;146(5):859-874. doi:10.1007/s007050170121

Ota MO, Ndhlovu Z, Oh S, et al. Hemagglutinin protein is a primary target of the measles virus-specific HLA-A2-restricted CD8+ T cell response during measles and after vaccination. *J Infect Dis*. 2007;195(12):1799-1807. doi:10.1086/518006

Pan CH, Greer CE, Hauer D, et al. A chimeric alphavirus replicon particle vaccine expressing the hemagglutinin and fusion proteins protects juvenile and infant rhesus macaques from measles. *J Virol*. 2010;84(8):3798-3807. doi:10.1128/JVI.01566-09

Pan CH, Valsamakis A, Colella T, et al. Modulation of disease, T cell responses, and measles virus clearance in monkeys vaccinated with H-encoding alphavirus replicon particles. *Proc Natl Acad Sci U S A*. 2005;102(33):11581-11588. doi:10.1073/pnas.0504592102

Parisien JP, Bamming D, Komuro A, et al. A shared interface mediates paramyxovirus interference with antiviral RNA helicases MDA5 and LGP2. *J Virol*. 2009;83(14):7252-7260. doi:10.1128/JVI.00153-09

Permar SR, Griffin DE, Letvin NL. Immune containment and consequences of measles virus infection in healthy and immunocompromised individuals. *Clin Vaccine Immunol*. 2006;13(4):437-443. doi:10.1128/CVI.13.4.437-443.2006

Permar SR, Klumpp SA, Mansfield KG, et al. Role of CD8(+) lymphocytes in control and clearance of measles virus infection of rhesus monkeys. *J Virol*. 2003;77(7):4396-4400. doi:10.1128/jvi.77.7.4396-4400.2003

Permar SR, Moss WJ, Ryon JJ, et al. Prolonged measles virus shedding in human immunodeficiency virus-infected children, detected by reverse transcriptase-polymerase chain reaction. *J Infect Dis*. 2001;183(4):532-538. doi:10.1086/318533

Phillips RS, Enwonwu CO, Okolo S, Hassan A. Metabolic effects of acute measles in chronically malnourished Nigerian children. *J Nutr Biochem*. 2004;15(5):281-288. doi:10.1016/j.jnutbio.2003.11.006

Plumet S, Herschke F, Bourhis JM, Valentin H, Longhi S, Gerlier D. Cytosolic 5'-triphosphate ended viral leader transcript of measles virus as activator of the RIG I-mediated interferon response. PLoS One. 2007;2(3):e279. Published 2007 Mar 14.

Polack FP, Auwaerter PG, Lee SH, et al. Production of atypical measles in rhesus macaques: evidence for disease mediated by immune complex formation and eosinophils in the presence of fusion-inhibiting antibody. *Nat Med*. 1999;5(6):629-634. doi:10.1038/9473

Polack FP, Hoffman SJ, Crujeiras G, Griffin DE. A role for nonprotective complement-fixing antibodies with low avidity for measles virus in atypical measles. *Nat Med*. 2003;9(9):1209-1213. doi:10.1038/nm918

Portais A, Le Marechal M, Nemoz B, et al. Measles-associated pneumonia in an immunocompromised patient: Persistent shortcomings in vaccination guidelines. *Infect Dis Now*. 2021;51(3):316-318. doi:10.1016/j.idnow.2020.11.004

Rana MS, Ikram A, Salman M, Usman M, Umair M. Negative impact of the COVID-19 pandemic on routine childhood immunization: experience from Pakistan. *Nat Rev Immunol*. 2021;21(11):689-690. doi:10.1038/s41577-021-00627-7

Randall RE, Goodbourn S. Interferons and viruses: an interplay between induction, signalling, antiviral responses and virus countermeasures. *J Gen Virol*. 2008;89(Pt 1):1-47. doi:10.1099/vir.0.83391-0

Reed LJ, Muench H. A simple method of estimating fifty per cent endpoints. Am J Hyg 1938; 27: 493-497

Rima B, Balkema-Buschmann A, Dundon WG, et al. ICTV Virus Taxonomy Profile: *Paramyxoviridae*. *J Gen Virol*. 2019;100(12):1593-1594. doi:10.1099/jgv.0.001328

Riddell MA, Moss WJ, Hauer D, Monze M, Griffin DE. Slow clearance of measles virus RNA after acute infection. *J Clin Virol*. 2007;39(4):312-317. doi:10.1016/j.jcv.2007.05.006

Rota JS, Heath JL, Rota PA, et al. Molecular epidemiology of measles virus: identification of pathways of transmission and implications for measles elimination. *J Infect Dis*. 1996;173(1):32-37. doi:10.1093/infdis/173.1.32

Rota PA, Bellini WJ. Update on the global distribution of genotypes of wild type measles viruses. *J Infect Dis*. 2003;187 Suppl 1:S270-S276. doi:10.1086/368042

Rota PA, Brown K, Mankertz A, et al. Global distribution of measles genotypes and measles molecular epidemiology. *J Infect Dis*. 2011;204 Suppl 1:S514-S523. doi:10.1093/infdis/jir118

Rota PA, Moss WJ, Takeda M, de Swart RL, Thompson KM, Goodson JL. Measles. *Nat Rev Dis Primers*. 2016;2:16049. Published 2016 Jul 14. doi:10.1038/nrdp.2016.49

Rümke HC, Loch HP, Hoppenbrouwers K, et al. Immunogenicity and safety of a measles-mumps-rubella-varicella vaccine following a 4-week or a 12-month interval between two doses. *Vaccine*. 2011;29(22):3842-3849. doi:10.1016/j.vaccine.2011.02.067

Ryon JJ, Moss WJ, Monze M, Griffin DE. Functional and phenotypic changes in circulating lymphocytes from hospitalized zambian children with measles. *Clin Diagn Lab Immunol*. 2002;9(5):994-1003. doi:10.1128/cdli.9.5.994-1003.2002

Sabidó M, Gavaldà L, Olona N, Ramon JM. Timing of hepatitis B vaccination: its effect on vaccine response in health care workers. *Vaccine*. 2007;25(43):7568-7572. doi:10.1016/j.vaccine.2007.08.025

Sampedro A, Rodríguez-Granger J, Gómez C, Lara A, Gutierrez J, Otero A. Comparative evaluation of a new chemiluminiscent assay and an ELISA for the detection of IgM against measles. *J Clin Lab Anal*. 2013;27(6):477-480. doi:10.1002/jcla.21630

Santibanez S, Niewiesk S, Heider A, et al. Probing neutralizing-antibody responses against emerging measles viruses (MVs): immune selection of MV by H protein-specific antibodies?. *J Gen Virol*. 2005;86(Pt 2):365-374. doi:10.1099/vir.0.80467-0

Schellens IM, Meiring HD, Hoof I, et al. Measles Virus Epitope Presentation by HLA: Novel Insights into Epitope Selection, Dominance, and Microvariation. *Front Immunol*. 2015;6:546. Published 2015 Nov 2. doi:10.3389/fimmu.2015.00546

Schneider-Schaulies S, Bieback K, Avota E, Klagge I, ter Meulen V. Regulation of gene expression in lymphocytes and antigen-presenting cells by measles virus: consequences for immunomodulation. *J Mol Med (Berl)*. 2002;80(2):73-85. doi:10.1007/s00109-001-0299-x

Schuhmann KM, Pfaller CK, Conzelmann KK. The measles virus V protein binds to p65 (RelA) to suppress NF-kappaB activity. *J Virol*. 2011;85(7):3162-3171. doi:10.1128/JVI.02342-10

Shi J, Zheng J, Huang H, et al. Measles incidence rate and a phylogenetic study of contemporary genotype H1 measles strains in China: is an improved measles vaccine needed?. *Virus Genes*. 2011;43(3):319-326. doi:10.1007/s11262-011-0638-0

Shivakoti R, Hauer D, Adams RJ, et al. Limited in vivo production of type I or type III interferon after infection of macaques with vaccine or wild-type strains of measles virus. *J Interferon Cytokine Res*. 2015;35(4):292-301. doi:10.1089/jir.2014.0122

Shivakoti R, Siwek M, Hauer D, Schultz KL, Griffin DE. Induction of dendritic cell production of type I and type III interferons by wild-type and vaccine strains of measles virus: role of defective interfering RNAs. *J Virol*. 2013;87(14):7816-7827. doi:10.1128/JVI.00261-13

Singh BK, Hornick AL, Krishnamurthy S, et al. The Nectin-4/Afadin Protein Complex and Intercellular Membrane Pores Contribute to Rapid Spread of Measles Virus in Primary Human Airway Epithelia [published correction appears in J Virol. 2016 Mar 15;90(6):3278]. *J Virol*. 2015;89(14):7089-7096. doi:10.1128/JVI.00821-15

Singh BK, Li N, Mark AC, Mateo M, Cattaneo R, Sinn PL. Cell-to-Cell Contact and Nectin-4 Govern Spread of Measles Virus from Primary Human Myeloid Cells to Primary Human Airway Epithelial Cells. *J Virol*. 2016;90(15):6808-6817. Published 2016 Jul 11. doi:10.1128/JVI.00266-16

Solomon T, Hart CA, Vinjamuri S, Beeching NJ, Malucci C, Humphrey P. Treatment of subacute sclerosing panencephalitis with interferon-alpha, ribavirin, and inosiplex. *J Child Neurol*. 2002;17(9):703-705. doi:10.1177/088307380201700911

Sparrer KM, Pfaller CK, Conzelmann KK. Measles virus C protein interferes with Beta interferon transcription in the nucleus. *J Virol*. 2012;86(2):796-805. doi:10.1128/JVI.05899-11

Stokke JL, Szymanski LJ, Bankamp B, et al. MMR Vaccine-Associated Disseminated Measles in an Immunocompromised Adolescent. *N Engl J Med*. 2021;385(13):1246-1248. doi:10.1056/NEJMc2103772

Suringa DW, Bank LJ, Ackerman AB. Role of measles virus in skin lesions and Koplik's spots. *N Engl J Med*. 1970;283(21):1139-1142. doi:10.1056/NEJM197011192832105

Sutcliffe PA, Rea E. Outbreak of measles in a highly vaccinated secondary school population. *CMAJ*. 1996;155(10):1407-1413.

Tabacchi G, Costantino C, Napoli G, et al. Determinants of European parents' decision on the vaccination of their children against measles, mumps and rubella: A systematic review and meta-analysis. *Hum Vaccin Immunother*. 2016;12(7):1909-1923. doi:10.1080/21645515.2016.1151990

Tahara M, Ito Y, Brindley MA, et al. Functional and structural characterization of neutralizing epitopes of measles virus hemagglutinin protein. *J Virol*. 2013;87(1):666-675.

Tahara M, Ohno S, Sakai K, et al. The receptor-binding site of the measles virus hemagglutinin protein itself constitutes a conserved neutralizing epitope. *J Virol*. 2013;87(6):3583-3586. doi:10.1128/JVI.03029-12

Tanaka M, Harada T. Koplik spots in measles. *Postgrad Med J*. 2019;95(1126):454. doi:10.1136/postgradmedj-2019-136739

Tanne JH. Measles cases and deaths are increasing worldwide, warn health agencies. *BMJ*. 2020;371:m4450. Published 2020 Nov 16. doi:10.1136/bmj.m4450

Tatsuo H, Ono N, Tanaka K, Yanagi Y. SLAM (CDw150) is a cellular receptor for measles virus. *Nature*. 2000;406(6798):893-897. doi:10.1038/35022579

Thibault PA, Watkinson RE, Moreira-Soto A, Drexler JF, Lee B. Zoonotic Potential of Emerging Paramyxoviruses: Knowns and Unknowns. *Adv Virus Res*. 2017;98:1-55. doi:10.1016/bs.aivir.2016.12.001.

Udem SA. Measles virus: conditions for the propagation and purification of infectious virus in high yield. *J Virol Methods*. 1984;8(1-2):123-136. doi:10.1016/0166-0934(84)90046-6

UNICEF. More than 117 million children at risk of missing out on measles vaccines, as COVID-19 surges. Statement by the Measles & Rubella Initiative: American Red Cross, U.S. CDC, UNICEF, UN Foundation and WHO. 2020. https://www.unicef.org/press-releases/more-117-million-children-risk-missing-out-measles-vaccines-covid-19-surges.

van der Vlist M, de Witte L, de Vries RD, et al. Human Langerhans cells capture measles virus through Langerin and present viral antigens to CD4$^+$ T cells but are incapable of cross-presentation. *Eur J Immunol*. 2011;41(9):2619-2631. doi:10.1002/eji.201041305

Vaz OM, Ellingson MK, Weiss P, et al. Mandatory Vaccination in Europe. *Pediatrics*. 2020;145(2):e20190620. doi:10.1542/peds.2019-0620

Weiss RA. The Leeuwenhoek Lecture 2001. Animal origins of human infectious disease. *Philos Trans R Soc Lond B Biol Sci*. 2001;356(1410):957-977. doi:10.1098/rstb.2001.0838

White SJ, Boldt KL, Holditch SJ, Poland GA, Jacobson RM. Measles, mumps, and rubella. *Clin Obstet Gynecol*. 2012;55(2):550-559. doi:10.1097/GRF.0b013e31824df256

WHO Global Surveillance . *Weekly Epidemiological Record Relevé Épidémiologique Hebdomadaire.* Volume 204. World Health Organization; Geneva, Switzerland: 2012; 73–80.

Wittwer K, Anderson DE, Pfeffermann K, et al. Small-molecule polymerase inhibitor protects non-human primates from measles and reduces shedding. *Nat Commun*. 2021;12(1):5233. Published 2021 Sep 2. doi:10.1038/s41467-021-25497-4

World Bank. Immunization, measles (% of children ages 12-23 months) 2021. https://data.worldbank.org/indicator/SH.IMM.MEAS.

World Health Organization Immunization, Vaccines and Biologicals—Measles Surveillance Data. Regional Summary of Reported Measles Cases. [(accessed on 30 March 2016)]. Available online: http://www.who.int/immunization/monitoring_surveillance/burden/vpd/surveillance_type/active/measles_monthlydata/en/index1.html.

World Health Organization. Measles - number of reported cases. 2021. https://www.who.int/data/gho/data/indicators/indicator-details/GHO/measles---number-of-reported-cases.

World Health Organization. Meeting of the Strategic Advisory Group of Experts on Immunization, October 2020: conclusions and recommendations Weekly Epidemiological Record, 2020;95 (48): 585 - 607

Xu S, Zhang Y, Rivailler P, et al. Evolutionary genetics of genotype H1 measles viruses in China from 1993 to 2012. *J Gen Virol*. 2014;95(Pt 9):1892-1899. doi:10.1099/vir.0.066746-0

Yanagi Y, Takeda M, Ohno S, Hashiguchi T. Measles virus receptors. *Curr Top Microbiol Immunol*. 2009;329:13-30. doi:10.1007/978-3-540-70523-9_2

Yoneyama M, Fujita T. Recognition of viral nucleic acids in innate immunity. *Rev Med Virol*. 2010;20(1):4-22. doi:10.1002/rmv.633

Yoneyama M, Onomoto K, Jogi M, Akaboshi T, Fujita T. Viral RNA detection by RIG-I-like receptors. Curr Opin Immunol. 2015;32:48-53.

Yu XL, Cheng YM, Shi BS, et al. Measles virus infection in adults induces production of IL-10 and is associated with increased CD4+ CD25+ regulatory T cells. *J Immunol*. 2008;181(10):7356-7366. doi:10.4049/jimmunol.181.10.7356

Zhang Y, Wang H, Xu S, et al. Monitoring progress toward measles elimination by genetic diversity analysis of measles viruses in China 2009-2010. *Clin Microbiol Infect*. 2014;20(9):O566-O577. doi:10.1111/1469-0691.12530

Zhou LJ, Tedder TF. CD14+ blood monocytes can differentiate into functionally mature CD83+ dendritic cells. *Proc Natl Acad Sci U S A*. 1996;93(6):2588-2592. doi:10.1073/pnas.93.6.2588

Zilliox MJ, Moss WJ, Griffin DE. Gene expression changes in peripheral blood mononuclear cells during measles virus infection. *Clin Vaccine Immunol*. 2007;14(7):918-923. doi:10.1128/CVI.00031-07

Chapter 8

Annexes

Article

Overview of Anti-SARS-CoV-2 Immune Response Six Months after BNT162b2 mRNA Vaccine

Claudia Gandolfo [1,†], Gabriele Anichini [1,†], Marco Mugnaini [2], Monica Bocchia [3], Chiara Terrosi [1], Anna Sicuranza [3], Gianni Gori Savellini [1], Alessandro Gozzetti [3], Federico Franchi [4] and Maria Grazia Cusi [1,*]

[1] Virology Unit, Department of Medical Biotechnologies, University of Siena, Azienda, Ospedaliera Universitaria Senese, V. le Bracci, 16, 53100 Siena, Italy; claudia.gandolfo@unisi.it (C.G.); gabriele.anichini@student.unisi.it (G.A.); chiara.terrosi@unisi.it (C.T.); gianni.gori@unisi.it (G.G.S.)
[2] Department of Information Engineering and Mathematical Sciences, University of Siena, 53100 Siena, Italy; marco.mugnaini@unisi.it
[3] Hematology Unit, Department of Medical Sciences, Surgery and Neurosciences, Azienda, Ospedaliera Universitaria Senese, V. le Bracci, 16, 53100 Siena, Italy; monica.bocchia@unisi.it (M.B.); sicuranza4@unisi.it (A.S.); gozzetti@unisi.it (A.G.)
[4] Anesthesia and Intensive Care Unit, Department of Medicine, Surgery and Neuroscience, University of Siena, 53100 Siena, Italy; federico.franchi@unisi.it
* Correspondence: mariagrazia.cusi@unisi.it; Tel.: +39-0577-233871
† These authors contributed equally to this work.

Abstract: Background: We have designed a prospective study aiming to monitor the immune response in 178 health care workers six months after BNT162b2 mRNA vaccination. Methods: The humoral immune response of all subjects was evaluated by chemiluminescence (CMIA); in 60 serum samples, a live virus-based neutralization assay was also tested. Moreover, 6 months after vaccination, B- and T-cell subsets from 20 subjects were observed by FACS analysis after restimulation with the trimeric SARS-CoV-2 Spike protein as an antigen, thus mimicking reinfection in vitro. Results: A significant decrease of circulating IgG levels and neutralizing antibodies over time were observed. Moreover, six months after vaccination, a variable T-cell immune response after in vitro antigen stimulation of PBMC was observed. On the contrary, the analysis of B-cell response showed a shift from unswitched to switched memory B-cells and an increase of Th17 cells. Conclusions: Although the variability of the CD4$^+$ and CD8$^+$ immune response and an antibody decline was observed among vaccinated subjects, the increase of switched memory B-cells and Th17 cells, correlating with the presence of neutralizing antibodies, opened the debate on the correct timing of vaccination.

Keywords: SARS-CoV-2; BNT162b2 mRNA vaccine; humoral immunity; cellular immunity; fuzzy system

1. Introduction

After the global diffusion of the severe acute respiratory infectious disease caused by the SARS-CoV-2 virus (COVID-19) in 2020, the World Health Organization (WHO) declared a pandemic status. Up to now, millions of COVID-19 cases have been confirmed worldwide (WHO, 2021) [1]. Considering its rapid spread, pharmaceutical industries promptly started intensive work to develop specific and efficacious vaccines, thanks to government support. The BNT162b2 mRNA vaccine (Pfizer-BioNTech) was the first vaccine available in Italy to prevent COVID-19 [2,3]. BNT162b2 is a lipid nanoparticle formulated nucleoside-modified messenger RNA (mRNA), encoding SARS-CoV-2 spike (S) protein, stabilized in the prefusion conformation [4]. Results from clinical trials showed that up to 6 months of follow-up and despite a gradually declining trend in vaccine efficacy, BNT162b2 had a favorable safety profile and a 91.3% effectiveness against COVID-19 disease [3].

However, on the basis of published results, 10–22% of people immunized against COVID-19, showing a steady decline of the humoral response [5], could present a major

risk of breakthrough infection, particularly with variants [6]. Many studies have been conducted on the duration of immunity after natural infection by SARS-CoV-2 [7], and results have been produced concerning the persistence of the antibody response over time and the durability of the cell-mediated immune response, in particular memory B and T cells, after two doses of vaccine [6,8–10].

Therefore, we designed a prospective study (MOTIVE study), (aiming) to explore and monitor the humoral immune response induced by the BNT162b2 mRNA vaccine in 178 vaccinated volunteers, (ii) to examine the memory B- and T-cell responses after the second BNT162b2 mRNA vaccine boost, and (iii) to run predictor models for the presence of a good protective antibody response against SARS-CoV-2. It is of primary interest to know the real correlates of protection from COVID-19 vaccines therefore a deeper knowledge of the type of immunity and its duration after vaccination could help to understand whether and when it is necessary to initiate further jabs and improve the vaccine performance against variants.

2. Materials and Methods

2.1. Study Design and Participants

In this current observational cohort study, we enrolled 178 volunteers among health-care workers (HCWs): 61 males and 117 females from 'Santa Maria alle Scotte' University Hospital in Siena, who had been subjected to periodical control (every 2 weeks) by molecular testing for SARS-CoV-2 virus with a nasopharyngeal swab and had never been infected. All subjects were vaccinated with two doses of BNT162b2 mRNA Vaccine (Pfizer Inc., New York, NY, USA) between 27 December 2020 and 31 January 2021. Among them, only 53 randomly selected subjects were screened 10 days after receiving the first dose of the vaccine. Then, blood samples were drawn to all subjects 10 days, one, three, and six months after the second dose of the BNT162b2 mRNA vaccine for humoral response analysis. Cell-mediated immune response was also investigated six months after vaccination in 20 vaccinated subjects, randomly selected for their high (10 subjects, neutralizing antibody titer one month after vaccination >64) or low (10 subjects, neutralizing antibody titer one month after vaccination <64) antibody response.

All subjects gave their informed consent to participate in this study in accordance with the principles of the Declaration of Helsinki. The study was approved by the local Ethical Committee (ID 19290).

2.2. Anti-SARS-CoV-2 Spike IgG Antibodies

In order to evaluate the humoral response induced by the vaccine, a blood sample was drawn from all HCWs 10 days, 1, 3, and 6 months after the second vaccine administration. To this aim, whole blood samples were collected and centrifuged at 1600 g for 15 min to separate the serum. Then they were stored at $-20\ ^\circ$C until serological assays were performed. Subjects' sera were analyzed using an Abbott SARS-CoV-2 IgG II Quant assay (Abbott Laboratories, Chicago, IL, USA), a chemiluminescent microparticle immunoassay (CMIA) for evaluating the immune status of individuals with quantitative measurement of IgG antibodies against the spike receptor-binding domain (RBD) of SARS-CoV-2. This assay was performed on an Abbott Architect i2000 (Abbott Diagnostics), according to the manufacturer's instructions. The cut-off value was 50.00 AU/mL. A sample was considered positive when the result was >50.0 AU/mL.

2.3. Microneutralization Assay

SARS-CoV-2 virus neutralization assay was carried out on Vero E6 cells (ATCC® CRL-1586™) in a 96-well microplate (COSTAR, Corning Incorporated, Corning, NY, USA). Twenty-five microliters of two-fold serial dilutions (1:8 to 1:1024) of sera samples were added to an equal volume of the SARS-CoV-2 strain (SARS-CoV-2/human/ITA/Siena-1/2020; GenBank: MT531537.2), containing 100 $TCID_{50}$ and incubated for 90 min at 37 $^\circ$C. Finally, 50 μL of Vero E6 cells suspension (2×10^5 cells/mL), prepared in complete DMEM,

was added to each well. After 72 h of incubation at 37 °C, cultures were daily examined for the presence of CPE under a microscope (Olympus IX51). The 50% endpoint titer was calculated using the Reed–Muench method [11]. A positive and negative control serum was included in each assay. Geometric mean titers (GMTs) of the neutralization assays were calculated. Serum from the National Institute for Biological Standards and Control, Blanche Lane, Ridge, Herts, UK (NIBSC) with known neutralization titer (Research reagent for anti-SARS-CoV-2 Ab NIBSC code 20/130) was used as a reference in MNTSera of subjects collected before 2019 were used as negative controls.

2.4. Peripheral Blood Mononuclear Cells Isolation and Stimulation

For the evaluation of the B- and T-cell response after stimulation with the Spike protein, peripheral blood mononuclear cells (PBMCs) were isolated from 20 selected subjects' whole blood and three unvaccinated, uninfected negative controls, using Lympholyte® Cell Separation Media (Cedarlane, Burlington, ON, Canada; Cat# DVCL5015). Afterwards, PBMCs were washed with RBC (Red Blood Cell) lysis buffer and seeded in quadruplicate at a concentration of 1×10^6 in 500 µL in 24-well plates in RPMI-1640 medium (Euroclone, Milan, Italy; Cat# ECB2000), supplemented with 10% heat-inactivated human serum (Euroclone, Milan, Italy; Cat# ECS5000L). Thereafter, IL-2 (20 U/mL), IL-10 (50 ng/mL), GM-CSF (50 ng/mL), and IL-4 (0.5 ng/mL) were added to each well and cells were incubated at 37 °C with 5% CO_2. After 48 h, Trimeric recombinant Spike protein (Leinco Technologies, Inc, St. Louis, MO, USA; Cat# S848) was added in two wells (for B- and T-subsets analysis, respectively) for each subject at a concentration of 5 µg/mL, while the other two wells were kept as unstimulated control cells. T- and B-cell populations were analyzed 24 h and 96 h after antigen stimulation, respectively. Responsiveness of each sample was assessed by stimulation with 5 µg/mL of phytohaemagglutinin (PHA) (Roche Diagnostics, Germany; Cat# 11249738001). After 24 h, cells were harvested and analyzed by flow cytometry.

2.5. Multiparameter Flow Cytometry Analysis

T- and B-cell subsets were stimulated in vitro for 24 and 96h with the recombinant Spike, respectively. Afterwards, PBMCs of 20 selected HCWs were harvested and washed, using PBS supplemented with 3% FCS, then stained with a fixable viability dye (LIVE/DEAD™ Fixable Aqua Dead Cell Stain Kit, Thermo Fisher Scientific, Waltham, MA, USA; Cat# L34957) for 20 min at 4 °C.

Surface staining with antibodies binding to CD3 (clone SK7), CD4 (clone SK3), CD8 (clone RPA-T8), CCR7 (clone 150503), CD45RA (clone HI100), CD38 (clone HIT2), HLA-DR (clone G46-6), CXCR3 (clone 1C6) and CCR6 (clone 11A9) for the analysis of T-helper and memory panels and with CD3 (clone SK7), HLA-DR (clone G46-6), CD19 (clone HIB19), CD27 (clone L128), IgD (clone IA6-2), CD20 (clone 2H7), CD24 (clone ML5), and CD38 (clone HIT2) for the analysis of B memory cells panel, according to manufacturer's instructions. All antibodies were supplied from BD Biosciences (New York, NY, USA). After fixation with PBS + 2% paraformaldehyde for 20 min at 4 °C, cells were washed and resuspended in PBS, supplemented with 0.5 mM EDTA before being acquired with SO LSRFortessa X20 flow cytometer (BD Biosciences, New York, NY, USA). Data analysis was performed using FlowJo v10 (TreeStar, Ashland, OR, USA).

2.6. Interferon-γ Quantification

Covi-FERON FIA (IFN-gamma/IFN-γ) (SD, BIOSENSOR), a fluorescent immunoassay, was used to quantify the interferon-γ production in the 20 selected subjects' whole blood six months after vaccination. Briefly, heparinized whole blood of each subject was incubated O/N at 37 °C in different blood collection tubes, which were antigen-sensitized. These tubes included: SARS-CoV-2 specific proteins tubes, Nil tube (Negative Control) and Mitogen tube (Positive Control). After centrifugation at 2300 g for 15 min, plasma was harvested and tested for the presence of IFN-γ, produced in response to the specific antigens by FIA. Results of each sample were automatically calculated in the analyzer. The concentration of

IFN-γ was provided as IU/mL. The test was considered valid if the Nil value was ≤ 8.0 and the Mitogen value greater than the Nil value by at least 0.5 IU/mL. Results were interpreted as described by the manufacturer's instructions.

2.7. Statistical Analysis

Differences among age, sex, circulating IgG levels, and neutralizing geometric mean titers (GMTs) were evaluated, and statistical significances were assessed with a two-tailed chi-square test. Results were considered statistically significant at $p < 0.05$. For each variable, a 95% confidence interval (95% CI)as calculated and reported. All analyses were performed by using Graph Pad Prism software (v.7.0). To represent data and to perform result comparisons, each single cell population analyzed by cytofluorimetry was normalized to the total amount of cells of interest for the specific subset of the cell population. After normalization, the obtained data were considered in terms of the relative difference between cells that had been non-exposed or exposed to SARS-CoV-2 Spike protein in order to investigate variations in cell counts after one (for T cells) or four days (for B cells) of antigen stimulation. CD4$^+$ CM represents the Central memory population, normalized with respect to total CD4$^+$ counted cells, CD4$^+$ EM are the effector memory population, normalized with respect to total CD4$^+$ counted cells as well as Th17 cells. CD8$^+$ CM and CD8$^+$ EM are the central and effector memory cells normalized for the CD8$^+$ population. Finally, the naïve, transitional, memory switched, and unswitched cells were normalized to the overall amount of B-cells for each subset of the cell population. Considering the fuzzy algorithm implemented, the authors used the Fuzzy MATLAB Toolbox and exploited the Mamdani model.

2.8. Limitations

This study has some limitations: the in vitro neutralization and stimulation assays were performed only with the WT virus since, at the beginning of this study, it was the only circulating strain.

In addition, another limitation could be represented by the low number of subjects analyzed for the T-cell response, mainly due to the complexity of the protocol used.

3. Results

3.1. Monitoring of Humoral Response after Vaccination

We analyzed sera from 178 healthcare workers, 61 males (34.2%; mean age 45.8 years, CI 95% 42.6–49.1) and 117 females (65.8%; mean age 44.4 years, CI 95% 42.1–46.6) who had never been infected by SARS-CoV-2 10 days, one month, three months, and six months after the second dose of BNT162b2 mRNA vaccine (Figure 1). Only two out of 53 randomly selected subjects, who were screened for the presence of specific IgG after the first dose of vaccine, were seronegative (3.8%), while all 178 HCWs were positive 10 days, one month, and three months after the second administration.

Results showed a significant difference in overall titers between 10 (21,394.9 AU/mL; CI 95% 19,600–23,200) and 30 (13,523.1 AU/mL; CI 95% 12,100–14,900), with an evident IgG decrease (36.64%) one month after vaccination ($p < 0.0001$). A similar decreasing pattern of circulating antibodies was observed both three months (4063.2 AU/mL; CI 95% 3600–4530, $p < 0.0001$ compared with results after 30 days) and six months (1431.6 AU/mL; CI 95% 1260–1,600, $p < 0.0001$ compared with results after three months) after the vaccine administration.

Antibody titers decayed over six months but remained detectable in all subjects, but two, who were previously tested positive. These data were confirmed by the decline of neutralizing antibodies.
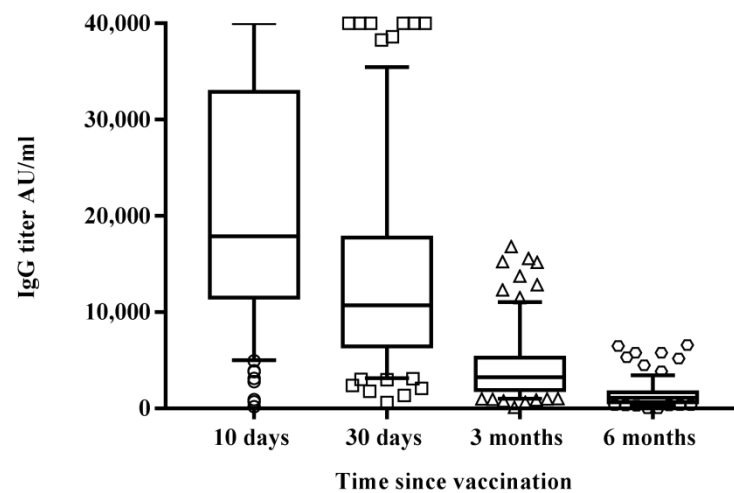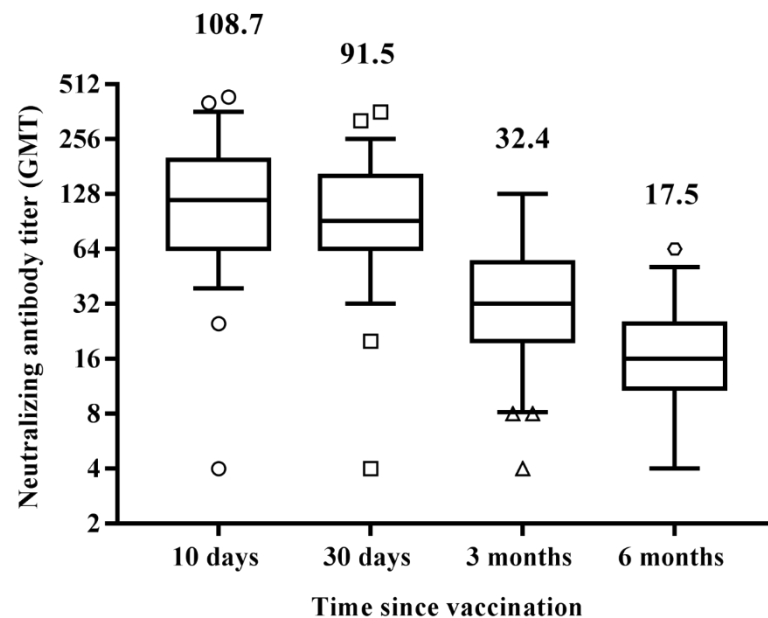
Figure 1. Differences in circulating IgG antibodies between the different time samplings after receiving the second vaccine administration reported as IgG titer in AU/mL. Results are reported in the box-whisker plots as median IgG and upper and lower quartiles. Differences in antibody titers were evaluated, and the statistical significance was assessed using the two-tailed chi-square test. Results were considered statistically significant at $p < 0.05$. Analyses were performed by using Graph Pad Prism software (v.7.0). Among the study group, 60 subjects were screened for the presence of specific neutralizing antibodies against SARS-CoV-2, 10 days, 1, 3, and 6 months after the second vaccine administration. The test was performed by assessing the protective activity of the humoral response against the live SARS-CoV-2 virus. Results did not show a significant difference ($p = 0.08$) in the antibody response, in terms of GMT 10days (GMT = 108.70) or 30 days (GMT = 91.50) after vaccination (Figure 2). However, in the following months, the decline of neutralizing antibodies was consistent, with a significant decrease both three months (GMT = 32.4; $p < 0.0001$ vs. 30 days) and six months (GMT = 17.5; $p < 0.0001$ vs. three months) after the vaccine administration.

Figure 2. Differences in neutralizing antibody titers (GMT) among the different time samplings after receiving the second vaccine administration. Results are reported in the box-whisker plots as median GMT and upper and lower quartiles. GMT, geometric mean titer. Differences in antibody titers were evaluated, and the statistical significance was assessed using the two-tailed chi-square test. Results were considered statistically significant at $p < 0.05$. Analyses were performed by using Graph Pad Prism software (v.7.0).

Finally, to better analyze the declining trend of neutralizing antibodies over time, we assessed the antibody profile of each subject. While those having a GMT > 128 (30 subjects) after 10 days showed a GMT decrease after 30 days (86.7%), the remaining (30 subjects), having a GMT < 128, behaved more heterogeneously. Seven of them (23.3%) showed a reduction in GMT, 17 (56.7%) developed a higher antibody titer, and 6 (20%) remained stable (Table 1).

Table 1. Neutralizing antibody profiles 1, 3 and 6 months after the second dose of vaccination in 60 subjects compared with the antibody response developed at 10 days.

	Neutralizing Antibody GMT > 128 at 10 Days Post-Vaccination			Neutralizing Antibody GMT < 128 at 10 Days Post-Vaccination		
	1 Month	3 Months	6 Months	1 Month	3 Months	6 Months
Ab level increase average	2 (6.66%) + 21.7%	0	0	17 (56.66%) + 22.0%	0	0
Ab level stability	2 (6.66%)	0	0	6 (20.0%)	0	0
Ab level decrease average	26 (86.66%) − 28.6%	30 (100%) − 70.7%	30 (100%) − 86.5%	7 (23.33%) − 6.8%	30 (100%) − 58.7%	30 (100%) − 76.9%

However, those having a higher GMT soon after vaccination showed a more pronounced decrease of neutralizing antibodies over time, suggesting that a leveling of antibody titer had occurred in all subjects over time (Table 1).

3.2. Cell-Mediated Immune Response to SARS-CoV-2 mRNA Vaccine

In addition to the analysis of the specific antibody developed in vaccinated subjects six months after vaccination, we analyzed the B- and T-cell immune responses in 20 subjects. We selected 10 subjects having a low neutralizing antibody response (<64) and 10 having a high antibody response (>64) one month after complete vaccination in order to investigate whether this parameter could correlate with a typical cell-mediated immune response. Three negative controls, represented by subjects who were not infected by SARS-CoV-2 and were not vaccinated, were also included.

We assessed the variation of the percentage of specific B- and T-cell populations between the basal level without antigen stimulation and the one induced by stimulation with the Spike antigen, as described in Section 2.4, in order to mimic the real-life event.

We analyzed $CD4^+$ central memory (CM $CD45RA^-$ $CCR7^+$), $CD4^+$ effector memory (EM $CD45RA^-$ $CCR7^-$), $CD4^+$ Th17 ($CXCR3$ $CCR6^+$), $CD8^+$ central memory (CM $CD45RA^-$ $CCR7^+$), $CD8^+$ effector memory (EM $CD45RA^-$ $CCR7^-$), naïve B ($CD19^+$ $CD27^-$ IgD^+), transitional B ($CD19^+$ $CD27^-$ IgD^+ $CD24^{high}$ $CD38^{high}$), unswitched memory B ($CD19^+$ $CD27^+$ IgD^+), and switched memory B cells ($CD19^+$ $CD27^+$ IgD^-). $CD4^+$ and $CD8^+$ naïve ($CD45RA^+$ $CCR7^+$) and effector memory cells re-expressing CD45RA (TEMRA $CD45RA^+$ $CCR7^-$) together with $CD4^+$ Th1 ($CXCR3^+$ $CCR6^-$) and Th2 ($CXCR3^-$ $CCR6^-$) helper cells were also analyzed, but no difference was recorded (data not shown). Full gating procedures are provided in Supplementary Materials Figures S1 and S2. As shown in Figure 3, wide variability was observed in T-cell response, indeed low and high responders did not show a relevant difference in behavior. An increasing trend of $CD4^+$ and $CD8^+$ effector memory cells after Spike stimulation was noted, however, without a significant difference (>0.05). On the contrary, an increase of Th17 cells was surprisingly evidenced upon stimulation with the Spike protein in low and high responders. This subset of $CD4^+$ cells produces several effector molecules, including IL-21, which stimulates B-cell differentiation and antibody class switching [12]. This feature correlates with the data clearly shown in Figure 3, where the unswitched memory B-cell differentiated in switched memory cells after exposure to the Spike, indicating that also people with a low neutralizing antibody titer could have a good memory B-cell immune response if reinfected with SARS-CoV-2. This relative variation is better represented in Figure 4, where only two out of twenty responders had a high level of unswitched and switched memory B cells, and one did not show any variations. The remaining samples, both from low and high responders, presented a shift to switched memory B-cells after antigen exposure. One of the controls

developed a weak variation in switched memory B cells, which might be attributable to a partial cross-reactive immunity to the common cold human coronaviruses.

Finally, we found an interesting correlation between Th17 cells and neutralizing antibodies to SARS-CoV-2. Figure 5 show that all samples had a positive percentage of Th17 variation corresponded to subjects having neutralizing antibodies; only five low responders (NT antibody titer <20 after one month) and a high responder (red circle in Figure 5) did not present a positive variation of Th17 after six months. A cut-off could be set with an NT value of 19.5.

Moreover, the transitional B-cells showed an increase after Spike stimulation, suggesting their role as developmental intermediates for human mature B-cell generation (Figure 6). We did not include the analysis of naïve and TEMRA cells in Figure 3 since no difference was evidenced between the stimulated and un-stimulated samples.

3.3. Fuzzy System

On the basis of these results, we tried to design an automated method based on a fuzzy algorithm that could provide a prognostic tool [13,14]. New computing methods based on fuzzy logic can be used in the development of intelligent systems for decision making, pattern recognition, and control. Figure 7 show the prediction probability of being a high/low responder with respect to an increase of Th17, which is always related to the presence of a good protective antibody response against SARS-CoV-2. The algorithm matches different membership functions designed to describe the likelihood of activating certain probability areas. When both Th17 and NT values are low, the chance to be a high responder is very low and close to zero.
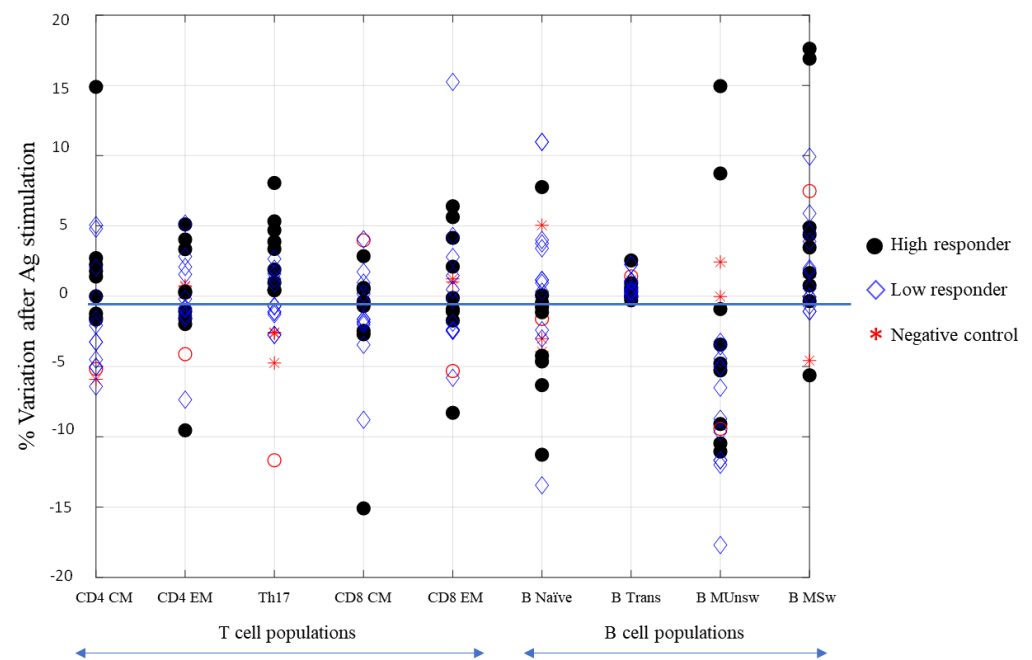
Figure 3. Representation of normalized parameters related to the immune cell populations with respect to their relative variations before and after stimulation with the SARS -CoV-2 Spike protein. High-responding subjects (black circles), low-responding ones (diamonds), and controls (stars). T cell populations: CD4$^+$ CM (central memory, CD45RA$^-$ CCR7$^+$), CD4$^+$ EM (effector memory, CD45RA$^-$ CCR7$^-$), CD4$^+$ Th17 (CXCR3$^-$ CCR6$^+$), CD8$^+$ CM (central memory, CD45RA$^-$ CCR7$^+$), CD8$^+$ EM (effector memory, CD45RA$^-$ CCR7$^-$). B-cell populations: B naïve (CD19$^+$ CD27$^-$ IgD$^+$), B transitional (CD19$^+$ CD27$^-$ IgD$^+$ CD24^{high} CD38^{high}), B MUnsw (memory unswitched CD19$^+$ CD27$^+$ IgD$^+$), and B MSw (memory switched CD19$^+$ CD27$^+$ IgD$^-$).
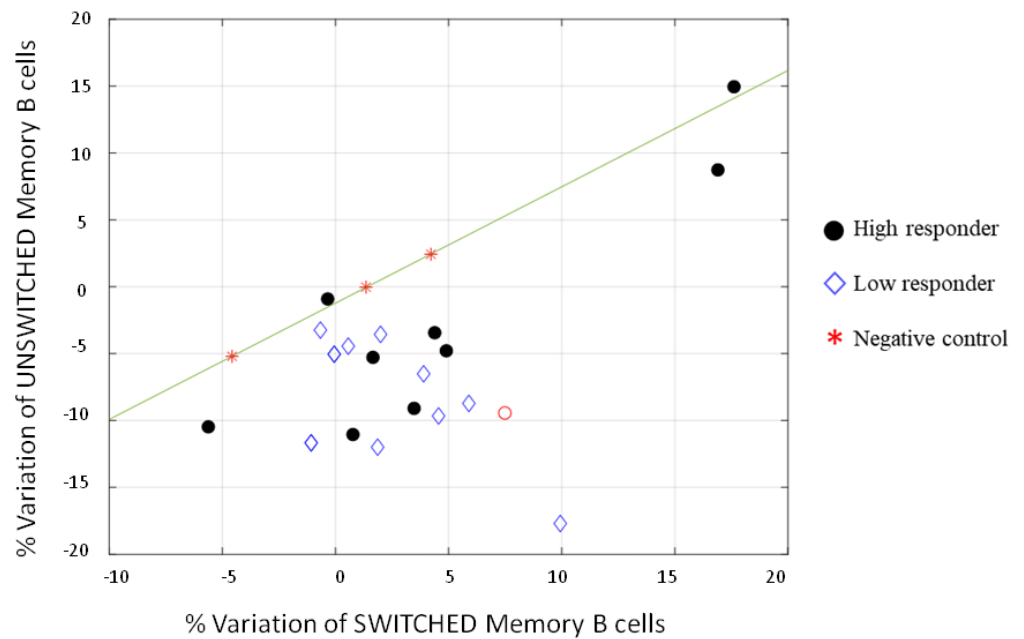
Figure 4. Representation of the relative variation of switched and unswitched memory B-cell populations normalized to the overall amount of B-cells. The mathematical expression $y = 0.8694 * x - 1.2207$ indicates that any point laying below y is, with high probability, a high or low responder.
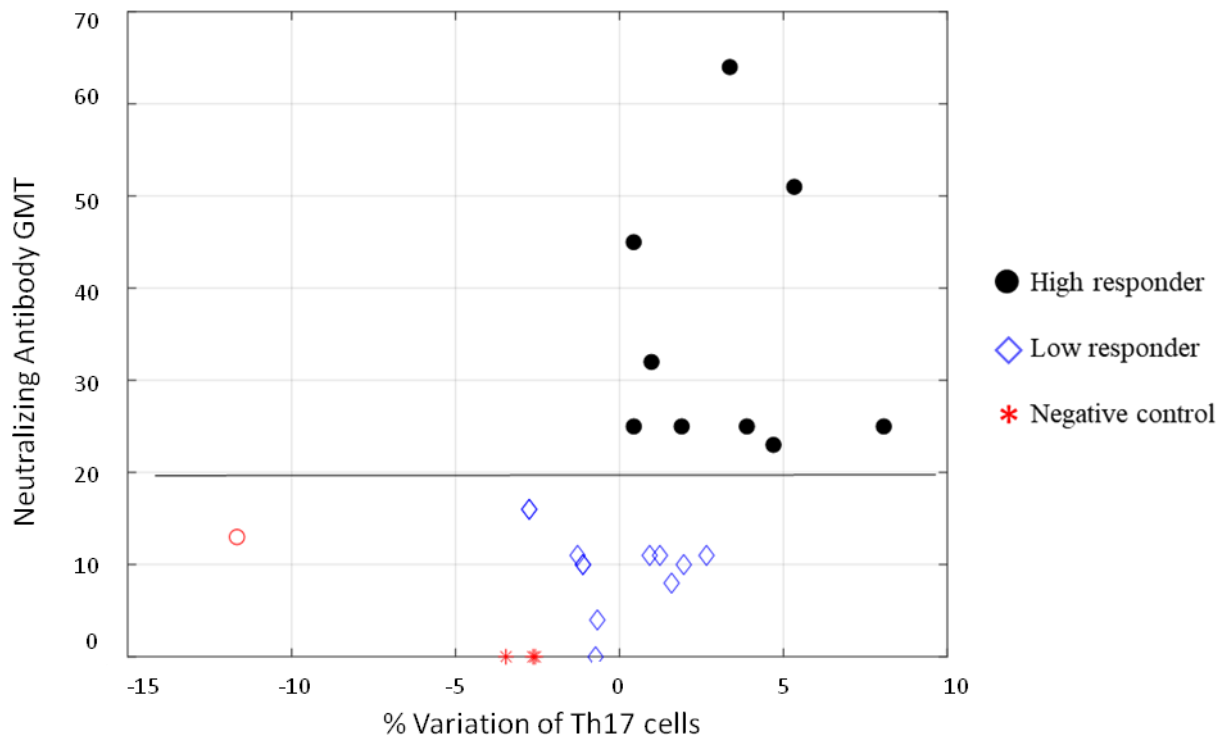

Figure 5. Representation of the % variation after stimulation of the $CD4^+$ Th17 population, normalized with respect to total $CD4^+$ counted cells, with respect to NT antibody GMT. It is possible to notice that a cut-off can be set with an NT value of 19.5 (calculated average). The red circle was considered an outlier.
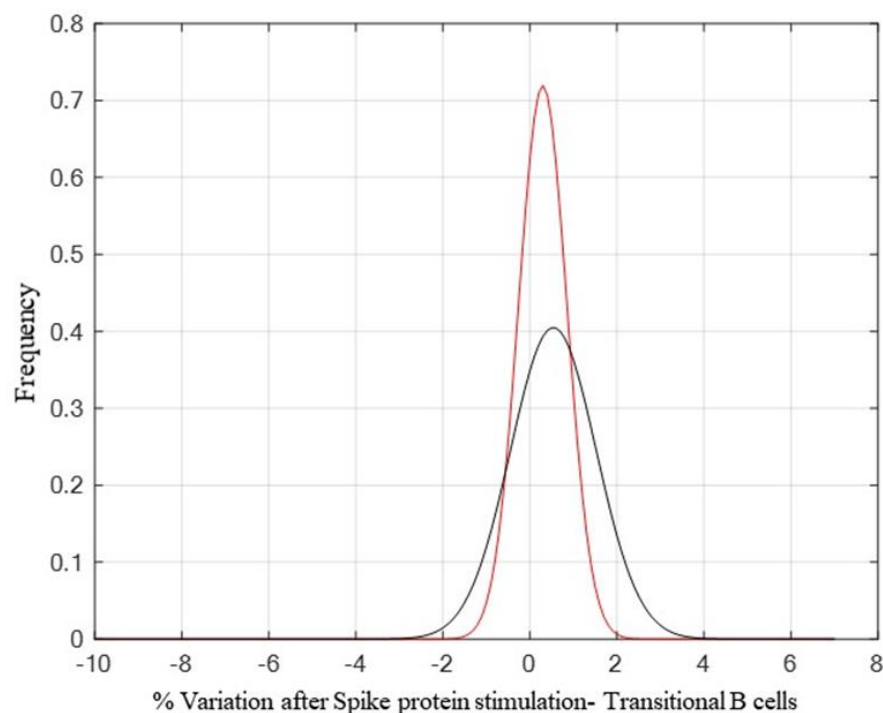
Figure 6. A comparison between the control probability density function (pdf) ($p = 0.4170$ and $h0 = 0$), shown in red, and the high responder population pdf ($p = 0.7146$ and $h0 = 0$), shown in black, highlights a small increase after antigen stimulation of transitional B-cells. Tests for the verification of pdf adherence have been conducted through the Chi2 square method.
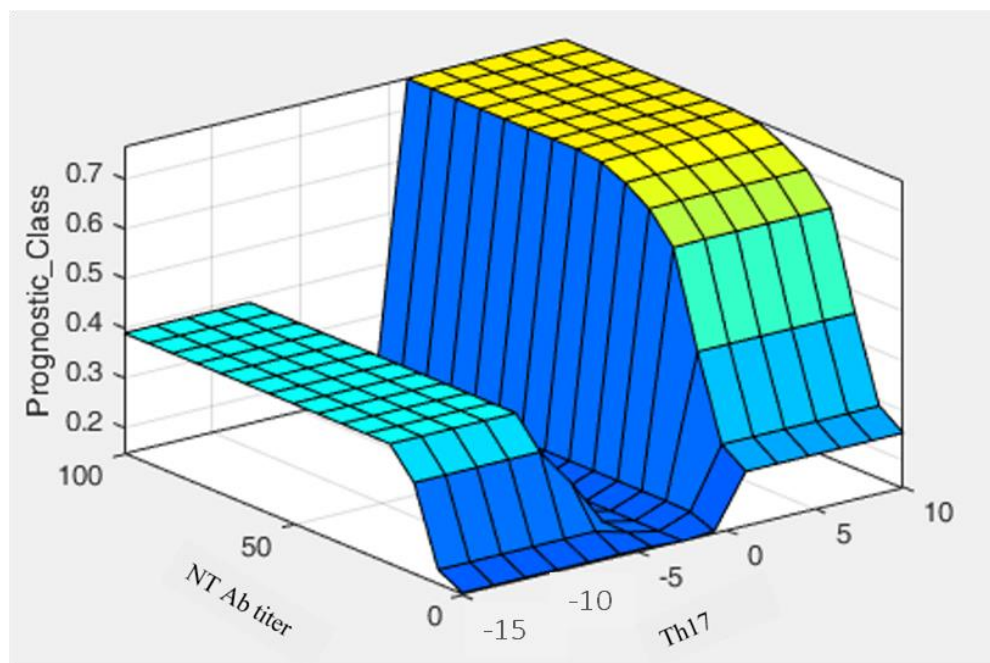
Figure 7. Graphical representation of a decision rule showing neutralizing antibody titer and Th17 population. Fuzzy MATLAB Toolbox and exploited the Mamdani model were used to generate the fuzzy algorithm.

3.4. Interferon-γ Production by SARS-CoV-2 Specific T Cells in the Whole Blood

As described in Section 2.6, a technically simple and rapid alternative to Elispot was performed to quantify the amount of interferon-γ in whole blood of the 20 previ-

ously selected subjects six months after vaccination, after O/N stimulation with a pool of SARS-CoV-2 peptides derived from the Spike amino acid sequence. A negative control, represented by uninfected and unvaccinated subjects, was included in the test. Table 2 show that 11 out of 20 subjects still had a Spike-specific T cell response, while both the 9 remaining vaccinated subjects and the negative control did not present an interferon-γ production. However, the amount of interferon-γ revealed in the responding subjects was correlated neither with the amount of specific CD4$^+$ or CD8$^+$ cells obtained by cytofluorimetric analysis nor with their antibody level six months after vaccination.

Table 2. The table shows the CoviFERON FIA results of the 20 samples previously analyzed by multiparametric flow cytofluorimetry.

N	CoviFERON FIA Results (IU/mL)			Results Interpretation	
	Nil	Original SP Antigen	Mitogen		
1	<0.145	1.42	>10.00	1.28	Reactive
2	<0.145	4.55	>10.00	4.41	Reactive
3	<0.145	1.12	>10.00	0.98	Reactive
4	<0.145	0.17	>10.00	0.03	Non-Reactive
5	<0.145	1.76	>10.00	1.62	Reactive
6	<0.145	0.93	>10.00	0.79	Reactive
7	<0.145	0.24	>10.00	0.10	Non-Reactive
8	<0.145	<0.145	>10.00	0.00	Non-Reactive
9	2.38	2.23	>10.00	−0.15	Non-Reactive
10	<0.145	0.56	>10.00	0.42	Reactive
11	<0.145	1.34	>10.00	1.20	Reactive
12	<0.145	<0.145	>10.00	0.00	Non-Reactive
13	<0.145	1.08	>10.00	0.94	Reactive
14	<0.145	2.74	>10.00	2.60	Reactive
15	<0.145	1.17	>10.00	1.03	Reactive
16	0.63	0.89	>10.00	0.26	Non-Reactive
17	0.27	7.00	>10.00	6.73	Reactive
18	<0.145	0.22	>10.00	0.08	Non-Reactive
19	<0.145	<0.145	>10.00	0.00	Non-Reactive
20	<0.145	0.18	>10.00	0.04	Non-Reactive
CTRL	<0.145	<0.145	>10.00	0.00	Non-Reactive

4. Discussion

In this study, the dynamic of the immune response six months after the BNT162b2 mRNA vaccine was analyzed. There are several articles in the scientific literature regarding the immunity after SARS-CoV-2 natural infection [15–19] and on the duration of the immune response after vaccination [4,9,10,20,21]. Here, we assessed the antibody response of 178 HCWs without any history of SARS-CoV-2 infection by chemiluminescent and microneutralization assays 10 days, 1, 3, and 6 months after two doses of the BNT162b2 mRNA vaccine. Only two out of the 53 randomly selected subjects, screened for the presence of specific IgG after the first dose of vaccine, were seronegative (3.8%), while all 178 HCWs were positive 10 days after the second dose. An antibody decline was observed over time, comparing the IgG levels at different time points after the second dose of vaccine.

Similarly, the neutralizing antibody response among the subjects showing no significant difference in GMT 10 (GMT = 109.78) and 30 (GMT = 92.90) days post-vaccination clearly declined in the following months. Indeed, a significant decrease in antibody response was found three (GMT = 32.4; $p < 0.0001$ vs. 30 days) and six months (GMT = 19.4; $p < 0.0001$ vs. three months) after vaccination (Figure 1).The NT antibody titer reached an average of 19.4, likely representing the cut-off to confer protection against the Wuhan strain of SARS-CoV-2 (19). Interestingly, we noticed that vaccinated subjects having a GMT > 128 10 days after the vaccine showed a slight decrease of the titer 30 days after, while those having a GMT < 128 showed quite different behavior. Most of them (56.6%) developed

a titer increase, a few (23.3%) showed a slight decrease, the remaining (20%) maintained the same titer (Table 1). However, it appeared that a levelling of the neutralizing antibody titer occurred over time, with a decreasing titer in subjects with a high amount of IgG and a titer increase in those showing a low–modest IgG level. Neutralizing antibodies are considered a good correlate of protection [22–24], and B-cells participate in the antiviral immune response. We stimulated human PBMCs with the Spike protein in vitro in order to understand whether a possible contact with SARS-CoV-2 in a vaccinated subject could mount an adequate immune response to protect the host in case of reinfection. After vaccination, memory B-cells capable of responding to a challenge were produced and distinguished in different subsets. This kind of response was present in all analyzed subjects, both high and low responders. We noticed that unswitched memory B-cells (IgD$^+$) shifted to switched memory B-cells (IgD$^-$) after in vitro stimulation with the Spike, indicating that the immune system is ready to defend the host in case of virus attack. Indeed, memory B cells play an important role in SARS-CoV-2 immunity and provide a good indication of vaccine efficacy [25,26]. While naïve B-cells showed a variable profile, transitional B-cells demonstrated a modest increase after antigen stimulation, particularly in high responders (Figure 6). Transitional B-cell subsets, identified within the CD24^{high}CD38^{high} B population display differential regulatory abilities. A subset of them is specialized in suppressing the production of proinflammatory cytokines and has the capacity to produce high levels of IL-10, which enhances B-cell survival, proliferation, and antibody production, thus providing support to the reported increase of memory B-cells. However, the biology of transitional B-cells still remains controversial [1]. Finally, we found a good correlation between Th17 cells after Spike stimulation and the presence of neutralizing antibodies. Th17 cells have a role in supporting B-cell responses. Indeed, under polarizing conditions, these cells can activate T-cells to support the expansion of B-cells and an enhanced antibody response [12,27,28]. In this study, we found that all high responders had an increase of Th17 cells after the exposure to the antigen, but only half of the low responders presented a similar behavior [22]. Thus, analysis of Th17 could be considered a useful biomarker correlated with an effective neutralizing antibody response for evaluating the efficacy of the vaccine over time. To this aim, we also implemented a prognostic tool based on fuzzy logic and artificial intelligence designed for this specific control task. By applying fuzzy logic, we were able to confirm this result. Indeed, in real life, things are not either white or black, but most are grey, thus in many practical situations, it is convenient to consider intermediate logical values, such as in these biological events that show variability among individuals. Fuzzy logic by intrinsic nature is not crisp, and therefore it weights, by means of specific membership function, the influence of several factors such as the Th17 and NT antibody titer amount for classification based on *a priori* knowledge.

Analyzing the virus-specific CD4$^+$ and CD8$^+$ T-cell immune response six months after vaccination, we noticed a variable profile both for CD4$^+$ and CD8$^+$ central memory lymphocytes, with a modest but not significant ($p > 0.05$) increase of the specific effector memory cells. Only 35% and 40% of the subjects revealed a 1% increase of CD4$^+$ and CD8$^+$ cells, respectively. We observed a clear heterogeneity of the T-cell-mediated response after BNT162b vaccination. These data were also supported by the low expression of interferon-γ non-correlated with the induced Spike cellular response in vaccinated subjects.

These data provide evidence that despite the antibody decline six months after BNT162b2 mRNA vaccination, the memory B-cell persists, and transitional B-cells could have a role together with Th17 cells in the proliferation and differentiation of B-lymphocytes. On the contrary, in this limited number of cases, a heterogeneity of CD4$^+$ and CD8$^+$ effector memory cell response to the Spike protein stimulation leads to hypothesize that in particular CD8+ cells do not represent the first class of defense against SARS-CoV-2 six months after mRNA vaccination. Humoral response against SARS-CoV-2 represents a valid correlate of protection; however, the T-cell response is also important, particularly for those who have a low antibody response and need to compensate for this shortage. Therefore, estimation of immunity over time is fundamental to improve the vaccine, evaluate the

variables that are useful to determine the real need for other boosts to protect people, and possibly develop an adequate time schedule of vaccination.

References

1. World Health Organization. WHO Coronavirus (COVID-19) Dashboard. Available online: https://covid19.who.int/ (accessed on 12 December 2021).
2. Polack, F.P.; Thomas, S.J.; Kitchin, N.; Absalon, J.; Gurtman, A.; Lockhart, S.; Perez, J.L.; Marc, G.P.; Moreira, E.D.; Zerbini, C.; et al. Safety and efficacy of the BNT162b2 mRNA COVID-19 vaccine. *N. Engl. J. Med.* **2020**, *383*, 2603–2615. [CrossRef]
3. Thompson, M.G.; Burgess, J.L.; Naleway, A.L.; Tyner, H.; Yoon, S.K.; Meece, J.; Olsho, L.E.W.; Caban-Martinez, A.J.; Fowlkes, A.L.; Lutrick, K.; et al. Prevention and Attenuation of Covid-19 with the BNT162b2 and mRNA-1273 Vaccines. *N. Engl. J. Med.* **2021**, *385*, 320–329. [CrossRef]
4. Thomas, S.J.; Moreira, E.D., Jr.; Kitchin, N.; Absalon, J.; Gurtman, A.; Lockhart, S.; Perez, J.L.; Marc, G.P.; Polack, F.P.; Zerbini, C.; et al. Safety and Efficacy of the BNT162b2 mRNA Covid-19 Vaccine through 6 Months. *N. Engl. J. Med.* **2021**, *385*, 1761–1773. [CrossRef]
5. Tartof, S.Y.; Slezak, J.M.; Fischer, H.; Hong, V.; Ackerson, B.K.; Ranasinghe, O.N.; Frankland, T.B.; Ogun, O.A.; Zamparo, J.M.; Gray, S.; et al. Effectiveness of mRNA BNT162b2 COVID-19 vaccine up to 6 months in a large integrated health system in the USA: A retrospective cohort study. *Lancet* **2021**, *398*, 1407–1416. [CrossRef]
6. Tarke, A.; Sidney, J.; Methot, N.; Yu, E.D.; Zhang, Y.; Dan, J.M.; Goodwin, B.; Rubiro, P.; Sutherland, A.; Wang, E.; et al. Impact of SARS-CoV-2 variants on the total CD4+ and CD8+ T cell reactivity in infected or vaccinated individuals. *Cell Rep. Med.* **2021**, *2*, 100355. [CrossRef]
7. Anichini, G.; Terrosi, C.; Gandolfo, C.; Savellini, G.G.; Fabrizi, S.; Miceli, G.B.; Cusi, M.G. SARS-CoV-2 Antibody Response in Persons with Past Natural Infection. *N. Engl. J. Med.* **2021**, *385*, 90–92. [CrossRef]
8. Brewer, R.C.; Ramadoss, N.S.; Lahey, L.J.; Jahanbani, S.; Robinson, W.H.; Lanz, T.V. BNT162b2 vaccine induces divergent B cell responses to SARS-CoV-2 S1 and S2. *Nat. Immunol.* **2021**, *23*, 33–39. [CrossRef] [PubMed]
9. Naaber, P.; Tserel, L.; Kangro, K.; Sepp, E.; Jürjenson, V.; Adamson, A.; Haljasmägi, L.; Rumm, A.P.; Maruste, R.; Kärner, J.; et al. Dynamics of antibody response to BNT162b2 vaccine after six months: A longitudinal prospective study. *Lancet Reg. Health-Eur.* **2021**, *10*, 100208. [CrossRef]
10. Almendro-Vázquez, P.; Laguna-Goya, R.; Ruiz-Ruigomez, M.; Utrero-Rico, A.; Lalueza, A.; de la Calle, G.M.; Delgado, P.; Perez-Ordoño, L.; Muro, E.; Vila, J.; et al. Longitudinal dynamics of SARS-CoV-2-specific cellular and humoral immunity after natural infection or BNT162b2 vaccination. *PLOS Pathog.* **2021**, *17*, e1010211. [CrossRef] [PubMed]
11. Reed, L.J.; Muench, H. A simple method of estimating fifty per cent endpoints. *Am. J. Epidemiol.* **1938**, *27*, 493–497. [CrossRef]
12. Maddur, M.S.; Miossec, P.; Kaveri, S.V.; Bayry, J. Th17 Cells: Biology, Pathogenesis of Autoimmune and Inflammatory Diseases, and Therapeutic Strategies. *Am. J. Pathol.* **2012**, *181*, 8–18. [CrossRef] [PubMed]
13. Liu, A.; Liu, B.; Ji, H.; Gao, D. Prognostic of electronic equipment based on adaptive neural network ensemble. *Jiefangjun Ligong Daxue Xuebao J. PLA Univ. Sci. Technol. Nat. Sci. Ed.* **2013**, *14*, 565–568.

14. Liang, D.; Wang, M.; Xu, Z. A novel approach of three-way decisions with information interaction strategy for intelligent decision making under uncertainty. *Inf. Sci.* **2021**, *581*, 106–135. [CrossRef]
15. Grifoni, A.; Weiskopf, D.; Ramirez, S.I.; Mateus, J.; Dan, J.M.; Moderbacher, C.R.; Rawlings, S.A.; Sutherland, A.; Premkumar, L.; Jadi, R.S.; et al. Targets of T Cell Responses to SARS-CoV-2 Coronavirus in Humans with COVID-19 Disease and Unexposed Individuals. *Cell* **2020**, *181*, 1489–1501.e1415. [CrossRef]
16. Gaebler, C.; Wang, Z.; Lorenzi, J.C.C.; Muecksch, F.; Finkin, S.; Tokuyama, M.; Cho, A.; Jankovic, M.; Schaefer-Babajew, D.; Oliveira, T.Y.; et al. Evolution of antibody immunity to SARS-CoV-2. *Nature* **2021**, *591*, 639–644. [CrossRef]
17. Dan, J.M.; Mateus, J.; Kato, Y.; Hastie, K.M.; Yu, E.D.; Faliti, C.E.; Grifoni, A.; Ramirez, S.I.; Haupt, S.; Frazier, A.; et al. Immunological memory to SARS-CoV-2 assessed for up to 8 months after infection. *Science* **2021**, *371*, eabf4063. [CrossRef]
18. Carsetti, R.; Zaffina, S.; Mortari, E.P.; Terreri, S.; Corrente, F.; Capponi, C.; Palomba, P.; Mirabella, M.; Cascioli, S.; Palange, P.; et al. Different Innate and Adaptive Immune Responses to SARS-CoV-2 Infection of Asymptomatic, Mild, and Severe Cases. *Front. Immunol.* **2020**, *11*, 3365. [CrossRef] [PubMed]
19. Anichini, G.; Gandolfo, C.; Terrosi, C.; Fabrizi, S.; Miceli, G.B.; Savellini, G.G.; Prathyumnan, S.; Franchi, F.; Cusi, M.G. Antibody response to SARS-CoV-2 in infected patients with different clinical outcome. *J. Med. Virol.* **2021**, *93*, 2548–2552. [CrossRef]
20. Goldberg, Y.; Mandel, M.; Bar-On, Y.M.; Bodenheimer, O.; Freedman, L.; Haas, E.J.; Milo, R.; Alroy-Preis, S.; Ash, N.; Huppert, A. Waning Immunity after the BNT162b2 Vaccine in Israel. *N. Engl. J. Med.* **2021**, *385*, e85. [CrossRef]
21. Levin, E.G.; Lustig, Y.; Cohen, C.; Fluss, R.; Indenbaum, V.; Amit, S.; Doolman, R.; Asraf, K.; Mendelson, E.; Ziv, A.; et al. Waning Immune Humoral Response to BNT162b2 Covid-19 Vaccine over 6 Months. *N. Engl. J. Med.* **2021**, *385*, e84. [CrossRef]
22. Khoury, D.S.; Cromer, D.; Reynaldi, A.; Schlub, T.E.; Wheatley, A.K.; Juno, J.A.; Subbarao, K.; Kent, S.J.; Triccas, J.A.; Davenport, M.P. Neutralizing antibody levels are highly predictive of immune protection from symptomatic SARS-CoV-2 infection. *Nat. Med.* **2021**, *27*, 1205–1211. [CrossRef] [PubMed]
23. McMahan, K.; Yu, J.; Mercado, N.B.; Loos, C.; Tostanoski, L.H.; Chandrashekar, A.; Liu, J.; Peter, L.; Atyeo, C.; Zhu, A.; et al. Correlates of protection against SARS-CoV-2 in rhesus macaques. *Nature* **2021**, *590*, 630–634. [CrossRef] [PubMed]
24. Krammer, F. Correlates of protection from SARS-CoV-2 infection. *Lancet* **2021**, *397*, 1421–1423. [CrossRef]
25. Mortari, E.P.; Russo, C.; Vinci, M.R.; Terreri, S.; Salinas, A.F.; Piccioni, L.; Alteri, C.; Colagrossi, L.; Coltella, L.; Ranno, S.; et al. Highly Specific Memory B Cells Generation after the 2nd Dose of BNT162b2 Vaccine Compensate for the Decline of Serum Antibodies and Absence of Mucosal IgA. *Cells* **2021**, *10*, 2541. [CrossRef]
26. Simon, Q.; Pers, J.-O.; Cornec, D.; Le Pottier, L.; Mageed, R.A.; Hillion, S. In-depth characterization of CD24 high CD38 high transitional human B cells reveals different regulatory profiles. *J. Allergy Clin. Immunol.* **2016**, *137*, 1577–1584.e10. [CrossRef] [PubMed]
27. Patakas, A.; Benson, R.A.; Withers, D.R.; Conigliaro, P.; McInnes, I.B.; Brewer, J.M.; Garside, P. Th17 Effector Cells Support B Cell Responses Outside of Germinal Centres. *PLoS ONE* **2012**, *7*, e49715. [CrossRef]
28. Mitsdoerffer, M.; Lee, Y.; Jäger, A.; Kim, H.-J.; Korn, T.; Kolls, J.K.; Cantor, H.; Bettelli, E.; Kuchroo, V.K. Proinflammatory T helper type 17 cells are effective B-cell helpers. *Proc. Natl. Acad. Sci. USA* **2010**, *107*, 14292–14297. [CrossRef]

Efficient Inactivation of SARS-CoV-2 and Other RNA or DNA Viruses with Blue LED Light

Chiara Terrosi [1], Gabriele Anichini [1], Jean Denis Docquier [1], Gianni Gori Savellini [1], Claudia Gandolfo [1], Francesco Saverio Pavone [2] and Maria Grazia Cusi [1,*]

[1] Department of Medical Biotechnologies, University of Siena, 53100 Siena, Italy; chiara.terrosi@unisi.it (C.T.); gabriele.anichini@student.unisi.it (G.A.); jddocquier@unisi.it (J.D.D.); gianni.gori@unisi.it (G.G.S.); claudia.gandolfo@unisi.it (C.G.)

[2] Department of Physics and Astronomy, European Laboratory for Non Linear Spectroscopy (LENS), University of Florence, 50121 Florence, Italy; francesco.pavone@unifi.it

[*] Correspondence: mariagrazia.cusi@unisi.it; Tel.: +39-0577-233871; Fax: +39-0577-233870

Abstract: Blue LED light has proven to have a powerful bacteria-killing ability; however, little is known about its mechanism of virucidal activity. Therefore, we analyzed the effect of blue light on different respiratory viruses, such as adenovirus, respiratory syncytial virus and SARS-CoV-2. The exposure of samples to a blue LED light with a wavelength of 420 nm (i.e., in the visible range) at 20 mW/cm^2 of irradiance for 15 min appeared optimal and resulted in the complete inactivation of the viral load. These results were similar for all the three viruses, demonstrating that both enveloped and naked viruses could be efficiently inactivated with blue LED light, regardless of the presence of envelope and of the viral genome nature (DNA or RNA). Moreover, we provided some explanations to the mechanisms by which the blue LED light could exert its antiviral activity. The development of such safe and low-cost light-based devices appears to be of fundamental utility for limiting viral spread and for sanitizing small environments, objects and surfaces, especially in the pandemic era.

Keywords: blue LED light; SARS-CoV-2; adenovirus; respiratory syncytial virus; viral inactivation

1. Introduction

A wide range of evidences about the use of blue light to inactivate pathogenic bacteria is currently present in literature [1,2]. In the past, several microbial species were studied for blue light antimicrobial activity in the spectral range of 400–470 nm, including Gram-positive and Gram-negative bacteria, mycobacteria and fungi. These studies were performed both in vitro and in vivo (preclinical studies and clinical trials) [3–14].

Antimicrobial properties of the blue light are the result of the absorption of these wavelengths by porphyrins and other chromophores within bacteria, such as flavins, leading to photochemical production of singlet oxygen and other reactive oxygen species (ROS). Bacterial exposure to ROS results in non-specific oxidative damage to vital structures and causes microbial inactivation [7–11,14–18].

Whilst the blue light effectiveness for bacterial inactivation is well studied in literature, there is a limited number of studies regarding possible virucidal effects of these wavelengths. A study on the inactivation efficacy of blue light (405 nm) on the bacteriophage/C31 indicated that the phage was susceptible to high doses of 405 nm light [19]. Richardson et al. showed that light, particularly the blue-violet part of the visible spectrum (wavelength 420–430 nm), is responsible for murine leukemia virus inactivation [20]. Likewise, another study demonstrated that a high dose of 405 nm light had a virucidal effect on feline calicivirus [21]. It is of paramount importance to find an effective tool with virucidal activity, to limit the virus spreading by aerosol and its survival on surfaces. However, as the mechanism of the inactivation through light is not elucidated, current knowledge on the antiviral efficacy of blue light requires further investigation. In this

study, we analyzed the effect of blue light on some viruses, such as adenovirus, respiratory syncytial virus and SARS-CoV-2. They are respiratory viruses that can be transmitted via aerosol [22–24]. SARS CoV-2, in particular, can survive in the environment and on surfaces for long time [24]. Blue light showed virucidal activity on all tested viruses.

2. Results and Discussion

Inactivation of microorganisms, and in particular of viruses that can be transmitted via aerosol, represents a crucial aspect of infection prevention and control procedures. In this study, we analyzed the virucidal activity of blue LED light against enveloped single strand RNA viruses, such as the respiratory syncytial virus and SARS-CoV-2, and a naked double strand DNA virus, such as the human adenovirus. We decided to test both enveloped and naked viruses in order to understand whether the envelope could be targeted with blue light leading to virus inactivation.

Preliminary trials were carried out to identify the optimal conditions (wavelength, exposure and power) for virus inactivation. The exposure of samples to a blue LED light with a wavelength of 420 nm (i.e., in the visible range) at 120 mW/cm^2 of irradiance for 15 min appeared optimal and resulted in the complete inactivation of the viral load (measured as described in the Materials and Methods section) for all viruses treated in this study (Figure 1).
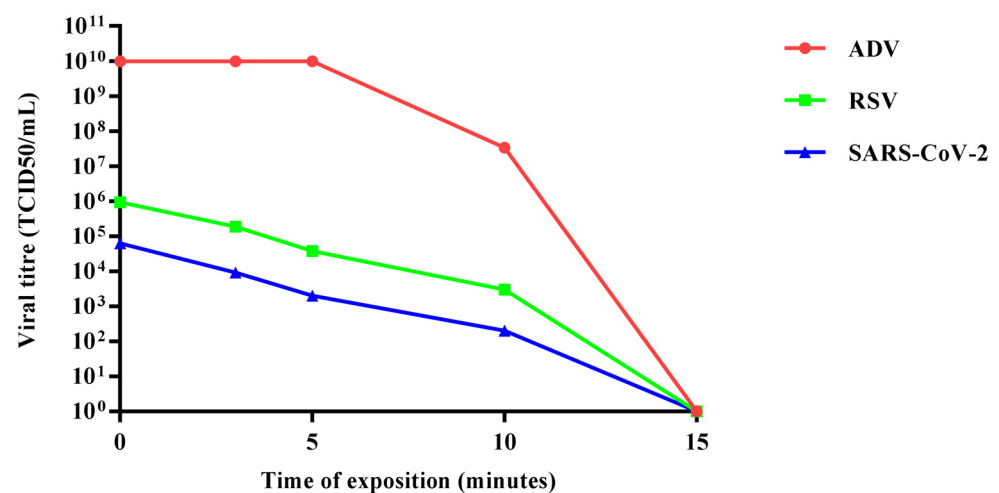

Figure 1. Representation of viral killing over time of adenovirus, respiratory syncytial virus and SARS-CoV-2 irradiated by blue LED light.

The results demonstrated that both enveloped and naked viruses could be efficiently inactivated by blue LED light, regardless of the presence of envelope or of the viral genome nature (DNA or RNA). In order to understand whether blue LED light could affect the integrity of the viral genome after LED irradiation, SARS-CoV-2 RNA was extracted and subjected to RT-PCR analysis. An amplified product of the expected size (≈500 bps) was obtained as well as for the non-irradiated virus (Figure 2), indicating that the viral nucleic acid was likely not degraded at 120 mW for 15 min.
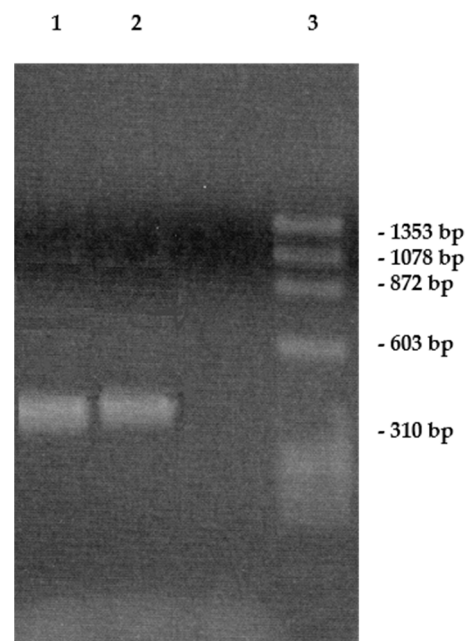
Figure 2. Agarose gel electrophoresis of irradiated SARS-CoV-2 (1), and non-irradiated SARS-CoV-2 (2). Standard is Thermo Scientific phiX174 DNA/BsuRI (HaeIII) Marker 9 (3).

Likewise, in order to investigate whether blue light could denature the proteins, we performed an immunoblot of the recombinant spike suspended in H_2O, after LED exposure, using an anti-spike monoclonal antibody. We did not observe a denaturing effect of blue light on the protein, which maintained the same molecular weight and showed the same profile of the control represented by the non-irradiated spike (Figure 3).
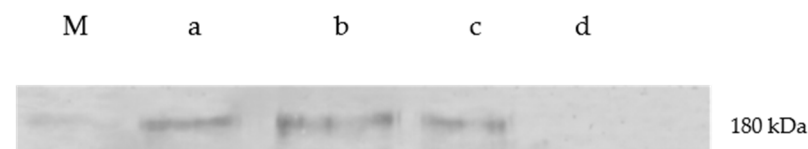

Figure 3. Immunoblot of transport medium + irradiated spike (**a**), irradiated transport medium + untreated spike (**b**), spike in water (**c**), irradiated transport medium (**d**), using anti-spike monoclonal antibody, as specified in Materials and Methods.

Thus, we tested the effect of LED on the nature of the matrix surrounding SARS-CoV-2.

Since the tested viruses were all in DMEM medium, likely containing photosensitizers, such as dye (phenol red) and porphyrins, their inactivation might rely on the presence of substances, whose exposure to blue LED light would generate reactive oxygen species (ROS) and, thus, oxidation of various molecules. It is known that cell membrane is the major target of ROS upon irradiation, causing alterations of the lipid structure. The envelope, being mostly constituted of phospholipids, could be subjected to the same fate. Moreover, ROS may induce damage of the proteins leading to their denaturation, thus explaining the effect of blue light on both enveloped and naked viruses [25–27].

Therefore, we focused on SARS-CoV-2, in order to see whether the presence of photosensitizers was necessary to activate LED. To this aim, we collected a nasopharyngeal swab from a COVID-19 positive subject in physiological solution (NaCl 0.9%), not containing any photosensitizers. Half of the sample was left at room temperature, the other part was irradiated as described above. Surprisingly, the viral load in the irradiated sample was reduced by 3 log ($TCID_{50}$ 2×10^2/mL) with respect to the untreated virus ($TCID_{50}$ 2×10^5/mL) ($p < 0.05$). We deduced that the liquid matrix where the swab was soaked, had a role in the viral inactivation. Organic materials, such as highly glycosylated mucins, containing cysteine-rich domains, which form disulfide bonds between mucin dimers [28], and other

substances present in the biological swab or human respiratory droplets could behave as photosensitizers [29]. These factors allowed the activation of LED and consequently the oxidation of molecules, damaging the virus itself. To confirm these data, we performed experiments on the SARS-CoV-2 recombinant trimeric spike, suspended in sterile water or in UTM medium and irradiated with LED blue light for 15 min. First, the fluorescence emission spectra of both the native and unfolded (after incubation of the protein sample in 4.5 M guanidinium chloride, commonly used as a chaotropic agent leading to protein denaturation) trimeric SARS-CoV-2 spike protein were obtained (Figure 4). Upon denaturation, a blue shift was clearly observed, with the maximum wavelength of emission varying from 345 to 365 nm, while the fluorescence intensity was less significantly affected. However, the fluorescence spectrum of the protein sample resuspended in water was not affected after exposure to blue LED light (Figure 4), supporting the hypothesis that irradiation with blue light would not directly induce the denaturation of the trimeric spike protein and would support the role of photosensitizers present in the liquid matrix.
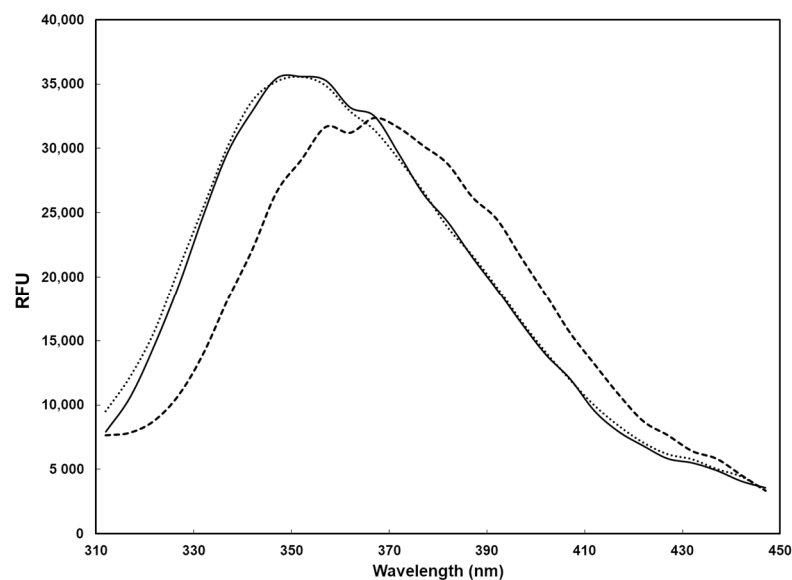

Figure 4. Fluorescence spectrum (excitation wavelength, 280 nm) of the recombinant trimeric SARS-CoV-2 spike protein (0.3 μM). Solid line, spectrum of the native protein in water; dashed line, spectrum of the denatured protein (obtained after incubation in the presence of 4.5 M GdmCl); dotted line, spectrum of the protein after exposure to blue LED light.

To further probe this hypothesis, the fluorescence spectra of the trimeric spike protein suspended in transport medium (UTM) were analyzed both before and after exposure to blue LED light (Figure 5). A significant reduction of fluorescence intensity was observed upon exposure to blue LED light, indicating that the irradiation had an effect on the protein, although the blue shift characterizing the denatured spike protein was not observed in this case. In addition, the spike protein added to a culture medium, previously subjected to blue LED light irradiation, showed no visible alteration of the fluorescence spectrum. Overall, these data indicate that the alteration of the trimeric spike protein likely requires the presence of photosensitizers contained in the culture medium. Since many viruses spread via droplet transmission, containing substances that can function as photosensitizers, the use of blue LED light can be exploited for virucidal activity. In conclusion, we provided some explanations to the mechanisms by which the blue LED light exerts its antiviral activity. Moreover, the development of safe low-cost light-based devices with the capability to inactivate viruses, sanitize equipment, hospital areas, particularly in pandemic era, appears of fundamental utility to limit the spread of viruses. The relevance of the decontamination of the environment, such as patient-care rooms, using blue light, will be evaluated by measuring its efficacy to reduce transmission of infectious pathogens.
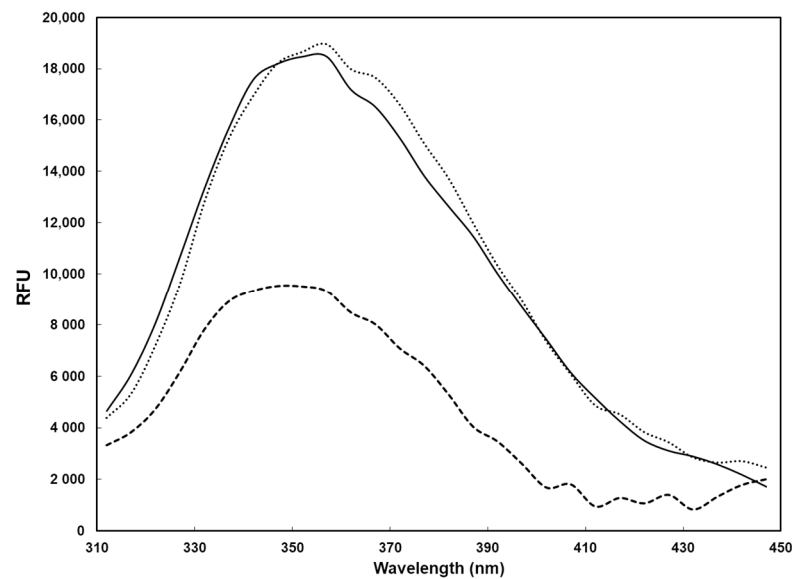
Figure 5. Fluorescence spectrum (excitation wavelength, 280 nm) of the recombinant trimeric SARS-CoV-2 spike protein (0.3 μM) in UTM culture medium. Solid line, spectrum of the protein in the culture medium without exposure; dashed line, spectrum of the protein in the culture medium after exposure of the sample to blue LED light; dotted line, spectrum of the protein after its addition to culture medium exposed to blue LED light.

3. Materials and Methods

3.1. Blue Light LED Instrument

The illuminator prototype used during the experiment was equipped of an array of blue LED emitting at 410–430 nm (Emoled Srl—Florence, Italy). The LED-based illuminator prototype was equipped on a steel stand in order to keep it at a distance of 4 cm from the samples during the illumination, giving an irradiance of 20 mW/cm^2 on the sample. The samples were irradiated for 3, 5, 10 or 15 min. The temperature of the medium was monitored by Ing. Domenico Alfieri; the temperature was not higher than 30 °C for the duration of the treatment.

3.2. Cells and Viruses

Vero E6 cells (ATCC CRL-1586) were cultured in Dulbecco's modified Eagle's medium (DMEM with phenol red dye) (Lonza, Milan, Italy) supplemented with 100 U/mL penicillin/streptomycin (Hyclone Europe, Milan, Italy) and 5% heat-inactivated fetal calf serum (FCS) (Lonza), at 37 °C. SARS-CoV-2 was isolated on Vero E6 cells from a clinical specimen in the Virology laboratory of 'S. Maria alle Scotte' Hospital in Siena, Italy. The respiratory syncytial virus (RSV) type A (ATCC VR-26) and adenovirus (VR-1516) were used for this study. All of them were suspended in DMEM.

3.3. Virus Exposure to the Blue LED Light

One mL of SARS-CoV-2, AdV or RSV was distributed in a Petri dish (35 × 11 mm^2, Thermo Fisher Scientific Inc.) and exposed for 3, 5, 10 or 15 min to the blue LED light at room temperature. The temperature was monitored during the irradiation. Likewise, for the control, 1 mL of each virus was put in a Petri dish and kept unexposed to the blue LED light, for the same time points at room temperature. After that, the viral suspension was collected and virus titration was performed. Fifty μL of the suspension was ten-fold serial diluted (10–10^{-8}) and distributed (in quadruplicate) in a 96 well plate. Furthermore, 50 μL (2 × 10^5/mL) of virus-susceptible Vero E6 cells were added in each well and incubated at 37 °C, 5% CO$_2$ incubator. The plate was daily observed under an optical microscope (Olympus IX51, magnification 100×). The final virus titer was evaluated after 3 days, when a cytopathic effect was evident in cells infected with the positive untreated virus control.

The viral titer was calculated according to the 'Reed and Muench' method [30]. This analysis calculates the 50% infectious dose of tissue cultures ($TCID_{50}$/mL). The test was performed in triplicate. The experiments carried out with SARS-CoV-2 were performed in BSL-3 laboratory.

3.4. SARS-CoV-2 Spike Protein Exposure to the Blue LED

The SARS-CoV-2 spike protein in its trimeric form (Recombinant SARS-CoV-2 Trimeric Spike Protein; Leinco Technologies, Fenton, MO, USA) was treated with blue LED light, as the virus. Therefore, the protein (0.12 µg/mL) was resuspended in complete sterile H_2O and irradiated for 30 min. The negative control was represented by the non-treated spike protein, at the same concentration (0.12 µg/mL) in H_2O. Likewise, the protein was resuspended in UTM medium (Copan, Italy; containing Hank's balanced salts bovine serum albumin, L-cysteine, gelatin, sucrose, L-glutamic acid, HEPES buffer, vancomycin, amphotericin B, colistin, phenol red) and irradiated with the blue light at the same conditions. Moreover, we irradiated only the UTM medium for 30 min, following which, the protein (0.12 µg/mL) was added. Lastly, a nasopharyngeal swab drawn from a COVID-19 infected patient (BIOBANK-MIU-2010, document approved by the Ethics Committee with amendment No. 1, on 17 February 2020) soaked in 1 mL of physiological buffer (NaCl 0.9%) was treated under blue light as above described. All the samples were then collected and tested for viral titration.

3.5. Immunoblot

Fifty microliters of each sample were loaded on an 8% SDS-PAGE gel, then transferred to a NitroBind nitrocellulose membrane (Santa Cruz Biotechnology, Heidelberg, Germany). Briefly, membrane blocking was accomplished with 5% non-fat dry milk, then filters were incubated o/n at 4 °C with anti-SARS-CoV-2 S monoclonal antibody (Clone LGSV201; Abnova, Taipei, Taiwan) (1:2000). After being washed with PBS 0.2% Tween-20 (PBS-T), membranes were incubated with horseradish peroxidase (HRP)-conjugated secondary antibody (Merck-Millipore) (1:5000). Immunocomplexes were detected with TMB Enhanced One Component HRP Membrane Substrate (Tebu-bio, Milan, Italy). Molecular weight markers were prestained protein SHARPMASS VI (Euroclone, Pero (MI), Italy)

3.6. Amplification of SARS-CoV-2 Spike Gene

Nucleic acid of the treated SARS-CoV-2 sample was extracted using the EZ1 Advanced XL system (Qiagen, Hilden, Germany), according to the manufacturer's instructions. Reverse transcription and PCR were performed using SuperScript III One-Step RT-PCR System with Platinum Taq DNA Polymerase (Invitrogen) by one cycle of 30 min at 45 °C and 2 min at 94 °C, 40 cycles of PCR, with each cycle consisting of 15 s at 94 °C, 30 s at 58 °C and 60 s at 68 °C, followed by a final elongation step for 5 min at 68 °C. Primer sequences for RT-PCR analysis were as follows:

Spike 2 For: 5′ CCTTTTGAGAGAGATATTTCAACTG 3′ (25 nt)
Spike 2 Rev: 5′ GATCAACTTACTCCTACTTGGCG 3′ (23 nt)
The final product was a fragment of 515 bps (nt 1387-1902 GeneBank No. MZ027646.1)

3.7. Protein Analysis Techniques

The potential of blue LED light to affect the three-dimensional structure of SARS-CoV-2 spike protein was investigated by fluorescence spectroscopy. Furthermore, 0.3 µM of SARS-CoV-2 spike protein was diluted in MilliQ water. Protein denaturation was carried out by incubating the protein sample in the presence 4.5 M guanidinium chloride (GdmCl) for up to 1 h. Fluorescence spectra (excitation wavelength, 280 nm; emission wavelength, 310–450 nm) of the native and denatured protein were recorded using an Envision microplate reader and black SpectraPlate microplates (Perkin Elmer, Waltham, Mass.) containing a final volume of 200 µL. To assess the effect of exposure to blue LED light, the protein was diluted either in MilliQ water or in the universal transport medium

(Copan Italia Sp.p.A, Brescia, Italy). Irradiation conditions were as previously mentioned (see 'Blue light LED instrument' and 'SARS-CoV-2 Spike Protein exposure').

References

1. Wang, Y.; Wang, Y.; Wang, Y.; Murray, C.K.; Hamblin, M.R.; Hooper, D.C.; Dai, T. Antimicrobial blue light inactivation of pathogenic microbes: State of the art. *Drug Resist. Updates* **2017**, *33–35*, 1–22. [CrossRef] [PubMed]
2. Tomb, R.M.; White, T.A.; Coia, J.E.; Anderson, J.G.; MacGregor, S.J.; Maclean, M. Review of the Comparative Susceptibility of Microbial Species to Photoinactivation Using 380–480 nm Violet-Blue Light. *J. Photochem. Photobiol. B Biol.* **2018**, *94*, 445–458. [CrossRef] [PubMed]
3. Zhou, W.; Kumer, A.; Ghate, V.; Kim, M.J.; Zhou, W.; Khoo, G.H.; Yuk, H.G. Antibacterial efficacy of 405, 460 and 520 nm light emitting diodes on Lactobacillus plantarum, Staphylococcus aureus and Vibrio parahaemolyticus. *J. Appl. Microbiol.* **2016**, *120*, 49–56. [CrossRef]
4. Masson-Meyers, D.S.; Bumah, V.V.; Biener, G.; Raicu, V.; Enwemeka, C.S. The relative antimicrobial effect of blue 405 nm LED and blue 405 nm laser on methicillin- resistant Staphylococcus aureus in vitro. *Lasers Med. Sci.* **2005**, *30*, 2265–2272. [CrossRef]
5. Enwemeka, C.S. Antimicrobial blue light: An emerging alternative to antibiotics. *Photomed. Laser Surg.* **2013**, *31*, 509–511. [CrossRef] [PubMed]
6. Bumah, V.V.; Masson-Meyers, D.S.; Enwemeka, C.S. Blue 470 nm light suppresses the growth of Salmonella enterica and methicillin-resistant Staphylococcus aureus (MRSA) in vitro. *Lasers Med. Surg.* **2015**, *47*, 595–601. [CrossRef]
7. Dai, T.; Gupta, A.; Murray, C.K.; Vrahas, M.S.; Tegos, G.P.; Hamblin, M.R. Blue light for infectious diseases: Propionibacterium acnes, Helicobacter pylori, and beyond? *Drug Resist. Updates* **2012**, *15*, 15223–15236. [CrossRef] [PubMed]
8. Hamblin, M.R.; Viveiros, J.; Yang, C.; Ahmadi, A.; Ganz, R.A.; Tolkoff, M.J. Helicobacter pylori accumulates photoactive porphyrins and is killed by visible light. *Antimicrob. Agents Chemother.* **2005**, *49*, 2822–2827. [CrossRef] [PubMed]
9. De Sous, N.T.A.; Santos, M.F.; Gomes, R.C.; Brandino, H.E.; Martinez, R.; de Jesus Guirro, R.R. Blue laser inhibits bacterial growth of Staphylococcus aureus, Escherichia coli, Pseudomonas aeruginosa. *Photomed. Laser Surg.* **2015**, *33*, 278–282. [CrossRef] [PubMed]
10. McKenzie, K.; Maclean, M.; Timoshkin, I.V.; MacGregor, S.J.; Anderson, J.G. Enhanced inactivation of Escherichia coli and Listeria monocytogenes by exposure to 405 nm light under sub-lethal temperature, salt and acid stress conditions. *Int. J. Food Microbiol.* **2013**, *170*, 91–98. [CrossRef] [PubMed]
11. Maclean, M.; MacGregor, S.J.; Anderson, J.G.; Woolsey, G.A. The role of oxygen in the visible light inactivation and wavelength sensitivity of Staphylococcus aureus. *J. Photochem. Photobiol. B* **2008**, *92*, 180–184. [CrossRef] [PubMed]
12. Enwemeka, C.S.; Williams, D.; Hollosi, D.; Yens, S.; Waynant, R.; Tata, D.B. *Blue Light Photo-Destroys Methicillin Resistant Staphylococcus aureus (MRSA) In Vitro*; Springer: Boston, MA, USA, 2008; pp. 33–37.
13. Guffey, J.S.; Wilborn, J. In vitro bactericidal effects of 405-nm and 470-nm blue light. *Photomed. Laser Surg.* **2006**, *24*, 684–688. [CrossRef]
14. Murdoch, L.E.; McKenzie, K.; Maclean, M.; MacGregor, S.J.; Anderson, J.G. Lethal effects of high-intensity violet 405-nm light on Saccharomyces cerevisiae, Candida albicans, and on dormant and germinating spores of Aspergillus niger. *Fungal Biol.* **2013**, *117*, 19–527. [CrossRef] [PubMed]
15. Anjos, C.; Sellera, F.P.; Gargano, R.G.; Lincopan, N.; Pogliani, F.C.; Ribeiro, M.G.; Jagielski, T.; Sabino, C.P. Algicidal effect of blue light on pathogenic Prototheca species. *Photodiagn. Photodyn. Ther.* **2019**, *26*, 210–213. [CrossRef]
16. Cieplik, F.; Spath, A.; Leibl, C.; Gollmer, A.; Regensburge, J.; Tabenski, L.; Hiller, K.A.; Maisch, T.; Schmalz, G. Blue light kills Aggregatibacter actinomycetemcomitans due to its endogenous photosensitizers. *Clin. Oral Investig.* **2014**, *18*, 1763–1769. [CrossRef]
17. Bumah, V.V.; Aboualizadeh, E.; Masson-Meyers, D.; Eells, J.; Enwemeka, C.S.; Hirschmugl, C. Resistance of B-DNA to blue light induced damage in methicillin- resistant Staphylococcus aureus. *J. Photochem. Photobiol. B Biol.* **2017**, *167*, 150–157. [CrossRef]

18. Pang, P.; Wang, N.; Wang, C.; Yao, Y.; Fu, X.; Yu, W.; Cai, R.; Yao, M. 460 nm visible light irradiation eradicates MRSA via inducing prophage activation. *J. Photochem. Photobiol. B Biol.* **2017**, *166*, 311–322. [CrossRef]

19. Tomb, R.M.; Maclean, M.; Herron, P.R.; Hoskisson, P.A.; MacGregor, S.J.; Anderson, J.G. Inactivation of Streptomyces phage /C31 by 405 nm light: Requirement for exogenous photosensitizers? *Bacteriophage* **2014**, *4*, e32129. [CrossRef] [PubMed]

20. Richardson, T.B.; Porter, C.D. Inactivation of murine leukaemia virus by exposure to visible light. *Virology* **2005**, *341*, 321–329. [CrossRef] [PubMed]

21. Tomb, R.M.; Maclean, M.; Coia, J.E.; Graham, E.; McDonald, M.; Atreya, C.D.; MacGregor, S.J.; Anderson, J.G. New Proof-of-Concept in Viral Inactivation: Virucidal Efficacy of 405 nm Light Against Feline Calicivirus as a Model for Norovirus Decontamination. *Food Environ. Virol.* **2017**, *9*, 159–167. [CrossRef] [PubMed]

22. Lynch, J.P.; Fishbein, M.; Echavarria, M. Adenovirus. *Semin. Respir. Crit. Care Med.* **2011**, *32*, 494–511. [CrossRef] [PubMed]

23. Griffiths, C.; Drews, S.J.; Marchant, D.J. Respiratory Syncytial Virus: Infection, Detection, and New Options for Prevention and Treatment. *Clin. Microbiol. Rev.* **2017**, *30*, 277–319. [CrossRef]

24. van Doremalen, N.; Bushmaker, T.; Morris, D.H.; Holbrook, M.G.; Gamble, A.; Williamson, B.N.; Tamin, A.; Harcourt, J.L.; Thornburg, N.J.; Gerber, S.I.; et al. Aerosol and Surface Stability of SARS-CoV-2 as Compared with SARS-CoV-1. *N. Engl. J. Med.* **2020**, *382*, 1564–1567. [CrossRef]

25. Ramakrishnan, P.; Maclean, M.; MacGregor, S.J.; Anderson, J.G.; Grant, M.H. Cytotoxic responses to 405nm light exposure in mammalian and bacterial cells: Involvement of reactive oxygen species. *Toxicol. In Vitro* **2016**, *33*, 54–62. [CrossRef]

26. Kuse, Y.; Ogawa, K.; Tsuruma, K.; Shimazawa, M.; Hara, H. Damage of photoreceptor-derived cells in culture induced by light emitting diode-derived blue light. *Sci. Rep.* **2014**, *4*, 5223. [CrossRef]

27. Bumah, V.V.; Morrow, B.N.; Cortez, P.M.; Bowman, C.R.; Rojas, P.; Masson-Meyers, D.S.; Suprapto, J.; Tong, W.G.; Enwemeka, C.S. The importance of porphyrins in blue light suppression of Streptococcus agalactiae. *J. Photochem. Photobiol. B Biol.* **2020**, *212*, 111996. [CrossRef] [PubMed]

28. Williams, O.W.; Sharafkhaneh, A.; Kim, V.; Dickey, B.F.; Evans, C.M. Airway mucus: From production to secretion. *Am. J. Respir. Cell Mol. Biol.* **2006**, *34*, 527–536. [CrossRef] [PubMed]

29. Niazi, S.; Groth, R.; Spann, K.; Johnson, G.R. The role of respiratory droplet physicochemistry in limiting and promoting the airborne transmission of human coronaviruses: A critical review. *Environ. Pollut.* **2021**, *276*, 115767. [CrossRef] [PubMed]

30. Reed, L.J.; Muench, H. A simple method of estimating fifty per cent endpoints. *Am. J. Hyg.* **1938**, *27*, 493–497.

Comparative Performance of a New SARS-CoV-2 Rapid Detection System

Gianni Gori Savellini,[a] Gabriele Anichini,[a] Chiara Terrosi,[a] Shibily Prathyumnan,[a] Claudia Gandolfo,[a] Stefano Marini,[c] Maria Grazia Cusi[a,b]

[a]Department of Medical Biotechnologies, University of Siena, Siena, Italy
[b]Microbiology and Virology Unit, S. Maria alle Scotte University Hospital, Siena, Italy
[c]Dati & Ricerca S.r.l., Rome, Italy

ABSTRACT The extraordinary global demand for reagents and diagnostic instruments needed for timely detection of severe acute respiratory syndrome coronavirus 2 (SARS-CoV-2) infection has rapidly affected their availability. In order to meet diagnostic needs, it has been necessary to develop new diagnostic procedures. To date, molecular diagnostic tools have represented the gold standard for diagnosis of SARS-CoV-2 infection, and thus an alternative and real-time PCR system was required. To this aim, a molecular rapid test which works with direct real-time RT-PCR may be a relevant aid. In the present work, the accuracy, sensitivity, and specificity of the bKIT Virus Finder COVID-19 rapid molecular test by Hyris Ltd. was evaluated. Moreover, the influence of a different swab storage medium composition was examined relative to that of a routinely used comparator assay. The Hyris Ltd. assay showed an overall agreement of 100% with the comparator based on a panel consisting of 74 retrospective positive nasopharyngeal swabs (NPSs), collected either in universal transport medium (UTM) or using ESwab. No false-positive result was achieved on samples that previously tested negative. Cross-reactivity screening on microorganisms that commonly colonize the human upper respiratory tract was not detected, excluding the risk of false-positive results. Simultaneously, drugs frequently administered to cure respiratory diseases did not interfere with the analytical performance of the assay. Our results showed that the Hyris Ltd. bKIT Virus Finder COVID-19 is a reliable assay for rapid qualitative detection of SARS-CoV-2, providing the advantage of less complex and unambiguous interpretation of results. Indeed, skilled technicians are not required, and thus the Hyris system is suitable as a rapid and easy system for SARS-CoV-2 diagnosis.

IMPORTANCE In order to overcome the increased demand for diagnostic tools for the timely detection of SARS-CoV-2 infection, we tested the bKIT Virus Finder COVID-19 molecular rapid test by Hyris Ltd. The new system was confirmed as a reliable assay for rapid SARS-CoV-2 detection, since sensitivity and specificity parameters were fully satisfied. Moreover, the bKIT Virus Finder COVID-19 provides the advantage of easy results interpretation, since skilled technicians are not required, and thus the Hyris system is a valuable SARS-CoV-2 rapid diagnosis system.

KEYWORDS SARS-CoV-2, molecular diagnosis, diagnostic platform

Severe acute respiratory syndrome coronavirus 2 (SARS-CoV-2), responsible for coronavirus disease 2019 (COVID-19), was first reported in 2019 in Wuhan, China, and the World Health Organization subsequently declared it a pandemic (https://www.who.int/emergencies/diseases/novel-coronavirus-2019). The high incidence of virus diffusion and COVID-19 reported during the first outbreak overwhelmed the capability of health care systems, since a rapid diagnostic procedure was not yet present. Moreover, also during the second outbreak, a simple, sensitive, and rapid diagnostic tool represented an important challenge to reduce the risk of SARS-CoV-2 transmission (1, 2). Therefore, the rapid identification of SARS-CoV-2-positive

TABLE 1 Tentative LoD of the bKIT Virus Finder COVID-19 assay in NPS or BAL negative matrices

LoD	SARS-CoV-2 ($TCID_{50}$/ml)	C_T (mean ± SD)		
		Reaction mix 1	Reaction mix 2	RP
Tentative, in NPS	1×10^4	26.89 ± 0.15	27.14 ± 0.19	25.26 ± 0.05
	1×10^3	30.45 ± 0.07	30.68 ± 0.15	25.28 ± 0.03
	1×10^2	33.33 ± 0.63	34.1 ± 0.16	25.2 ± 0.04
	10	38.18 ± 0.53	37.68 ± 1.01	25.09 ± 0.16
	1	N/A	N/A	25.18 ± 0.02
Tentative, in BAL	1×10^4	27.74 ± 0.06	29.30 ± 2.02	29.91 ± 0.17
	1×10^3	31.14 ± 0.47	33.33 ± 0.44	30.82 ± 0.19
	1×10^2	34.13 ± 0.08	36.44 ± 0.04	31.88 ± 0.15
	10	37.29 ± 1.54	39.72 ± 0.23	33.16 ± 1.00
	1	38.52 ± 1.10	41.60 ± 0.42	32.41 ± 0.57

patients still represents a critical aspect in COVID-19 management and is highly required for efficient and timely isolation of patients. The quantitative reverse transcription-PCR (RT-qPCR) assay for SARS-CoV-2 on nasopharyngeal swabs (NPSs) or bronchoalveolar lavage fluid (BAL) samples represents the gold standard procedure for COVID-19 diagnosis (3–5). Several diagnostic strategies have been quickly developed, including fully automated RT-qPCR, encompassing RNA extraction and direct report of results, and RNA extraction-free RT-qPCR systems (6, 7). High test sensitivity and short time to results are mandatory for SARS-CoV-2 diagnosis. Indeed, some nucleic acid amplification tests (NAATs) allow single samples to be run on demand, providing results in less than 1 h with no need for highly skilled laboratory technicians (8, 9). In the effort to develop an alternative diagnostic method, Hyris Ltd. is offering an innovative and comprehensive product for COVID-19 testing in the form of the Hyris system implemented with a new diagnostic assay for SARS-CoV-2. In this study, we examined the sensitivity and specificity of the direct real-time RT-PCR method (without RNA extraction) of the bKIT Virus Finder COVID-19. Furthermore, we assessed the influence of swab transport medium on rRT-PCR performance, demonstrating that the limit of viral detection is highly affected by the use of saline solution storage medium compared to universal transport medium (UTM), as previously reported by other competitors (7). We showed that Hyris bKIT Virus Finder COVID-19 assays provide an efficiency similar to that of the comparator without risks of cross-reaction effects or false-negative results, supporting sensitivity parameters described during preliminary studies (10, 11). Importantly, the simplicity and diagnostic quality standards of the bKIT Virus Finder COVID-19 make the Hyris system ideal for a SARS-CoV-2 rapid diagnosis.

RESULTS

Sensitivity performance of bKIT Virus Finder COVID-19. The sensitivity of the bKIT Virus Finder COVID-19 detection kit was evaluated at an early step by determining the limit of detection (LoD) on both live SARS-CoV-2 virus and a defined number of viral genome copies. Live virus was diluted in pools of previously tested negative NPS and BAL matrices in order to obtain a final virus titer ranging from 1×10^4 50% tissue culture infective doses ($TCID_{50}$/ml) down to 1 $TCID_{50}$/ml. Each viral dilution was tested in triplicate by using a modified run protocol without the automatic interpretation of results, which allowed the performance of these types of tests, assessing the cycle threshold (C_T) values of each sample. Since the amplification protocol consists of 45 PCR cycles, a sample with a C_T value of 40 or below was considered positive, and thus all samples with a C_T of ≥40 were excluded from the trial. A tentative LoD of 10 $TCID_{50}$/ml was assumed for both BALs and NPSs. Thus, 10 $TCID_{50}$/ml represented the limit of the viral dilution that tested positive with both targets (reaction mix 1 and reaction mix 2) in all replicates, displaying a mean C_T value below the set limit (Tables 1 and 2). The LoD was further confirmed by 20 repetitions of the previously identified tentative LoD. The NPSs displayed mean C_T values of 36.746 ± 0.344 (95% confidence interval [CI], 36.402 to 37.090) for mix 1 and 37.346 ± 0.318 (95% CI, 37.029 to 37.664) for mix 2, while in the BAL

TABLE 2 CIs of LoD of the bKIT Virus Finder COVID-19 assay in NPS or BAL negative matrices

Sample	Mix	LoD (95% CI)
NPS	Mix 1	36.746 ± 0.344 (36.402–37.090)
	Mix 2	37.3465 ± 0.318 (37.029–37.664)
	RNase P	25.009 ± 0.0436 (24.965–25.053)
BAL	Mix 1	32.94894737 ± 0.256 (32.693–33.205)
	Mix 2	34.325 ± 0.207 (34.118–34.532)
	RNase P	24.5455 ± 0.152 (24.394–24.697)

matrix, the C_T values were 32.948 ± 0.256 (95% CI, 32.693 to 33.205) and 34.325 ± 0.207 (95% CI, 34.118 to 34.532) for mix 1 and mix 2, respectively (Tables 1 and 2). The high sensitivity of the test was further confirmed by determining the LoD for viral genome copies. In this case, the limit of detection of the bKIT Virus Finder COVID-19 was set to 10 copies/μl for both NPS and BAL matrices (Table 3). Indeed, both reaction mixes (mix 1 and mix 2) detected up to 10 copies/μl of viral target with a mean C_T of 36.640 ± 3.97 (95% CI, 32.473 to 40.806) and 36.070 ± 3.40 (95% CI, 32.501 to 39.638), respectively. In contrast, reaction mix 2 displayed a lower sensitivity at a lower dilution (2 copies/μl) of SARS-CoV-2 RNA (Table 3).

Specificity features of the new diagnostic assay. The diagnostic specificity of the bKIT Virus Finder COVID-19 was also evaluated to check cross-reactivity against pathogens normally present in the upper respiratory tract. For analytical specificity evaluation, clinical specimens, culture isolates, or purified nucleic acids were added to NPS or BAL native matrix to determine cross-reactivity in three replicates. As reported in Table 4, the bKIT Virus Finder COVID-19 did not show potential false-positive RT-PCR results, especially with closely related SARS and Middle East respiratory syndrome (MERS) coronaviruses. Moreover, no interference in the detection of positive samples ($n = 8$) was noticed when commonly used substances, such as oseltamivir, mupirocin, tobramycin, fluticasone, blood, oxymetazoline, and Tonimer, were added (Table 5). Likewise, the same substances failed to positively interfere with the test when added to negative samples ($n = 8$). Thus, specificity and sensitivity parameters required for diagnostic purposes of the bKIT Virus Finder COVID-19 were fully confirmed.

Diagnostic potential of the Hyris assay. To evaluate the diagnostic performance of the bKIT Virus Finder COVID-19 assay, samples previously confirmed positive by a real-time PCR comparator assay were selected and retested with the Hyris system for SARS CoV-2. In total, 76 NPSs, of which 51 were ESwabs and 25 were in standard UTM transport medium, were collected and included in the trial for comparison. Among them, two (2/51) of the ESwab positive samples were detected as negative for SARS-CoV-2 RNA, while the RNase P internal control was successfully amplified, suggesting a partial degradation of the viral genome. Indeed, repetition of the test with a comparator assay confirmed the absence of viral target. Thus, these two samples were omitted from the final statistical evaluation. Regarding the remaining 49 specimens, a concordance of 100% (49/49) was obtained with respect to the comparator data (Tables 6 and 7). However, a discrepancy in the over-

TABLE 3 Diagnostic sensitivity evaluated by testing serial dilutions of standard viral genome copies

Sample	SARS-CoV-2 (copies/μl)	C_T (mean $\pm$ SD)		
		Mix 1	Mix 2	RP
NPS	20	37.23 ± 0.91	38.61 ± 1.29	25.39 ± 0.04
	10	39.44 ± 1.58	38.47 ± 0.49	25.3 ± 0.007
	2	39.46	N/A	25.2 ± 0.03
	1	41.95 ± 1.83	N/A	25.18 ± 0.04
BAL	20	32.83 ± 0.34	32.77 ± 0.30	23.52 ± 0.46
	10	33.83 ± 0.10	33.66 ± 0.03	23.47 ± 0.17
	2	35.39	N/A	23.40 ± 0.27
	1	N/A	N/A	23.32 ± 0.25

TABLE 4 Specificity of the Hyris assay assessed by testing the reaction mixes with pathogens commonly present in the upper respiratory tract

	No. of positive results/total no. (%)			
Pathogen	Reaction mix 1		Reaction mix 2	
Adenovirus	0/3 (0)	0/3 (0)	0/3 (0)	0/3 (0)
Metapneumovirus	0/3 (0)	0/3 (0)	0/3 (0)	0/3 (0)
Influenza A virus	0/3 (0)	0/3 (0)	0/3 (0)	0/3 (0)
Influenza B virus	0/3 (0)	0/3 (0)	0/3 (0)	0/3 (0)
Respiratory syncytial virus	0/3 (0)	0/3 (0)	0/3 (0)	0/3 (0)
Enterovirus	0/3 (0)	0/3 (0)	0/3 (0)	0/3 (0)
Rhinovirus	0/3 (0)	0/3 (0)	0/3 (0)	0/3 (0)
Parainfluenza virus 1 to 4	0/3 (0)	0/3 (0)	0/3 (0)	0/3 (0)
Mycoplasma pneumoniae	0/3 (0)	0/3 (0)	0/3 (0)	0/3 (0)
Pneumocystis jirovecii	0/3 (0)	0/3 (0)	0/3 (0)	0/3 (0)
Chlamydia pneumoniae	0/3 (0)	0/3 (0)	0/3 (0)	0/3 (0)
Streptococcus pneumoniae	0/3 (0)	0/3 (0)	0/3 (0)	0/3 (0)
Streptococcus pyogenes	0/3 (0)	0/3 (0)	0/3 (0)	0/3 (0)
Mycobacterium tuberculosis	0/3 (0)	0/3 (0)	0/3 (0)	0/3 (0)
Pseudomonas aeruginosa	0/3 (0)	0/3 (0)	0/3 (0)	0/3 (0)
Candida albicans	0/3 (0)	0/3 (0)	0/3 (0)	0/3 (0)
Staphylococcus epidermidis	0/3 (0)	0/3 (0)	0/3 (0)	0/3 (0)
Streptococcus salivarius	0/3 (0)	0/3 (0)	0/3 (0)	0/3 (0)
Bordetella pertussis	0/3 (0)	0/3 (0)	0/3 (0)	0/3 (0)
Legionella pneumoniae	0/3 (0)	0/3 (0)	0/3 (0)	0/3 (0)
Pooled human nasal wash	0/3 (0)	0/3 (0)	0/3 (0)	0/3 (0)
Pooled SARS-CoV and MERS-CoV	0/3 (0)	0/3 (0)	0/3 (0)	0/3 (0)
Pooled OC43, NL63, 229E, and HKU-1CoVs	0/3 (0)	0/3 (0)	0/3 (0)	0/3 (0)

all cycle threshold (C_T) values was noticed for most of the ESwabs tested with the Hyris system, with a mean C_T of 27.7 ± 4.52 (95% CI, 26.332 to 29.068) for mix 1 ($P < 0.0001$) and 28.94 ± 5.05 (95% CI, 27.488 to 30.391) for mix 2 ($P < 0.0001$), relative to the comparator C_T value of 20.46 ± 3.78 (95% CI, 19.31 to 21.60) (Tables 6 and 7). In contrast, NPSs collected in the UTM medium, all (25/25) confirmed positive, provided results overlapping with the comparator values, with a mean C_T of 28.74 ± 6.66 (95% CI, 25.990 to 31.489) ($P = 0.660$) and 30.01 ± 6.99 (95% CI, 27.124 to 32.895) ($P = 0.287$) for reaction mix 1 and 2, respectively (Tables 6 and 7). Although a direct comparison of C_T values obtained with different assays is not appropriate, our data suggested that samples collected in UTM provide greater accuracy than those obtained using ESwab. Along with NPSs, a few BAL samples were included in the trial. Among them, only two (33.3%) were detected as positive, while the remaining samples were considered negative (2/6; 33.3%), since the viral genome was not recognized or was indeterminate (2/6; 33.3%) as the RNase P internal control probe was not reacting, suggesting a complete degradation of the clinical sample (Table 8). Similar results were obtained with the comparator assay. Finally, to confirm the diagnostic specificity of the new diagnostic platform, 100 NPSs confirmed SARS-CoV-2 negative were further

TABLE 5 Assessment of false-negative results risk

	C_T (mean ± SD)					
	Reaction mix 1		Reaction mix 2		RP	
Substance	Untreated	Treated	Untreated	Treated	Untreated	Treated
Oseltamivir	25.28 ± 3.12	25.31 ± 2.58	26.14 ± 2.68	26.30 ± 2.81	25.98 ± 2.14	26.23 ± 2.27
Mupirocin	25.28 ± 3.12	25.80 ± 2.78	26.09 ± 2.72	26.80 ± 3.03	25.98 ± 2.14	26.33 ± 2.23
Tobramycin	25.22 ± 3.17	24.38 ± 1.58	26.11 ± 2.70	25.23 ± 2.20	26.15 ± 2.08	26.34 ± 2.18
Fluticasone	25.20 ± 3.18	25.40 ± 2.51	26.14 ± 2.68	26.15 ± 2.96	26.00 ± 2.13	26.84 ± 1.61
Blood	25.20 ± 3.18	25.03 ± 2.61	26.14 ± 2.68	24.98 ± 9.08	26.00 ± 2.13	26.16 ± 1.97
Oxymetazoline	25.20 ± 3.18	25.26 ± 2.50	26.14 ± 2.68	25.64 ± 9.28	26.00 ± 2.13	26.18 ± 2.19
Tonimer	25.20 ± 3.18	25.04 ± 2.63	26.14 ± 2.68	25.11 ± 9.08	26.00 ± 2.13	26.31 ± 2.40

TABLE 6 Diagnostic sensitivity and specificity evaluation of retrospective positive and negative samples

Parameter and sample type	No. of positive samples/total no. (%)	No. of negative samples/total no. (%)
Sensitivity		
ESwab	49/49 (100)	0/49
UTMs	25/25 (100)	0/25 (0)
BALs	2/4 (50)	2/4 (50)
Specificity		
ESwab	0/100 (0)	100/100 (100)

investigated by the bKIT Virus Finder COVID-19 assay. Total accordance with the standard procedure (Seegene assay) was shown for detection of negative samples (0/100; 0%) (Tables 6 and 7).

DISCUSSION

Diagnostic performance of COVID-19 assays is the major limiting aspect of diagnostic procedures for SARS-CoV-2. Moreover, timely detection of symptomatic and asymptomatic infected subjects is crucial for stopping virus spread and for limiting its diffusion in the population, especially to vulnerable people suffering from preexisting injuries or the elderly (12). Based on these observations, it is critical that diagnostic procedures are as accurate as possible and provide results in a rapid manner to promptly isolate infected patients (8, 9, 13). Rapid tests for COVID-19 infection without underestimated diagnostic performance are urgently needed, as reported in European Directive 98/79/EC on *in vitro* diagnostic device (IVDD) guidelines (14–16). In the present study, the bKIT Virus Finder COVID-19 was evaluated, and its feasible application in routine diagnostic procedures was confirmed. Sensitivity was first evaluated based on the limit of detection (LoD) of the bKIT Virus Finder COVID-19 assay on both nasopharyngeal swabs (NPSa) and bronchoalveolar lavage fluid (BAL) samples. Our test evaluation completely satisfied sensitivity parameters. Indeed, the LoD was set with both viral N1 and N2 targets at 10 $TCID_{50}$/ml either in NPS or in BAL. These data completely fit with the LoD reported in viral copies number. Indeed, the Hyris direct qRT-PCR method showed a viral LoD of 10 copies/μl, confirming the high sensitivity of the test. False-negative results were obtained mainly because of improper specimen collection or degradation of the viral RNA during shipping or storage. Moreover, some automatic systems for SARS CoV-2 molecular testing could be affected by the presence of high salt content in NPS transport medium, such as ESwab, providing false-negative results (7, 17). Thus, the use of NPS in UTM is strongly recommended. We noticed that the saline diluent (ESwab) for NPSs could affect the results, providing C_T values higher than those obtained using UTM buffer, because of their different compositions. Therefore, we recommend the use of UTM for this system, since it better fits the gold standard parameters of the reaction. Nevertheless, in this trial, most of the clinical specimens tested using bKIT Virus Finder COVID-19, although in saline solution (ESwab), were correctly diagnosed, offering added value to this diagnostic system. Moreover, specificity (cross-reactivity) was absent, based on the analysis of several pathogens commonly present in the upper respiratory tract. Most importantly, the Hyris assay did not show reactivity with other human coronaviruses, including OC43, NL63, 229E, and HKU-1 strains, and

TABLE 7 Comparison of C_T values of ESwabs and UTMs

bKIT mix or comparator	Mean C_T ± SD (95% CI)	
	ESwabs	UTMs
Reaction mix 1	27.7 ± 4.52 (26.33–29.06)	28.74 ± 6.66 (25.99–31.48)
Reaction mix 2	28.94 ± 5.05 (27.48–30.39)	30.01 ± 6.99 (27.12–32.89)
Comparator	20.46 ± 3.78 (19.31–21.60)	27.89 ± 6.94 (25.02–30.75)

TABLE 8 Results evaluation based on sample reactivity with the two virus-specific (mix 1 and mix 2) probes and the internal control (RNase P) probe[a]

Result	Reaction mix 1	Reaction mix 2	RNase P
Positive	Pos	Pos	Pos
Negative	Neg	Neg	Pos
Inconclusive	Pos (Neg)	Neg (Pos)	Pos (Pos)
Indeterminate	Neg	Neg	Neg

[a]Results in parentheses indicate possible combinations of data leading to inconclusive diagnosis.

the two SARS-CoV-2-related pandemic coronaviruses, SARS-CoV and MERS-CoV. The addition of an endogenous human RNase P gene (RP) as an internal control of the assay enabled the correct evaluation of the quality of swab sampling. Although the new kit was tested on few BAL specimens, our data demonstrated that the Hyris approach is suitable for COVID-19 diagnosis in samples other than NPSs, as long as the samples are timely processed or properly stored. In conclusion, the bKIT Virus Finder COVID-19 direct qRT-PCR by Hyris can be considered a valid and rapid diagnostic tool, providing the advantage of a less complex and unambiguous results interpretation. Moreover, the use of the Hyris platform provides the advantage of using a webpage connected to the instruments that allows remote interpretation and validation of results.

MATERIALS AND METHODS

Sample collection. SARS-CoV-2-positive samples represented by nasopharyngeal swabs (NPSs) in both universal transport medium (UTM; Copan, Brescia, Italy) ($n = 25$) and modified liquid Amies (ESwab; Copan) ($n = 49$) were collected during the first (March to April 2020) and the second (September to October 2020) pandemic periods at the Azienda Ospedaliera Universitaria Senese Santa Maria alle Scotte Hospital in Siena, Italy. Based on comparator results with the Allplex SARS-CoV-2 assay (Seegene Inc., Seoul, Republic of Korea), we selected samples with C_T values ranging from 10 to 37. One hundred previously tested negative samples were selected to evaluate the specificity of the new nucleic acid-based technology. The use of the samples was explicitly authorized for research purposes by patients at the time of their biological sampling; the study protocol (DR20003) was reviewed by the local Institutional Ethics Review Board (IERB) of the AOU Hospital of Siena (Italy), and a "favorable opinion" was expressed. The samples retrieved for the new test were anonymized and numbered in sequence. Pools of negative NPS or bronchoalveolar lavage fluid (BAL) were prepared for further validation assays. All samples were stored at −80°C until tested by the Hyris kit.

bKIT Virus Finder COVID-19 assay. The bKIT Virus Finder COVID-19 amplification kit was intended for use with the bCUBE instrument (Hyris Ltd.). The diagnostic procedure was based on extraction-free real-time RT-PCR by using reaction mix 1 and mix 2 containing reverse transcriptase, DNA polymerase, RNase inhibitor, buffer with magnesium chloride, deoxynucleoside triphosphates (dNTPs), and two 6-carboxyfluorescein (FAM)-labeled fluorescent probes/primers targeting different sequences of the SARS-CoV-2 N gene (reaction mix 1 and reaction mix 2). An internal control was represented by amplification of the human RNase P gene (RP) with a HEX (6-carboxy-2,4,4,5,7,7-hexachlorofluorescein)-labeled fluorescent probe present in reaction mix 1. The testing procedure required the loading into two reaction wells of a bCUBE 16-well cartridge of each sample (5 μl) in both reaction mixes (15 μl). Positive and negative controls were also loaded in both reaction mixes. The cartridge was sealed with adhesive film in order to avoid liquid evaporation and cross-contamination among samples and the positive control. Samples and controls were loaded on the cartridge in accordance with the manufacturer's instructions (Fig. 1). The prepared cartridge was then slotted into the bCUBE, and the experiment was run by standard protocol as defined by the manufacturer. Results were obtained within 2 h and expressed as described in Table 8.

Pathogenic microorganisms and cross-reactivity assay. *Mycobacterium tuberculosis* DNA, purified from a clinical sample, was kindly provided by F. Santoro (Laboratory of Molecular Microbiology and Biotechnologies, S. Maria delle Scotte University Hospital, Siena). *Mycoplasma pneumoniae*, *Pneumocystis jirovecii*, *Chlamydia pneumoniae* genomic DNA, and HKU-1 human coronavirus (CoV) genomic RNA were purified by the EZ1 system (Qiagen, Milan, Italy) from clinical samples collected at the Microbiology and Virology Unit of the S. Maria delle Scotte University Hospital in Siena. Whole genomic RNA for OC43, NL63, and 229E CoV strains and highly pathogenic SARS-CoV and MERS-CoV were purchased from the European Virus Archive (EVAg; reference number SKU 011N-03). Preliminary quality tests for purified nucleic acids were done by conventional RT-PCR or PCR. The minimum amount of DNA/RNA giving a detectable signal ($C_T \leq$ 35) was selected for further analysis with the bKIT Virus Finder COVID-19. The selected volume of nucleic acids was directly added to the NPS and BAL negative matrices for cross-reactivity screening. Pools of SARS/MERS-CoV or OC43, NL63, 229E, and HKU-1 CoV extracts were tested. In the event of a positive result, each pathogen was individually tested to identify which one was responsible for cross-reactivity. Where applicable, virus cultures were directly added to negative matrices (NPS or BAL) to a minimum concentration of 1×10^4 TCID$_{50}$/ml. Bacteria were collected from freshly streaked plates and diluted in sterile isotonic solution to a final concentration of 1×10^8 CFU/ml by using the McFarland method. After predilution in sterile isotonic solution, 1×10^6 CFU/ml were inoculated in both negative matrices.
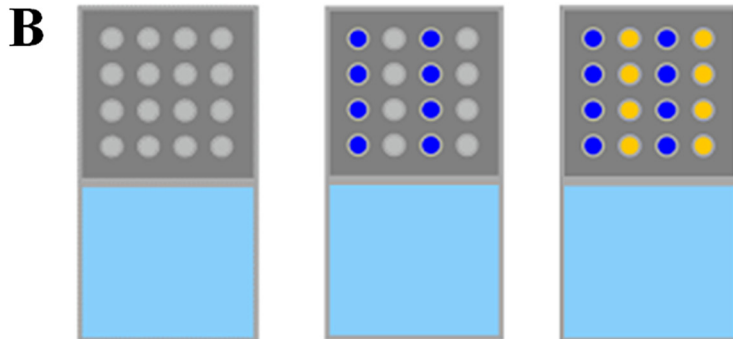
FIG 1 Scheme of the Hyris bCUBE cartridge. Clinical samples and positive and negative controls should be loaded on the cartridge two times, as shown by the cartridge layout (A) for testing with reaction mix 1 (blue) and reaction mix 2 (yellow) (B). Evaluation of results is automatically performed, matching all the included controls in order to avoid the generation of false-positive or false-negative data.

Limit of detection. SARS-CoV-2 was isolated at the University Hospital Santa Maria alle Scotte of Siena (Tuscany, Italy) from a nasopharyngeal swab seeded on Vero E6 cells (ATCC CRL-1586). Virus isolate Siena-1/2020 was fully sequenced and annotated in GenBank (accession no. MT531537). Live viral stock was used to test the sensitivity of the bKIT Virus Finder COVID-19 assay by limit of detection (LoD). Sample preparation was performed in a biosafety level 3 (BSL3) laboratory by serial dilution of the virus in NPS or BAL negative matrix starting from 1×10^5 to 10 $TCID_{50}$/ml. Three repeats for each dilution were tested in the trial, and the tentative LoD of the assay was determined as the lowest detectable virus titer at which >95% of replicates tested positive. The LoD of the assay was confirmed by 20 repeats of the tentative LoD. The significance of the results was evaluated by the 95% confidence interval. The limit of detection (LoD) was further evaluated on the SARS-CoV-2 RNA standard (Exact Diagnostics, TX, USA). The reference RNA standard was serially diluted (ranging from 20 to 1 copy/μl) in negative NPS or BAL matrices before bKIT Virus Finder COVID-19 test assessment. Results are presented as the mean C_T value $\pm$ standard deviation (SD) of two independent trials.

Interference assay. Eight retrospective known positive specimens and 8 known negative specimens were tested again with and without the addition of potential interfering substances. Mupirocin, tobramycin, and oseltamivir were purchased from Sigma-Aldrich (Milan, Italy). Stock solutions were prepared according to the manufacturer's instructions and then diluted to 6.6 mg/ml, 4 μg/ml, and 3.3 mg/ml, respectively, in the matrices. Commercial pharmaceutical formulations containing oxymetazoline (Vicks Sinex), fluticasone (Flixonase), and isotonic saline solution (Tonimer Lab) have been used as a source of the corresponding interfering substances. Each pharmaceutical product was diluted in the positive or negative matrices to 15% (vol/vol), 5% (vol/vol), and 5% (vol/vol) final concentrations. Whole blood containing anticoagulant was drawn from healthy donors and diluted in sterile physiological saline solution to obtain a 20% (vol/vol) stock solution and then to 2% (vol/vol) in the matrices. Each positive sample added with the potentially interfering substance was tested in triplicate, while each negative sample added with the interfering substance was tested in a single replicate. Results are presented as the mean $\pm$ standard deviation (SD) of C_T values.

REFERENCES

1. Rong XM, Yang L, Chu HD, Fan M. 2020. Effect of delay in diagnosis on transmission of COVID-19. Math Biosci Eng 17:2725–2740. https://doi.org/10.3934/mbe.2020149.
2. Lilleri D, Zavaglio F, Gabanti E, Gerna G, Arbustini E. 2020. Analysis of the SARS-CoV-2 epidemic in Italy: the role of local and interventional factors in the control of the epidemic. PLoS One 15:e0242305. https://doi.org/10.1371/journal.pone.0242305.
3. Sethuraman N, Jeremiah SS, Ryo A. 2020. Interpreting diagnostic tests for SARS-CoV-2. JAMA 323:2249–2251. https://doi.org/10.1001/jama.2020.8259.
4. Li C, Zhao C, Bao J, Tang B, Wang Y, Gu B. 2020. Laboratory diagnosis of coronavirus disease-2019 (COVID-19). Clin Chim Acta 510:35–46. https://doi.org/10.1016/j.cca.2020.06.045.
5. Dinnes J, Deeks JJ, Berhane S, Taylor M, Adriano A, Davenport C, Dittrich S, Emperador D, Takwoingi Y, Cunningham J, Beese S, Domen J, Dretzke J, Ferrante di Ruffano L, Harris IM, Price MJ, Taylor-Phillips S, Hooft L, Leeflang MM, McInnes MD, Spijker R, Van den Bruel A, Cochrane COVID-19 Diagnostic Test Accuracy Group. 2021. Rapid, point-of-care antigen and molecular-based tests for diagnosis of SARS-CoV-2 infection. Cochrane

Database Syst Rev 3:CD013705. https://doi.org/10.1002/14651858.CD013705 .pub2.

6. Cobb B, Simon CO, Stramer SL, Body B, Mitchell PS, Reisch N, Stevens W, Carmona S, Katz L, Will S, Liesenfeld O. 2017. The cobas 6800/8800 system: a new era of automation in molecular diagnostics. Expert Rev Mol Diagn 17:167–180. https://doi.org/10.1080/14737159.2017.1275962.

7. Merindol N, Pépin G, Marchand C, Rheault M, Peterson C, Poirier A, Houle C, Germain H, Danylo A. 2020. SARS-CoV-2 detection by direct rRT-PCR without RNA extraction. J Clin Virol 128:104423. https://doi.org/10.1016/j.jcv .2020.104423.

8. Michael J Loeffelholz MJ, Alland D, Butler-Wu SM, Pandey U, Perno CF, Nava A, Carroll KC, Mostafa H, Davies E, McEwan A, Rakeman JL, Fowler RC, Pawlotsky JM, Fourati S, Banik S, Banada PP, Swaminathan S, Chakravorty S, Kwiatkowski RW, Chu VC, Kop J, Gaur R, Sin MLY, Nguyen D, Singh S, Zhang N, Persing DH. 2020. Multicenter evaluation of the Cepheid Xpert Xpress SARS-CoV-2 test. J Clin Microbiol 58:e00926-20. https://doi.org/10 .1128/JCM.00926-20.

9. Zhen W, Smith E, Manji R, Schron D, Berry GJ. 2020. Clinical evaluation of three sample-to-answer platforms for detection of SARS-CoV-2. J Clin Microbiol 58:e00783-20. https://doi.org/10.1128/JCM.00783-20.

10. Miscio L, Olivieri A, Labonia F, De Feo G, Chiodini P, Portella G, Atripaldi L, Parrella R, Conenna R, Buonaguro FM, Cavalcanti E, Ascierto P, Botti G, Bianchi A. 2020. Evaluation of the diagnostic accuracy of a new point-of-care rapid test for SARS-CoV-2 virus detection. J Transl Med 18:488. https://doi.org/10.1186/s12967-020-02651-y.

11. Martinelli F, Perrone A, Della Noce I, Colombo L, Lo Priore S, Romano S. 2020. Application of a portable instrument for rapid and reliable detection of SARS-CoV-2 infection in any environment. Immunol Rev 295(Suppl s1):4–10. https://doi.org/10.1111/imr.12857.

12. CDC. 2020. Groups at higher risk for severe illness. Centers for Disease Control and Prevention, Atlanta, Georgia. https://www.cdc.gov/coronavirus/2019 -ncov/community/health-equity/racial-ethnic-disparities/disparities-illness.html. Accessed 10 December 2020.

13. Tang YW, Schmitz JE, Persing DH, Stratton CW. 2020. Laboratory diagnosis of COVID-19: current issues and challenges. J Clin Microbiol 58: e00512-20. https://doi.org/10.1128/JCM.00512-20.

14. Anonymous. 1998. Direttiva 98/79/Ce Del Parlamento Europeo E Del Consiglio del 27 ottobre 1998, relativa ai dispositivi medico-diagnostici in vitro. Gazzetta ufficiale delle Comunità europee, L 331/1, 7.12.1998.

15. European Commission. 2020. Current performance of COVID-19 test methods and devices and proposed performance criteria. Working Document of Commission Services. European Commission, Brussels, Belgium.

16. European Commission. 2016. Guidelines on medical devices MEDDEV 2.7/1 rev. 4. Clinical evaluation: a guide for manufacturers and notified bodies under directives 93/42/EEC and 90/385/EEC. European Commission, Brussels, Belgium.

17. Liu M, Li Q, Zhou J, Ai W, Zheng X, Zeng J, Liu Y, Xiang X, Guo R, Li X, Wu X, Xu H, Jiang L, Zhang H, Chen J, Tian L, Luo J, Luo C. 2020. Value of swab types and collection time on SARS-COV-2 detection using RT-PCR assay. J Virol Methods 286:113974. https://doi.org/10.1016/j.jviromet.2020.113974.

SARS-CoV-2 N Protein Targets TRIM25-Mediated RIG-I Activation to Suppress Innate Immunity

Gianni Gori Savellini [1,*] **, Gabriele Anichini** [1] **, Claudia Gandolfo** [1] **and Maria Grazia Cusi** [1,2]

1 Department of Medical Biotechnologies, University of Siena, 53100 Siena, Italy;
   gabriele.anichini@student.unisi.it (G.A.); claudia.gandolfo@unisi.it (C.G.); mariagrazia.cusi@unisi.it (M.G.C.)
2 "S. Maria delle Scotte" Hospital, Viale Bracci, 1, 53100 Siena, Italy
* Correspondence: gianni.gori@unisi.it

Abstract: A weak production of INF-β along with an exacerbated release of pro-inflammatory cytokines have been reported during infection by the novel SARS-CoV-2 virus. SARS-CoV-2 encodes several proteins able to counteract the host immune system, which is believed to be one of the most important features contributing to the viral pathogenesis and development of a severe clinical picture. Previous reports have demonstrated that SARS-CoV-2 N protein, along with some non-structural and accessory proteins, efficiently suppresses INF-β production by interacting with RIG-I, an important pattern recognition receptor (PRR) involved in the recognition of pathogen-derived molecules. In the present study, we better characterized the mechanism by which the SARS-CoV-2 N counteracts INF-β secretion and affects RIG-I signaling pathways. In detail, when the N protein was ectopically expressed, we noted a marked decrease in TRIM25-mediated RIG-I activation. The capability of the N protein to bind to, and probably mask, TRIM25 could be the consequence of its antagonistic activity. Furthermore, this interaction occurred at the SPRY domain of TRIM25, harboring the RNA-binding activity necessary for TRIM25 self-activation. Here, we describe new findings regarding the interplay between SARS-CoV-2 and the IFN system, filling some gaps for a better understanding of the molecular mechanisms affecting the innate immune response in COVID-19.

Keywords: innate immunity; SARS-CoV-2 N protein; RIG-I activation

1. Introduction

Coronaviruses (CoVs) are a large family of single-stranded, positive-sense RNA viruses that belong to the family *Coronaviridae* [1,2]. Coronavirus has a large RNA genome consisting of the open reading frames (ORFs) 1a and 1b encoding for two polyproteins which are proteolytically cleaved into 16 nonstructural proteins (nsp1–16) that play pivotal roles in the life cycle of CoVs [3–6]. Almost one-third of the viral genome consists of genes encoding structural proteins, including spike (S), envelope (E), membrane (M), and nucleocapsid (N) proteins. Additionally, the CoVs contain accessory proteins encoded by ORFs located at the 3′ end of their genome [5,6]. Coronaviruses can infect humans and animals (bats, mice and birds) [7,8]; among them, CoV-229E, CoV-OC43, CoV-NL63, CoV-HKU1, SARS-CoV and MERS-CoV have been associated with human diseases [7–10]. Furthermore, SARS-CoV and MERS-CoV caused severe respiratory illness during the 2002–2003 and 2012 epidemics, respectively [11–14]. The outbreak of the novel coronavirus SARS-CoV-2, which emerged at the end of 2019, is currently spread worldwide, and the World Health Organization (WHO) declared it a pandemic in March 2020 [15]. SARS-CoV-2 causes coronavirus disease 2019 (COVID-19), which includes a variable spectrum of symptoms, ranging from mild influenza-like syndrome to severe pneumonia, acute respiratory distress and even death [16–22]. In general, the population that is most affected by COVID-19 are adults, as well as those with pre-existing chronic diseases [23,24]. However, neonates and children can also be infected by SARS-CoV-2 [25]. Many young people or healthy subjects develop asymptomatic or pauci-symptomatic infection with

a high risk of human-to-human transmission [26–29]. SARS-CoV-2 infection mainly targets the respiratory tract. Differences in transmissibility and viral shedding suggest that SARS-CoV-2 significantly differs from other epidemic coronaviruses [29–31]. SARS-CoV and MERS-CoV have tropism for the lower respiratory tract, whereas the emergent SARS-CoV-2 virus presents with high viral load in the upper respiratory tract [30,31]. The type I interferon-mediated immune response represents the first line of host defense against viral infection [32]. Viral pathogen-associated molecular patterns (PAMPs), such as viral mRNA and dsRNAs, are produced during early virus infection/replication and recognized by pattern recognition receptors (PRPs), including retinoic-acid inducible gene-I (RIG-I), melanoma differentiation-associated protein 5 (MDA-5) and Toll-like receptors (TLRs) [33]. Both RIG-I and MDA-5 contain two N-terminal caspase activation and recruitment domains (CARDs) that enable interaction with the mitochondrial adaptor protein MAVS [34–42] which, in turn, triggers the activation of transcription factors (IRF-3/7; NF-kB and AP-1) involved in IFN expression [34–37]. Ubiquitination by TRIM25 is a well-characterized regulatory mechanism of RIG-I [36–42]: the delivery of K63-linked ubiquitin moiety by TRIM25 to the lysine residue at position 172 on RIG-I N-terminal first CARD domain (RIG-IN) results in a marked increase in RIG-I downstream signaling activity [38,39]. Moreover, recent data have demonstrated that unanchored K63 poly-ubiquitin chains play a fundamental role in the full stabilization and activation of the RIG-I tetramer [42]. In order to overcome this first-line defense implemented by the host, viruses have evolved by expressing protein(s) able to block IFN-β production and its downstream activity at different steps in the signaling cascade.

SARS-CoV and MERS-CoV are known to produce several proteins with antagonistic properties on the interferon signaling. Papain-like protease (PLPro), ORF8b, the nucleocapsid (N), and the ORF3b proteins are well-characterized interferon antagonists [43–51].

The SARS-CoV N protein was found to abrogate the activity of the transcription factors IRF3 and NF-κB, resulting in the inhibition of IFN-β synthesis. Furthermore, the antagonistic nature of SARS-CoV N was achieved by hindering RIG-I ubiquitination and activation by TRIM25 [44,45]. A similar mechanism was also described for MERS-CoV [49], suggesting that the SARS-CoV N protein may target multiple factors to overcome the host immune system [50,51]. Different factors are involved in the induction of IFN-β production; therefore, they may act independently during different stages of the viral life cycle, rendering the antagonistic activity of the N protein indispensable as its structural activity in virus replication context. As in other coronaviruses, the nucleocapsid protein is one of the most crucial structural components of the SARS-CoV-2 virus. Hence, major attention has been focused on the characterization of this protein. Studies conducted by other groups have elucidated the IFN-β antagonistic function of this protein [52,53].

In COVID-19 infection, a low induction of type I interferons was detected in the peripheral blood or lungs of patients with a severe clinical picture [54–56]. Thus, the expression of SARS-CoV-2 proteins with suppressive activity on innate immunity was analyzed, and a detailed study evidenced the antagonistic properties of some viral proteins [57–62]. More details are still needed in order to understand the molecular mechanism residing on SARS-CoV2 escape from the host immune system. For this reason, this study focused on the investigation of the mechanism by which the nucleoprotein N of SARS-CoV2 circumvents IFN-α/β secretion.

2. Materials and Methods

2.1. Cells, Virus and Chemicals

Human embryonic kidney Lenti-X 293T cells (Clontech, Milan, Italy) were cultured in Dulbecco's modified Eagle's medium (DMEM) (Lonza, Milan, Italy) supplemented with 100 U/mL penicillin/streptomycin (Hyclone Europe, Milan, Italy) and 10% heat-inactivated fetal calf serum (FCS) (Lonza, Basel, Switzerland), respectively, at 37 °C. SARS-CoV-2 was isolated on Vero E6 cells (ATCC CRL-1586) from a clinical specimen in the Virology laboratory of "S. Maria alle Scotte" Hospital in Siena, Italy. Transfections were performed

using the jetPRIME Transfection Reagent (Polyplus, Illkirch, France). The proteasome inhibitor MG-132 was purchased from Merck Millipore.

2.2. Plasmids

Viral RNA was extracted from Vero E6 supernatant of SARS-CoV-2-infected cells using a QIAamp viral RNA mini kit (Qiagen, Hilden, Germany). The N (nt 28218-29477) coding gene was amplified by reverse transcriptase (RT)-polymerase chain reaction (PCR) from purified viral RNA with the following primers (Sigma-Aldrich, Milan, Italy): N BamHI sense 5′-CGCGGACCCCTCTGATAATGGACCCCAAAAT-3′ and N EcoRV antisense 5′-CCGGATATCTGATTAGGCCTGAGTTGAGTCAGC-3′, whereas the HA-tag containing TRIM25 SPRY domain was generated by PCR using the forward 5′-CCGCTCGAGAAGGTGCTGGAGACCTTCCTG-3′ and reverse 5′-ATAGTTTAGCGGCCG CCTAAGCGTAATCTGGAACATCGTATGGGTACTTGGGGGAGCAGA-3′ primers. The reaction was carried out using the SuperScript III One-Step RT-PCR with Platinum Taq (Life Technologies, Milan, Italy) by one cycle of reverse transcription at 55 °C for 30 min and 94 °C for 5 min followed by 40 cycles of PCR (1 min at 94 °C; 30 s at 60 °C; 1 min at 68 °C). The gene was cloned in pcDNA4HisMax-C plasmid (Life Technologies) in frame with the 6xHis tag or in pEF-Bos. The correct sequence of the constructs was confirmed by sequencing (Eurofins Genomics, Milan, Italy). The reporter plasmid encoding Firefly Luciferase downstream of the complete interferon-beta promoter (p125-Luc), the minimal interferon-beta promoter (p55A2) and the plasmids coding the FLAG-tagged RIG-I CARD domains (RIG-IN) were kindly provided by Prof. Takashi Fujita (Tokyo Metropolitan Institute of Medical Science, Tokyo, Japan). The FLAG-tagged human RIG-I and MDA-5 expression plasmids were kindly provided by Prof. A. García-Sastre (Mount Sinai School of Medicine, New York, NY, USA). The plasmids expressing human IRF3 and HA-tagged TRIM25 were kindly provided by L. Martinez-Sobrido (University of Rochester Medical Center School of Medicine and Dentistry, Rochester, NY, USA) and Hiroyuki Oshiumi (Graduate School of Medical Sciences, Kumamoto University, Kumamoto, Japan), respectively. The Renilla Luciferase reporter plasmid was purchased from Promega (Promega, Milan, Italy); HA-tagged K63-only ubiquitin mutant-expressing plasmid was from Addgene (Cambridge, MA, USA).

2.3. Transfection and Immunoblotting

Transient expression of the recombinant proteins was carried out using jetPRIME Transfection Reagent (Polyplus, Illkirch, France) following the manufacturer's instructions. Lenti-X 293T cells were seeded in a 6-well culture plate at a density of 1×10^6 cells per well and incubated at 37 °C in a 5% CO_2 atmosphere. The next day, cell monolayers were transfected with selected plasmids and cells were collected at 48 h post-transfection for protein analysis. Where necessary, protein concentration of the whole cell lysates was determined by BCA assay (Pierce, Milan, Italy). Fifty micrograms of total proteins were loaded on SDS-PAGE and, after being transferred to a NitroBind nitrocellulose membrane (Santa Cruz Biotechnology, Heidelberg, Germany), protein expression was detected using anti-Flag M2 (Merck-Millipore) (1:2000), anti-SARS-CoV-2 N rabbit polyclonal antibody (Life Technologies) (1:1000), anti-HA monoclonal antibody (Sigma-Aldrich, St. Louis, MO, USA) (1:1000) or anti-actin (BioLegend, London, UK) (1:500) as loading controls. Horseradish peroxidase (HRP)-conjugated secondary antibody (Merck-Millipore) (1:5000) was used as a secondary antibody. Quantitative comparisons among samples were performed by densitometric analysis using ImageJ software.

2.4. Co-Immunoprecipitations (Co-IP)

Lenti-X 293T cells were plated in 9 cm Petri dishes and transfected with 1 μg of RIG-I-expressing plasmid along with 0.2 μg of both TRIM25- and HA-ubiquitin K63-only-expressing plasmids. For protein ubiquitination detection, 36 h post-transfection exhausted medium was replaced with fresh DMEM supplemented with 1 μM of MG-132 proteasome

inhibitor. Samples were collected after additional 12 h. For immuno-precipitations, cell lysates were prepared in RIPA buffer (50 mM TrisHCl (pH 7.5); 150 mN NaCl; 1 mM EDTA; 1% Triton X-100) supplemented with a cOmplete anti-protease cocktail (Roche, Milan, Italy). Cleared lysates were incubated overnight at 4 °C with anti-FLAG M2 magnetic beads with gentle rotation. For RIG-I ubiquitination detection, denaturing immuno-precipitations were performed. Cell samples were lysed in 1% SDS by boiling for 10 min. Then, SDS was diluted to 0.1% final concentration with RIPA buffer supplemented with the cOmplete anti-protease cocktail (Roche, Milan, Italy). Proteins were captured with anti-FLAG M2 magnetic beads overnight at 4 °C, after which they were collected using a magnetic stand and extensively washed with phosphate buffered-solution (PBS). Bound proteins were eluted by boiling with 2× denaturing sample buffer, loaded on SDS-PAGE and probed by immunoblotting, as described above.

2.5. Luciferase Reporter Assay

For analyses, 2×10^5 Lenti-X 293T cells were seeded in 24-well plates and transfected with indicated plasmids, as previously described. Briefly, 0.2 µg of p125-FFLuc, 0.05 µg of RIG-I, MDA-5 or RIG-IN and, where indicated, 0.5 µg of N expressing plasmid were co-transfected. Where indicated, 50 ng of HA-TRIM25, HA-Riplet or hIRF3 plasmids were co-transfected. Empty plasmids were used to normalize the total amount of DNA. Twenty nanograms of pSV40-RL were co-transfected as internal controls. Thirty-six hours post-transfection, cells were stimulated by transfection with 2 µg/well of poly (I:C). After an additional 12 h, cells were collected and luciferase activities were measured on lysates using the Dual Luciferase reporter assay reagent (Promega, Madison, WI, USA), according to the manufacturer's instructions. Results are given as mean values of several experiments ± standard deviations (SD).

2.6. Statistics

The mean differences were statistically analyzed using GraphPad Prism 6 (GraphPad Software San Diego, CA, USA) by means of the Fisher test to compare prevalence rates among different study groups. Statistical significance was set at $p < 0.05$, and was two-tailed.

3. Results

3.1. SARS-CoV-2 N Protein Specifically Impairs RIG-I Signaling Pathway

Previous studies conducted on SARS-CoV-2 demonstrated that the N structural viral protein was able to suppress RIG-I-mediated IFN-β promoter activation, a key sensor of RNA virus infection [52]. A recent publication reported that SARS-CoV-2 virus N protein exhibited such behavior presumably due to its ability to bind RIG-I [53]. Here, we confirmed that SARS-CoV-2 N protein was able to block IFN-β promoter activation in a highly specific manner by inhibiting RIG-I, but not MDA-5, upon poly(I:C) stimulation. Indeed, the transient expression of the N protein in Lenti-X 293T cells affected the luciferase reporter gene expression when RIG-I ($p = 0.0016$) but not MDA-5 ($p = 0.205$) was over-expressed (Figure 1A, Table S1).
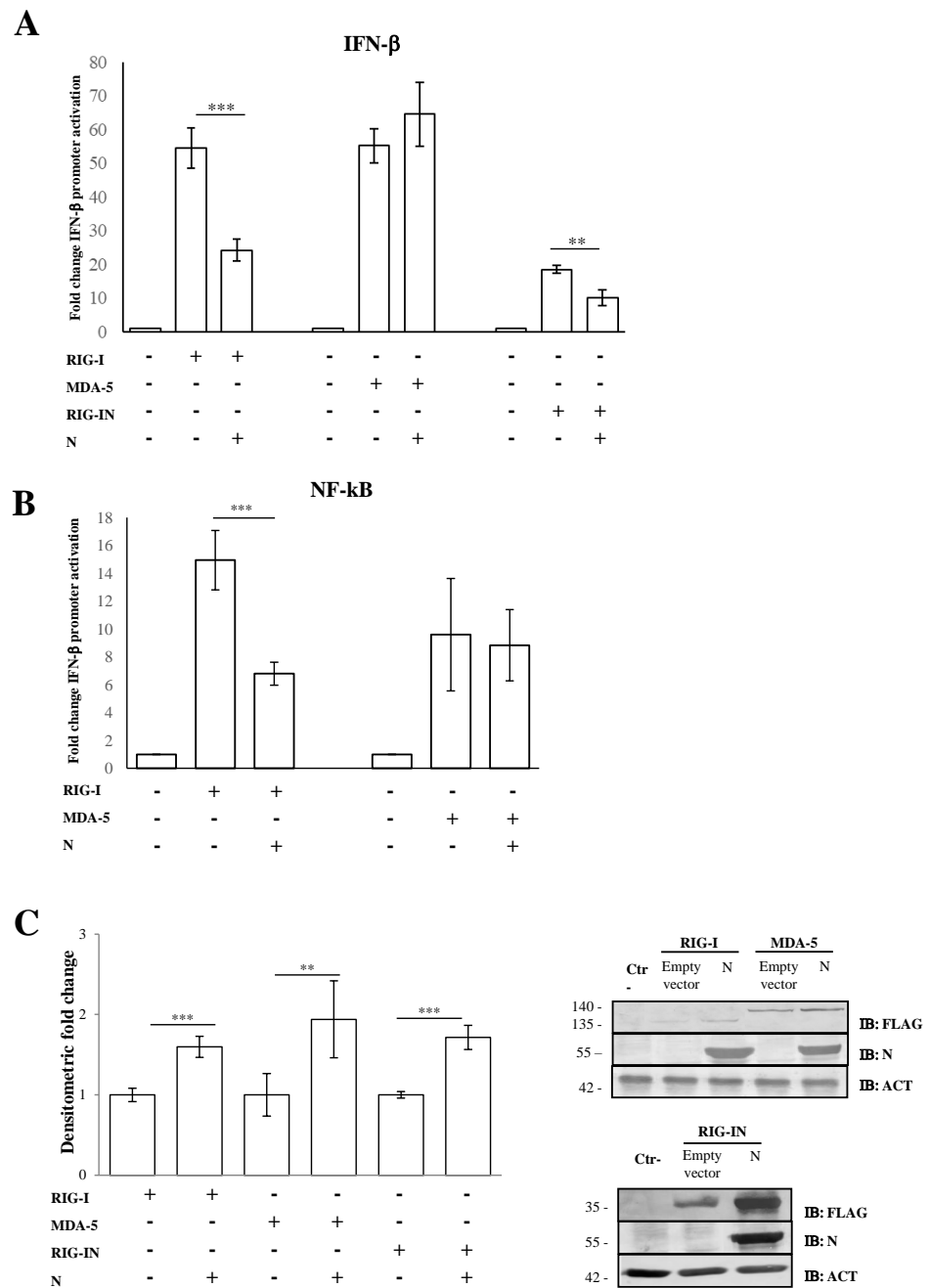
Figure 1. SARS-CoV-2 N counteracts RIG-I-mediated signaling. (**A**) SARS-CoV-2 N protein inhibited IFN-β promoter activation. Lenti-X 293T cells were co-transfected with the IFN-β Firefly luciferase reporter plasmid, RIG-I-, RIG-IN- or MDA-5-expressing plasmids, with or without the N-expressing plasmid. Renilla luciferase control reporter plasmid was included as an internal control for further normalization. Firefly luciferase activities were normalized with respect to Renilla luciferase values, and fold induction was estimated with respect to the relative mock-treated sample. (**B**) The inhibitory effect of SARS-CoV-2 N protein on the minimal IFN-β promoter containing the NF-κB responsive element was assessed by a luciferase reporter assay, as described above. (**C**) Fifty micrograms of whole cell lysates (WCLs) were further analyzed by immunoblotting for RIG-I, RIG-IN, MDA-5 and N proteins using anti-FLAG M2 and anti-N monoclonal antibodies. Loading control was represented by the immuno-detection of actin protein. Densitometric analyses of reactive bands were performed with ImageJ software. Results are plotted as the mean fold change in RIG-I, RIG-IN or MDA-5 with respect to relative actin levels from (n = 3) independent experiments ± SD. Significance was determined with p-values (*** $p < 0.005$, $0.005 < $ ** $p < 0.01$).

Afterwards, we evaluated the N protein activity on RIG-I CARD domains (RIG-IN). RIG-IN, lacking the repressor and helicase domains (RD and CTD) [33], is known to be constantly active in the absence of stimuli; therefore, IFN-β induction inevitably occurs. In this system, a small amount of RIG-IN expression was sufficient to induce IFN-β promoter activation, which showed significant abrogation by the presence of the N protein (Figure 1A, Table S1). In parallel, the antagonistic behavior of the N protein was tested on the minimal IFN-β promoter containing the NF-κB responsive element. Additionally, in this case, the activation of the minimal IFN-β promoter was hindered when RIG-I ($p = 0.002$) was expressed along with the viral protein. In contrast, N protein did not interfere with the MDA-5 signaling pathway (Figure 1B, Table S1). The capability of the N protein to block the NF-κB transcription factor activity confirmed the N antagonistic function mostly on the early stage of the signaling cascade leading to IFN-β production. To address whether the antagonistic properties of the N protein were due to a down-regulation of RIG-I cellular levels, the cytoplasmic amount of RIG-I was evaluated. As shown in Figure 1C, the presence of SARS-CoV-2 N protein did not negatively affect the cellular accumulation of RIG-I, which, in turn, was stabilized by the presence of the viral protein ($p = 0.004$), as reported by semi-quantitative immunoblotting (Figure 1C, Table S1). Likewise, MDA-5 and RIG-IN levels were significantly increased ($p = 0.01$; $p < 0.0001$, respectively) when the N protein was co-expressed (Figure 1C, Table S1).

3.2. SARS-CoV-2 Nucleoprotein Prevents RIG-I Activation by TRIM25

The activation of RIG-I is tightly controlled by its ubiquitination by the E3 ligase TRIM25 on lysine residues at the 172-position on the second RIG-I CARD domain [38,39]. To assess whether the N protein inhibitory activity was due to a direct effect on early RIG-I activation or on a downstream step in the cascade, an IFN-β reporter assay was performed in the presence of TRIM25 over-expression. The presence of TRIM25 significantly enhanced RIG-I signaling (2.4-fold induction; $p = 0.0006$) (Figure 2A, Table S2).

However, the N protein completely abrogated TRIM25-mediated RIG-I activity (0.4-fold decrease; $p = 0.009$, Table S2), as shown in Figure 2A. In a similar manner, the N protein showed its antagonistic properties on RIG-IN activation by TRIM25 (Figure 2A, Table S2). Thereafter, the SARS-CoV-2 N protein substantially attenuated the RIG-I/TRIM25 signaling pathway in a dose-dependent manner, as evidenced by expressing an increasing amount of the protein (Figure 2B, Table S2). Moreover, the antagonistic nature of the viral protein was not detected on the $T_{55}I$ RIG-I mutant ($p = 0.929$), which lacks a TRIM25 binding site, confirming a direct effect of the N protein on TRIM25-mediated RIG-I activation rather than on other RIG-I domains (Figure 2C, Table S2). To support these observations, we also evaluated the specific activity of the N protein on Riplet, another E3 ubiquitin ligase involved in the control of RIG-I functions. The N protein was unable to counteract the stimulatory activity of Riplet on RIG-I (Figure 2D, Table S2). To further verify the inhibitory effect of N protein on TRIM25, we tested whether N protein affected endogenous RIG-I activation by transfecting Lenti-X 293T cells with TRIM25 alone. As expected, RIG-I activation was induced upon overexpression of the E3 ubiquitin ligase ($p = 0.0153$), although this induction was counteracted by ectopic expression of the N protein (Figure 2E, Table S2).
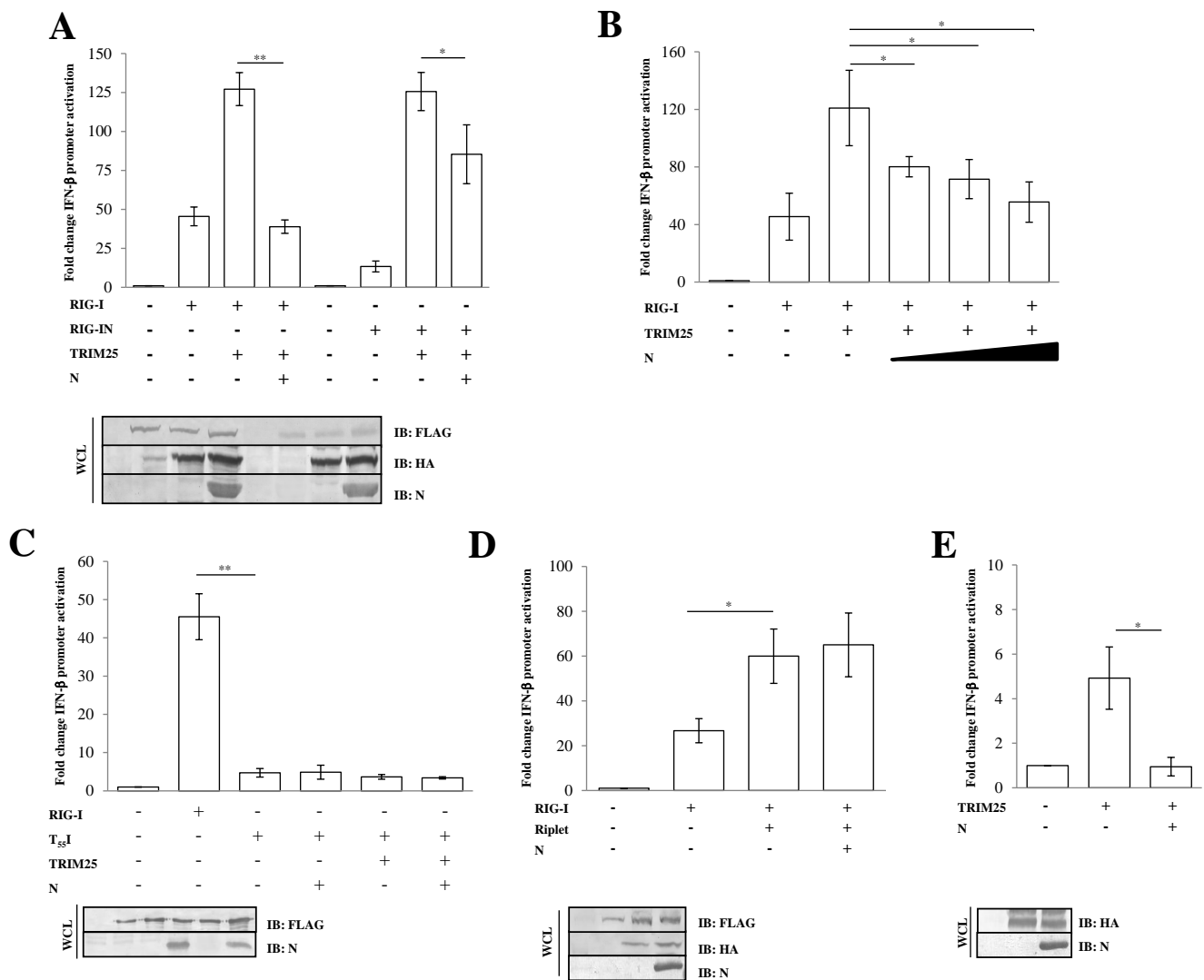
Figure 2. SARS-CoV-2 N protein inhibits TRIM25-mediated RIG-I activation to counteract IFN-β secretion. Lenti-X 293T cells were co-transfected with the IFN-β-Luc Firefly luciferase reporter plasmid and the Renilla luciferase control reporter plasmid along with RIG-I- and TRIM25-expressing plasmids. Where indicated, fixed (**A**) or increasing (**B**) amounts of SARS-CoV-2 N were co-expressed. (**C**) Wild-type RIG-I was replaced by its $T_{55}I$ mutated counterpart. Cells were collected at 48 h post-transfection, prior to 12 h of stimulation with poly(I:C). The luciferase activity of the cell lysates was analyzed with the dual luciferase reporter assay system (Promega). Fold changes in IFN-β promoter activation were calculated with respect to the relative reference sample based on Firefly luciferase values normalized to Renilla luciferase activities. (**D**) The specificity of SARS-CoV-2 N on TRIM25 was achieved by enhancing RIG-I activation through the over-expression of the stimulatory protein Riplet or (**E**) solely on TRIM25 expression. Luciferase assays were assessed and the fold change in activation was calculated as previously described. Results were plotted as mean values ($n = 4$) ± standard deviation (SD), and significance was determined by *p*-values $0.005 < ** \, p < 0.01$, $0.01 < * \, p < 0.05$). Cell lysates from reporter gene assays were analyzed by immunoblotting. Fifty micrograms of WCLs were loaded on SDS-PAGE and probed with specific monoclonal antibodies for protein detection.

3.3. IRF3 Activation Is Impaired by N-Mediated RIG-I-TRIM25 Axes Inhibition

The nucleocapsid (N) protein of SARS-CoV was shown to inhibit the activation and nuclear translocation of the transcription factor IRF3 induced by poly(I:C), a synthetic double-stranded RNA analogue, thus resulting in a potent antagonist of type-I IFNs. Several studies on SARS-CoV demonstrated that the N protein inhibited IRF3 activation through the early PRR recognition stage of the signaling pathway [44]. Further studies showed that SARS-CoV N protein inhibited IRF3 activity through the suppression of RIG-I

ubiquitination/activation by TRIM25 [45]. Regarding SARS-CoV-2, we observed that the IFN-β promoter activation due to IRF3 overexpression was not perturbed by the presence of the N protein (fold decrease 0.85; p = 0.373, Table S3). In contrast, the antagonistic function of the viral protein was fully restored when IRF3 activation was induced by RIG-I (fold decrease 0.3; p = 0.0012), TRIM25 (fold decrease 0.27; p = 0.005, Table S3) or both (fold decrease 0.2; p = 0.0018, Table S3) proteins co-expression, confirming the specificity of SARS-CoV-2 N protein for the RIG-I–TRIM25 protein complex (Figure 3).
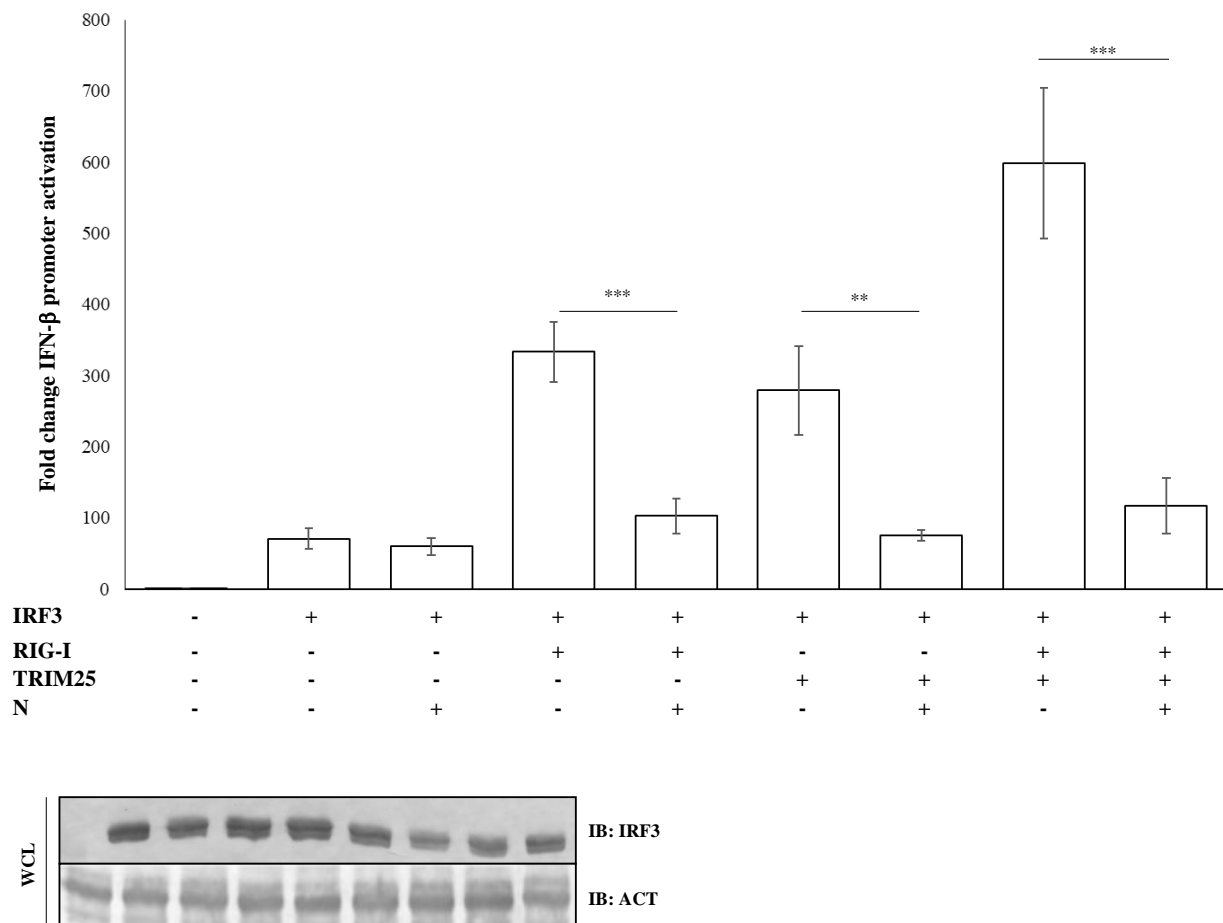

Figure 3. IRF3 activation is impaired due to inhibition of the RIG-I-TRIM25 pathway. Lenti-X 293T cells were co-transfected with the IFN-β-Luc Firefly luciferase reporter plasmid and the Renilla luciferase control reporter plasmid along with the IRF3-expressing plasmid. Where indicated, co-transfections were performed, including expressing plasmids for RIG-I, TRIM25 or SARS-CoV-2 N. Cells, previously stimulated for 12 h with poly(I:C), were collected at 48 h post-transfection. The luciferase activity of the cell lysates was analyzed with the dual luciferase reporter assay system (Promega). Fold changes in IFN-β promoter activation were calculated with respect to the relative reference sample based on Firefly luciferase values normalized to Renilla luciferase activities. Results were plotted as mean values (n = 4) ± standard deviation (SD) and significance was determined by p-value (*** p < 0.005, 0.005 < ** p < 0.01). Cell lysates from reporter gene assays were analyzed by immunoblotting.

3.4. The SARS-CoV-2 N Protein Forms a Stable Complex with TRIM25

To further dissect the involvement of the SARS-CoV-2 N protein on the RIG-I and TRIM25 cascade, lysates of Lenti-X 293T cells exogenously expressing the N protein, along with HA-TRIM25, were extracted with anti-HA antibody. The immunoblotting performed on co-immunoprecipitation complexes revealed that SARS-CoV-2 N protein is associated with TRIM25 because it was readily detected as being associated to the anti-HA precipitated protein (Figure 4A).
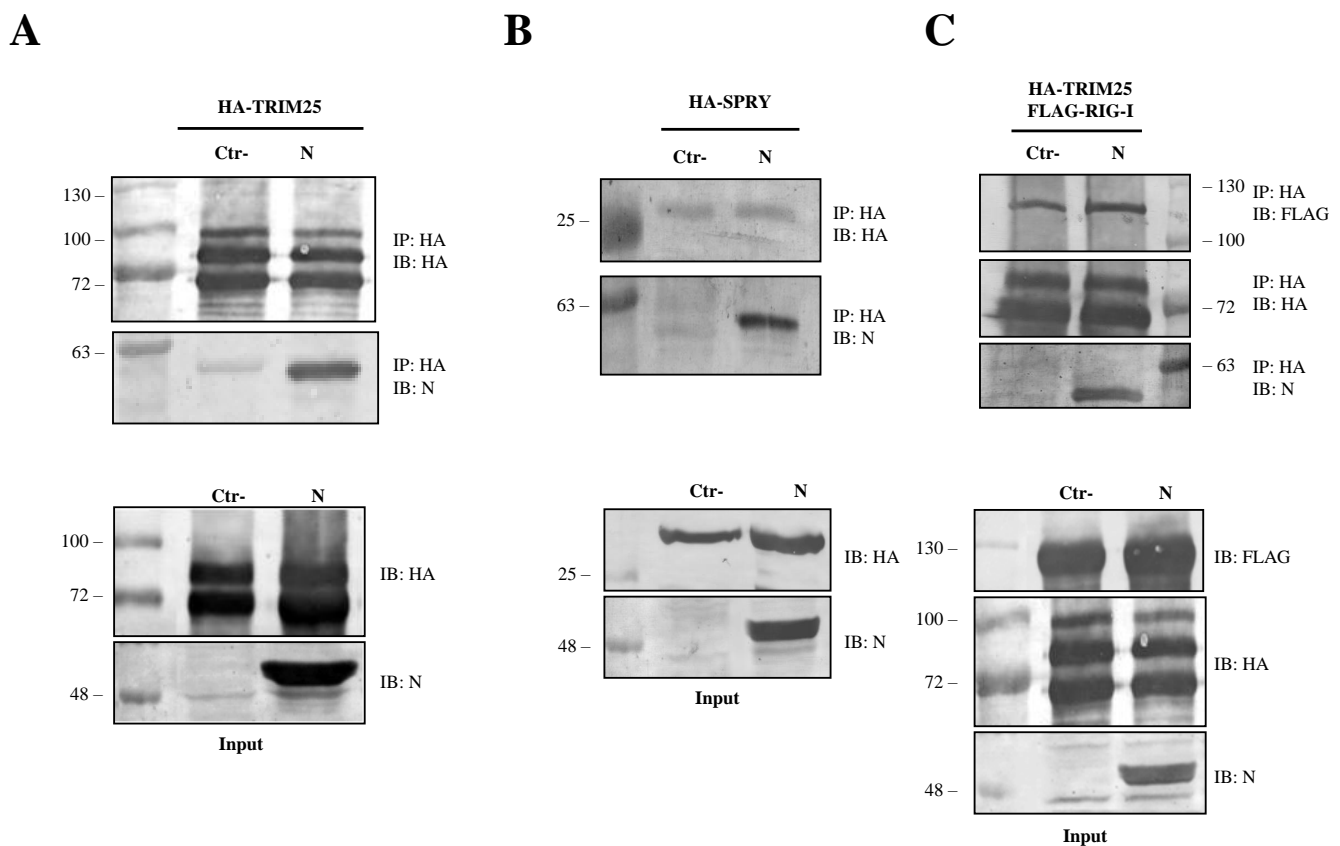
Figure 4. SARS-CoV-2 N protein is an interacting partner of TRIM25. The ability of SARS-CoV-2 N protein to interact with TRIM25 and RIG-I was determined by co-immunoprecipitation (Co-IP) on lysates of transfected Lenti-X 293T cells. (**A**) The formation of a stable immune complex was detected when TRIM25 was transiently over-expressed along with the N protein following Co-IP with anti-HA. (**B**) The N viral protein presented affinity with the SPRY domain of TRIM25 because the viral protein was detected in the anti-HA Co-IP performed on lysates of Lenti-X 293T cells expressing HA-SPRY, alone or in combination with the N protein. (**C**) The capability of SARS-CoV-2 N protein to disturb the RIG-I-TRIM25 interaction was then investigated by Co-IP on lysates of Lenti-X 293T cells simultaneously expressing RIG-I, TRIM25 and N. The interaction between RIG-I and TRIM25 was not affected by the presence of the viral protein. Indeed, their interaction was detected as co-immunoprecipitating with anti-HA antibody in the samples in which the N protein was either present or absent. Blots are representative of (*n* = 3) independent experiments. Fifty micrograms of WCLs were loaded on SDS-PAGE and immunostained as protein expression controls.

Co-immunoprecipitation experiments further confirmed that SARS-CoV-2 N protein interacted with the TRIM25 functional domain SPRY. The anti-HA Co-IP performed on cell lysates expressing HA-SPRY and N showed that the interaction between N and TRIM25 occurred at the SPRY sequence of the ubiquitin ligase (Figure 4B). These findings clearly showed that TRIM25 was an association partner of the SARS-CoV-2 N protein in transfected human cells. Next, we hypothesized that TRIM25-RIG-I interaction might be influenced by the presence of SARS-CoV N protein. To corroborate this hypothesis, SARS-CoV-2 N protein was expressed in Lenti-X 293T cells along with FLAG-RIG-I and HA-TRIM25. The interaction profile determined by Co-IP clearly demonstrated that the three proteins formed a multi-complex (Figure 4C). Indeed, immunoblotting performed on the immune-complex of the TRIM25 Co-IP sample evidenced the presence of both RIG-I and N (Figure 4C). Thus, we can speculate that the N protein interposes between RIG-I and TRIM25, which causes depletion and impedes full RIG-I activation. To further support this hypothesis, the level of TRIM25-mediated RIG-I ubiquitination was evaluated. In Lenti-X 293T cells, RIG-I underwent substantial ubiquitination by the overexpression of TRIM25 and K63-only ubiquitin (Figure 5, Table S4). Such ubiquitination was significantly reduced (*p* = 0.006) by the presence of the N protein which, consistently with previous results, reduced RIG-

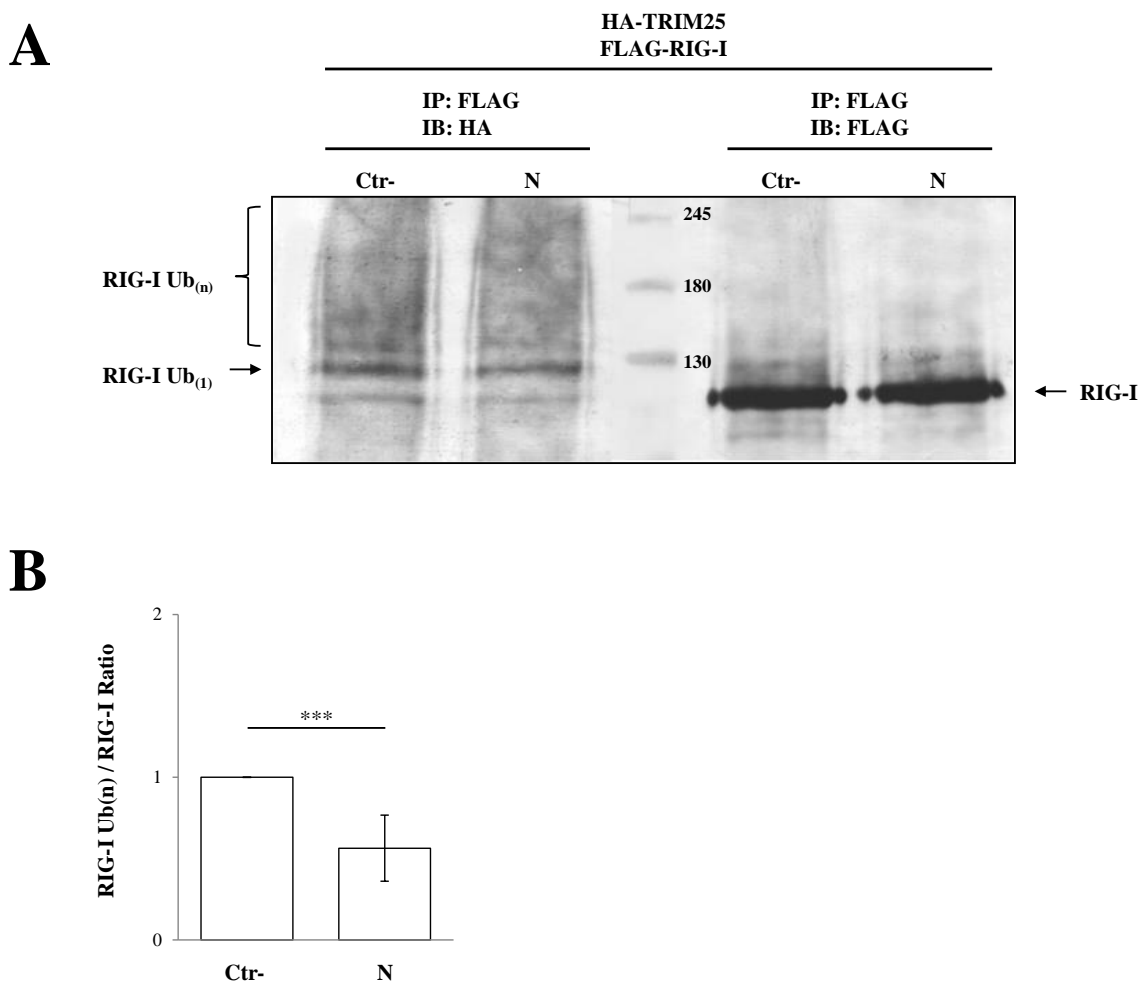I ubiquitination and activation by TRIM25 without affecting its cellular accumulation (Figure 5, Table S4).

Figure 5. TRIM25 E3 ubiquitin ligase activity was impaired by the presence of SARS-CoV-2 N protein. The transient expression of SARS-CoV-2 N protein affected the ability of TRIM25 to mediate RIG-I ubiquitination in Lenti-X 293T cells. (**A**) Cells transfected with plasmids expressing FLAG-RIG-I, HA-TRIM25, HA-K63-only ubiquitin mutant and, where indicated, the SARS-CoV-2 N protein, were treated with the proteasome inhibitor MG-132 for 12 h. Lysates, prepared under denaturing conditions as described in the Material and Methods section, were immunoprecipitated with anti-FLAG magnetic beads, and precipitated proteins were resolved by SDS-PAGE. Pulled proteins were detected by immunoblotting with anti-HA or anti-FLAG monoclonal antibodies. Blots are representative of at least two biologically independent experiments. (**B**) The RIG-I ubiquitination rate was determined by densitometric analysis calculating the ratio between mono- and poly-ubiquitinated RIG-I (anti-HA) and relative RIG-I levels (anti-FLAG). Fold changes in RIG-I ubiquitination were calculated for N-containing samples relatively to the control sample. Results are expressed as mean ($n = 3$) fold change $\pm$ standard deviation (SD), and significance was determined by *p*-value (*** $p < 0.005$).

4. Discussion and Conclusions

Antagonism to the host innate immune response by viral proteins is a crucial point in virus replication and could affect the outcome of the infection [32,58–62]. Viral escape from a host innate immune response reflects an efficient and unperturbed viral replication due to the absence of type I interferon secretion [43–58]. The lack of an adequate IFN-β production and antiviral protein expression may be critical to COVID-19 pathogenesis. SARS-CoV, a virus closely related to SARS-CoV-2, utilizes multiple strategies to antagonize the host antiviral response [43–48]. Notably, ORF6 and the nucleoprotein N play a critical role in type I IFN production [44,45]. Notwithstanding, the N protein represents the most

important viral antagonistic factor due to its multi-functional activity on the signaling pathway leading to IFN-β production [50]. Based on the similarity between SARS-CoV and SARS-CoV-2, a conserved antagonistic function to the innate immunity for the SARS-CoV-2 N protein has already been described [52,53]. In the present study, we demonstrated a mechanism by which SARS-CoV-2 N protein was able to inhibit IFN-β secretion. Moreover, despite genetic variability among SARS-coronaviruses, the N protein shared the ability to antagonize the host innate immune response, suggesting that this function was evolutionarily conserved and fundamental for virus replication, survival and spread. An in-depth analysis revealed that the SARS-CoV-2 N displayed an IFN-β antagonistic mechanism similar to that of SARS-CoV, because it was involved in this mechanism at a very early step in viral infection, in particular, targeting RIG-I.

Viral antagonistic proteins can exert their activity at different steps in the RIG-I- and MDA-5-mediated signaling cascades in order to block IFN-β production; therefore, we improved the characterization of the SARS-CoV-2 N inhibitory mechanism by investigating its effects on the PRRs or downstream effectors (IRF3). Although SARS-CoV-2 N protein did not lead to a negative regulation of RIG-I or MDA-5 cellular accumulation, it displayed an IFN-β counteractive mechanism similar to that of SARS-CoV. Indeed, the antagonistic properties of the SARS-CoV-2 N protein were addressed to RIG-I and its CARD domains (RIG-IN), because a significant inhibition of IFN-β promoter activation was evidenced in vitro through the IFN-β promoter reporter assay, when an overexpression of N protein was tested with RIG-I and its CARD domains (RIG-IN). Moreover, this inhibitory function was also confirmed using the minimal IFN-β promoter plasmid, consisting of only the NF-κB responsive element. We demonstrated that the antagonistic property of the SARS-CoV-2 N protein was addressed to the TRIM25-mediated activation of RIG-I. A significant inhibition was noticed when the overexpression of the co-stimulatory protein TRIM25 was associated with the viral N protein. The affinity of the N protein for TRIM25 was clearly demonstrated by co-immunoprecipitation experiments, where the two proteins were detected as associated partners. Similarly to SARS-CoV, this interaction was mapped to the SPRY domain of TRIM25, harboring the catalytic domain and the interface for RIG-I recognition. Further proof of this mechanism came from the ability of N protein to block the ubiquitinating activity of TRIM25 on RIG-I which, however, remained accumulated into the cell. These results led to the hypothesis that TRIM25-RIG-I axis could be altered by the presence of the N protein. Several lines of evidence point toward TRIM25 as a key modulator of RIG-I, although it is one of the multiple host proteins having this function. Among them, Riplet plays a similar role, having the ability to ubiquitinate and control RIG-I signaling. Notwithstanding, SARS-CoV-2 N protein seemed to exert a highly specific action only on TRIM25, because its presence did not affect Riplet activity. The detailed interactions among the RIG-I/TRIM25/N triple complex is currently being investigated [52,53]. In this study, the results suggested that the N protein intervened on the RIG-I and TRIM25 axis by hindering TRIM25, whose E3 ligase activity on RIG-I was suppressed and, consequently, triggered the sequential steps culminating in IFN production. In this context, IRF3 activity was not directly affected by the presence of the N protein. The presently described N protein activity, combined with the ability of several viral proteins (ORF3, ORF6, nsp13 and nsp14) to suppress host innate immunity, establishes a comprehensive suppression of type I IFN production during SARS-CoV-2 viral infection; in particular, suppressing IFN-β by directly antagonizing the enzymatic function of TRIM25. Moreover, these data help to increase our knowledge on immune responses to SARS-CoV2 virus, which represents an important worldwide threat for humanity.

In the light of recent outbreak of SARS-CoV-2 variants, much attention is focused on mutations occurring in the spike protein, the major concern in vaccination trials. Notwithstanding, conserved mutations among virus variants have also been reported in the N protein [61,62]. The nucleoprotein modulates the innate immune response; therefore, mutations in its sequence can play an important role, rather than in virus infectivity and

transmissibility, in determining its antagonistic properties and the clinical outcomes to SARS-CoV-2 infection.

References

1. Cui, J.; Li, F.; Shi, Z. Origin and evolution of pathogenic coronaviruses. *Nat. Rev. Microbiol.* **2019**, *17*, 181–192. [CrossRef]
2. Ren, L.L.; Wang, Y.M.; Wu, Z.Q.; Xiang, Z.C.; Guo, L.; Xu, T.; Jiang, Y.Z.; Xiong, Y.; Li, Y.J.; Li, X.W.; et al. Identification of a novel coronavirus causing severe pneumonia in human: A descriptive study. *Chin. Med. J.* **2020**, *133*, 1015–1024. [CrossRef] [PubMed]
3. Lu, R.; Zhao, X.; Li, J.; Niu, P.; Yang, B.; Wu, H.; Wang, W.; Song, H.; Huang, B.; Zhu, N.; et al. Genomic characterisation and epidemiology of 2019 novel coronavirus: Implications for virus origins and receptor binding. *Lancet* **2020**, *395*, 565–574. [CrossRef]
4. Marra, M.A.; Jones, S.J.; Astell, C.R.; Holt, R.A.; Brooks-Wilson, A.; Butterfield, Y.S.; Khattra, J.; Asano, J.K.; Barber, S.A.; Chan, S.Y.; et al. The Genome sequence of the SARS-associated coronavirus. *Science* **2003**, *300*, 1399–1404. [CrossRef] [PubMed]
5. Tan, Y.J.; Lim, S.G.; Hong, W. Characterization of viral proteins encoded by the SARS-coronavirus genome. *Antivir. Res.* **2005**, *65*, 69–78. [CrossRef]
6. Tan, Y.J.; Lim, S.G.; Hong, W. Understanding the accessory viral proteins unique to the severe acute respiratory syndrome (SARS) coronavirus. *Antivir. Res.* **2006**, *72*, 78–88. [CrossRef]
7. Zhou, P.; Yang, X.L.; Wang, X.G.; Hu, B.; Zhang, L.; Zhang, W.; Si, H.R.; Zhu, Y.; Li, B.; Huang, C.L.; et al. A pneumonia outbreak associated with a new coronavirus of probable bat origin. *Nature* **2020**, *579*, 270–273. [CrossRef]
8. Tao, Y.; Shi, M.; Chommanard, C.; Queen, K.; Zhang, J.; Markotter, W.; Kuzmin, I.V.; Holmes, E.C.; Tong, S. Surveillance of bat coronaviruses in Kenya identifies relatives of human coronaviruses NL63 and 229E and their recombination history. *J. Virol.* **2017**, *91*, e01953-16. [CrossRef]
9. Corman, V.M.; Baldwin, H.J.; Tateno, A.F.; Zerbinati, R.M.; Annan, A.; Owusu, M.; Nkrumah, E.E.; Maganga, G.D.; Oppong, S.; Adu-Sarkodie, Y.; et al. Evidence for an ancestral association of human coronavirus 229E with bats. *J. Virol.* **2015**, *89*, 11858–11870. [CrossRef]
10. Corman, V.M.; Muth, D.; Niemeyer, D.; Drosten, C. Hosts and Sources of Endemic Human Coronaviruses. *Adv. Virus Res.* **2018**, *100*, 163–188.
11. De Wit, E.; van Doremalen, N.; Falzarano, D.; Munster, V.J. SARS and MERS: Recent insights into emerging coronaviruses. *Nat. Rev. Microbiol.* **2016**, *14*, 523–534. [CrossRef]
12. Yin, Y.; Wunderink, R.G. MERS, SARS and other coronaviruses as causes of pneumonia. *Respirology* **2018**, *23*, 130–137. [CrossRef] [PubMed]
13. Channappanavar, R.; Perlman, S. Pathogenic human coronavirus infections: Causes and consequences of cytokine storm and immunopathology. *Semin. Immunopathol.* **2017**, *39*, 529–539. [CrossRef]
14. Hui, D.S.; Memish, Z.A.; Zumla, A. Severe acute respiratory syndrome vs. the Middle East respiratory syndrome. *Curr. Opin. Pulm. Med.* **2014**, *20*, 233–241. [CrossRef]
15. World Health Organization. *Coronavirus Disease 2019 (COVID-19): Situation Summary Mar. 2020*; World Health Organization: Geneva, Switzerland, 2020.
16. Huang, C.; Wang, Y.; Li, X.; Ren, L.; Zhao, J.; Hu, Y.; Zhang, L.; Fan, G.; Xu, J.; Gu, X.; et al. Clinical features of patients infected with 2019 novel coronavirus in Wuhan, China. *Lancet* **2020**, *395*, 497–506. [CrossRef]
17. Chen, N.; Zhou, M.; Dong, X.; Qu, J.; Gong, F.; Han, Y.; Qiu, Y.; Wang, J.; Liu, Y.; Wei, Y.; et al. Epidemiological and clinical characteristics of 99 cases of 2019 novel coronavirus pneumonia in Wuhan, China: A descriptive study. *Lancet* **2020**, *395*, 507–513. [CrossRef]
18. Guan, W.J.; Ni, Z.Y.; Hu, Y.; Liang, W.H.; Ou, C.Q.; He, J.X.; Liu, L.; Shan, H.; Lei, C.L.; Hui, D.S.C.; et al. Clinical Characteristics of Coronavirus Disease 2019 in China. *N. Engl. J. Med.* **2020**, *382*, 1708–1720. [CrossRef] [PubMed]

19. Yang, X.; Yu, Y.; Xu, J.; Shu, H.; Xia, J.; Liu, H.; Wu, Y.; Zhang, L.; Yu, Z.; Fang, M.; et al. Clinical course and outcomes of critically ill patients with SARS-CoV-2 pneumonia in Wuhan, China: A single-centered, retrospective, observational study. *Lancet Respir. Med.* **2020**, *8*, 475–481. [CrossRef]

20. Lippi, G.; Plebani, M.; Henry, B.M. Thrombocytopenia is associated with severe coronavirus disease 2019 (COVID-19) infections: A meta-analysis. *Clin. Chim. Acta* **2020**, *506*, 145–148. [CrossRef] [PubMed]

21. Pan, Y.; Yu, X.; Du, X.; Li, Q.; Li, X.; Qin, T.; Wang, M.; Jiang, M.; Li, J.; Li, W.; et al. Epidemiological and Clinical Characteristics of 26 Asymptomatic Severe Acute Respiratory Syndrome Coronavirus 2 Carriers. *J. Infect. Dis.* **2020**, *221*, 1940–1947. [CrossRef]

22. Wu, Z.; McGoogan, J.M. Characteristics of and Important Lessons from the Coronavirus Disease 2019 (COVID-19) Outbreak in China: Summary of a Report of 72,314 Cases from the Chinese Center for Disease Control and Prevention. *JAMA* **2020**, *323*, 1239–1242. [CrossRef]

23. Ryu, S.; Chun, B.C. An interim review of the epidemiological characteristics of 2019 novel coronavirus. *Epidemiol. Health* **2020**, *42*, e2020006. [CrossRef]

24. Yang, Y.; Lu, Q.; Liu, M.; Wang, Y.; Zhang, A.; Jalali, N. Epidemiological and clinical features of the 2019 novel coronavirus outbreak in China. *medRxiv* **2020**, *11*. [CrossRef]

25. Lai, C.C.; Liu, Y.H.; Wang, C.Y.; Wang, Y.H.; Hsueh, S.C.; Yen, M.Y.; Ko, W.C.; Hsueh, P.R. Asymptomatic carrier state, acute respiratory disease, and pneumonia due to severe acute respiratory syndrome coronavirus 2 (SARS-CoV-2): Facts and myths. *J. Microbiol. Immunol. Infect.* **2020**, *53*, 404–412. [CrossRef] [PubMed]

26. Lai, C.C.; Shih, T.P.; Ko, W.C.; Tang, H.J.; Hsueh, P.R. Severe acute respiratory syndrome coronavirus 2 (SARS-CoV-2) and coronavirus disease-2019 (COVID-19): The epidemic and the challenges. *Int. J. Antimicrob. Agents* **2020**, *55*, 105924. [CrossRef] [PubMed]

27. Liu, Y.C.; Liao, C.H.; Chang, C.F.; Chou, C.C.; Lin, Y.R. A locally transmitted case of SARS-CoV-2 infection in Taiwan. *N. Engl. J. Med.* **2020**, *382*, 1070–1072. [CrossRef]

28. Bai, Y.; Yao, L.; Wei, T.; Tian, F.; Jih, D.Y.; Chen, L. Presumed asymptomatic carrier transmission of COVID-19. *J. Am. Med. Assoc.* **2020**, *323*, 1406–1407. [CrossRef] [PubMed]

29. Rothe, C.; Schunk, M.; Sothmann, P.; Bretzel, G.; Froeschl, G.; Wallrauch, C. Transmission of 2019-nCoV infection from an asymptomatic contact in Germany. *N. Engl. J. Med.* **2020**, *382*, 970–971. [CrossRef]

30. Hui, K.P.Y.; Cheung, M.C.; Perera, R.A.P.M.; Ng, K.C.; Bui, C.H.T.; Ho, J.C.W.; Ng, M.M.T.; Kuok, D.I.T.; Shih, K.C.; Tsao, S.W.; et al. Tropism, replication competence, and innate immune responses of the coronavirus SARS-CoV-2 in human respiratory tract and conjunctiva: An analysis in ex-vivo and in-vitro cultures. *Lancet Respir. Med.* **2020**, *8*, 687–695. [CrossRef]

31. Zou, L.; Ruan, F.; Huang, M.; Liang, L.; Huang, H.; Hong, Z.; Yu, J.; Kang, M.; Song, Y.; Xia, J.; et al. SARS-CoV-2 Viral Load in Upper Respiratory Specimens of Infected Patients. *N. Engl. J. Med.* **2020**, *382*, 1177–1179. [CrossRef]

32. García-Sastre, A.; Biron, C.A. Type 1 Interferons and the Virus-Host Relationship: A Lesson in Détente. *Science* **2006**, *312*, 879–882. [CrossRef]

33. Reikine, S.; Nguyen, J.B.; Modis, Y. Pattern Recognition and Signaling Mechanisms of RIG-I and MDA5. *Front. Immunol.* **2014**, *5*, 342. [CrossRef]

34. Rehwinkel, J.; Gack, M.U. RIG-I-like receptors: Their regulation and roles in RNA sensing. *Nat. Rev. Immunol.* **2020**, *3*, 1–15. [CrossRef]

35. Sato, M.; Suemori, H.; Hata, N.; Asagiri, M.; Ogasawera, K.; Nakao, K.; Nakaya, T.; Katsuki, M.; Noguchi, S.; Tanaka, N.; et al. Distinct and essential roles of transcription factors IRF-3 and IRF-7 in response to viruses for IFN-alpha/beta gene induction. *Immunity* **2000**, *13*, 539–548. [CrossRef]

36. Peisley, A.; Wu, B.; Xu, H.; Chen, Z.J.; Hur, S. Structural basis for ubiquitin-mediated antiviral signal activation by RIG-I. *Nature* **2014**, *509*, 110–114. [CrossRef] [PubMed]

37. Wu, B.; Peisley, A.; Tetrault, D.; Li, Z.; Egelman, E.H.; Magor, K.E.; Walz, T.; Penczek, P.A.; Hur, S. Molecular Imprinting as a Signal-Activation Mechanism of the Viral RNA Sensor RIG-I. *Mol. Cell* **2014**, *55*, 511–523. [CrossRef] [PubMed]

38. Gack, M.U.; Shin, Y.C.; Joo, C.H.; Urano, T.; Liang, C.; Sun, L.; Takeuchi, O.; Akira, S.; Chen, Z.; Inoue, S.; et al. TRIM25 RING-finger E3 ubiquitin ligase is essential for RIG-I-mediated antiviral activity. *Nature* **2007**, *446*, 916–920. [CrossRef] [PubMed]

39. Gack, M.U.; Kirchhofer, A.; Shin, Y.C.; Inn, K.S.; Liang, C.; Cui, S.; Myong, S.; Ha, T.; Hopfner, K.P.; Jung, J.U. Roles of RIG-I N-terminal tandem CARD and splice variant in TRIM25-mediated antiviral signal transduction. *Proc. Natl. Acad. Sci. USA* **2008**, *105*, 16743–16748. [CrossRef]

40. Jiang, X.; Kinch, L.N.; Brautigam, C.A.; Chen, X.; Du, F.; Grishin, N.V.; Chen, Z.J. Ubiquitin-induced oligomerization of the RNA sensors RIG-I and MDA5 activates antiviral innate immune response. *Immunity* **2012**, *36*, 959–973. [CrossRef]

41. Peisley, A.; Wu, B.; Yao, H.; Walz, T.; Hur, S. RIG-I forms signalling-competent filaments in an ATP-dependent, ubiquitin-independent manner. *Mol. Cell* **2013**, *51*, 573–583. [CrossRef]

42. Zeng, W.; Sun, L.; Jiang, X.; Chen, X.; Hou, F.; Adhikari, A.; Xu, M.; Chen, Z.J. Reconstitution of the RIG-I pathway reveals a signaling role of unanchored polyubiquitin chains in innate immunity. *Cell* **2010**, *141*, 315–330. [CrossRef] [PubMed]

43. Chen, X.; Wang, K.; Xing, Y.; Tu, J.; Yang, X.; Zhao, Q.; Li, K.; Chen, Z. Coronavirus membrane-associated papain-like proteases induce autophagy through interacting with Beclin1 to negatively regulate antiviral innate immunity. *Protein Cell* **2014**, *5*, 912–927. [CrossRef] [PubMed]

44. Lu, X.; Pan, J.; Tao, J.; Guo, D. SARS-CoV nucleocapsid protein antagonizes IFN-β response by targeting initial step of IFN-β induction pathway, and its C-terminal region is critical for the antagonism. *Virus Genes* **2011**, *42*, 37–45. [CrossRef]

45. Hu, Y.; Li, W.; Gao, T.; Cui, Y.; Jin, Y.; Li, P.; Ma, Q.; Liu, X.; Cao, C. The Severe Acute Respiratory Syndrome Coronavirus Nucleocapsid Inhibits Type I Interferon Production by Interfering with TRIM25-Mediated RIG-I Ubiquitination. *J. Virol.* **2017**, *91*, e02143-16. [CrossRef]

46. Devaraj, S.G.; Wang, N.; Chen, Z.; Chen, Z.; Tseng, M.; Barretto, N.; Lin, R.; Peters, C.J.; Tseng, C.T.K.; Baker, S.C.; et al. Regulation of IRF-3-dependent innate immunity by the papain-like protease domain of the severe acute respiratory syndrome coronavirus. *J. Biol. Chem.* **2007**, *282*, 32208–32221. [CrossRef]

47. Siu, K.L.; Chan, C.P.; Kok, K.H.; Chiu-Yat Woo, P.; Jin, D.Y. Suppression of innate antiviral response by severe acute respiratory syndrome coronavirus M protein is mediated through the first transmembrane domain. *Cell Mol. Immunol.* **2014**, *11*, 141–149. [CrossRef]

48. Siu, K.L.; Kok, K.H.; Ng, M.H.; Poon, V.K.; Yuen, K.Y.; Zheng, B.J. Severe acute respiratory syndrome coronavirus M protein inhibits type I interferon production by impeding the formation of TRAF3/TANK/TBK1/IKKepsilon complex. *J. Biol. Chem.* **2009**, *284*, 16202–16209. [CrossRef]

49. Chang, C.Y.; Liu, H.M.; Chang, M.F.; Chang, S.C. Middle East Respiratory Syndrome Coronavirus Nucleocapsid Protein Suppresses Type I and Type III Interferon Induction by Targeting RIG-I Signaling. *J. Virol.* **2020**, *94*, e00099-20. [CrossRef] [PubMed]

50. McBride, R.; van Zyl, M.; Fielding, B.C. The coronavirus nucleocapsid is a multifunctional protein. *Viruses* **2014**, *6*, 2991–3018. [CrossRef]

51. Surjit, M.; Lal, S.K. The SARS-CoV nucleocapsid protein: A protein with multifarious activities. *Infect. Genet. Evol.* **2008**, *8*, 397–405. [CrossRef] [PubMed]

52. Chen, K.; Xiao, F.; Hu, D.; Ge, W.; Tian, M.; Wang, W.; Pan, P.; Wu, K.; Wu, J. SARS-CoV-2 Nucleocapsid Protein Interacts with RIG-I and Represses RIG-Mediated IFN-β Production. *Viruses* **2021**, *13*, 47. [CrossRef]

53. Oh, S.J.; Shin, O.S. SARS-CoV-2 Nucleocapsid Protein Targets RIG-I-Like Receptor Pathways to Inhibit the Induction of Interferon Response. *Cells* **2021**, *10*, 530. [CrossRef]

54. Blanco-Melo, D.; Nilsson-Payant, B.E.; Liu, W.C.; Uhl, S.; Hoagland, D.; Møller, R.; Jordan, T.X.; Oishi, K.; Panis, M.; Sachs, D.; et al. Imbalanced Host Response to SARS-CoV-2 Drives Development of COVID-19. *Cell* **2020**, *181*, 1036–1045. [CrossRef]

55. Hadjadj, J.; Yatim, N.; Barnabei, L.; Corneau, A.; Boussier, J.; Smith, N.; Péré, H.; Charbit, B.; Bondet, V.; Chenevier-Gobeaux, C.; et al. Impaired type I interferon activity and exacerbated inflammatory responses in severe Covid-19 patients. *Science* **2020**, *369*, 718–724. [CrossRef]

56. Acharya, D.; Liu, G.; Gack, M.U. Dysregulation of type I interferon responses in COVID-19. *Nat. Rev. Immunol.* **2020**, *20*, 397–398. [CrossRef]

57. Yuen, C.K.; Lam, J.Y.; Wong, W.M.; Mak, L.F.; Wang, X.; Chu, H.; Cai, J.P.; Jin, D.Y.; To, K.K.W.; Chan, J.F.W.; et al. SARS-CoV-2 nsp13, nsp14, nsp15 and orf6 function as potent interferon antagonists. *Emerg. Microbes. Infect.* **2020**, *9*, 1418–1428. [CrossRef] [PubMed]

58. Frieman, M.; Baric, R. Mechanisms of severe acute respiratory syndrome pathogenesis and innate immunomodulation. *Microbiol. Mol. Biol. Rev.* **2008**, *72*, 672–685. [CrossRef] [PubMed]

59. Nelemans, T.; Kikkert, M. Viral Innate Immune Evasion and the Pathogenesis of Emerging RNA Virus Infections. *Viruses* **2019**, *11*, 961. [CrossRef]

60. Tay, M.Z.; Poh, C.M.; Rénia, L.; MacAry, P.A.; Ng, L.F.P. The trinity of COVID-19: Immunity, inflammation and intervention. *Nat. Rev. Immunol.* **2020**, *20*, 363–374. [CrossRef] [PubMed]

61. Rahman, M.S.; Islam, M.R.; Alam, A.S.M.R.U.; Islam, I.; Hoque, M.N.; Akter, S.; Rahaman, M.M.; Sultana, M.; Hossain, M.A. Evolutionary dynamics of SARS-CoV-2 nucleocapsid protein and its consequences. *J. Med. Virol.* **2021**, *93*, 2177–2195. [CrossRef]

62. Thorne, L.G.; Bouhaddou, M.; Reuschl, A.K.; Zuliani-Alvarez, L.; Polacco, B.; Pelin, A.; Batra, J.; Whelan, M.V.X.; Ummadi, M.; Rojc, A.; et al. Evolution of enhanced innate immune evasion by the SARS-CoV-2 B.1.1.7 UK variant. *bioRxiv* **2021**, 1–36. [CrossRef]

Reports on Global Health Research

Case Report

Successful Treatment of SARS-CoV2 Delta Variant Infected Patient with a Monoclonal Antibody Cocktail

Maria Grazia Cusi[1,2]*, Danilo Tacconi[3], Gianni Gori Savellini[1], Gabriele Anichini[1], Beatrice Valoriani[3], Claudia Gandolfo[1]

[1]Virology Unit, Department of Medical Biotechnologies, University of Siena, Italy

[2]Microbiology and Virology Unit, 'S. Maria alle Scotte' Hospital, Italy

[3]Infectious Diseases Unit, S. Donato Hospital, Italy

***Corresponding author:** Maria Grazia Cusi, Virology Unit, Department of Medical Biotechnologies, University of Siena, Siena, Italy

Abstract

We report the successful effect of mAbs therapy against SARS-CoV-2 Delta variant (also known as B.1.617.2) in a woman aged 59, affected by secondary immunodepression due to a rheumatoid arthritis currently treated with biological drugs.

Introduction

The COVID-19 pandemic is still ongoing and a variety of prophylactic and therapeutic interventions has been developed. Monoclonal Antibodies (mAbs), able to block the virus in the infected host, are becoming more important in treating specific categories of subjects infected by SARS CoV-2 and within a context of viral variants' emergency. Being biological drugs, monoclonal antibodies have lately become an important class of drugs treating multiple conditions in infectious diseases. However, an important limit when using these mAbs is antibody escape, due to the virus mutation in the region responsible for antibody binding, making the antibody unarmed. Several companies have developed antibody therapeutics for Covid-19, including Lilly with etesevimab and bamlanivamab [1] and Regeneron with casirivimab and imdevimab [2,3]; other new mAbs are on clinical trials [4]. These antibodies bind two distinct and non-overlapping sites on the Receptor Binding Domain (RBD). The rationale for this antibody combination is that it is unlikely that a mutation in the S protein of SAR-CoV-2 simultaneously renders both antibodies ineffective.

First identified in India and already spread in many countries, the Delta variant represents a new source of risk and a new challenge for humans, because of the mutations in the spike gene. These mutations found in the Receptor Binding Domain (RBD),

which is the neutralizing antibodies major target, can impair the monoclonal antibody efficacy in COVID-19 therapy. The Delta variant, also known as B.1.617.2, is considered a 'variant of concern' by the Center for Disease Control and Prevention (CDC) [5]. This variant has four mutations of interest in the Spike protein: L452R, T478K, D614G, P681R; in particular, the substitution at position 452 confers a stronger affinity of the spike protein to the ACE2 receptor and seems to decrease the recognition capability of the immune system, while the substitution at position 681, near the furin cleavage, may facilitate the cleavage of S precursor protein into the active S1/S2 subunits, resulting in better transmissibility [6].

B.1.617.2 shows increased transmissibility, potential reduction in neutralization by some monoclonal antibody treatments under emergency authorization and potential reduction in neutralization in sera after vaccination in lab tests [7]. Here, we report the successful effect of mAbs therapy in a woman aged 59, affected by secondary immunodepression due to a rheumatoid arthritis currently treated with biological drugs.

Materials and methods

Prior to participating in this study, the subject, living in Arezzo area (Tuscany, Italy), signed a written informed consent. This research was crried out according to the principles of Helsinki declaration.

Nasopharyngeal swab was collected in viral transport media on May 25th, 2021. Then, RT-PCR targeting *N1* and N2 genes

(Cepheid GeneExpert, Sunnyvale, CA, USA) was performed for SARS-CoV-2 detection. Viral RNA was extracted using the EZ1 Advanced XL system (Qiagen, Hilden, Germany) according to the manufacturer's instructions. Moreover, amplification through molecular PCR was done. Finally, Sanger sequencing of the entire Spike protein (Table 1) was performed using the following primers and the sequence was uploaded on Gisaid (EPI_ISL_2550732):

Position	Gene	Ref /TUS-Siena-33 (nt)	Ref/TUS-Siena-33 (aa)
21618	S	C/G	Thr/Arg
21987	S	G/A	Gly/Asp
22029-22034	S	AGTTCA/del	Phe, Arg/del
22227	S	C/T	Ala/Val
22917	S	T/G	Leu/Arg
22995	S	C/A	Thr/Lys
23403	S	A/G	Asp/Gly
23604	S	C/G	Pro/Arg
24410	S	G/A	Asp/Asn

1) 1173 bp, nt 21289-22461

SARS-S-F3 5' TATCTTGGCAAACCACGCGAACAA 3'

SARS-S-R7 5' TTTGTTTCTGAGAGAGGGTC 3'

2) 1326 bp, nt 22342-23668

SARS-S-F7 5' TGGTGCTGCAGCTTATTAT 3'

SARS-S-R6 5' TTCTGCACCAAGTGACATAGTGTAGGCA 3'

3) 1140 bp, nt 23398-24537

SARS-S-F6 5' TCAGGATGTTAACTGCACAGAAGTCC 3'

SARS-S-R8 5' TGCACTTCAGCCTCAACTT 3'

4) 1156 bp, nt 24465-23310

SARS-S-F8 5' CCAATTTTGGTGCAATTT 3'

SARS-S-R3 5' ACCCTTGGAGAGTGCTAGTTGCCATCTC 3'

Table 1: Genetic variations of hCoV-19/Italy/TUS-Siena-33/2021 isolate compared to the SARS-CoV-2 reference genome isolated in Wuhan (NC_045512.2).

Moreover, to test subject's seronegativity for SARS-CoV-2 before the treatment with monoclonal cocktail, serum was analyzed using the Abbott SARS-CoV-2 IgG/IgM Chemiluminescent Microparticle Immunoassay (CMIA) (Abbott Laboratories, Chicago, IL) on an Abbott Architect i2000 (Abbott Diagnostics) according to the manufacturer's instructions. This method is a qualitative assay that detects IgG/IgM binding to an undisclosed epitope of the SARS-CoV-2 nucleocapsid protein, with the results expressed as Relative Light Units (RLU). The final interpretation of positivity was determined by the ratio above a threshold value, with positive ratio ³1.4 or negative ratio <1.4.

Results

On May 20th, 2021 she presented fever (39°C), arthralgia, headache; thus, the day after, her family doctor recommended her to do a swab for SARS-CoV-2, which was positive by molecular real-time PCR (Ct 28), (Cepheid GeneeXpert, Sunnyvale, CA, USA).

The Sanger sequence limited to the viral spike protein revealed the presence of SARS-CoV-2 Delta variant (B.1.617.2) (GISAID EPI_ISL_2550732).

The woman had a mild disease and normal oxygen saturation without lung involvement.

She was, however, treated with monoclonal cocktail considering her chronic assumption of biological drugs for rheumatoid arthritis, therapies related whit high risk of developing a severe form of COVID-19 and hospitalization. She had received no SARS-CoV-2 vaccine and was seronegative (Abbott Laboratories, Chicago, IL). On May 25th, in the morning, she was treated with a cocktail of monoclonal antibodies (casirivimab 1200 mg + imdevimab 1200 mg; Regeneron, Tarrytown, NY, USA). On the infusion day, vital parameters were stable with Sp02: 98%, BP: 120/80, HR: 85. During the night, the high fever, that was present for four days, disappeared. She turned negative to SARS-CoV-2 after a control swab on June 5th. The patient recovered from Covid-19, reporting persistence of a moderate asthenia.

Discussion

This is the first reported case of a patient infected by the Delta variant, treated with the combination of casirivimab and imdevimab in the early stage of COVID-19 and recovered after 12 days, suggesting the therapeutic role of these mAbs against this emergent SARS-CoV-2 variant. Because of high incidence of B.1.1.7 and P.01 variants in the area, she was suggested to be treated with Regeneron mAbs, based on the observation of Hoffmann et all. that found the casirivimab/imdevimab combination efficient in inhibiting viral entry into cells for all variants, while bamlanivimab failed to inhibit B.1.351 and P.1 variants[8]. Although this analysis only includes one patient, this is an *in vivo* confirmation that this mAbs cocktail was successful in hindering the Delta variant.

Authors' Contributions

M.G.C. conceptualized the work and wrote the first draft of the manuscript. G.G.S., G.A. and C.G. performed the experiments. D.T. and B.V. provided the study samples.

References

1. Chen P, Nirula A, Heller B, Gottlieb RL, Boscia J, et al. (2020) SARS-CoV-2 neutralizing antibody LY-CoV555 in outpatients with Covid-19. N Engl J Med 384: 229-237.

2. U.S. Food & Drug Administration Coronavirus (COVID-19) update: FDA authorizes monoclonal antibodies for treatment of COVID-19. 2020.

3. Weinreich DM, Sivapalasingam S, Norton T, Ali S, Gao H, et al. (2020) REGN-COV2, a neutralizing antibody cocktail, in outpatients with Covid-19. N Engl J Med 384: 238-251.

4. DeFrancesco L (2020) COVID-19 antibodies on trial. Nat Biotechnol 38: 1242-1252.

5. https://www.cdc.gov/coronavirus/2019-ncov/variants/variant.html

6. Cherian S, Potdar V, Jadhav S, Yadav P, Gupta N, et al. NIC team, INSACOG Consortium. Convergent evolution of SARS-CoV-2 spike mutations, L452R, E484Q and P681R, in the second wave of COVID-19 in Maharashtra, India. BioRXiv.

7. Torjesen I (2021) Covid-19: Delta variant is now UK's most dominant strain and spreading through schools. BMJ 373: n1445.

8. Hoffmann M, Arora P, Groß R, Seidel A, Hörnich BF, et al. (2021) SARS-CoV-2 variants B.1.351 and P.1 escape from neutralizing antibodies. Cell 184:2384-2393.e12.

Claudia Gandolfo [1], Shibily Prathyumn [1], Chiara Terrosi [1], Gabriele Anichini [1], Gianni Gori Savellini [1], Davide Corti [2], Luisa Bracci [3], Antonio Lanzavecchia [2], Gleyder Roman-Sosa [4,†] and Maria Grazia Cusi [1,*]

[1]   Virology Unit, Department of Medical Biotechnologies, University of Siena, 53100 Siena, Italy; claudia.gandolfo@unisi.it (C.G.); shibily.prathyumn@student.unisi.it (S.P.); chiara.terrosi@unisi.it (C.T.); gabriele.anichini@student.unisi.it (G.A.); gianni.gori@unisi.it (G.G.S.)

[2]   Institute for Research in Biomedicine, 6501 Bellinzona, Switzerland; davide.corti@humabs.ch (D.C.); alanzavecchia@vir.bio (A.L.)

[3]   Biochemistry Unit, Department of Medical Biotechnologies, University of Siena, 53100 Siena, Italy; luisa.bracci@unisi.it

[4]   Structural Virology Unit, Virology Department, Institut Pasteur, 25-28 rue du Dr Roux, 75015 Paris, France; gleyder.roman-sosa@vetmed.uni-giessen.de

*   Correspondence: mariagrazia.cusi@unisi.it; Tel.: +39-0577-233871

†   Current address: Institut für Virologie (FB10), Justus-Liebig-Universität Giessen, Schubert Str. 81, 35392 Giessen, Germany.

Abstract: Emerging and re-emerging viral infections have been an important public health problem in recent years. We focused our attention on Toscana virus (TOSV), an emergent neurotropic negative-strand RNA virus of the *Phenuiviridae* family. The mechanisms of protection against phlebovirus natural infection are not known; however, it is supposed that a virus-neutralizing antibody response against viral glycoproteins would be useful to block the first stages of infection. By using an improved memory B cell immortalization method, we obtained a panel of human mAbs which reacted with TOSV antigens. We identified three epitopes of TOSV Gn glycoproteins by neutralizing mAbs using synthetic peptide arrays on membrane support (SPOT synthesis). These epitopes, separated in primary structure, might be exposed near one another as a conformational epitope in their native structure. In vivo studies were conducted to evaluate the humoral response elicited in mice immunized with the identified peptides. The results underlined the hypothesis that the first two peptides located in the NH_2 terminus could form a conformational epitope, while the third, located near the transmembrane sequence in the carboxyl terminus, was necessary to strengthen neutralizing activity. Our results emphasize the importance of identifying neutralizing epitopes shared among the various phleboviruses, which could be exploited for the development of a potential epitope-based diagnostic assay or a polyvalent protective vaccine against different phleboviruses.

Keywords: Toscana virus; glycoprotein; epitope; vaccine

1. Introduction

Toscana virus (TOSV) belongs to the phlebovirus genus within the *Phenuiviridae* family under the order Bunyavirales [1]. TOSV was first isolated in 1971 in central Italy (in Monte Argentario, Grosseto Province) from two different species of sandflies, *Phlebotomus perniciosus* (*P. perniciosus*) and *Phlebotomus perfiliewi* (*P. perfiliewi*) [2–4]. TOSV is considered an emergent pathogen associated with acute neurological disease, such as meningitis, and occurs in Mediterranean countries during the summer months [5–9].

Despite the important role played by TOSV in central nervous system (CNS) infections, it remains a neglected agent and is rarely considered by physicians [10]. Like all members of the genus *Phlebovirus*, TOSV contains a segmented negative-strand RNA genome consisting of three non-covalently closed circular RNA segments that code, respectively, for the large protein (L) [11], the envelope glycoproteins (Gn and Gc) plus a non-structural protein (NSm) [12,13], and the nucleocapsid protein (N) together with the non-structural protein (NSs) [14].

The mechanisms of protection against natural infection of *Phlebovirus* are not known; however, it is supposed that a neutralizing antibody response against the viral glycoproteins could be necessary to block the first stages of infection. In several members of the family, such as Rift Valley fever virus (RVFV), La Crosse virus (LACV), Hantaan virus (HTNV), and TOSV, this neutralizing activity is a property of anti Gn-Gc antibodies [15–21]. In TOSV, however, a partial neutralizing activity was also shown for anti-N antibodies [22].

In this study, we focused our attention on TOSV Gn glycoprotein, since studies on the antigenicity of glycoproteins could be helpful to design epitopes that can be exploited as potential targets for the production of epitope-based diagnostics and vaccines against TOSV and other related *Phleboviruses*. In particular, we tried to identify viral Gn epitopes by using specific neutralizing antibodies. By immortalization of human memory B cells of a seropositive subject and parallel high-throughput screening for TOSV antigens, we localized three neutralizing epitopes. Two of these epitopes (Region 1 and Region 2) were located in the amino-terminal half of the Gn protein, while the third (Region 3) was close to the transmembrane region. To evaluate their immunogenicity, different combinations of these peptides were used for in vivo studies. All sera of immunized mice elicited, to a different extent, a good antibody response against Gn, laying the basis for the development of a polyvalent protective vaccine against different phleboviruses.

2. Materials and Methods

2.1. Viruses and Cells

Vero cells (ATCC CCL-81) were grown as a monolayer in Dulbecco's modified Eagle's medium (DMEM) (Lonza, Milan, Italy) supplemented with 5% heat-inactivated fetal calf serum (FCS) (Lonza) and 100 U/mL penicillin-streptomycin (HyClone Europe, Milan, Italy) at 37 °C. Human embryonic kidney (HEK)-Lenti-X 293 cells (Clontech, Milan, Italy) were grown as a monolayer in DMEM (Lonza, Milan, Italy) supplemented with 10% heat-inactivated FCS (Lonza) and 100 U/mL penicillin-streptomycin at 37 °C. Spodoptera frugiperda cells (Sf9) were propagated in SF-900II medium (GIBCO InVitrogen, Milan, ITALY) containing streptomycin (100 mg/mL; Life Technologies), and penicillin (100 UI/mL; Life Technologies).

Toscana virus (TOSV) strain 1812 cultured on Vero cells (isolated from a clinical specimen S. Maria alle Scotte Hospital, Siena, Italy) was plaque purified and propagated for viral stock preparation. Sandfly fever Naples virus (SFNV strain Sabin, kindly provided by ISS), sandfly fever Sicilian virus (SFSV, strain Sabin, provided by ISS), and Punique virus (PUNV, strain P1_B4_2008, isolated from a sandfly pool collected in Tunisia) were grown on Vero cells at the virology laboratory of the University of Siena. Purified TOSV for ELISA screening was prepared as described elsewhere [23].

2.2. Human PBMC Isolation

Peripheral blood mononuclear cells (PBMCs) were isolated from human blood, diluted in an equal volume of phosphate buffered saline (PBS) and further separated by Ficoll-Hypaque gradient by centrifugation at 1800 rpm for 20 min at RT. Cells were collected from the plasma/Ficoll interface, resuspended in PBS and centrifuged at 1300 rpm for 10 min at RT. Cells were finally resuspended in RPMI 1640 medium (Hyclone, Cramligton, UK) and counted. This research was carried out according to the principles of Helsinki declaration. Ethical approval was obtained from the local ethical committee for clinical trials (authorization TOSV2016_19/04/2016) (Comitato Etico Regione Toscana-Area Vasta Sud Est) in terms of General Data Protection and Regulation (GDPR) upon written informed consent signed by all subjects prior to participating in this study [24,25].

2.3. Immortalization of Human Memory B Cells

PBMCs and plasma samples were obtained from a patient with meningitis, infected by TOSV, during the acute phase and one year after the infection. At the Institute for Research in Biomedicine (Bellinzona Switzerland), frozen PBMCs were thawed and immortalized

using EBV in the presence of CpG, as previously described [26]. Briefly, IgG⁺ memory B cells were isolated using magnetic cell separators (MACS) and negative and positive selection kits (Miltenyi Biotec, Bergisch Gladbach, Germany). Then, memory B cells were seeded at 10 or 50 cells per well in 96 U-bottom microplates (Greiner, ThermoFisher Scientific) in complete medium containing 2.5 μg/mL CpG 2006, in the presence of EBV (30% supernatant of B95-8 cells) and irradiated allogeneic mononuclear cells (50,000 per well). After 2 weeks, the culture supernatants were screened for specific antibodies by Intellicyt Cytometer against TOSV-infected VERO cells. Specific TOSV antibodies were purified from culture supernatants by affinity chromatography on protein A columns (Amersham) and stored at −20 °C for further testing.

2.4. SPOT Peptide Synthesis

A set of 82 overlapping peptides of 15 aa, shifted by five residues, spanning aa 1–416 of TOSV Gn glycoprotein (GenBank accession no: AEM36009.1 from aa 308–834) was synthesized as an array on derivatized cellulose based membranes using SPOT technology [27,28]. In the sequence, the cysteines were replaced by serine. The membrane immobilized peptides were first saturated in MBS (pH 7.0) containing 2% non-fat milk and 0.05% Tween 20 in Tris Buffered Saline (TBS) o/n at 4°C. After three washing steps with TBS containing 0.05% Tween 20 (TTBS), peptides were probed with each human mAb at a concentration of 5 μg/mL in MBS for 90 min at 37 °C. Following the other three washing steps, the membrane was incubated with HRP-conjugated goat anti-mouse IgG (Merk Life Science S.r.l., Milano, Italy) at 1:8000 dilution and, after three washing steps, an enhanced chemiluminescent substrate kit was used for detection of HRP development (Thermo SCIENTIFIC, Monza, Italy) according to the manufacturer's instructions. The spots were evaluated with a gray scale of intensity after image acquisition using ImageQuantTL, as described [29].

2.5. Expression and Purification of Recombinant Proteins and Peptides

Plasmid vector pGex-2T (Amersham Biosciences, Milano, Italy) was used for the construction of a plasmid-containing defined peptide sequence of TOSV Gn glycoprotein. The gene sequence, containing peptides 1 and 2 (Figure 1), was amplified from the purified viral RNA by reverse transcriptase PCR (RT-PCR) using specific primers. The reaction was carried out using the Super Script III one-step RT-PCR mix (Invitrogen) by one cycle of reverse transcription at 50 °C for 30 min and 94 °C for 2 min, followed by 40 cycles of PCR (15 min at 94 °C, 30 s at 56 °C and 1 min at 68 °C) and 5 min at 68 °C. The primers used were:
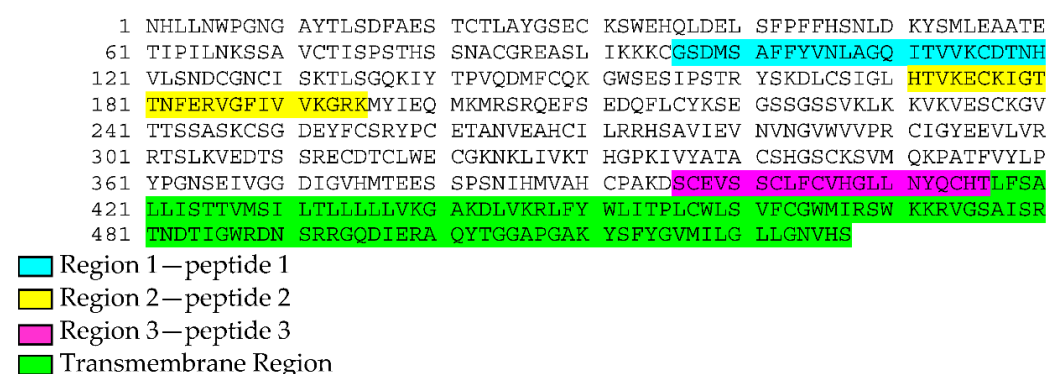
```
  1  NHLLNWPGNG  AYTLSDFAES  TCTLAYGSEC  KSWEHQLDEL  SFPFFHSNLD  KYSMLEAATE
 61  TIPILNKSSA  VCTISPSTHS  SNACGREASL  IKKKCGSDMS  AFFYVNLAGQ  ITVVKCDTNH
121  VLSNDCGNCI  SKTLSGQKIY  TPVQDMFCQK  GWSESIPSTR  YSKDLCSIGL  HTVKECKIGT
181  TNFERVGFIV  VKGRKMYIEQ  MKMRSRQEFS  EDQFLCYKSE  GSSGSSVKLK  KVKVESCKGV
241  TTSSASKCSG  DEYFCSRYPC  ETANVEAHCI  LRRHSAVIEV  NVNGVWVVPR  CIGYEEVLVR
301  RTSLKVEDTS  SRECDTCLWE  CGKNKLIVKT  HGPKIVYATA  CSHGSCKSVM  QKPATFVYLP
361  YPGNSEIVGG  DIGVHMTEES  SPSNIHMVAH  CPAKDSCEVS  SCLFCVHGLL  NYQCHTLFSA
421  LLISTTVMSI  LTLLLLLVKG  AKDLVKRLFY  WLITPLCWLS  VFCGWMIRSW  KKRVGSAISR
481  TNDTIGWRDN  SRRGQDIERA  QYTGGAPGAK  YSFYGVMILG  LLGNVHS
```

▢ Region 1—peptide 1
▢ Region 2—peptide 2
▢ Region 3—peptide 3
▢ Transmembrane Region

Figure 1. Three aminoacid sequences identified by pepscan analysis.

Forward primer: 5′-AAGGATCCGGAAGTGATATGTCG-3′
Reverse primer: 5′-GGGGAATTCTCATCTTCATCTGCTC-3′

The amplified gene was then cloned into a pGex-2T vector and linearized with Bam HI and EcoRI. The plasmid was named GC683. Another plasmid, named GC727, containing peptide 1, 2 and 3 sequences of TOSV Gn glycoprotein was constructed by inserting the sequence coding for peptide 3 (Figure 1) in GC683 plasmid after linearization with EcoRI

(Infusion cloning Takara Bio Inc, Kusatsu, Shiga Japan). A five-alanine coding sequence upstream of peptide 3 was fused with the linearized vector:

5′-GAG CAG ATG AAG ATG AGA ATT CAT GCG GCGGCGGCGGCG TCC TGT GAG GTT AGC AGC TGC CTA TTC TGT GTG CAC GGA CTG CTT AAC TAC CAG TGC CAC ACC TGA CTC GAG GAA TTC ATC GTG ACT GAC TGA CGA-3′.

The top 10 competent cells were transformed with GC683 and GC727 plasmids, and protein expression was induced by 1mM IPTG (Thermo Fisher Scientific (Ultrospec 2100 pro, Amersham Biosciences, Milano, Italy). Cultures were allowed to grow for 3 h at 37 °C, and cells were harvested by centrifugation at 4500 rpm for 20 min. The expressed recombinant proteins, pep GC683 and pep GC727, were purified from the cells as previously described [30]. The purified proteins were then quantified by Bradford reagent (Avantor, Leuven, Belgium) at 595 nm. SDS PAGE was then performed to evaluate the purity of the protein by staining the gel with Coomassie Brilliant Blue (CBB) (Bio-rad, Milano, Italy). The specificity of the protein was confirmed by Western blot analysis (data not shown). The protein was then stored at −80 °C until further use. Assessment of endotoxin concentration (<0.5 endotoxin units/mL) during the protein purification process was performed by using the ToxinSensor Chromogenic LAL Endotoxin Assay Kit (GeneScript, Leiden, Holland) according to the the manufacturer's instructions. The construct encoding the ectodomain fragment (Arg307-Thr725) of TOSV Gn protein from the strain Sotkamo (AMY16460.1) with a carboxyl terminal double Strep-Tag was generated by PCR (Forward primer: 5′-GACGATGACGATAAGGCCGGTTGG-3′ and Reverse primer: 5′-GGTGTGGCACTGGTAGTTCAGCAGGCC-3′) and followed by religation of the PCR product. The template used was a synthetic gene that encodes the full-length glycoprotein precursor with a double Strep-Tag at the carboxyl terminus already cloned in the pMT/V5-His A plasmid (Invitrogen, Monza, Italy) for expression in Drosophila S2 cells. The recombinant plasmid was co-transfected with the puromycin resistance gene-expressing plasmid pCoPuro in Drosophila S2 cells at a ratio of 1:20, and stable cell lines were established in the presence of puromycin (7 μg mL^{-1}). The protein was purified from the cell supernatants as previously described [31] and kept at −80 °C until use.

2.6. Mice Immunization

Four-week-old female BALB/c mice (Charles River, Milan, Italy) were used in the immunization experiments. Each experiment was repeated three times to assess the reproducibility of results. Twelve groups of five mice each were immunized with 100μg/mice of Gn peptides in different combinations every 2 weeks by four intraperitoneal (IP) injections (Table 1). All animal experiments were approved by the local ethics committee and carried out in strict compliance with the Institutional Animal Care and Use Committee (IACUC) guidelines and in accordance with the 2010/63/EUDirective (http://eurlex.europa.eu/LexUriServ/LexUriSev.do?uri=OJ:L:2010:276:0033:0079:EN:PDF, accessed on 22 September 2010) of the European Parliament and the Council for the Protection of Animals Used for Scientific Purposes. Peptide 1, 2 and 3 as single units conjugated with the KLH carrier were purchased from Peptide Facility (CRIBI—Centro di Biotecnologie Università di Padova). All the combinations of antigens contained an equal volume of Montanide (50 μL/mouse) as adjuvant.

Two weeks after the last immunization, all mice were sacrificed, blood was drawn, and serum was collected and stored at −20 °C for further analysis.

Table 1. Mice immunization chart.

Group of Mice	Antigens Injected for Immunization
Group 1	Peptide 1-KLH
Group 2	Peptide 2-KLH
Group 3	Peptide 3-KLH
Group 4	Peptide 1-KLH and peptide 2-KLH
Group 5	Peptide 1-KLH and peptide 3-KLH
Group 6	Peptide 2-KLH and peptide 3-KLH
Group 7	Peptide 1-KLH, peptide 2-KLH and peptide 3-KLH
Group 8	Pep GC683
Group 9	Pep GC683 and peptide 3-KLH
Group 10	Pep GC727
Group 11	rGn
Group 12	PBS

2.7. ELISA

Microtiter plates (Labsystem, Helsinki, Finland) were coated with 100 μL per well of either purified whole TOSV or purified Gn glycoprotein protein (1 μg/mL conc.) in 0.1 M carbonate buffer (pH 9.6) and incubated o/n at 4 °C. To prevent non-specific binding, 100 μL of non-fat dry milk (0.5%) was added to each well for 1 h at RT. After three washing steps with PBS containing 0.05% Brij, 100 μL of mice sera or human mAbs diluted 1:50 in dilution buffer (PBS + 0.05% Brij + 10% FBS) were added to each well and the plates were incubated at 37 °C for one hour. Post incubation, the plates were washed and 100 μL of peroxidase-conjugated anti-mouse IgG or anti-human IgG (Sigma-Aldrich) were added followed by incubation at 37 °C for one hour in dark. The plates were then washed prior to adding 100 μL of 3,3′,5,5′-tetramethylbenzidine to each well (TMB One Component HRP Microwell Substrate, Tebu-bio laboratories) for 15 min. A negative control corresponding to a pool of TOSV seronegative human sera (previously screened in our lab) was included in the assay. The reaction was stopped by adding 100 μL of 1 N H_2SO_4 solution, and the plates were read immediately at 450 nm.

2.8. Neutralization Test

Virus neutralization was carried out on Vero cells in a 96 well microplate. Briefly, two-fold serial dilutions (50 μL) of immunized mice serum or human mAbs were added to an equal volume of TOSV containing 100 $TCID_{50}$ and incubated for 90 min at 37 °C. Fifty μL of cells (10^6/mL) were suspended in Minimum Essential Media (MEM, InVitrogen, Milan, Italy) with 5% FCS and added to each well. Five days after incubation at 37 °C, the cultures were examined microscopically for the presence of a cytopathic effect. The 50% end point titer of the neutralizing serum was calculated using the Reed and Muench method [32]. A titer <1/4 was considered negative. The same protocol was used for the neutralization assay versus SFNV, SFSV and PUNV.

2.9. Indirect Immunofluorescence Assay

Sf9 cells were infected with baculovirus expressing the ectodomains of TOSV glycoproteins (Bac-Gn and Bac-Gc) as described elsewhere [22]. Lenti-X HEK293 were transfected with 1μg of Gn-expressing plasmid using the GeneJuice reagent (Merck-Millipore, Milan, Italy), as suggested by the manufacturer. Vero cells were infected with TOSV 1812. All these cells were spotted on slides and fixed for 10 min at room temperature with cold methanol/acetone and screened by indirect immunofluorescence (IFA).

Diluted mice sera (1:50 in PBS) or human mAbs were added to the slides, followed by incubation at 37 °C for 30 min. Subsequently, the slides were washed with PBS for 5 min, and FITC-conjugated anti-mouse or anti-human secondary antibody (Sigma, Milan, Italy) was added to the slides and incubated for 20 min at 37 °C. After the final wash, immunofluorescence was visualized using a Diaplan microscope (Leica Microsystems, Milan, Italy). The cross-reactivity of mouse sera against Sicilian virus (SFSV), Naples

virus (SFNV), and Cyprus Virus (CYPR) was tested using a commercially available kit "sandfly fever virus Mosaic 1 types: Sicilian, Naples, Toscana, Cyprus IFA" (EUROPattern) following the manufacturer's instructions.

2.10. Statistical Analysis

The statistical analysis of differences between means was performed using Stat View statistical software (Abacus Concepts, Berkeley, CA, USA). Neutralization titers were presented as geometric mean ± standard deviation. $p < 0.05$ was considered significant.

3. Results

3.1. Isolation and Screening of a Panel of TOSV Human Monoclonal Antibodies

PBMCs and serum were collected from a patient infected by TOSV during the acute phase and one year later. After immortalization, B cell culture supernatants containing Ig were screened by high-throughput FACS analysis using TOSV infected VERO cells (Figure 2).
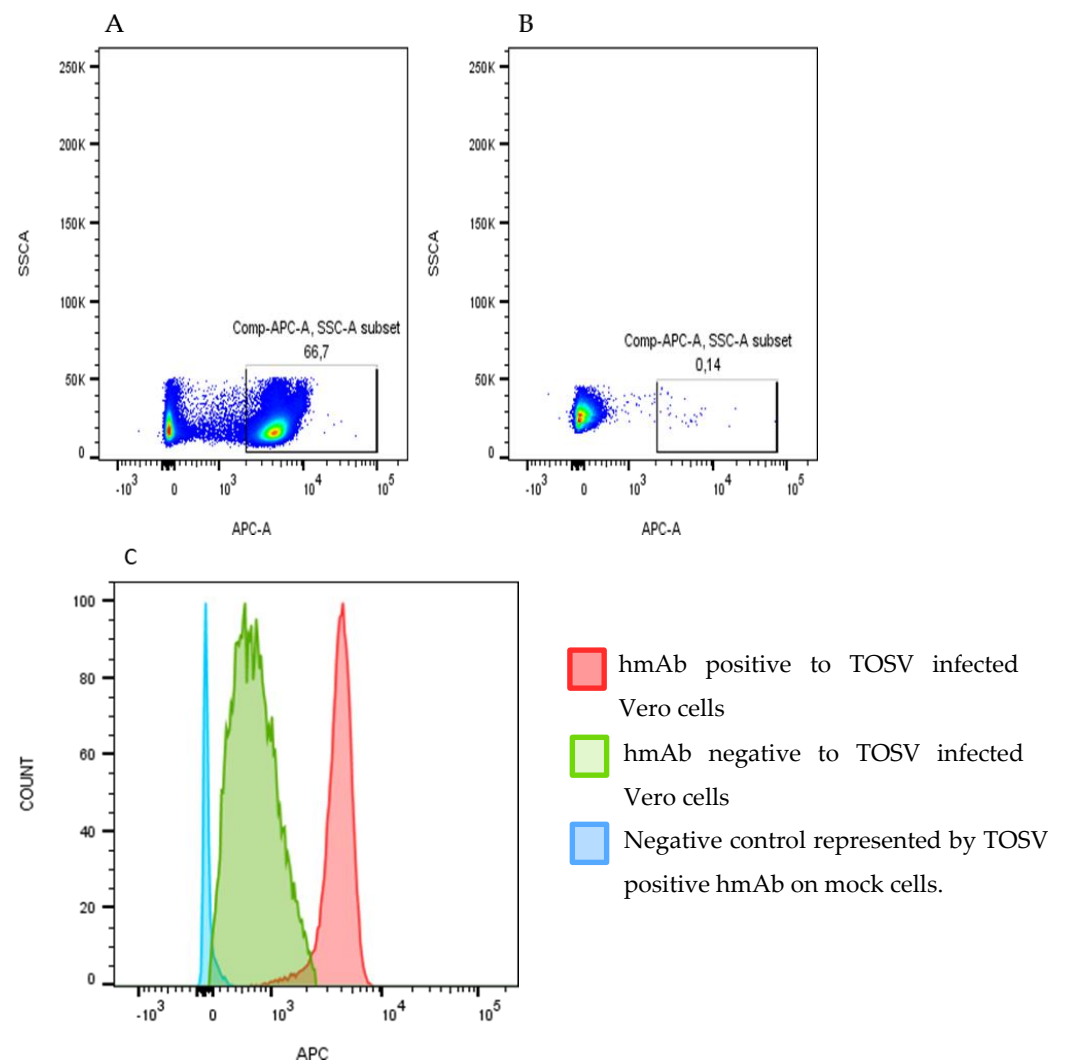

Figure 2. High-throughput FACS analysis using TOSV-infected VERO cells. (**A**) shows the identification of TOSV-positive human mAb by using an anti-hFc-APC secondary antibody (BD Biosciences) reacted with infected cells, while (**B**) shows a TOSV-negative hmAb. (**C**) shows the difference between the fluorescence of a positive and a negative hmAb to TOSV-infected Vero cells versus mock cells.

Based on this primary screening, 112 mAbs which were positively reactive against TOSV infected cells were selected. Among them, 7 antibodies were derived from PBMCs of

the acute phase (identified as TVA mAbs), while 105 were from PBMCs collected one year post infection (TVB mAbs). The whole mAbs panel was first screened against recombinant TOSV N protein by ELISA in order to exclude those positive to the N protein.

Fifty-eight mAbs (5 from the acute phase and 53 from the convalescent phase) were then analyzed by immunofluorescence with Sf9 cells infected with recombinant baculoviruses, Bac-Gn or Bac-Gc, expressing the ectodomains of TOSV Gn and Gc proteins, respectively. Thirteen out of 58 mAbs were positive to Sf9-Gn and five showed positivity to Sf9-Gc; 40 tested negative to both the proteins. The 58 mAbs were also screened by neutralization assay with a TOSV strain 1812. We did not find any neutralizing activity among the monoclonal antibodies derived from the acute phase sample, although the human serum of the acute phase had a neutralizing titer of 1/161. However, twenty mAbs obtained from the convalescent phase sample had a high neutralization activity with titer values ranging from 1/128 to >1/512 (Table 2). These neutralizing mAbs were analyzed by immunofluorescence with Lenti-X HEK293 cells transfected with plasmids expressing the whole glycoproteins. Our attention was first addressed to the Gn glycoprotein, because all the mAbs with a high neutralization titer were positive to the Gn glycoprotein. Twelve mAbs, previously negative by IFA on Sf9-Gn cells and lacking the transmembrane region, were positive on Lenti-X HEK293-Gn, expressing the whole protein and suggesting that these antibodies recognized a region close to the transmembrane domain (data not shown).

Table 2. Human mAbs tested for neutralizing activity against TOSV.

mAbs of Acute Phase	
mAbs	**NT Titer**
5	neg
mAbs of Convalescent Phase	
mAbs	**NT Titer**
26	neg
7	<1/128
8	1/128–1/512
12	>1/512

No mAbs of the acute phase had a neutralizing activity, while twenty mAbs obtained from the convalescent phase sample had high neutralization activity with titer values ranging from 1/128 to >1/512.

3.2. Identification of Neutralizing TOSV Gn Epitopes by Pepscan Analysis

SPOT peptide synthesis [27,28] was used to generate membranes of 82 spots of 15 aa–long peptides shifted by 5 residues, covering TOSV Gn glycoprotein from aa 1 to aa 416 (GenBank accession no: AEM36009.1 from aa 308–834). These membranes were used to identify Gn epitopes recognized by previously selected neutralizing mAbs. We also included three aspecific mAbs as negative controls.

Most of the mAbs, in particular those with a neutralizing activity >1/128, reacted with the same strings of Gn peptides. Two of these linear peptides were localized in the amino-terminal half of the protein; one was instead close to the transmembrane region of the glycoprotein (Figure 1). The three regions identified by the neutralizing mAbs were also recognized by the sera of the acute as well as the convalescent phase. Furthermore, the serum drawn during the convalescent phase showed a higher reactivity against the spotted peptides, compared with the serum of the acute phase.

The three regions identified by pepscan analysis were as follows: the first two regions, 1 and 2, were localized in the amino-terminal of the Gn glycoprotein, while region 3 was located near the transmembrane sequence.

3.3. Cross-Reactivity of Human mAbs

Since cross-reactivity of sera among phleboviruses is quite common, we analyzed the ability of some mAbs to neutralize viruses of the phlebovirus genus, such as sandfly fever Naples virus (SFNV), sandfly fever Sicilian virus (SFSV), and Punique virus (PUNV). A preliminary screening detected one anti-TOSV mAb that neutralizes SFNV. Unfortunately, because of the small amount of purified mAbs, we could not test them against other phleboviruses. On the contrary, none of the tested mAbs against SFSV and PUNV showed neutralizing activity (Table 3).

Table 3. Neutralization assay of mAbs against SFNV, PUNV and SFSV.

Antibody ID	NT Titer			
	TOSV	**SFNV**	**PUNV**	**SFSV**
TVB 27	1/161	1/25	-	-
TVB 73	>1/512	-	-	-
TVB 147	1/645	-	-	-
TVB 161	1/645	-	-	-
TVB 164	1/6	-	-	-

3.4. Immunization of Mice with Peptides

Different combinations of these peptides were used for in vivo studies to determine their immunogenicity. The peptides were used as a single antigen linked with KLH as carrier, or in combination, or fused with GST as carrier protein. Peptides 1 and 2 were expressed by a plasmid named GC683, whereas peptides 1, 2 and 3 were expressed by a plasmid named GC727 as described in Materials and Methods (Figure 3).
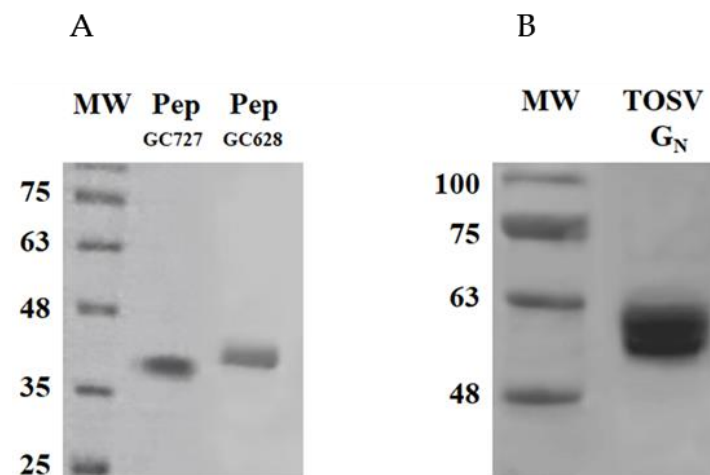

Figure 3. SDS_PAGE of TOSV recombinant proteins. (**A**) 5 µg of purified pep GC683 and GC727 and (**B**) TOSV Gn protein were analyzed on a 12% polyacrylamide gel under reducing conditions and stained with Coomassie Blue. MW: SharpmassVI, Euroclone.

Four weeks-old female Balb/c mice were immunized intraperitoneally as described in Table 1. Four consecutive immunizations of 5 mice/group were carried out at two weeks interval.

The antibody response to the different combinations of peptides was evaluated in mice. After four cycles of immunizations, mice were sacrificed, and the sera obtained from each group were tested for the presence of antibodies against both Gn protein and purified TOSV by ELISA.

All the mice elicited, to a different extent, an antibody response against all combinations of the peptides. ELISA results, using Gn as antigen, showed that sera of mice immunized with single synthetic peptides or combinations of them were all reactive. The

group immunized with Pep1-KLH developed a low level of antibodies, while those immunized with Pep 2-KLH and Pep 3-KLH or other combinations containing peptides 2 and 3 were able to induce a high level of antibodies reacting with Gn. Sera screened by using the purified whole TOSV as antigen showed positivity in all the immunized mice groups, although at varying levels. Mice immunized with Pep 3-KLH or combinations containing peptide 3 showed a good response. Moreover, the mice group immunized with Pep GC683 alone or with Peptide 3-KLH showed the best response (Figure 4A).
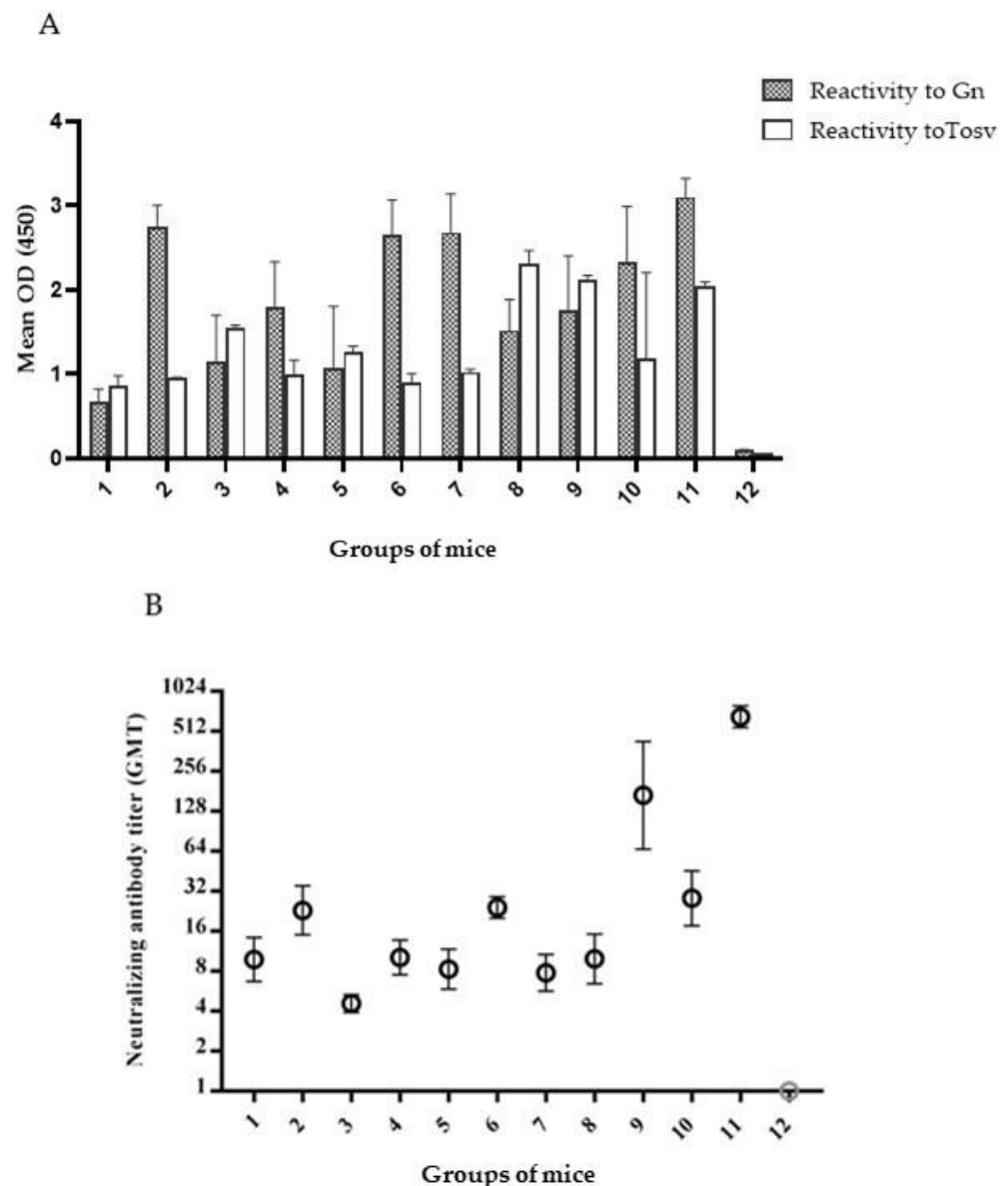

Figure 4. (**A**) Evaluation of the humoral response of immunized mice with different combinations of antigens, either against rGn or whole TOSV, by ELISA. (**B**) Evaluation of the neutralizing antibody response in immunized mice measured in quadruplicate. Results are reported as geometric mean titer (GMT, black circles) with 95% confidence interval (95% CI). **Group 1**: peptide 1-KLH; **Group 2**: peptide 2-KLH; **Group 3**: peptide 3-KLH; **Group 4**: peptide 1-KLH and peptide 2-KLH; **Group 5**: peptide 1-KLH and peptide 3-KLH; **Group 6**: peptide 2-KLH and peptide 3-KLH; **Group 7**: peptide 1-KLH, peptide 2-KLH and peptide 3-KLH; **Group 8**: pep GC683; **Group 9**: pep GC683 and peptide 3-KLH; **Group 10**: pep GC727; **Group 11**: rGn; **Group 12**: PBS.

Mice sera were also tested by immunofluorescence on TOSV-infected Vero cells. Only the sera of mice immunized with Pep 2-KLH or Pep3-KLH did not react with the viral glyco-

protein in immunofluorescence, indicating that it is possible that each single conformomer was not similar to that of the original protein (data not shown).

A neutralization assay was also performed to determine specific neutralizing activity against TOSV. The mice groups immunized with the single peptides 1, 2 and 3 showed low neutralization titers of 1/10, 1/23 and 1/5, respectively. Additionally, the groups immunized with different combinations of single peptides showed a modest neutralization titer (range 1/8–1/24), as did the mice immunized with Pep GC683 and Pep GC727 (titer of 1/10 and 1/28, respectively). On the contrary, the mice group immunized with a combination of Pep GC683 + Pep3-KLH showed a significantly higher titer value (1/183) (Figure 4B).

3.5. Serological Cross-Reactivity of Immunized Mice

The immunized mice sera were tested for cross-reactivity against some viruses of the Phlebovirus genus, including SFNV, SFSV, CYPR (Cyprus viruses) and PUNV using a commercially available IFA kit. The sera of all groups showed cross-reactivity with SFNV, but only the serum of mice immunized with Pep1-KLH+ Pep 2-KLH recognized SFSV and CYPR. PUNV reacted only with sera of groups receiving Pep 3-KLH alone or in combination, as an immunogen (Table 4).

Table 4. Cross-reactivity among mice sera and SFNV, SFSV, CYPR, PUNV Phleboviruses.

GROUPS	CROSS-REACTIVITY			
	SFNV	SFSV	CYPR	PUNV
Group 1 (Pep 1-KLH)	+	−	−	−
Group 2 (Pep 2-KLH)	+	−	−	−
Group 3 (Pep 3-KLH)	+	−	−	+
Group 4 (Pep 1-KLH + Pep2-KLH)	+	+	+	−
Group 5 (Pep 1-KLH + Pep 3-KLH)	+	−	−	+
Group 6(Pep2-KLH + Pep3-KLH)	+	−	−	+
Group7(Pep1-KLH+Pep2-KLH + Pep3-KLH)	+	−	−	+
Group 8 (PepGc 683)	+	−	−	−
Group 9 (PepGc 683 + Pep3-KLH)	+	−	−	+
Group 10 (Pep Gc 727)	+	−	−	+
Group 11 (rGn)	−	−	−	−
Group 12 (PBS)	−	−	−	−

4. Discussion

By using an improved memory B cell immortalization method [26], combined with parallel high-throughput screening for TOSV antigens, we isolated a panel of human mAbs which were characterized with regard to epitope specificity and neutralizing activity. We demonstrated that most of the antibodies were directed to TOSV Gn glycoprotein and that they acquired a high degree of magnitude of response with the maturation of the adaptative immune response; indeed, they were all obtained from PBMCs of the convalescent phase blood sample.

With pepscan analysis, we were able to identify three amino acid regions that were always recognized by the neutralizing mAbs. Two of these epitopes (Region 1 and Region 2) were located in the amino-terminal half of Gn protein, while the third (Region 3) was close to the transmembrane region. We first hypothesized that they were a part of a larger conformational epitope that could be recognized when exposed on the viral envelope in the natural structure of the protein.

To evaluate their immunogenicity, different combinations of these peptides were used for in vivo studies. All the sera of immunized mice were positive to Gn in the ELISA assay. This result demonstrated that the mice elicited, to different extents, a good antibody response against the viral glycoprotein. Likewise, the sera tested against the whole virus showed a high antibody level.

In particular, sera of mice immunized with Pep GC683 or Pep GC727 expressing peptides 1 and 2 or 1, 2, and 3 fused with GST, respectively, showed very good results once tested against the whole TOSV either in ELISA (Figure 4) or IFA (data not shown). This finding indicates that peptides 1 and 2 might represent a conformational structure similar to that of the original protein which is recognized by TOSV specific sera, although we cannot exclude that a linear epitope with a dominant sequence for peptide 3 could also be a favourable target.

Concerning the induction of neutralizing antibodies, all combinations of peptides induced a modest response with a range varying from 1/8 to 1/28, but Pep GC683 + Pep3-KLH induced a better response (GMT 1/183). Therefore, this result supports the hypothesis that Pep 1 and Pep 2 could be part of a conformational epitope capable of inducing neutralizing antibodies, and Pep 3, located near the transmembrane region, could strengthen this activity by hindering the binding of TOSV to the cell receptor. Indeed, Pep GC683 alone did not mount a high titer of neutralizing antibodies, but the addition of Pep 3-KLH enhanced the neutralizing response in vivo. Thus, it appears that both epitopes are involved in the neutralization of virus infectivity. In particular, they might act in synergy by reacting with distinct domains of the Gn glycoprotein and inducing a steric hindrance at the binding site with the receptor, a phenomenon already known to occur [33]. Thus, this binding could block the virus entry into the cell, mediated by the glycoproteins, and, consequently, inhibit viral replication. Moreover, considering the importance of identifying neutralizing epitopes shared by other phleboviruses, we evaluated the serological cross-reactivity of TOSV mAbs with neutralizing activity to other phleboviruses. Cross-reactivity is associated with linear as well as conformational epitopes [34]. The well-documented serological relationships among viruses of the same genus provides the rationale behind identifying conserved epitope regions on viral proteins [35] and their use for diagnostic as well as treatment purposes.

We found only one mAb (TVB 27) which neutralized SFNV, which has a Gn sharing 90% homology with TOSV Gn. This was only a preliminary screening, and a larger analysis must be carried out with the aim of detecting the epitopes shared by other phleboviruses that could be exploited for a potential vaccine against other sandfly viruses.

The sera of all groups of mice were also tested by immunofluorescence against SFNV, SFSV, PUNV and CYPR. All sera cross-reacted with SFNV; sera of mice immunized either with Peptide 3-KLH alone or its combinations reacted with Punique virus, which had 70% sequence similarity with Peptide 3. Unexpectedly, only the sera obtained from mice immunized with peptides 1-KLH + 2-KLH cross-reacted with SFNV, SFSV and CYPR, probably because this combination induced antibodies with a higher affinity than those elicited by single peptides.

Finally, it is worthy to note that these results were based only on the screening of mAbs derived from one patient. Thus, this study will be enlarged to other TOSV-positive patients to characterize further antibodies and extend the spectrum of functional epitopes. The results could be exploited for the development of potential epitope-based diagnostic assays or as the starting point for the development of a polyvalent vaccine protective against several sandfly viruses.

Author Contributions: Conceptualization, M.G.C.; methodology, C.G., S.P. and G.R.-S.; software, G.A.; validation, D.C., M.G.C., L.B.; investigation, L.B.; D.C.; A.L.; data curation, C.T.; G.G.S.; writing—original draft preparation, C.G.; writing—review and editing, C.G.; S.P.; M.G.C.; supervision, M.G.C. All authors have read and agreed to the published version of the manuscript.

Institutional Review Board Statement: The study was conducted according to the guidelines of the Declaration of Helsinki, and approved by the Institutional Review Board of the University of Siena (protocol code MGC-08/2014, Health Ministry authorization no. 342/2015PR).

Informed Consent Statement: Not applicable.

Conflicts of Interest: We declare no competing interest.

References

1. Abudurexiti, A.; Adkins, S.; Alioto, D.; Alkhovsky, S.V.; Avšič-Županc, T.; Ballinger, M.J.; Bente, D.A.; Beer, M.; Bergeron, É.; Blair, C.D.; et al. Taxonomy of the order *Bunyavirales*: Update 2019. *Arch. Virol.* **2019**, *164*, 1949–1965. [CrossRef]
2. Verani, P.; Ciufolini, M.G.; Nicoletti, L.; Balducci, M.; Sabatinelli, G.; Coluzzi, M.; Paci, P.; Amaducci, L. Ecological and epidemiological studies of Toscana virus, anarbovirus isolated from Phlebotomus. *Ann. Ist. Super. Sanita* **1982**, *18*, 397–399.
3. Verani, P.; Nicoletti, L.; Ciufolini, M.G. Antigenic and biological characterization of Toscana virus, a newPhlebotomus fever group virus isolated in Italy. *Acta Virol.* **1984**, *28*, 39–47.
4. Verani, P.; Ciufolini, M.G.; Caciolli, S.; Renzi, A.; Nicoletti, L.; Sabatinelli, G.; Bartolozzi, D.; Volpi, G.; Amaducci, L.; Coluzzi, M.; et al. Ecology of viruses isolated from sand flies in Italy and characterized of a new Phlebovirus (Arabia virus). *Am. J. Trop. Med. Hyg.* **1988**, *38*, 433–439. [CrossRef] [PubMed]
5. Valassina, M.; Cusi, M.G.; Valensin, P.E. A Mediterranean arbovirus: The Toscana virus. *J. NeuroVirology* **2003**, *9*, 577–583. [CrossRef]
6. Valassina, M.; Valentini, M.; Pugliese, A.; Valensin, P.E.; Cusi, M.G. Serological survey of toscana virus infections in a high-risk population in Italy. *Clin. Diagn. Lab. Immunol.* **2003**, *10*, 483–484. [CrossRef] [PubMed]
7. Charrel Rèmi, N.; Pierre, G.; Josè-Maria, N.; Loredana, N.; Anna, P.; Paz, S.; Antonio, T.; de Lambelleire, X.E. Emergence of Toscana Virus in Europe. *Emerg. Infect. Diseas.* **2005**, *11*, 1657–1663. [CrossRef] [PubMed]
8. Sanbonmatsu-Gàmez, S.; Pèrez-Ruiz, M.; Palop-Borràs, B.; Navarro-Marì, J.M. Unusual Manifestation of Toscana virus Infection, Spain. *Emerg. Infect. Dis.* **2009**, *15*, 347–348. [CrossRef] [PubMed]
9. Cusi, M.G.; GoriSavellini, G.; Zanelli, G. Toscana virus epidemiology: From Italy to beyond. *Open Virol. J.* **2010**, *4*, 22–28. [CrossRef]
10. Charrel, R.N.; Bichaud, L.; De Lamballerie, X. Emergence of Toscana virus in the Mediterranean area. *World J. Virol.* **2012**, *1*, 135–141. [CrossRef]
11. Accardi, L.; Gro, M.C.; Di Bonito, P.; Giorgi, C. Toscana virus genomic L segment: Molecular cloning, coding strategy and amino acid sequence in comparison with other negative strand RNA viruses. *Virus Res.* **1993**, *27*, 119–131. [CrossRef]
12. Di Bonito, P.; Mochi, S.; Gro, M.C.; Fortini, D.; Giorgi, C. Organization of the M genomic segment of Toscana phlebovirus. *J. Gen. Virol.* **1997**, *76*, 77–81. [CrossRef]
13. Gro, M.C.; Di Bonito, P.; Fortini, D.; Mochi, S.; Giorgi, C. Completion of molecular characterization of Toscana phlebovirus genome: Nucleotide sequence, coding strategy of M genomic segment and its aminoacid sequence comparison to other phleboviruses. *Virus Res.* **1997**, *51*, 81–91. [CrossRef]
14. Giorgi, C.; Accardi, L.; Nicoletti, L.; Gro, M.C.; Takehara, K.; Hilditch, C.; Morikawa, S.; Bishop, D.H. Sequences and coding strategies of the SRNAs of Toscana and Rift Valley fever viruses compared to those of Punta Toro, Sicilian Sandfly fever, and Uukuniemi viruses. *Virology* **1991**, *180*, 738–753. [CrossRef]
15. Saluzzo, J.F.; Anderson, G.W., Jr.; Hodgson, L.A.; Digoutte, J.P.; Smith, J.F. Antigenic and biological properties of Rift Valley fever virus isolated during the 1987 Mauritanian epidemic. *Res. Virol.* **1989**, *140*, 155–164. [CrossRef]
16. Saluzzo, J.F.; Anderson, G.W., Jr.; Smith, J.F.; Fontenille, D.; Coulanges, P. Biological and antigenic relationship between Rift Valley fever virus strains isolated in Egypt and Madagascar. *Trans. R. Soc. Trop. Med. Hyg.* **1989**, *83*, 701. [CrossRef]
17. Gonzalez-Scarano, F.; Shope, R.E.; Calisher, C.E.; Nathanson, N. Characterization of monoclonal antibodies against Gn and N proteins of La Crosse and Tahyna, two California serogroup bunyaviruses. *Virology* **1982**, *120*, 42–53. [CrossRef]
18. Grady, L.; Kinch, W. Two monoclonal antibodies against La Crosse virus show host-dependent neutralizing activity. *J. Gen. Virol.* **1985**, *66*, 2773–2776. [CrossRef] [PubMed]
19. Arikawa, J.; Schmaljohn, A.L.; Dalrymple, J.M.; Schmaljohn, C.S. Characterization of Hantaan virus envelope glycoprotein antigenic determinants defined by monoclonal antibodies. *J. Gen. Virol.* **1989**, *70*, 615–624. [CrossRef]
20. Di Bonito, P.; Bosco, S.; Mochi, S.; Accardi, L.; Ciufolini, M.G.; Nicoletti, L.; Giorgi, C. Human antibody response to Toscana virus glycoproteins expressed by recombinant baculovirus. *J. Med. Virol.* **2002**, *68*, 615–619. [CrossRef]
21. Cusi, M.G.; Valentini, M.; Valensin, P.E.; Valassina, M. Immune response to the neurotropic Toscana virus infection: Preliminary data. In Proceedings of the 1st SIV International Workshop on Neurovirology, Alghero, Italy, 23–25 June 2002.
22. Cusi, M.G.; Valensin, P.E.; Donati, M.; Valassina, M. Neutralization of Toscana virus is partially mediated by antibodies to the nucleocapsid protein. *J. Med. Virol.* **2001**, *63*, 72–75. [CrossRef]
23. Soldateschi, D.; dal Maso, G.M.; Valassina, M.; Santini, L.; Bianchi, S.; Cusi, M.G. Laboratory diagnosis of Toscana virus infection by enzyme immunoassay with recombinant viral nucleoprotein. *J. Clin. Microbiol.* **1999**, *37*, 649–652. [CrossRef] [PubMed]
24. Authorisation, no. 9/2014—General Authorisation to Process Personal Data for Scientific Research Purposes. Available online: https://www.gazzettaufficiale.it/atto/serie_generale/caricaDettaglioAtto/originario?atto.dataPbblicazioneGazzetta=2014-1230&atto.codiceRedazionale=14A09916&elenco30giorni=true (accessed on 30 December 2014).
25. Law Decree 22 December 2017, No. 219, published in the Ocial Gazette No. 12 of 16 January 2018. Available online: https://www.gazzettaufficiale.it/eli/gu/2018/01/16/12/sg/pdf (accessed on 16 January 2016).

26. Traggiai, E.; Becker, S.; Subbarao, K.; Kolesnikova, L.; Uematsu, Y.; Gismondo, M.R.; Murphy, B.R.; Rappuoli, R.; Lanzavecchia, A. An efficient method to make human monoclonal antibodies from memory B cells: Potent neutralization of SARS coronavirus. *Nat. Med.* **2004**, *10*, 871–875. [CrossRef]

27. Hilpert, K.; Winkler, D.F.; Hancock, R.E. Peptide arrays on cellulose support: SPOT synthesis, a time and cost-efficient method for synthesis of large numbers of peptides in a parallel and addressable fashion. *Nat. Protoc.* **2007**, *2*, 1333–1349. [CrossRef]

28. Winkler, D.F.; Campbell, W.D. The spot technique: Synthesis and screening of peptide macroarrays on cellulose membranes. *Methods. Mol. Biol.* **2008**, *494*, 47–70. [PubMed]

29. Lin, M.; Mcrae, H.; Dan, H.; Tangorra, E.; Laverdiere, A.; Pasick, J. High-resolution epitope mapping for monoclonal antibodies to the structural protein Erns of classical swine fever virus using peptide array and random peptide phage display approaches. *J. Gen. Virol.* **2010**, *138*, 2928–2940. [CrossRef] [PubMed]

30. Di Bonito, P.; Nicoletti, L.; Mochi, S.; Accardi, L.; Marchi, A.; Giorgi, C. Immunological characterization of Toscana virus proteins. *Arch. Virol.* **1999**, *144*, 1947–1960. [CrossRef] [PubMed]

31. Backovic, M.; Johansson, D.X.; Klupp, B.G.; Mettenleiter, T.C.; Persson, M.A.; Rey, F.A. Efficient method for production of high yields of Fab fragments in Drosophila S2 cells. *Protein Eng. Des. Sel.* **2010**, *23*, 169–174. [CrossRef]

32. Reed, L.J.; Muench, H. A simple method of estimating fifty per cent endpoints. *Am. J. Hyg.* **1938**, *27*, 493–497.

33. Hlavacek, W.S.; Posner, R.G.; Perelson, A.S. Steric effects on multivalent ligand-receptor binding: Exclusion of ligand sites by bound cell surface receptors. *Biophys. J.* **1999**, *76*, 3031–3043. [CrossRef]

34. Rizk, R.Z.; Christensen, N.D.; Michael, K.M.; Müller, M.; Sehr, P.; Waterboer, T.; Pawlita, M. Reactivity pattern of 92 monoclonal antibodies with 15 human papillomavirus types. *J. Gen. Virol.* **2008**, *89 Pt 1*, 117–129. [CrossRef]

35. Elliott, R.M.; Brennan, B. Emerging phleboviruses. *Curr. Opin. Virol.* **2014**, *5*, 50–57. [CrossRef] [PubMed]

CASE REPORT

Hyperimmune plasma in three immuno-deficient patients affected by non-severe, prolonged COVID-19: a single-center experience

Maria Grazia Cusi[1*], Edoardo Conticini[2*] [iD], Claudia Gandolfo[1], Gabriele Anichini[1], Gianni Gori Savellini[1], Serafina Valente[3,4], Federico Franchi[4,5], Sabino Scolletta[4,5], Elena Percivalle[6] and Bruno Frediani[2,4]

Abstract

Background: Convalescent plasma (CP) and hyperimmune plasma (HP) are passive immunotherapies consisting in the infusion of plasma from recovered people into infected patients. Following pre-existing evidence in many other viral diseases, such as SARS, MERS and Ebola, CP and HP have also been proposed for the treatment of COVID-19. Nevertheless, due to the lack of large, well-designed, clinical trials, no clear-cut guidelines exist about what subtype of patient CP and HP should be administered to.

Case presentation: We have reported the cases of 3 patients, all immunosuppressed and affected by non-severe, prolonged COVID-19. They were treated with HP, whose neutralizing titer was higher than 1/80. The first patient was a 55-year-old male, who had undergone lung transplant. He was under therapy with Tacrolimus and developed non-neutralizing antibodies against SARS-CoV2. The second patient was a 77-year-old female, affected by follicular lymphoma. She had tested positive for SARS-CoV2 after 6 months. The third was a 60-year-old patient, affected by chronic leukemia. He did not develop antibodies after 2-month disease. All 3 patients received HP and had tested negative for SARS-CoV2 within 2 weeks.

Conclusion: Despite encouraging initial data, no strong evidence exist in support of CP and HP to treat COVID-19. In our experience, although limited due to the reduced number of patients, we found a good safety and efficacy of HP in 3 immuno-deficient subjects. Further data are needed in order to assess whether this subtype of patients may particularly benefit from passive immunization.

Keywords: Convalescent plasma, Hyperimmune plasma, SARS-CoV2, COVID-19, Immunodeficiency

* Correspondence: mariagrazia.cusi@unisi.it; conticini.edoardo@gmail.com
[1]Virology Unit, Department of Medical Biotechnologies, University of Siena, Siena, Italy
[2]Rheumatology Unit, Department of Medicine, Surgery and Neurosciences, University of Siena, viale Mario Bracci, 16, Siena, Italy
Full list of author information is available at the end of the article

Background

Convalescent plasma (CP) is a promising therapy to treat patients affected by Coronavirus disease 2019 (COVID-19) [1, 2]. CP is a passive immunotherapy consisting in the infusion of plasma from recovered people into infected patients and it is thought to act by transferring neutralizing antibodies [3]. Hyperimmune plasma (HP) is another blood component sharing the same mechanism of action of CP, but with the advantage of a better standardization in terms of neutralizing antibodies titer, lower volume, and easier storage, no need of group matching, these *pros* are nevertheless counterbalanced by a lower availability [4].

Despite some encouraging data coming from the first published papers, displaying a reduced mortality in patients treated with CP [5]), it should be remarked that only 10 of them are randomized control trials (RCTs), [5] while many others do not have a control group [6, 7]. Thus, findings from larger and well-designed clinical trials with both CP and HP are urgently needed in order to better assess efficacy and safety in COVID-19.

Moreover, an even larger uncertainty exists about the role of CP and HP in the treatment of COVID-19 patients: no clear-cut findings display whether this procedure should be performed in severely ill or asymptomatic subjects, in association with steroids, antivirals or immunosuppressive drugs, before or after the failure of a first-line treatment.

We experienced the administration of HP in 3 immunosuppressed patients, with mild to moderate disease and a prolonged positivity of nasopharyngeal swab, at the COVID Unit, University Hospital of Siena.

Cases presentation

Plasma collection

Collected plasma, kindly provided by the Service of Immunohematology and Transfusion Medicine, 'San Matteo Hospital' Pavia, Italy, showed a neutralizing titer of 1/80 or more. Donor plasma, obtained by symptomatic subjects, was tested for specific neutralizing antibody titer as previously described [8].

Neutralizing antibody assay

Serum samples were titrated in a four-fold dilution series starting from 1/8 in 96-well tissue culture microtiter plate and mixed with a working dilution of a SARS-CoV-2 (SARS-CoV-2/human/ITA/Siena-1/2020; GenBank: 96 MT531537.2) ($100TCID_{50}$). After 1 h incubation at 37 °C and 5% CO_2, VERO E6 (ATCC® CRL-1586 M) cells were added. After 72 h incubation, the cultures were daily examined under the microscope (Olympus 120 IX51) for the presence of the cytopathic effect (CPE). The 50% end point titer was calculated using the Reed-Muench method [9]. A positive and negative

control serum was included in each assay. A positive titer was equal to or greater than 1/20.

Molecular testing

Nasopharyngeal swabs were analyzed by using the Allplex 2019-nCoV assay (Arrow Diagnostics S.r.l., Italy) for molecular testing. The analysis included genes encoding the envelope (E), the RNA-dependent RNA polymerase (RdRp) and the nucleocapsid (N). A cycle threshold (C_T) value of less than 40 was defined as a positive test, while a C_T value of 40 or more was considered as a negative test.

Patient 1

The first patient treated with HP was a 55-year-old male, who had undergone lung transplant due to a congenital bullous emphysema and was under therapy with oral glucocorticoids and Tacrolimus. He had previously suffered from diffuse alveolar damage, leading to lung fibrosis and Aspergillus fumigatus infection in the transplanted lung. He had tested positive for SARS-CoV2 in April 2020, despite the presence of IgG, which were found to be non-neutralizing (titer< 1/20). Further tests after two months evidenced a persistent positivity of nasopharyngeal swab (E Ct 17.5, RdRp Ct 18.3 and N Ct 18.2). Lymphocytes subpopulation evidenced very low levels of B cells (28/ul, normal value 90–660). In June, he was treated with two administrations of HP compatible for ABO and RhD grouping and neutralizing titer of 1/80. Seven days since the second infusion, he had eventually tested negative for SARS-CoV-2.

Patient 2

The second patient, a 77-year-old female suffering from mild symptoms (ageusia, anosmia, fever) had tested positive in April. Her previous medical history evidenced gastric follicular lymphoma, in treatment with Rituximab and Bendamustine, and ulcerative colitis, for which the patient was assuming Mesalazine. After 6 months, further nasopharyngeal swabs displayed a persistent positivity (E Ct 31.6, RdRp Ct 34 and N Ct 32.2) and no specific IgG or IgM antibodies were developed. Total serum IgG and IgM were below normal values, too. For these reasons, the patient underwent two administrations of HP ABO and RhD grouping and neutralizing titer of 1/80. She was discharged with low viral load and eventually tested negative 7 days later.

Patient 3

The third and last patient of our case series was a 60-year-old male, affected by stage IV chronic lymphocytic leukemia and in treatment with Bendamustine, Cotrimoxazole and Aciclovir. He had been admitted to our COVID Unit with a diagnosis of bilateral interstitial

Cusi *et al. BMC Infectious Diseases*   (2021) 21:630

Page 3 of 4

pneumonia and blood examination revealed leukopenia and thrombocytopenia.

After two months, the patient did not develop any specific antibody response against SARS-CoV-2 and his nasopharyngeal swab was persistently positive (E Ct 24.3, RdRp Ct 24.3 and N Ct 23), thus he was treated with two administrations of HP ABO and RhD grouping and neutralizing titer of 1/100. The patient was subsequently discharged and he had eventually tested negative after two weeks.

Discussion and conclusions

Due to the lack of effective drugs in the treatment of COVID-19, several authors [1–3] have proposed the use of CP and HP. Passive immunization proved variable efficacy in several infectious diseases, such as Spanish flu, Middle East Respiratory Syndrome (MERS), Severe Acute Respiratory Syndrome (SARS) and Ebola [7, 8, 10–12], all linked by a similar physiopathology of the lung damage.

To date, more than 100 trials have been registered worldwide, but only few data have been published [5, 6], providing conflicting data in terms of mortality, duration and progression of disease in hospitalized, critically ill, subjects treated with CP [5, 6, 13]. Moreover, all these studies, as well as the other ones stopped or still ongoing, are affected by a notable variety of the sample and by the uncertainty of the serological status of the patients, since many of them had anti-SARS-CoV-2 antibodies.

HP improved radiological findings and reduced mortality, markers of inflammation and viral load in an Italian cohort of moderate-to-severe COVID-19 patients [8], but, due to the lack of a control group, these findings still have to be confirmed in larger controlled studies. Indeed, no RCT investigating the efficacy of HP in COVID-19 has been published yet [6].

On the other hand, CP and HP appear to be quite safe, with no serious or unexpected adverse events (AEs) in the majority of patients who underwent this treatment [14, 15]. Nevertheless, no clear-cut-conclusion can be drawn about the safety of CP and HP, due to the limited information about grade 3 and 4 adverse events (AEs) [5].

Moreover, as previously mentioned, a profound uncertainty exists about what subset of COVID-19 patients may benefit from passive immunization and when the treatment is more efficacious during the course of the disease. Data from the currently available literature seem to suggest that, in case of severe COVID-19 infection, the highest efficacy of the treatment is achieved when CP is infused within the first 7 days [16].

Conversely, in our experience, we chose to administer HP in 3 patients affected by different conditions (hematological malignancies and organ transplant) leading to prolonged immunodeficiency, with a marked reduction in number and functionality of B lymphocytes. All these patients had been previously treated with intravenous and/or oral steroids and, due to their comorbidities, they were not considered eligible for further pharmacological treatments.

HP was effective in reducing viral load in all patients and led to their hospital discharge, with no further complications, AEs or need to invasive ventilation.

It is well known that the major complication of severe COVID-19 infection is an acute respiratory distress syndrome (ARDS), presumably mediated by an aberrant and exaggerate response of immune system. On the other hand, immunodeficient patients probably lack those immune stimuli leading to ARDS [17] but, conversely, they also lack defense mechanisms involved in viral clearance and antibodies production and associated to a higher viral load and a lower viral clearance [18, 19].

For these reasons, if a combined treatment of both antiviral and immunosuppressive drugs may represent a promising option for the first and more common subtype of COVID-19 patients, CP or HP should be administered to all those subjects whose immune system is impaired by concomitant treatments or diseases. Indeed, passive immunization, whose antiviral activity may probably not provide substantial benefits in severely ill patients, may be conversely more indicated in those subjects at risk for a sudden worsening, due to an impaired viral clearance [4].

A growing number of evidence is currently witnessing the potential role of passive immunization in patients affected by different conditions, such as malignancies, congenital and acquired immunodeficiencies and organ transplants, all with an impaired immune humoral response [20].. Nevertheless, these data only rely on case reports or case series, and no RCT has currently included immunocompromised subjects. At the same time, the vast majority of papers focuses on CP, while only a few of them have reported the use of HP. [21]).

In conclusion, our findings, although limited by the small number of patients, provide some interesting insights: first, HP also proved to be effective and safe in fragile and compromised subjects, burdened by severe comorbidities, low life expectancy and prolonged duration of disease; secondly, our paper may help paving the way in defining a tailored therapy for particular subsets of patients.

Due to the limited number of patients, we cannot exclude the risk of re-infection in these patients connected with their persistent immunosuppression; however, the HP treatment was successful to make them COVID-free. The patients were followed-up after discharge and they

Cusi *et al. BMC Infectious Diseases*   (2021) 21:630

Page 4 of 4

did not show persistence of the virus three months later. Nevertheless, the recent emergence of variants is underscoring the need to use HP more wisely, particularly taking into account the epidemiological picture and considering the circulating viral variants in specific geographic areas. This aspect is aiming to use only HP having antibodies which can cross-neutralize the viral variant.

Abbreviations
AEs: Adverse events; ARDS: Acute respiratory distress syndrome; COVID-19: Coronavirus disease-19; CP: Convalescent plasma; HP: Hyperimmune plasma; MERS: Middle East Respiratory Syndrome; SARS: Severe Acute Respiratory Syndrome

Declarations

Ethics approval and consent to participate
All patients gave their informed consent to the administration of convalescent plasma. The study was conducted according to Helsinki declaration and an authorization from Local Ethical Committee was obtained.

Consent for publication
All patients provided their written consent to the publication of data.

Competing interests
Authors declare no conflict of interest or competing interest.

Author details
[1]Virology Unit, Department of Medical Biotechnologies, University of Siena, Siena, Italy. [2]Rheumatology Unit, Department of Medicine, Surgery and Neurosciences, University of Siena, viale Mario Bracci, 16, Siena, Italy. [3]Clinical and Surgical Cardiology Unit, Cardio-Thoracic and Vascular Department, University Hospital of Siena, Siena, Italy. [4]COVID Unit, University Hospital of Siena, Siena, Italy. [5]Anesthesia and Intensive Care Unit, Department of Medicine, Surgery and Neuroscience, University of Siena, Siena, Tuscany, Italy. [6]Microbiology /Virology Unit, Department of Diagnostic Medicine, Fondazione IRCCS San Matteo, Pavia, Italy.

References
1. Shen C, Wang Z, Zhao F, Yang Y, Li J, Yuan J, et al. Treatment of 5 critically ill patients with COVID-19 with convalescent plasma. JAMA. 2020;323(16):1582–9. https://doi.org/10.1001/jama.2020.4783.
2. Roback JD, Guarner J. Convalescent plasma to treat COVID-19: possibilities and challenges. JAMA. 2020;323(16):1561–2. https://doi.org/10.1001/jama.2020.4940.
3. Marano G, Vaglio S, Pupella S, Facco G, Catalano L, Liumbruno GM, et al. Convalescent plasma: new evidence for an old therapeutic tool? Blood Transfus. 2016;14(2):152–7. https://doi.org/10.2450/2015.0131-15.
4. Subbarao K, Mordant F, Rudraraju R. Convalescent plasma treatment for COVID-19: tempering expectations with the influenza experience. Eur J Immunol. 2020 Oct;50(10):1447–53. https://doi.org/10.1002/eji.202048723.
5. Klassen SA, Senefeld JW, Johnson PW, Carter RE, Wiggins CC, Shoham S, et al. The effect of convalescent plasma therapy on mortality among patients with COVID-19: systematic review and meta-analysis. Mayo Clin Proc. 2021 May;96(5):1262–75. https://doi.org/10.1016/j.mayocp.2021.02.008.
6. Piechotta V, Chai KL, Valk SJ, Doree C, Monsef I, Wood EM, Lamikanra A, Kimber C, McQuilten Z, So-Osman C, Estcourt LJ, Skoetz N. Convalescent plasma or hyperimmune immunoglobulin for people with COVID-19: a living systematic review. Cochrane Database Syst Rev. 2020;7(7):CD013600.
7. Wood EM, Estcourt LJ, McQuilten ZK. How should we use convalescent plasma therapies for the management of COVID-19? Blood. 2021;137(12):1573-81.
8. Perotti C, Del Fante C, Baldanti F, Franchini M, Percivalle E, Vecchio Nepita E, et al. Plasma from donors recovered from the new coronavirus 2019 as therapy for critical patients with COVID-19 (COVID-19 plasma study): a multicentre study protocol. Intern Emerg Med. 2020 Aug;15(5):819–24. https://doi.org/10.1007/s11739-020-02384-2.
9. Reed LJ, Muench HA. simple method of estimating fifty per cent endpoints. Am J Hyg. 1938;27:493–7.
10. Mair-Jenkins J, Saavedra-Campos M, Baillie JK, Cleary P, Khaw FM, Lim WS, et al. The effectiveness of convalescent plasma and hyperimmune immunoglobulin for the treatment of severe acute respiratory infections of viral etiology: a systematic review and exploratory meta-analysis. J Infect Dis. 2015;211:80–90.
11. Wong HK, Lee CK. Pivotal role of convalescent plasma in managing emerging infectious diseases. Vox Sang. 2020;115(7):545–7. https://doi.org/10.1111/vox.12927.
12. Zhou B, Zhong N, Guan Y. Treatment with convalescent plasma for influenza a (H5N1) infection. N Engl J Med. 2007;357(14):1450–1. https://doi.org/10.1056/NEJMc070359.
13. Piechotta V, Chai KL, Valk SJ, Doree C, Monsef I, Wood EM, et al. Convalescent plasma or hyperimmune immunoglobulin for people with COVID-19: a living systematic review. Cochrane Database Syst Rev. 2020 Jul 10;7(7):CD013600.
14. Duan K, Liu B, Li C, Zhang H, Yu T, Qu J, et al. Effectiveness of convalescent plasma therapy in severe COVID-19 patients. Proc Natl Acad Sci U S A. 2020;117(17):9490–6. https://doi.org/10.1073/pnas.2004168117.
15. Joyner MJ, Bruno KA, Klassen SA, Kunze KL, Johnson PW, Lesser ER, et al. Safety update: COVID-19 convalescent plasma in 20,000 hospitalized patients. Mayo Clin Proc. 2020;95(9):1888–97. https://doi.org/10.1016/j.mayocp.2020.06.028.
16. Focosi D, Franchini M. COVID-19 convalescent plasma therapy: hit fast, hit hard! Vox sang; 2021. https://doi.org/10.1111/vox.13091. Epub ahead of print. PMID: 33794556, COVID-19 convalescent plasma therapy: hit fast, hit hard!
17. Minotti C, Tirelli F, Barbieri E, Giaquinto C, Donà D. How is immunosuppressive status affecting children and adults in SARS-CoV-2 infection? A systematic review. J Inf Secur. 2020;81(1):e61–6.
18. Hatzl S, Eisner F, Schilcher G, Kreuzer P, Gornicec M, Eller P, et al. Response to "COVID-19 in persons with haematological cancers". Leukemia. 2020 Aug; 34(8):2265–70. https://doi.org/10.1038/s41375-020-0914-x.
19. Westblade LF, Brar G, Pinheiro LC, et al. SARS-CoV-2 viral load predicts mortality in patients with and without cancer who are hospitalized with COVID-19. Published online ahead of print 15 September 2020. Cancer Cell. 2020. https://doi.org/10.1016/j.ccell.2020.09.007.
20. Focosi D, Franchini M. COVID-19 neutralizing antibody-based therapies in humoral immune deficiencies: a narrative review. Transfus Apher Sci. 2021; 27:103071.
21. Senefeld JW, Klassen SA, Ford SK, Wiggins CC, Bostrom BC, Thompson MA. Therapeutic use of convalescent plasma in COVID-19 patients with immunodeficiency. medRxiv. 2020. https://doi.org/10.1101/2020.11.08.20224790 11.08.20224790.

Publisher's Note

Neutralizing Antibody Response of Vaccinees to SARS-CoV-2 Variants

Gabriele Anichini [1] , **Chiara Terrosi** [1], **Gianni Gori Savellini** [1] , **Claudia Gandolfo** [1] , **Federico Franchi** [2] and **Maria Grazia Cusi** [1,*]

1. Virology Unit, Department of Medical Biotechnologies, Siena University Hospital, 53100 Siena, Italy; gabriele.anichini@student.unisi.it (G.A.); chiara.terrosi@unisi.it (C.T.); gianni.gori@unisi.it (G.G.S.); claudia.gandolfo@unisi.it (C.G.)
2. Emergency, Anesthesia and Intensive Care Unit, Department of Medicine, Surgery and Neurosciences, Siena University Hospital, 53100 Siena, Italy; federico.franchi@unisi.it
* Correspondence: mariagrazia.cusi@unisi.it

Abstract: Due to their increased transmissibility, three variants of high concern have emerged in the United Kingdom (also known as B.1.1.7 lineage or VOC-202012/01), South Africa (B.1.351 lineage), and Brazil (P1 lineage) with multiple substitutions in the spike protein. Since neutralizing antibodies elicited by vaccination are likely considered as correlates of protection for SARS-CoV-2 infection, it is important to analyze whether vaccinees with mRNA BNT162b2 are equally protected against these emerging SARS-CoV-2 variants. To this aim, we enrolled healthy subjects one month after complete vaccination with Comirnaty and evaluated the neutralizing response against the native Wuhan strain and the emerging B.1.1.7, B.1.351 and P1 lineages, by using the microneutralization assay, currently considered the gold standard test for the evaluation and detection of functional neutralizing antibodies. The most remarkable finding of this study was the significantly lower neutralizing antibody titer against B.1.351 lineage, compared to the wild-type virus. No significant differences were observed with the other two lineages. These findings provide evidence that vaccinated subjects may not be equally protected against all SARS-CoV-2 lineages.

Keywords: SARS-CoV-2; vaccine; variants; neutralizing antibody

1. Introduction

The severe acute respiratory syndrome coronavirus 2 (SARS-CoV-2) circulating in the human population has acquired multiple mutations, particularly in the spike protein, necessary to bind to the cell-surface angiotensin-converting enzyme 2 (ACE2) receptor. The same viral protein has been targeted for vaccine development and therapeutic antibody interventions [1,2]. On 11 December 2020, the United States of America (U.S.A) Food and Drug Administration issued the first emergency use authorization (EUA) to Pfizer BioNTech (Pfizer Inc., New York, NY, USA)) to use their COVID-19 mRNA BNT162b2 vaccine Comirnaty. It showed a high efficacy (95%) in preventing symptomatic infections in individuals aged 16 years and older [1]. The emergency use authorization allowed the Pfizer-BioNTech COVID-19 vaccine to be distributed with a two-dose formulation, 21 days apart. This formulation is able to induce a strong specific neutralizing antibody response against the wild-type strain [3,4]. Meanwhile, due to their increased transmissibility, three variants of high concern have emerged in the United Kingdom (also known as B.1.1.7 lineage or VOC-202012/01), South Africa (B.1.351 lineage), and Brazil (P1 lineage) with multiple substitutions in the spike protein, including the N-terminal domain (NTD) and the receptor binding domain (RBD). Shared by all the three variants and located in the RBD, the N501Y substitution appears to be highly relevant to increase the affinity to ACE2 [5]. Other significant variations in the UK strain are the amino acid 69 and 70 deletion (Δ69/70) and D614G substitution, which affects higher infectivity and transmissibility [6]. Differently

from the B.1.1.7 lineage, P1 and B.1.351 contain the E484K substitution, which is also located in the viral RBD and is known to confer resistance to several monoclonal antibodies [7,8]. Moreover, both P1 and B.1.351 lineages are, respectively, characterized by the K417N and K417T substitutions, which interfere with the neutralizing activity of antibody response [9]. Since neutralizing antibodies elicited by vaccination are likely considered as correlates of protection from SARS-CoV-2 infection, it is important to analyze whether vaccinees with mRNA BNT162b2 are equally protected against these emerging SARS-CoV-2 variants. To this aim, we enrolled healthy subjects one month after complete vaccination with Comirnaty and evaluated the neutralizing response against the native Wuhan strain and the emerging B.1.1.7, B.1.351 and P1 lineages, by using the microneutralization assay (MN). Currently considered as the gold standard test, MN is the most specific and sensitive serological assay when evaluating and detecting functional neutralizing antibodies [10].

2. Materials and Methods

2.1. Study Design and Participants

In this current observational cohort study, we enrolled 60 healthcare workers (HCWs) from 'Santa Maria alle Scotte' University Hospital in Siena, aged 25 to 65 (mean age 45.8; CI 95% 42.9–48.7), 22 males (36.7%; mean age 45.1 years, CI 95% 40.1–50.2) and 38 females (63.3%; mean age 45.6 years, CI 95% 42.0–49.2. They had been subjected to periodical control (every 2 weeks) by molecular testing for SARS-CoV-2 virus with nasopharyngeal swab and had never been infected. All subjects were vaccinated with two doses of BioNTech COVID-19 vaccine (Pfizer Inc.). In order to evaluate the humoral response induced by the vaccine, a blood sample was drawn thirty days after the second dose of vaccine. All subjects were tested for the presence of neutralizing antibodies against the wild-type and three variant lineages of SARS-CoV-2: B.1.1.7 lineage (VOC-202012/01), South Africa (B.1.351 lineage), and Brazil (P1 lineage) by microneutralization test. This research was carried out according to the principles of the Helsinki declaration, with reference to BIOBANK-MIU-2010 document approved by the Ethics Committee with amendment No. 1, on 17 February 2020. Prior to participating in this study, all subjects signed a written informed consent.

2.2. Cells and Viruses

Vero E6 cells were grown as a monolayer in Dulbecco's modified Eagle's medium (DMEM) (Euroclone, Milan, Italy) supplemented with 100U/mL penicillin/streptomycin (Euroclone) and 5% heat-inactivated fetal calf serum (FCS) (Euroclone) at 37 °C in a humidified 5% CO_2 atmosphere. SARS-CoV-2 wild-type (SARS-CoV-2/human/ITA/Siena-1/2020; GenBank: MT531537.2), B.1.1.7 (GSAID EPI_ISL_1163688), B.1.351 (GSAID EPI_ISL_1163689) and P.1 (GSAID EPI_ISL_1163690) strains were isolated from clinical swabs and propagated on Vero cells until a cytopathic effect (CPE) appeared. Viral stocks were prepared, titrated on Vero cells and stored at −80 °C for long term.

2.3. SARS-CoV-2 Microneutralization Test

SARS-CoV-2 virus neutralization assay was carried out on Vero E6 cells in a 96-well microplate. Twenty-five microliters of two-fold serial dilutions (1:8 to 1:1024) of sera samples were added to an equal volume of the wild-type (SARS-CoV-2/human/ITA/Siena-1/2020; GenBank: MT531537.2), B.1.1.7 (GSAID EPI_ISL_1163688), B.1.351 (GSAID EPI_ISL_1163689) and P.1 (GSAID EPI_ISL_1163690) SARS-CoV-2 strains containing 100 $TCID_{50}$ in four replicates and incubated for 90 min at 37 °C. Finally, 50 μL of Vero E6 cells suspension (2×10^5 cells/ml) prepared in complete DMEM were added to each well. After incubation at 37 °C, cultures were daily examined for the presence of CPE under microscope (Olympus IX51, Olympus Corporation, Tokyo, Japan) by the same observer (Figure 1) [11]. The 50% end point geometric mean titer (GMT) was calculated using the Reed−Muench method [12]. A positive and negative control serum were included in each assay. All neutralization assays were performed in duplicate. The test was conducted in a BSL3 lab.
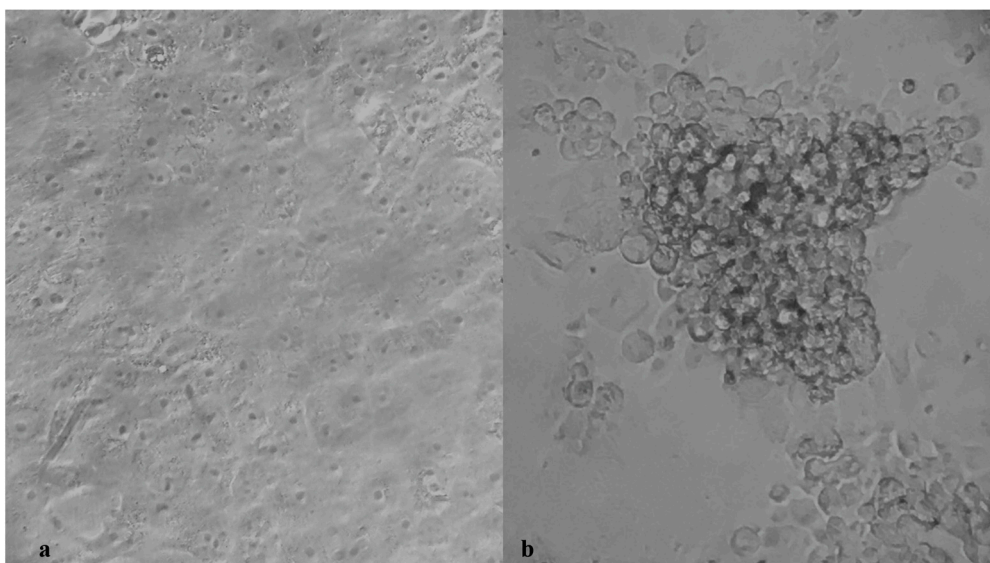
Figure 1. Viral cytopathic effect (CPE) (**b**) observed in cultured Vero E6 cells after infection with 100 TCID of the SARS-CoV-2 strain. (**a**) shows the uninfected control cells. (Magnification 400×).

In addition, a regression analysis of the neutralizing antibodies of the study subjects was assessed thirty days after vaccination, according to subject age.

2.4. Statistical Analysis

Age differences and neutralizing GMTs were evaluated and statistical significances were assessed with the Mann−Whitney−Wilcoxon test. Results were considered statistically significant at $p < 0.05$. A 95% confidence interval (CI 95%) has been calculated and reported for each variable. Regression analysis of the neutralizing antibodies according to the participants' age was assessed. All analyses were performed by using Graph Pad Prism 7.0 software (GraphPad Software, San Diego, CA, USA)).

3. Results

3.1. Study Group

We analyzed sera from 60 healthcare workers (HCWs), aged 25 to 65 (mean age 45.8; CI 95% 42.9–48.7), 22 males (36.7%; mean age 45.1 years, CI 95% 40.1–50.2) and 38 females (63.3%; mean age 45.6 years, CI 95% 42.0–49.2), who had never been infected with SARS-CoV-2 virus.

All subjects were found to be positive for specific IgG antibodies one month after the second dose of vaccine.

3.2. Neutralizing Antibody Response against SARS-CoV-2 Variants

To better characterize the humoral response induced by vaccination, neutralizing antibodies against the wild-type virus and the three variant lineages were investigated. Only one subject, who tested weak positive for IgG by the chemiluminescent assay (CMIA), did not develop a neutralizing response against all four lineages. With regard to the remaining 59 subjects, the neutralizing antibody titers elicited against the wild-type strain (GMT = 95.6, CI 95% 79.1–112.0) showed a slight decrease (1.2 fold, $p = 0.03$) versus P1 lineage (GMT = 78.5, CI 95% 76.6–100.0) and a significant decrease (4.2 fold, $p < 0.001$) to the B.1.351 lineage (GMT = 22.8, CI 95% 17.8–27.9). No significant differences were found in comparison with the B.1.1.7 (UK) lineage (GMT = 89.1, CI 95% 73.6–105.0) (Figure 2).
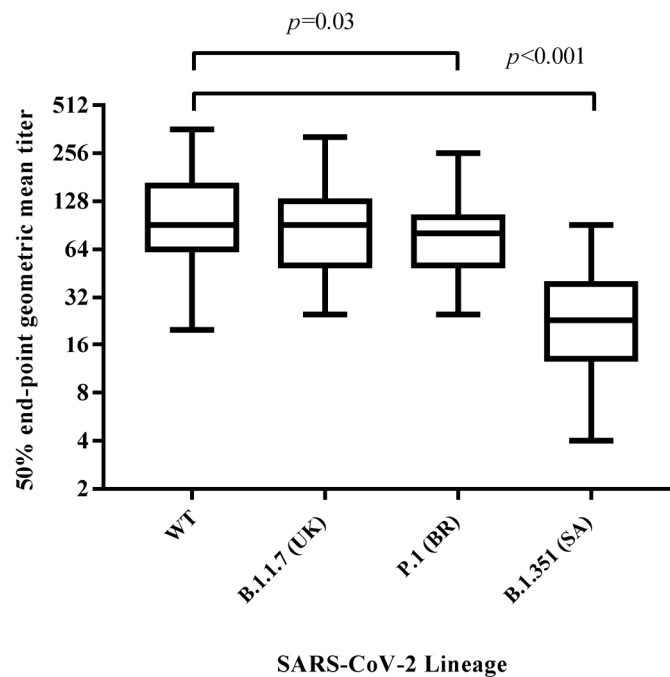
Figure 2. Differences in neutralizing antibody titers among vaccinated subjects against the wild-type, B.1.1.7, B.1.351, and P.1 SARS-CoV-2 lineages thirty days after receiving the second dose of vaccine. Results are reported in the box−whiskers plots as GMTs and upper and lower quartiles. GMT, geometric mean titer.

3.3. Regression Analysis of Neutralizing Titers According to Subject Age

Moreover, neutralizing titers were analyzed considering the subjects' age. To this aim, they were divided into two groups according to their age: 25–45 and 46–65 years. No relevant differences were found between the two groups, either in circulating IgG values or in neutralizing GMTs, to all four lineages, although a very slight decrease was observed with increasing age (Figure 3).
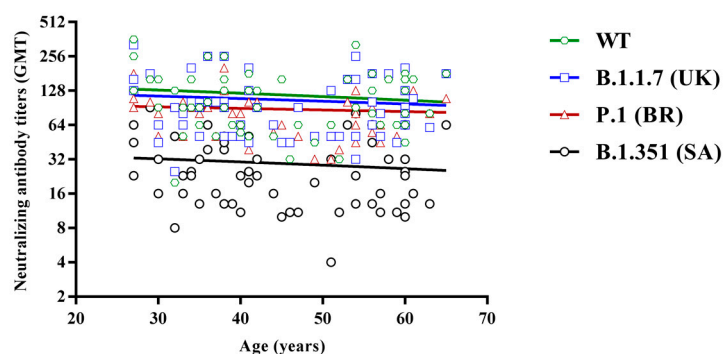
Figure 3. Regression analysis of neutralizing antibody titers against the wild-type (green, R2 = −0.12), B.1.1.7 (blue, R2 = −0.09), P.1 (red, R2 = −0.07) and B.1.351 lineages (black, R2 = −0.11), according to subjects' age.

4. Discussion

In this study, we evaluated the neutralizing activity against recently emerging variants of SARS-CoV-2 in subjects vaccinated with two doses of BioNTech COVID-19 vaccine.

Instead of pseudoviruses, we used clinical isolates of variants in the neutralization assay, thus providing a relevant method to assess the viral sensitivity to neutralizing antibodies in the presence of all SARS-CoV-2 antigen epitopes. We preferred to perform this procedure, considered as the gold standard, because the neutralizing antibody titers against

SARS-CoV-2 variants are so different, depending on the test used [13]. We realized that, although different, the antibody response trend was similar. Indeed, the results reported in this study are similar to others that used different methods to measure the efficacy of the vaccine against variants after about a month [4,13–16]. However, despite the unquestionable scientific relevance of different methods that may be carried out, a uniformity in reporting absolute titer values in International Standard Units is desirable, in order to avoid diverse interpretations of the antibody trend several months after vaccination.

The B.1.351 variant is currently of greater concern, being less sensitive to sera from immunized people [14–17]. The most remarkable finding of this study is the significantly lower neutralizing antibody titer against B.1.351 lineage, compared to the Wuhan-Hu-1 virus. Indeed, we found that B.1.351 was approximately 4-fold less sensitive to neutralization by vaccinees' sera, whereas P.1 variant was only 1.2-fold less sensitive. On the other hand, the GMT against B.1.1.7 was similar to that obtained against the wild type virus (89.1 vs. 95.6). Moreover, the neutralizing response appeared reduced, particularly against variants carrying the K417N/T and E484K mutations. Both of them are located in the receptor binding domain (RDB) of the spike protein and can mediate antibody escape. However, since the cross-reactivity to B.1.351 of antibody response appeared very low, other mutations were likely to be involved, particularly affecting the N-terminal domain of the viral spike [18–20]. These findings provide evidence that vaccinated subjects may not be equally protected against all SARS-CoV-2 lineages. Therefore, considering the up to four-fold decrease in the GMT tested against B.1.351 lineage, it is likely that only people having a high antibody titer could be protected, although a threshold of protection still needs to be defined.

Author Contributions: Conceptualization, M.G.C.; methodology, C.T., G.G.S. and C.G.; validation: M.G.C.; investigation, G.A.; resources, F.F.; writing—original draft, G.A.; writing—review and editing, M.G.C. All authors have read and agreed to the published version of the manuscript.

Institutional Review Board Statement: The study was conducted according to the guidelines of the Declaration of Helsinki, and approved by the Ethics Committee (protocol code BIOBANK-MIU-2010 approved with amendment No. 1, on 17 February 2020).

Informed Consent Statement: Informed consent was obtained from all subjects involved in the study.

Data Availability Statement: The authors declare that the data supporting the findings of this study are available within the paper or available from the corresponding author(s) upon reasonable request.

Conflicts of Interest: The authors declare no competing interest.

References

1. Polack, F.P.; Thomas, S.J.; Kitchin, N.; Absalon, J.; Gurtman, A.; Lockhart, S.; Perez, J.L.; Pérez Marc, G.; Moreira, E.D.; Zerbini, C.; et al. C4591001 Clinical Trial Group. Safety and Efficacy of the BNT162b2 mRNA Covid-19 Vaccine. *N. Engl. J. Med.* **2020**, *383*, 2603–2615. [CrossRef] [PubMed]
2. Baden, L.R.; El Sahly, H.M.; Essink, B.; Kotloff, K.; Frey, S.; Novak, R.; Diemert, D.; Spector, S.A.; Rouphael, N.; Creech, C.B.; et al. COVE Study Group. Efficacy and Safety of the mRNA-1273 SARS-CoV-2 Vaccine. *N. Engl. J. Med.* **2021**, *384*, 403–416. [CrossRef] [PubMed]
3. Sahin, U.; Muik, A.; Derhovanessian, E.; Vogler, I.; Kranz, L.M.; Vormehr, M.; Baum, A.; Pascal, K.; Quandt, J.; Maurus, D.; et al. COVID-19 vaccine BNT162b1 elicits human antibody and T_H1 T cell responses. *Nature* **2020**, *586*, 594–599. [CrossRef] [PubMed]
4. Liu, Y.; Liu, J.; Xia, H.; Zhang, X.; Fontes-Garfias, C.R.; Swanson, K.A.; Cai, H.; Sarkar, R.; Chen, W.; Cutler, M.; et al. Neutralizing Activity of BNT162b2-Elicited Serum. *N. Engl. J. Med.* **2021**, *384*, 1466–1468. [CrossRef] [PubMed]
5. Starr, T.N.; Greaney, A.J.; Addetia, A.; Hannon, W.W.; Choudhary, M.C.; Dingens, A.S.; Li, J.Z.; Bloom, J.D. Prospective mapping of viral mutations that escape antibodies used to treat COVID-19. *Science* **2020**, *371*, 850–854. [CrossRef] [PubMed]
6. Zhang, L.; Jackson, C.B.; Mou, H.; Ojha, A.; Peng, H.; Quinlan, B.D.; Rangarajan, E.S.; Pan, A.; Vanderheiden, A.; Suthar, M.S.; et al. SARS-CoV-2 spike-protein D614G mutation increases virion spike density and infectivity. *Nat. Commun.* **2020**, *11*, 6013. [CrossRef] [PubMed]

7. Liu, Z.; VanBlargan, L.A.; Bloyet, L.M.; Rothlauf, P.W.; Chen, R.E.; Stumpf, S.; Zhao, H.; Errico, J.M.; Theel, E.S.; Liebeskind, M.J.; et al. Identification of SARS-CoV-2 spike mutations that attenuate monoclonal and serum antibody neutralization. *Cell Host Microbe* **2021**, *29*, 477–488.e4. [CrossRef] [PubMed]
8. Chen, R.E.; Zhang, X.; Case, J.B.; Winkler, E.S.; Liu, Y.; VanBlargan, L.A.; Liu, J.; Errico, J.M.; Xie, X.; Suryadevara, N.; et al. Resistance of SARS-CoV-2 variants to neutralization by monoclonal and serum-derived polyclonal antibodies. *Nat. Med.* **2021**, *27*, 717–726. [CrossRef]
9. Garcia-Beltran, W.F.; Lam, E.C.; St Denis, K.; Nitido, A.D.; Garcia, Z.H.; Hauser, B.M.; Feldman, J.; Pavlovic, M.N.; Gregory, D.J.; Poznansky, M.C.; et al. Multiple SARS-CoV-2 variants escape neutralization by vaccine-induced humoral immunity. *Cell* **2021**, *8674*, 298–3001. [CrossRef]
10. Muruato, A.E.; Fontes-Garfias, C.R.; Ren, P.; Garcia-Blanco, M.A.; Menachery, V.D.; Xie, X.; Shi, P.Y. A high-throughput neutralizing antibody assay for COVID-19 diagnosis and vaccine evaluation. *Nat. Commun.* **2020**, *11*, 4059. [CrossRef]
11. Anichini, G.; Terrosi, C.; Gandolfo, C.; Gori Savellini, G.; Fabrizi, S.; Miceli, G.B.; Cusi, M.G. SARS-CoV-2 Antibody Response in Persons with Past Natural Infection. *N. Engl. J. Med.* **2021**, *14*, 3825. [CrossRef]
12. Reed, L.J.; Muench, H. A simple method of estimating fifty per cent endpoints. *Am. J. Hyg.* **1938**, *27*, 493–497.
13. mRNA-1273 Vaccine Induces Neutralizing Antibodies against Spike Mutants from Global SARS-CoV-2 Variants. Available online: https://www.biorxiv.org/content/10.1101/2021.01.25.427948v1.abstract (accessed on 13 May 2021).
14. Shen, X.; Tang, H.; Pajon, R.; Smith, G.; Glenn, G.M.; Shi, W.; Korber, B.; Montefiori, D.C. Neutralization of SARS-CoV-2 Variants B.1.429 and B.1.351. *N. Engl. J. Med.* **2021**, *7*, 429. [CrossRef]
15. Stamatatos, L.; Czartoski, J.; Wan, Y.H.; Homad, L.J.; Rubin, V.; Glantz, H.; Neradilek, M.; Seydoux, E.; Jennewein, M.F.; MacCamy, A.J. mRNA vaccination boosts cross-variant neutralizing antibodies elicited by SARS-CoV-2 infection. *Science* **2021**, *25*, 9175. [CrossRef] [PubMed]
16. Hoffmann, M.; Arora, P.; Groß, R.; Seidel, A.; Hörnich, B.F.; Hahn, A.S.; Krüger, N.; Graichen, L.; Hofmann-Winkler, H.; Kempf, A. SARS-CoV-2 variants B.1.351 and P.1 escape from neutralizing antibodies. *Cell* **2021**, *184*, 2384–2393. [CrossRef] [PubMed]
17. Greaney, A.J.; Starr, T.N.; Gilchuk, P.; Zost, S.J.; Binshtein, E.; Loes, A.N.; Hilton, S.K.; Huddleston, J.; Eguia, R.; Crawford, K.H.D. Complete Mapping of Mutations to the SARS-CoV-2 Spike Receptor-Binding Domain that Escape Antibody Recognition. *Cell Host Microbe* **2021**, *29*, 44–57. [CrossRef] [PubMed]
18. Brouwer, P.J.M.; Caniels, T.G.; van der Straten, K.; Snitselaar, J.L.; Aldon, Y.; Bangaru, S.; Torres, J.L.; Okba, N.M.A.; Claireaux, M.; Kerster, G.B. Potent neutralizing antibodies from COVID-19 patients define multiple targets of vulnerability. *Science* **2020**, *369*, 643–650. [CrossRef]
19. Liu, L.; Wang, P.; Nair, M.S.; Yu, J.; Rapp, M.; Wang, Q.; Luo, Y.; Chan, J.F.; Sahi, V.; Figueroa, A. Potent neutralizing antibodies against multiple epitopes on SARS-CoV-2 spike. *Nature* **2020**, *584*, 450–456. [CrossRef] [PubMed]
20. Chi, X.; Yan, R.; Zhang, J.; Zhang, G.; Zhang, Y.; Hao, M.; Zhang, Z.; Fan, P.; Dong, Y.; Yang, Y. A neutralizing human antibody binds to the N-terminal domain of the Spike protein of SARS-CoV-2. *Science* **2020**, *369*, 650–655. [CrossRef] [PubMed]

CORRESPONDENCE

SARS-CoV-2 Antibody Response in Persons with Past Natural Infection

TO THE EDITOR: Whether or not persons who have already been infected with severe acute respiratory syndrome coronavirus 2 (SARS-CoV-2) should be vaccinated is unclear. Only a few studies have shown that vaccinees who were previously infected with SARS-CoV-2 had a significantly higher antibody response than previously uninfected vaccinees.[1-4] In an observational cohort study, we enrolled 100 health care workers, including 38 (9 men and 29 women) with a documented history of SARS-CoV-2 infection (mean duration between infection and vaccination, 111 days). The mean age of these previously infected participants was 35.1 years (95% confidence interval [CI], 31.7 to 38.6). Our study also included 62 participants (25 men and 37 women) who had not been previously infected. The mean age of those participants was 44.7 years (95% CI, 41.0 to 47.6).

Both groups of participants received the messenger RNA vaccine BNT162b2 (Pfizer–BioNTech).

Serum samples were obtained from the previously infected participants 10 days after the administration of the first dose and from the previously uninfected participants 10 days after the administration of the second dose. Thereafter, all the participants were screened for the presence of specific anti–SARS-CoV-2 spike IgG by means of a chemiluminescence microparticle immunoassay.
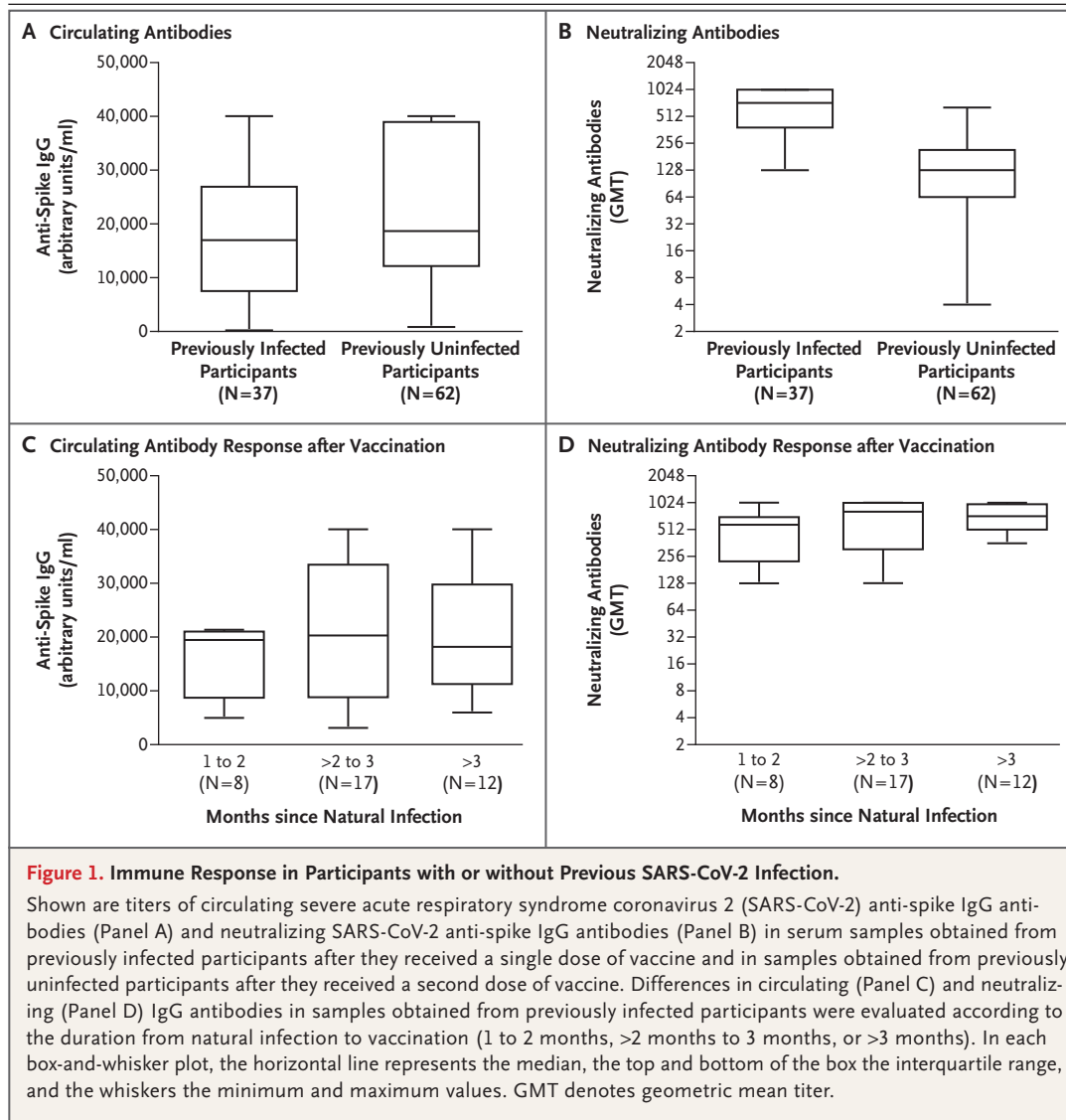
No significant difference in circulating anti-spike IgG antibody titers was observed between the samples from previously infected participants (mean level, 20,120 arbitrary units per milliliter; 95% CI, 16,400 to 23,800) and those from previously uninfected participants (mean level, 22,639 arbitrary units per milliliter; 95% CI, 19,400 to 25,900) (median levels are shown in Fig. 1A). Circulating anti-spike IgG antibodies were not detected in only one previously infected participant; that participant did not have an antibody response to natural infection with SARS-CoV-2.

The same serum samples were also analyzed for the presence of specific anti–SARS-CoV-2 neutralizing antibodies. We observed a difference in levels of neutralizing antibodies between samples from the previously infected participants (geometric mean titer, 569; 95% CI, 467 to 670) and those from the previously uninfected participants (geometric mean titer, 118; 95% CI, 85 to 152) (P<0.001) (median levels are shown in Fig. 1B). No substantial differences were noted between the titers from the previously infected and the previously uninfected participants according to age (Fig. S1 in the Supplementary Appendix, available with the full text of this letter at NEJM.org) or sex (data not shown).

The previously infected participants were categorized into three groups according to the

Figure 1. Immune Response in Participants with or without Previous SARS-CoV-2 Infection.
Shown are titers of circulating severe acute respiratory syndrome coronavirus 2 (SARS-CoV-2) anti-spike IgG antibodies (Panel A) and neutralizing SARS-CoV-2 anti-spike IgG antibodies (Panel B) in serum samples obtained from previously infected participants after they received a single dose of vaccine and in samples obtained from previously uninfected participants after they received a second dose of vaccine. Differences in circulating (Panel C) and neutralizing (Panel D) IgG antibodies in samples obtained from previously infected participants were evaluated according to the duration from natural infection to vaccination (1 to 2 months, >2 months to 3 months, or >3 months). In each box-and-whisker plot, the horizontal line represents the median, the top and bottom of the box the interquartile range, and the whiskers the minimum and maximum values. GMT denotes geometric mean titer.

time that had elapsed from infection to vaccination: 1 to 2 months (8 participants), more than 2 months to 3 months (17 participants), and more than 3 months (12 participants). The previously infected patient in whom circulating anti-spike IgG antibodies were not detected was not included in this categorization. The circulating IgG mean titers differed between the group vaccinated at 1 to 2 months and the group vaccinated at more than 2 months to 3 months after natural infection (mean level, 15,837 arbitrary units per milliliter [95% CI, 11,265 to 20,410] vs. 21,450 arbitrary units per milliliter [95% CI,

15,377 to 27,523]) (median levels are shown in Fig. 1C); however, because the number of participants was limited, a real distinction cannot be made. No further significant difference was observed between the group of participants vaccinated at more than 2 months to 3 months and the group of those vaccinated more than 3 months after infection (mean level, 21,090 arbitrary units per milliliter [95% CI, 14,702 to 27,477]).

The differences among the three groups were more evident with respect to levels of neutralizing antibodies, with geometric mean titers rang-

ing from 437 (95% CI, 231 to 643) in participants vaccinated 1 to 2 months after infection to 559 (95% CI, 389 to 730) in those vaccinated more than 2 months to 3 months after infection to 694 (95% CI, 565 to 823) in those vaccinated more than 3 months after infection (median levels are shown in Fig. 1D). Although these findings indicate that the booster response was more efficacious when the vaccine was administered more than 3 months after infection, not enough information is available to draw a definitive conclusion.

The most remarkable finding of this study was the significantly lower neutralizing antibody titer after administration of a second dose of vaccine in previously uninfected patients than the titer after only a single dose of vaccine in previously infected participants. It is unclear how the neutralizing antibody titers influence the ability of the host to transmit the virus. These findings provide evidence that after the administration of a single dose of vaccine, the humoral response against SARS-CoV-2 in persons with a history of SARS-CoV-2 infection is greater than the response in previously uninfected participants who have received a second dose.

Gabriele Anichini, M.S.
Chiara Terrosi, M.S.
Claudia Gandolfo, Ph.D.
Gianni Gori Savellini, Ph.D.
University of Siena
Siena, Italy

Simonetta Fabrizi, M.D.
Giovanni B. Miceli, M.D.
Santa Maria alle Scotte University Hospital
Siena, Italy

M. Grazia Cusi, Ph.D.
University of Siena
Siena, Italy
mariagrazia.cusi@unisi.it

1. Wise J. Covid-19: people who have had infection might only need one dose of mRNA vaccine. BMJ 2021;372:n308.
2. Manisty C, Otter AD, Treibel TA, et al. Antibody response to first BNT162b2 dose in previously SARS-CoV-2-infected individuals. Lancet 2021;397:1057-8.
3. Saadat S, Tehrani ZR, Logue J, et al. Binding and neutralization antibody titers after a single vaccine dose in health care workers previously infected with SARS-CoV-2. JAMA 2021 March 1 (Epub ahead of print).
4. Krammer F, Srivastava K, Alshammary H, et al. Antibody responses in seropositive persons after a single dose of SARS-CoV-2 mRNA vaccine. N Engl J Med 2021;384:1372-4.

Sotatercept for Pulmonary Arterial Hypertension

TO THE EDITOR: Humbert et al. (April 1 issue)[1] report that in the PULSAR trial, sotatercept reduced pulmonary vascular resistance in patients with pulmonary arterial hypertension by correcting dysregulated activin–growth differentiation factor signaling.[2] Sotatercept is also effective in increasing hemoglobin levels in patients with β-thalassemia.[3,4] The PULSAR trial excluded patients with hemoglobin levels above 16 g per deciliter at initial screening and above 18 g per deciliter after at least one dose of sotatercept. Depending on the prevalence of anemia and polycythemia among patients with pulmonary arterial hypertension, the erythropoietic effects of sotatercept could be consequential.

We performed a cross-sectional analysis involving a cohort of 366 patients referred because of dyspnea. On catheterization, these patients were categorized as having World Health Organization (WHO) group 1 pulmonary arterial hypertension, WHO group 2 to 5 pulmonary hypertension, or no pulmonary hypertension. Among the patients with group 1 pulmonary arterial hypertension, 49.4% had anemia (hemoglobin level, <12 g per deciliter in women and <13 g per deciliter in men). Patients with pulmonary arterial hypertension had lower hemoglobin levels, hematocrits, red-cell counts, and mean corpuscular hemoglobin concentrations and higher red-cell distribution widths than controls who did not have pulmonary arterial hypertension; these findings are similar to those in previous studies.[5]

In most patients with pulmonary arterial hypertension in our cohort (93.7%), the hemoglobin level was 16 g per deciliter or less. These patients would be expected to have a margin for the treatment-mediated increases of 1.2 to 1.5 g per

Short Communication

How long can SARS-CoV-2 persist in human corpses?

Mario Gabbrielli[a], Claudia Gandolfo[b], Gabriele Anichini[b], Tommaso Candelori[a], Matteo Benvenuti[a], Gianni Gori Savellini[b], Maria Grazia Cusi[b,*]

[a] Department of Molecular and Developmental Medicine, Forensic Medicine Unit, University of Siena, Siena, Italy
[b] Department of Medical Biotechnologies, Virology Unit, University of Siena, Siena, Italy

ARTICLE INFO

ABSTRACT

We report the finding of the SARS-CoV-2 genome in the corpse of an exhumed infected person, one month after her death. The viral gene targets were still present in her lungs and heart, however, the virus was no longer alive. Infectious risks from human corpses should be considered.

© 2021 The Author(s). Published by Elsevier Ltd on behalf of International Society for Infectious Diseases. This is an open access article under the CC BY-NC-ND license (http://creativecommons.org/licenses/by-nc-nd/4.0/).

How long can SARS-CoV-2 persist in a body? This is question everyone asks but that cannot yet be answered. Many articles have reported the presence of the virus in infected people for more than 5 months (Zapor, 2020), but it is not clear how long SARS-CoV-2 can persist in a human body. The finding of SARS-CoV-2 genomic fragments in tissues of infected people does not say whether the virus is alive and can infect others or whether these are simple fragments of the viral genome, which do not constitute a threat to humans. We were interested to know how long SARS-CoV-2 could remain viable in a dead body. It is known that influenza virus genomic RNA could persist for decades in frozen bodies (Taubenberger et al., 2007). Here we demonstrate that SARS-CoV-2 genomic fragments were still present in the body of an exhumed person who died from COVID-19. SARS-CoV-2 belongs to the *Coronaviridae* family and contains a single-stranded RNA genome. Like a lot of viruses, it has an envelope, which makes it more sensitive to the environment. Indeed, temperature and humidity are important factors that influence the virus survival. SARS-CoV-2 can survive in cadavers for a long time; it depends on the amount of virus detected before death, on which organ and tissue the virus had been detected in, and also on the burial process. Few data are available on this topic. In Ebola virus-infected macaques, the virus remained easily detectable in samples 3 days postmortem, but its genome was still detected 7 weeks later (Prescott, 2015). In this study, autopsy was performed on a person

who died of COVID-19 one month earlier. A forensic autopsy was authorized for this study. The autopsy was performed in the Institute of Legal Medicine of the University of Siena, in a special autopsy room for infectious corpses (air suction directly at the autopsy table downwards). All people involved wore FFP3 masks and the usual protective clothing (WHO, 2020). The body was buried in a zinc casket, thus advanced corification processes were visible and organs were clearly identifiable and relatively well preserved. All the drawn organs, lungs, heart and kidneys were analyzed for the presence of SARS-CoV-2 by molecular testing. We revealed N and RdRp gene targets by real time PCR (Argene SARS-CoV-2 R-gene, Biomerieux, Italy) in both lungs (RdRp Ct 31, N Ct 31) and N target in heart (Ct 36); on the contrary, viral genes were not detected in kidneys. We infected Vero E6 cells (ATCC CRL-1586) with the samples, which were observed daily for the presence of viral cytopathic effect for one week. However, trials to grow the virus *in vitro* were unsuccessful, but we do not exclude that the use of an alternative cellular system, such as TMPRSS2-expressing Vero E6 cells and organoids, could be more useful in virus isolation (Matsuyama et al., 2020; Zhou et al. 2020). We could speculate that, despite cell lysis, the virus could persist in tissues at a temperature of 20 °C for a long time, as previously reported for other pathogens (Prescott, 2015; Douceron et al., 1993). We cannot assess how long SARS-CoV-2 could remain alive in a deceased body, but we can certainly assert that its viral genome could persist in tissues for more than 30 days, hypothesizing that transmission from deceased people could be possible for a certain period after death, despite the fact that the corpse was sprayed with disinfectant or a sodium hypochlorite solution. Furthermore, the risk of infection transmission is higher when it concerns positive-stranded naked-RNA viruses, such as SARS-CoV-2, because of the

---

* Corresponding author at: Department of Medical Biotechnologies, Virology Unit, University of Siena, S. Maria delle Scotte Hospital, V.le Bracci, 1, 53100 Siena, Italy.
E-mail address: mariagrazia.cusi@unisi.it (M.G. Cusi).

intrinsic nature of viral genome, defined as infectious. We can conclude that the autopsy (including histological and virological examinations) gives the opportunity to investigate on the virus spreading in bodies, tissues and organs affected by the infection and by the late and obscure effects of the disease. Moreover, the autopsy could provide answers to some questions that are not yet solved, such as the persistence of SARS-CoV-2 in human bodies. Lastly, it is worth noting that infectious risks from human corpses should be considered for pathologists and technicians in autopsy rooms and for people in contact with corpses during mourning and funeral practices. This fact becomes particularly important when certain funeral rites require different treatments of the corpse, putting dedicated personnel at risk.

Authors' contributions

Conceptualization, MG and MGC; methodology, GA and CG; formal analysis, GGS, CG, GA, TC and MB; investigation, GGS, GA, CG, TC and MB; data curation, MG and MGC; writing—original draft preparation, MG and MGC; supervision, MGC MG.

Declaration of interests

The authors declare that they have no known competing financial interests or personal relationships that could have appeared to influence the work reported in this paper.

Funding

No funding.

Ethical approval

Approved.

Declaration of Competing Interest

The authors report no declarations of interest.

References

Douceron H, et al. Long-lasting postmortem viability of human immunodeficiency virus: a potential risk in forensic medicine practice. Forensic Sci Int 1993;60:61–6, doi:http://dx.doi.org/10.1016/0379-0738(93)90093-p.

Matsuyama S, et al. Enhanced isolation of SARS-CoV-2 by TMPRSS2-expressing cells. Proc Natl Acad Sci U S A 2020;117:7001–3, doi:http://dx.doi.org/10.1073/pnas.2002589117.

Prescott J, et al. Postmortem stability of Ebola virus. Emerg Infect Dis 2015;21:856–9, doi:http://dx.doi.org/10.3201/eid2105.150041.

Taubenberger JK, et al. Discovery and characterization of the 1918 pandemic influenza virus in historical context. Antivir Ther 2007;12:581–91.

WHO. Infection prevention and control for the safe management of a dead body in the context of COVID-19. 2020. https://apps.who.int/iris/handle/10665/331538.

Zapor M. Persistent detection and infectious potential of SARS-CoV-2 virus in clinical specimens from COVID-19 patients. Viruses 2020;12:1384, doi:http://dx.doi.org/10.3390/v12121384.

Zhou J, et al. Infection of bat and human intestinal organoids by SARS-CoV-2. Nat Med 2020;26:1077–83, doi:http://dx.doi.org/10.1038/s41591-020-0912-6.

SHORT COMMUNICATION

JOURNAL OF
MEDICAL VIROLOGY WILEY

Antibody response to SARS-CoV-2 in infected patients with different clinical outcome

Gabriele Anichini[1] | Claudia Gandolfo[1,2] | Chiara Terrosi[1] | Simonetta Fabrizi[3] | Giovanni Battista Miceli[3] | Gianni Gori Savellini[1] | Shibily Prathyumnan[1] | Federico Franchi[4] | Maria Grazia Cusi[1,2] 🆔

[1]Virology Unit, Department of Medical Biotechnologies, University of Siena, Siena, Tuscany, Italy

[2]Microbiology and Virology Unit, Santa Maria alle Scotte University Hospital, Siena, Tuscany, Italy

[3]Preventive Medicine and Health Surveillance Unit, Santa Maria alle Scotte University Hospital, Siena, Tuscany, Italy

[4]Anesthesia and Intensive Care Unit, Department of Medicine, Surgery and Neuroscience, University of Siena, Siena, Tuscany, Italy

Correspondence
Maria Grazia Cusi, Virology Unit, Department of Medical Biotechnologies, University of Siena, Rettorato, via Banchi di Sotto 55, Siena 53100, Italy.
Email: mariagrazia.cusi@unisi.it

Abstract

Data regarding antibody responses to severe acute respiratory syndrome coronavirus-2 (SARS-CoV-2) in patients infected with COVID-19 are not yet available. In this study, we aimed to evaluate serum antibody responses in patients regardless of the outcome. We measured the circulating immunoglobulin G (IgG) antibody levels in 60 subjects with a certified history of SARS-CoV-2 infection by using immunoenzymatic, chemiluminescent, and Neutralization assays. Half patients had a severe infection, the other half were pauci-symptomatic. We analyzed their antibody response to see the trend of the humoral response. Our results showed a significant difference in circulating IgG level among the two groups. The neutralizing antibody response against SARS-CoV-2 was significantly higher among those who had severe disease. Furthermore, ten subjects from each group were screened twice, and a declining antibody trend was observed in pauci-symptomatic individuals. These findings provide evidence that humoral immunity against SARS-CoV-2 in pauci-symptomatic people is weak and may not be long-lasting. This may have implications for immunity strategy and prevention, since it is still not clear whether a time-dependent decrease of both circulating and neutralizing antibodies to nonprotective levels could occur in a longer time span and whether potential vaccines are able to induce a herd immunity and a durable response.

KEYWORDS
coronavirus, humoral immunity, neutralization

1 | INTRODUCTION

In December 2019, a cluster of patients with pneumonia of unknown cause was identified in Wuhan, Hubei Province, China.[1] On January 7, 2020, China centers for disease control and prevention identified a novel beta-coronavirus from lower respiratory tract samples of patients with pneumonia.[2] This novel coronavirus was later named "severe acute respiratory syndrome coronavirus-2" (SARS-CoV-2). As an emerging acute respiratory infectious disease, SARS CoV-2 primarily spreads through the respiratory tract, by droplets,

respiratory secretions, and direct contact,[3] with a high human-to-human transmissibility.

Most adults or children with SARS-CoV-2 infection present mild flu-like symptoms; only a minority of patients have a severe outcome and rapidly develop acute respiratory distress syndrome, respiratory and multiple organ failure, bleeding and coagulation dysfunction, even death.[4] So far, the golden clinical diagnostic method of COVID-19 is nucleic acid detection in the nasopharyngeal swab or other lower respiratory tract samplings by real-time PCR, which can be further confirmed by next-generation sequencing.

Apart from RT-PCR testing, serological testing is an additional emerging option in COVID-19 diagnostics[5] primarily as a proof of past infection but also to support the diagnosis of suspected COVID-19 patients.[6,7] Serological assays for the evaluation of the humoral responses against Spike (S) and Nucleoprotein (N) in COVID-19 patients have been assessed, because of their high immunogenicity. Spike plays an important role in viral binding and entry into target cells,[8] while the Nucleoprotein in viral replication and assembly.[9] The kinetics of anti-N response has been described as similar to that of the anti-S, although N responses might appear earlier.[7] Anti-SARS-CoV-2 antibody titers seem to correlate with disease severity, likely reflecting higher viral replication rates and/or immune activation in patients with severe outcome.[10]

In hospitalized patients, seroconversion is typically detected between 5 and 14 days postsymptoms onset, with a median time of 5–12 days for anti-S immunoglobulin M and 14 days for immunoglobulin G (IgG), and immunoglobulin A.[6,7,11,11,12]

Neutralizing antibodies have been detected in symptomatic individuals[13,14] and their potency seems to be associated with high levels of circulating antibodies. On the other hand, despite representing the majority of SARS-CoV-2 infections, asymptomatic infections are currently poorly documented[15] and whether this immunity is mediated by neutralizing antibodies remains an outstanding question.[16]

Moreover, it is still unknown how long SARS-CoV-2 infected subjects could maintain long-term immunity and long-lasting protective antibodies, regardless of the outcome.

In this study, we measured the circulating IgG antibody levels in 60 subjects with a certified history of SARS-CoV-2 infection, by using three different assays based on different methods. Subjects were equally divided into two groups: those hospitalized, who had a severe outcome, and those pauci-symptomatic. We analyzed their antibody response to see the trend of the humoral response in individuals with different disease outcomes. Moreover, 10 patients of each group were screened a second time to evaluate the persistence of anti-SARS-CoV-2 antibody 2 months after symptoms onset.

2 | MATERIALS AND METHODS

2.1 | Study design and participants

The participants in this study were subjects with an assessed history of SARS-CoV-2 infection, between March and May 2020. Half of them were hospitalized in "Santa Maria alle Scotte" University Hospital, in Siena with a severe outcome. Instead, the other half consisted of pauci-symptomatic subjects reporting mild signs compatible with COVID-19 (fever, cough), who were placed in isolation at home. All infections were confirmed by RT-qPCR Test (nasopharyngeal swab) (in case of current infection) and/or by serological testing (for past infections). This research was carried out according to the principles of Helsinki declaration, with reference to BIOBANK-MIU-2010 document approved by the Ethics Committee

with amendment No 1, on February 17, 2020 in terms of General Data Protection and Regulation. A total of 60 subjects, 30 who had a severe outcome and 30 who had mild infection were screened for the presence of anti-SARS-CoV-2 IgG antibodies. Moreover, 10 subjects selected from each group were screened twice, respectively, 30 and 60 days after symptoms, to evaluate the trend of their immune response.

2.2 | Cells and viruses

Vero E6 cells (ATCC CRL-1586[M]) were cultured in Dulbecco's modified Eagle's medium (DMEM) (Euroclone) supplemented with 100 U/ml penicillin/streptomycin and 5% heat-inactivated fetal calf serum (Euroclone) at 37°C in a humidified 5% CO_2 atmosphere. SARS-CoV-2 virus (SARS-CoV-2/human/ITA/Siena-1/2020; GenBank: MT531537.2), isolated from a COVID infected patient in the Virology lab at "S. Maria alle Scotte" Hospital, was propagated on Vero E6 cells until a cytopathic effect (CPE) appeared. Viral stocks were prepared, titrated on Vero E6 cells, and stored at −80°C.

2.3 | SARS-CoV-2 IgG antibody detection

Subjects' sera were analyzed using two separate immunoassays. The Abbott SARS-CoV-2 IgG chemiluminescent microparticle immunoassay (CMIA) (Abbott Laboratories) was performed on an Abbott Architect i2000 (Abbott Diagnostics) according to the manufacturer's instructions. This method is a qualitative assay that detects IgG binding to an undisclosed epitope of the SARS-CoV-2 nucleocapsid protein, with the results expressed as relative light units. The other assay was the Enzywell SARS-CoV-2 IgG (DIESSE Diagnostica Senese; Monteriggioni), an enzyme-linked immunosorbent assay (ELISA)-based 96-well plate format assay which detects anti-SARS-CoV-2 IgG directed against the inactivated native virus, with the result given in optical density at 450 nm. The final interpretation of positivity was determined by the ratio above a threshold value, with positive ratio ≥1.4 or negative ratio less than 1.4 for CMIA assay, and a positive ratio ≥1.1, borderline ratio more than 0.9 and less than 1.1, or negative ratio less than 0.9 for the ELISA. Each value represented the mean of triplicate determinations.

2.4 | SARS-CoV-2 microneutralization test

SARS-CoV-2 virus neutralization assay was carried out on Vero E6 cells in a 96-well microplate. Twenty-five microliters of twofold serial dilutions (1:8–1:1024) of sera samples were added to an equal volume of the SARS-CoV-2 strain containing 150 $TCID_{50}$ and incubated for 90 min at 37°C. Finally, 50 µl of Vero E6 cells suspension (2×10^5 cells/ml) prepared in complete DMEM were added to each well. After incubation at 37°C, the cultures were daily examined at the microscope (Olympus IX51) for the presence of the CPE. The 50% end

point titer was calculated using the Reed-Muench method.[17] A positive and negative control serum were included in each assay. Geometric mean titers (GMTs) of the neutralization assay were calculated.

2.5 | Statistical analysis

The differences between age, time of blood sample collection, circulating IgG levels, and neutralizing titers were evaluated and the statistical significances assessed with two-tailed χ^2 test. Results were considered statistically significant at $p < .05$. Spearman's rank correlation coefficient was used to assess correlations of log-transformed continuous variables between the groups.

3 | RESULTS

3.1 | Study group

We analyzed sera from 60 subjects with a certified history of SARS-CoV-2 infection. Half of them had a severe infection and needed hospital recovery (H) and the other half was pauci-symptomatic with mild signs (fever and/or cough). Mean age was 66.1 years for the hospitalized (95% confidence interval [CI]: 61.0–71.0) and 45.0 for the pauci-symptomatic (95% CI: 38.6–51.4) subjects ($p < .0001$). All these subjects were screened for the presence of specific anti-SARS-CoV-2 IgG antibodies either by indirect ELISA or CMIA. Blood samples were collected about 30 days since symptoms onset (T_0). Finally, only 10 subjects of each group were screened twice (T_0 = average 30 days; T_1 = average 60 days) for the presence of both circulating IgG levels and specific anti-SARS-CoV-2 neutralizing antibodies.

3.2 | Anti-SARS-CoV-2 specific IgG

Results obtained by ELISA and CMIA, respectively, showed a significant difference in circulating IgG level among patients with a severe outcome and those with mild symptoms at T_0 ($n = 30$; 7.31 vs. 4.06; $p = .0018$ and 6.21 vs. 4.95; $p = .048$) (Table 1A).

Concerning those subjects who were screened twice ($n = 10+10$), no significant differences in IgG levels were found between the two samplings (T_0, T_1) of both the groups, using both ELISA and CMIA ($p > .05$), although a lower IgG level was noticed among those with mild symptoms (Table 1B).

On the contrary, regarding the neutralizing activity, an evident GMT difference was found between the two groups at T_0 (Figure 1); indeed, a higher titer was present in severe cases in comparison with those having mild disease (87.7 vs. 23.3; $p = .0002$). This difference was also confirmed for the patients tested twice ($p = .046$), although no significant difference in neutralizing antibody titer was found between the first and the second samples drawn 1 month apart from

the same subjects, probably due to the limited number of samples (Table 1B). It is worthy mentioning that a different trend of antibody response was observed in the H group, where the tendency of neutralizing antibodies was increasing over time, while it was decreasing in pauci-symptomatic individuals.

3.3 | Neutralizing antibody titer and correlation with circulating IgG levels

We correlated the IgG titers obtained in the two serological assays, ELISA and CMIA, to the neutralizing antibody titers, to evaluate whether circulating IgG antibody levels could partly be associated to a neutralizing activity. As expected, we observed a moderate positive correlation between the neutralizing response and circulating IgG by using the whole virus proteins-based ELISA ($r = .60$) and a weak correlation using SARS CoV-2 N antigen-based CMIA ($r = .44$) (data not shown).

4 | DISCUSSION

In this study, we analyzed the titer of anti-SARS-CoV-2 IgG antibodies with three different serological assays in a cohort of subjects with a certified history of COVID-19, equally distributed with a severe outcome or mild symptoms.

Despite the limited number of subjects, the most remarkable finding of this study was the significantly lower antibody titer in patients who experienced mild infection with respect to those affected by a severe respiratory syndrome. Both ELISA and CMIA, although based on different antigens, such as all virus proteins in the first assay and the nucleoprotein in the second one, showed an antibody response, which was significantly higher in patients with severe disease than in pauci-symptomatic subjects in the same time frame since symptoms onset.

Previous studies on humoral response in SARS and MERS demonstrated that the humoral response could wane over time.[18,19] We do not know how long this immunity could last in individuals affected by COVID-19.[20] However, although the decay of total specific IgG was similar in both the groups, we noticed that the neutralizing antibodies, representing the protective response, only raised in severe cases 2 months after symptoms onset. On the contrary, the neutralizing response was very low in pauci-symptomatic individuals (GMT: 29.2) with an evident decrease after 2 months (GMT: 21.52). These data raise concern that humoral immunity against SARS-CoV-2 may not be long-lasting in people with mild illness, threatening their protective status. Moreover, neutralizing antibody titers from all study subjects did not show a good correlation with the level of circulating IgG antibodies evaluated in ELISA or CMIA. In particular, only a modest correlation ($r = .60$) was found with ELISA values, while weak correlation ($r = .44$) was shown with CMIA. This can be easily explained on the basis of the antigen used in each test. Indeed, ELISA was based on all the viral proteins,

Table 1A	Severe cases (H) T$_0$ (30)	Pauci-symptomatic (P) T$_0$ (30)
CMIA IgG (S/SCO)	6.21 (5.47–6.95)	4.95 (3.97–5.93)
ELISA IgG (AU)	7.31 (5.82–8.80)	4.06 (2.81–5.31)
NT Ab (GMT)	87.7 (54.9–121.0)	23.3 (10.4–36.2)

TABLE 1 Serological analysis of the study population according to the clinical outcome in subjects screened once (Table 1A) and twice (Table 1B)

including the Spike protein, responsible for cell binding to the receptor and containing the sequence recognized by neutralizing antibodies. CMIA was only using the immunogenic nucleoprotein, to which the humoral response is promptly mounted in the host, but it is not involved in the neutralizing activity. The observational time considered in this study was quite short, but the preliminary results indicated that a part of the population, particularly young people who presented a very mild disease, developed a weak humoral response, mainly characterized by a low neutralizing activity that could wane over time. For this reason, patients with high levels of circulating antibodies, especially those who had a severe outcome, could be more likely protected, while subjects with a favorable outcome, who showed low levels of neutralizing antibodies, may not maintain a long-lasting response and be susceptible to reinfection. Therefore, it could be important to keep monitoring both kind of subjects and see
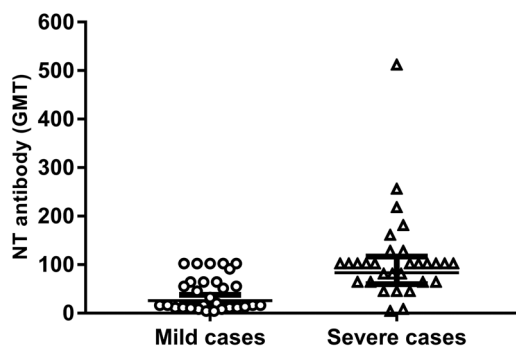
whether a time-dependent decrease of both circulating and neutralizing IgG antibodies to nonprotective levels could occur in a longer time course.

This finding may have implications for immunity strategy and prevention, since it is still not clear whether the immunity is long-lasting and the potential vaccines, based on the spike antigen, are able to induce a durable response and herd immunity. Further studies are necessary to understand the role of cellular immune response and identify the correlates of protection for COVID-19.

CONFLICT OF INTERESTS

The authors declare that there are no conflict of interests.

AUTHOR CONTRIBUTIONS

Conceptualization: Maria Grazia Cusi. Data curation: Maria Grazia Cusi, Gabriele Anichini. Investigation: Gianni Gori Savellini. Methodology: Gabriele Anichini, Claudia Gandolfo, Chiara Terrosi and Shibily Prathyumnan. Resources: Simonetta Fabrizi, Giovanni Battista Miceli and Federico Franchi. Supervision: Maria Grazia Cusi. Writing—original draft: Gabriele Anichini. Writing—review and editing: Maria Grazia Cusi. All authors revised and approved the final version of the manuscript.

ORCID

Maria Grazia Cusi http://orcid.org/0000-0001-8869-8164

FIGURE 1 Differences in neutralizing antibody titers between SARS-CoV-2 infected patients with mild or severe outcome. The whiskers represent the values from the 5th to the 95th percentiles; the GMTs are depicted by the horizontal lines in the boxes. Individual data points are shown. The *p* value of the GMT between the two groups is 0.0002. GMT, Geometric mean titer; SARS-CoV-2, severe acute respiratory syndrome coronavirus-2

REFERENCES

1. Zhu N, Zhang D, Wang W, et al. China novel coronavirus investigating and research team. A novel coronavirus from patients with pneumonia in China. *N Engl J Med*. 2020;382:727-733.
2. Lu R, Zhao X, Li J, et al. Genomic characterisation and epidemiology of 2019 novel coronavirus: implications for virus origins and receptor binding. *Lancet*. 2020;395:565-574.
3. Li X, Wang W, Zhao X, et al. Transmission dynamics and evolutionary history of 2019-nCoV. *J Med Virol*. 2020;92:501-511.

4. Lu H, Stratton CW, Tang YW. Outbreak of pneumonia of unknown etiology in Wuhan, China: the mystery and the miracle. *J Med Virol.* 92, 2020:401-402.

5. Patel R, Babady E, Theel ES, et al. Report from the American Society for Microbiology COVID-19 International Summit, 23 March 2020: value of diagnostic testing for SARS-CoV-2/COVID-19. *mBio.* 2020; 11:e00722-20.

6. Guo L, Ren L, Yang S, et al. Profiling early humoral response to diagnose novel coronavirus disease (COVID-19). *Clin Infect Dis.* 2020;71:778-785.

7. Zhao J, Yuan Q, Wang H, et al. Antibody responses to SARS-CoV-2 in patients of novel coronavirus disease. *Clin Infect Dis.* 2020:28ciaa344.

8. Ou X, Liu Y, Lei X, et al. Characterization of spike glycoprotein of SARS-CoV-2 on virus entry and its immune cross-reactivity with SARS-CoV. *Nat Commun.* 2020;11:1620.

9. Zeng W, Liu G, Ma H, et al. Biochemical characterization of SARS-CoV-2 nucleocapsid protein. *Biochem Biophys Res Commun.* 2020;527:618-623.

10. Long QX, Liu BZ, Deng HJ, et al. Antibody responses to SARS-CoV-2 in patients with COVID-19. *Nat Med.* 2020;26:845-848.

11. Amanat F, Stadlbauer D, Strohmeier S, et al. A serological assay to detect SARS-CoV-2 seroconversion in humans. *Nat Med.* 2020;26: 1033-1036.

12. Okba NMA, Müller MA, Li W, et al. Severe acute respiratory syndrome coronavirus 2-specific antibody responses in coronavirus disease patients. *Emerg Infect Dis.* 2020;26:1478-1488.

13. Wölfel R, Corman VM, Guggemos W, et al. Virological assessment of hospitalized patients with COVID-2019. *Nature.* 2020;581:465-469.

14. Wu F, Wang A, Liu M, et al. Neutralizing antibody responses to SARS-CoV-2 in a COVID-19 recovered patient cohort and their implications. *medRxiv.* 2020. https://doi.org/10.1101/2020.03.30. 20047365

15. Li R, Pei S, Chen B, et al. Substantial undocumented infection facilitates the rapid dissemination of novel coronavirus (SARS-CoV-2). *Science.* 2020;368:489-493.

16. Grzelak L, Temmam S, Planchais C, et al. A comparison of four serological assays for detecting anti-SARS-CoV-2 antibodies in human serum samples from different populations. *Sci Transl Med.* 2020;12(559). https://doi.org/10.1101/2020.04.21.20068858

17. Reed LJ, Muench H. A simple method of estimating fifty per cent endpoints. *Am J Hyg.* 1938;27:493-497.

18. Cao WC, Liu W, Zhang PH, Zhang F, Richardus JH. Disappearance of antibodies to SARS-associated coronavirus after recovery. *N Engl J Med.* 2007;357:1162-1163.

19. Chang SC, Wang JT, Huang LM, et al. Longitudinal analysis of Severe Acute Respiratory Syndrome (SARS) coronavirus-specific antibody in SARS patients. *Clin Diagn Lab Immunol.* 2005;12:1455-1457.

20. Ibarrondo FJ, Fulcher JA, Goodman-Meza D, et al. Rapid decay of Anti-SARS-CoV-2 antibodies in persons with mild Covid-19. *N Engl J Med.* 2020;383:1085-1087NEJMc2025179.

Perspective

Residual SARS-CoV-2 RNA in nasal swabs of convalescent COVID-19 patients: Is prolonged quarantine always justified?

Antonio Piralla[a], Matteo Ricchi[b], Maria Grazia Cusi[c,d], Paola Prati[e], Nadia Vicari[e], Giada Scarsi[e], Claudia Gandolfo[c,d], Gabriele Anichini[d], Chiara Terrosi[d], Elena Percivalle[a], Edoardo Vecchio Nepita[a], Federica Bergami[a], Monica Tallarita[a], Raffaella Di Martino[a], Alessandro Ferrari[a], Francesca Rovida[a], Giovanna Lunghi[f], Roberta Schiavo[g], Fausto Baldanti[a,h,*]

[a] Molecular Virology Unit, Microbiology and Virology Department, Fondazione IRCCS Policlinico San Matteo, Pavia, Italy
[b] Diagnostic Section of Piacenza, Istituto Zooprofilattico Sperimentale della Lombardia e dell'Emilia Romagna, (IZSLER), Piacenza, Italy
[c] Microbiology and Virology Unit, S. Maria delle Scotte University Hospital of Siena, Siena, Italy
[d] Virology Unit, Department of Medical Biotechnologies, University of Siena, Siena, Italy
[e] Diagnostic Section of Pavia, Istituto Zooprofilattico Sperimentale della Lombardia e dell'Emilia Romagna (IZSLER), Pavia, Italy
[f] Virology Unit, Fondazione IRCCS Ca' Granda Ospedale Maggiore Policlinico, Milan, Italy
[g] Microbiology Unit, Clinical Pathology Department, Guglielmo da Saliceto Hospital, Piacenza, Italy
[h] Department of Clinical, Surgical, Diagnostic and Pediatric Sciences, University of Pavia, Pavia, Italy

ABSTRACT

Real-time reverse transcription PCR is currently the most sensitive method to detect severe acute respiratory syndrome coronavirus 2 (SARS-CoV-2). Defining whether a patient could be contagious or not contagious in the presence of residual SARS-CoV-2 RNA is of extreme importance in the context of public health. In this prospective multicenter study, virus isolation was prospectively attempted in 387 nasal swabs from clinically recovered patients showing low viral load (quantification cycle, Cq, value greater than 30). The median Cq value was 36.8 (range 30.0–39.4). Overall, a cytopathic effect was detected in nine samples, corresponding to a culture positivity rate of 2.3% (9/387). The results of this study help to dissect true virus replication and residual viral RNA detection in recovered patients.

© 2020 The Authors. Published by Elsevier Ltd on behalf of International Society for Infectious Diseases. This is an open access article under the CC BY-NC-ND license (http://creativecommons.org/licenses/by-nc-nd/4.0/).

Introduction

On February 20, 2020, Lombardy, a region in northern Italy, was struck by an outbreak of severe acute respiratory syndrome coronavirus 2 (SARS-CoV-2) infection. Soon afterward, the epidemic involved other Italian regions, with a north-south gradient. Several containment measures were adopted, including lockdown of affected areas, social distancing, and quarantining of individuals with laboratory-confirmed COVID-19 as well as their close contacts. Laboratory confirmation of SARS-CoV-2 infection relied on positivity of a nasopharyngeal swab on virus-specific real-time reverse transcription PCR (RT-PCR) targeting several SARS-CoV-2 genes (Centers for Disease Control and Prevention, 2020; WHO, 2020a; Wang et al., 2020).

In the early phases of the epidemic, when containment of the infection was the most urgent goal, prudence required that even minimal amounts of SARS-CoV-2 RNA were considered sufficient for imposing quarantine on a suspected COVID-19 patient. Similarly, quarantine relief rules required two negative nasal swab results from samples taken at least 24 h apart. All these measures were somewhat effective in limiting SARS-CoV-2 circulation, as shown by the marked reduction of new COVID-19 cases by the end of May. On the other hand, while most clinically recovered patients tested negative at the end of the quarantine period and were able to return to their normal working and social life, a substantial proportion (about 16.6%) still tested positive on the required second testing, sometimes forcing them into a never-ending quarantine–positive test loop (Wu et al., 2020). Previous reports indicated that viable virus could not be isolated from samples with low SARS-CoV-2 genome loads (Huang et al., 2020; Atkinson and Petersen, 2020; Wölfel et al., 2020). In the initial phase of the

* Corresponding author at: Department of Clinical, Surgical, Diagnostic and Pediatric Sciences, University of Pavia, 27100 Pavia, Italy.
E-mail addresses: f.baldanti@smatteo.pv.it, fausto.baldanti@unipv.it (F. Baldanti).

infection (when viable virus is obviously present and the patient is infectious), this finding could be due to sampling bias or culturing inconsistencies (e.g., delayed delivery of the sample to the laboratory). On the other hand, in clinically recovered patients, the presence of residual viral RNA is more likely related to elimination of degrading viral materials.

Our hypothesis is that despite the high sensitivity of SARS-CoV-2-specific molecular assays, in the monitoring of the presence SARS-CoV-2 for release of individuals from quarantine, this approach could be a double-edged sword because of detection of the prolonged presence of a single gene.

Methods

To understand whether residual SARS-CoV-2 RNA load in clinically recovered patients could be associated with ongoing virus replication or is a result of catabolism of the virus or virus-infected cells, we submitted to cell culture isolation 387 nasal swabs from patients resident in the Lombardy, Emilia-Romagna, and Toscana regions showing low SARS-CoV-2 RNA amounts with a quantification cycle (Cq) value greater than 30, according to MIQE guidelines (Bustin et al., 2009). Clinical samples were obtained at the time of discharge from the hospital or during the quarantine period from hospitalized patients, symptomatic healthcare workers, or persons tested as part of the early epidemic response. Samples were anonymized before the analysis, and no clinical information was available.

This study was conduced in collaboration with five different centers: (1) Molecular Virology Unit, Microbiology and Virology Department, Fondazione IRCCS Policlinico San Matteo, Pavia, (2) Istituto Zooprofilattico Sperimentale della Lombardia e dell'Emilia Romagna, (3) Microbiology and Virology Unit, S. Maria delle Scotte University Hospital of Siena, Siena, (4) Virology Unit, Fondazione IRCCS Ca' Granda Ospedale Maggiore Policlinico, Milan, and (5) Microbiology Unit, Clinical Pathology Department, Guglielmo da Saliceto Hospital, Piacenza. Nasal swabs collected in universal transport medium (UTM™, Copan Italia, Brescia, Italy) were prospectively analyzed for the diagnosis of SARS-CoV-2 infection by real-time RT-PCR targeting the E gene according to WHO guidelines (WHO, 2020b) and protocols of Corman et al. (2020) at

centers 1 and 2, while at centers 3–5, a commercial multiplex assay including the N gene as a target (Allplex™ 2019-nCoV assay; Seegene, Korea) was used. A series of nasal swabs collected from convalescent patients from April 1 to August 1, 2020, and positive for SARS-CoV-2 RNA with Cq value greater than 30 with the E or N gene were included in the study. To investigate the infectious potential of samples, a 200 μL sample was inoculated into a Vero E6 (VERO C1008 (Vero 76, clone E6, Vero E6); ATCC® CRL-1586™) confluent 24-well microplate for virus isolation. All samples were inoculated between 8 and 24 h after positivity results and kept at 4 °C before processing. After 1 h incubation at 33 °C in 5% CO_2 in air, the inoculum was discarded and 1 mL of medium for respiratory viruses (Eagle's minimum essential medium supplemented with 1% penicillin, streptomycin, and glutamine and trypsin at 5 μg/mL) was added to each well. Cells were incubated at 33 °C in 5% CO_2 in air and observed with a light microscope every day for a cytopathic effect. After incubation for 7 days, 200 μL of supernatant from a well showing a cytopathic effect was tested for the presence of SARS-CoV-2 by molecular assay (gene E real-time RT-PCR) or SARS-CoV-2-specific immunofluorescence assays using antibodies to N protein.

In a subset of samples positive for the N gene (with Cq value of 35 or greater), both direct RNA and amplicon sequencing approaches was performed with a MinION instrument (Oxford Nanopore Technologies, UK). The sequencing run was managed by MinKNOW (version 19.12.5), and amplicon reads were mapped to the reference genome Wuhan Wu-1 (GenBank accession no. MN908947).

Results

Among the samples tested by real-time RT-PCR, 89.4% (346/387) had Cq values greater than 30 for the E gene and 10.6% (41/387) had Cq values greater for the N gene (Figure 1A). The median Cq value was 36.8 (range 30.0–39.4). In detail, the median Cq value was 36.9 (range 30.0–39.4) for the E gene and 35.5 (range 32.0–39.4) for the N gene (Figure 1A). A cytopathic effect was observed in only nine samples, corresponding to a culture positivity rate of 2.3% (9/387). Among these samples, five had a high Cq value for the E gene, while the others had a high Cq value for the N gene (Figure
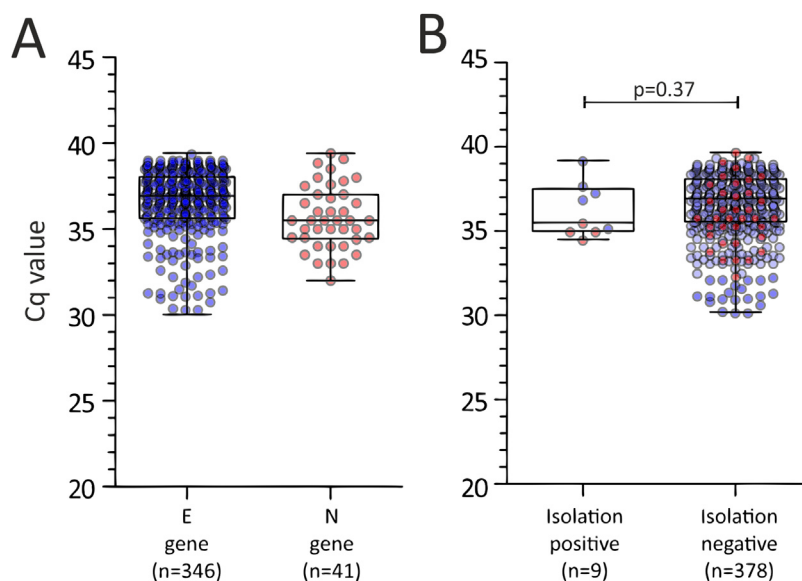

Figure 1. Cq values observed in samples included in the study according to (A) the target gene used in the diagnostic severe acute respiratory syndrome coronavirus 2 (SARS-CoV-2)-specific real-time reverse transcription PCR and (B) isolation positive or negative.

1B). In these samples, the occurrence of active replication of SARS-CoV-2 was determined by real-time RT-PCR in five samples (median Cq value 14.5; range 12.4–16.8) and immunofluorescence assays in the other four samples.

The median Cq value of culture-positive samples was not significantly different from that observed in culture-negative samples (35.6 vs. 36.9; p = 0.37, Figure 1B).

In a series of five samples, long-read *sequencing* data analysis was performed by third-generation sequencing with Nanopore technology. Bioinformatic reconstruction of sequenced RNA showed how samples did not have the whole viral genome, but only few and very short gene fragments (<600 nucleotides). This finding indicates that the residual RNA detected by molecular testing was not functional and represented only pieces of the degraded viral genome.

Discussion

This prospective multicenter observational study demonstrates that residual SARS-CoV-2 RNA load, with a minimum amount of only one gene target, is not substantially associated with ongoing virus replication. Indeed, less than 3% of samples that were positive by real-time RT-PCR with low or very low RNA amounts were still able to transmit infection in cell monolayers. Our data are in agreement with a French study that reported an isolation rate lower than 50.0% in samples with a Cq value between 30 and 35 (only 24 samples) and no isolation for samples with a Cq value greater than 35 (only four samples) (La Scola et al., 2020). Similar results were very recently reported by Singanayagam et al. (2020), where the estimated probability of recovery of virus from samples with a Cq value of 35 or greater was 8.3%. The concept that medium/high viral load is needed for virus isolation was assessed in a recent publication aimed at clarifying the correlation between the culturability of the virus and the RNA copy number (Huang et al., 2020). In that study, the mean Cq value of culturable samples was always less than 30 (Huang et al., 2020). Our data are even more straightforward when one considers that samples were inoculated early after collection, thus minimizing the infectivity loss during transport to the laboratory. In addition, all samples were drawn from clinically recovered patients. The implications of the results of the present study are important at both the individual level and the epidemiologic level. On the individual side, dissection between true virus replication and residual detection of virus genes has the immediate effect of releasing patients from prolonged quarantine, safely allowing them to return to work and social activities. From an epidemiologic standpoint, these data pose the question of whether it is correct to consider these molecular "low-positivity" cases as real virus positives. Indeed, while the analytical positivity of highly sensitive real-time RT PCR methods is correct (a fragment of SARS-CoV-2 RNA is detected), their clinical significance is less than certain (a fragment of viral RNA does not indicate either the presence of the whole virus or that the patient is still contagious). The number of messenger RNAs that originate during SARS-CoV-2 replication is largely different, although they are collinear with the viral genome and are simultaneously targeted by real-time RT PCR methods. Thus, the results of molecular assays have to take into account the virus biology (Huang et al., 2020). Finally, in the infection recovery phase, neutralizing antibodies are generated, and an impact of seroconversion on virus infectivity must be considered. However, specific studies are needed to address this hypothesis.

One limitation of this study is the impossibility to score the quality of sampling and storage before samples are sent to the laboratory and, nevertheless, the sensitivity of cell culture isolation. Comparison of Cq values between E and N gene results

could be biased by different sensitivities of the assays; however, WHO and CDC reports showed comparable sensitivity for both assays (WHO, 2020b; Corman et al., 2020; Canters for Disease Control and Prevention, 2020). Indeed, a nationwide external quality assessment conducted for more than 100 Korean laboratories showed overlapping results for Cq values obtained by real-time RT-PCR assays used in the present study (Sung et al., 2020).

An additional limitation was the unavailability of clinical information because of the anonymization of samples. However, these data, which were consistent among the five different laboratories in northern and central Italy, lead us to propose that the individuals are no longer contagious when the molecular diagnosis is based on a high Cq value ($\geq$35) of one gene target, and this is supported by clinical data. The major caveat of this study is the evidence that most recovered patients (97%) with a high Cq value do not carry infectious virus, and that prolonged quarantine periods are not justified. Thus, revision of current guidelines is highly recommended.

Funding

Conflict of interest

The authors declare that they have no competing interests.

Ethics statement

This study was performed according to the guidelines of the Institutional Review Board of our Institute on the use of biological specimens for scientific purposes, in keeping with Italian law (art 13 D. Lgs 196/2003) Samples were anonymized before the analysis and therefore informed consent was not required.

Author contributions

AP collated and analyzed the data and wrote the first draft of the manuscript. MR performed the statistical analysis and constructed the figures. MGC, PP, GL, and RS provided samples for the study. EP and MGC supervised the isolation team. EVN, RD, AF, GS, and CG performed isolation experiments. NV, FB, MT, and FR performed the laboratory PCR work. CG, GA, and CT performed next-geneteration sequencing experiments. MGC and FB supervised and coordinated the samples and testing and critically revised the first version of the manuscript.

Acknowledgment

References

Atkinson B, Petersen E. SARS-CoV-2 shedding and infectivity. Lancet 2020;395 (10233):1339–40, doi:http://dx.doi.org/10.1016/S0140-6736(20)30868-0.

Bustin SA, Benes V, Garson JA, Hellemans J, Huggett J, Kubista M, et al. The MIQE guidelines: minimum information for publication of quantitative real-time PCR experiments. Clin Chem 2009;55(4):611–22, doi:http://dx.doi.org/10.1373/clinchem.2008.112797.

Canters for Disease Control and Prevention. CDC's diagnostic multiplex assay for Flu *and* COVID-19 at public health laboratories and supplies. 2020. . (Accessed 14 September 2020) https://www.cdc.gov/coronavirus/2019-ncov/lab/multiplex.html.

Centers for Disease Control and Prevention. CDC 2019-novel coronavirus (2019-nCoV) real-time RT-PCR diagnostic panel. 2020. . [Accessed 18 June 2020] https://www.fda.gov/media/134922/download.

Corman VM, Landt O, Kaiser M, Molenkamp R, Meijer A, Chu DK, et al. Detection of 2019 novel coronavirus (2019-nCoV) by real-time RT-PCR. Euro Surveill 2020;25(3):2000045, doi:http://dx.doi.org/10.2807/1560-7917.ES.2020.25.3.2000045.

Huang CG, Lee KM, Hsiao MJ, Yang SL, Huang PN, Gong YN, et al. Culture-based virus isolation to evaluate potential infectivity of clinical specimens tested for COVID-19. J Clin Microbiol 2020;58(8):e01068–20, doi:http://dx.doi.org/10.1128/JCM.01068-20.

La Scola B, Le Bideau M, Andreani J, Hoang VT, Grimaldier C, Colson P, et al. Viral RNA load as determined by cell /culture as a management tool for discharge of SARS-CoV-2 patients from infectious disease wards. Eur J Clin Microbiol Infect Dis 2020;39(6):1059–61, doi:http://dx.doi.org/10.1007/s10096-020-03913-9.

Singanayagam A, Patel M, Charlett A, Lopez Bernal J, Saliba V, Ellis J, et al. Duration of infectiousness and correlation with RT-PCR cycle threshold values in cases of COVID-19, England, January to May 2020. Euro Surveill 2020;25(32):2001483, doi:http://dx.doi.org/10.2807/1560-7917.ES.2020.25.32.2001483.

Sung H, Han MG, Yoo CK, Lee SW, Chung YS, Park JS, et al. Nationwide external quality assessment of SARS-CoV-2 molecular testing, South Korea. Emerg Infect Dis 2020;26(10):2353–60, doi:http://dx.doi.org/10.3201/eid2610.202551.

Wang W, Xu Y, Gao R, Lu R, Han K, Wu G, et al. Detection of SARS-CoV-2 in different types of clinical specimens. JAMA 2020;323(18):1843–4, doi:http://dx.doi.org/10.1001/jama.2020.3786.

WHO.2020a Real-time RT-PCR assays for the detection of SARS-CoV-2. https://www.who.int/docs/default-source/coronaviruse/whoinhouseassays.pdf?sfvrsn=de3a76aa_2. [Accessed 18 June 2020].

WHO. https://www.who.int/docs/default-source/coronaviruse/protocol-v2-1.pdf. [Accessed 18 June 2020].

Wölfel R, Corman VM, Guggemos W, Seilmaier M, Zange S, Müller MA, et al. Virological assessment of hospitalized patients with COVID-2019. Nature 2020;581(7809):465–9, doi:http://dx.doi.org/10.1038/s41586-020-2196-x.

Wu J, Liu X, Liu J, Liao H, Long S, Zhou N, et al. Coronavirus disease 2019 test results after clinical recovery and hospital discharge among patients in China. JAMA Netw Open 2020;3(5):e209759, doi:http://dx.doi.org/10.1001/jamanetworkopen.2020.9759.

Ubiquitin and Not Only Unfolded Domains Drives Toscana Virus Non-Structural NSs Protein Degradation

Gianni Gori Savellini [1,*] ![ORCID]**, Luca Bini** [2] ![ORCID]**, Assunta Gagliardi** [3]**, Gabriele Anichini** [1] ![ORCID]**, Claudia Gandolfo** [1,4]**, Shibily Prathyumnan** [1] **and Maria Grazia Cusi** [1,4] ![ORCID]

[1] Department of Medical Biotechnologies, University of Siena, 53100 Siena, Italy; gabriele.anichini@student.unisi.it (G.A.); claudia.gandolfo@unisi.it (C.G.); shibilyps@gmail.com (S.P.); mariagrazia.cusi@unisi.it (M.G.C.)
[2] Department of Life Sciences, University of Siena, 53100 Siena, Italy; luca.bini@unisi.it
[3] Department of Cellular, Computational and Integrative Biology (CIBIO), University of Trento, Laboratory of Synthetic and Structural Vaccinology, 38122 Trento, Italy; assunta.gagliardi@unitn.it
[4] S. Maria delle Scotte Hospital, V.le Bracci, 1, 53100 Siena, Italy
[*] Correspondence: gianni.gori@unisi.it; Tel.: +39-0577-233864

Abstract: The non-structural protein NSs of the *Phenuiviridae* family members appears to have a role in the host immunity escape. The stability of Toscana virus (TOSV) NSs protein was tested by a cycloheximide (CHX) chase approach on cells transfected with NSs deleted versions fused to a reporter gene. The presence of intrinsically disordered regions (IDRs) both at the C- and N-terminus appeared to affect the protein stability. Indeed, the NSsΔC and NSsΔN proteins were more stable than the wild-type NSs counterpart. Since TOSV NSs exerts its inhibitory function by triggering RIG-I for proteasomal degradation, the interaction of the ubiquitin system and TOSV NSs was further examined. Chase experiments with CHX and the proteasome inhibitor MG-132 demonstrated the involvement of the ubiquitin-proteasome system in controlling NSs protein amount expressed in the cells. The analysis of TOSV NSs by mass spectrometry allowed the direct identification of K_{104}, K_{109}, K_{154}, K_{180}, K_{244}, K_{294}, and K_{298} residues targeted for ubiquitination. Analysis of NSs K-mutants confirmed the presence and the important role of lysine residues located in the central and the C-terminal parts of the protein in controlling the NSs cellular level. Therefore, we directly demonstrated a new cellular pathway involved in controlling TOSV NSs fate and activity, and this opens the way to new investigations among more pathogenic viruses of the *Phenuiviridae* family.

Keywords: ubiquitin-proteasome system; NSs protein; protein stability

1. Introduction

Toscana virus (TOSV) is a member of the *Phenuiviridae* family (*Phlebovirus genus*) classified as an emergent sandfly-borne virus. It is mainly transmitted to humans by *Phlebotomus perfiliewi*, *P. perniciosus*, and *P. papatasi* sandfly species [1–3]. Although pauci-symptomatic infections are described in endemic countries [4], TOSV infection is mostly associated to meningitis or more severe central nervous system (CNS) injuries, such as encephalitis and cerebral ischemia [4–6]. Nowadays, TOSV is widely present in the Mediterranean basin [7–11] and represents a significant public health threat.

The non-structural protein (NSs) of the *Phenuiviridae* and *Bunyaviridae* family members represents an important virulence factor, inhibiting the host innate immunity to viral infections, mainly mediated by type I interferons (IFN-α/β) [12–21]. In order to overcome this first-line defense implemented by

the host, viruses evolved protein(s) able to block the IFN-β production and its downstream activity at different steps in the signaling cascade.

However, TOSV is the first Phlebovirus described to date, whose behavior is different from that observed among the *Bunyaviridae* or *Phenuiviridae* members, since interferons are not inhibited during viral infection and replication, despite its NSs protein. TOSV NSs protein is rapidly degraded by the ubiquitin-proteasome system, as previously demonstrated [19–21]. Therefore, during TOSV infection in humans, the ubiquitination and degradation of the NSs protein occur very early in virus replication to prevent IFN-β inhibition in the host.

The proteasomal degradation of proteins is triggered by ubiquitination, a process consisting of covalent attachment of poly-ubiquitin (poly-Ub) chains at lysine residues on the target protein. The assembly of poly-Ub chains to the target protein is accomplished by the cooperation of ubiquitin-activating enzymes (E1), ubiquitin-conjugating enzymes (E2), and ubiquitin-ligases (E3), which work in a sequential cascade [22–34]. A well-characterized cellular complex, which mediates ubiquitination of target proteins, is represented by the Skp, Cullin, and F-box (SCF)-containing complex. Cullin activity is regulated by their NEDdylation, which is the covalent attachment of the small ubiquitin-like protein NEDD8 (neural precursor cell expressed developmentally downregulated 8) to the cullin subunit via the NEDD8 activating enzyme (NAE) [25,26]. In this context, the E3 ubiquitin ligase is the only enzyme that confers specificity to this system by recognizing selected target proteins [24–26].

The structure of the poly-Ub chain assembled by the E3 ligase is crucial for target protein fate and function [22,33]. Covalent bonding between ubiquitin monomers occurs at one of the seven lysine residues in the previously attached ubiquitin molecule, resulting in the formation of ubiquitin chains containing distinctive linkages between the ubiquitin moieties, thus creating a different structure. Based on the linkage generated between ubiquitin moieties, the cognate proteins undergo regulation of their physiological functions, although the role of some chains is still elusive [34–38]. Notably, Lys_{48} (K_{48}) ubiquitin linkage has been reported to be involved in targeting proteins for degradation by the 26S proteasome, while the Lys_{63} (K_{63}) linkage has been proved to regulate protein functions, especially those involved in signal transduction, cell cycle, and gene expression [23,28,31]. So far, the involvement of the ubiquitin system in virus replication, latency, oncogenic properties, and immunity escape has been widely demonstrated [39–59].

Among *Phenuiviridae* members, Rift Valley fever virus (RVFV) is the most investigated virus in terms of antagonistic effects of its NSs protein. The involvement of the ubiquitin system, and in particular of the SCF E3 ubiquitin ligase complex, has been recently elucidated [59–61]. However, despite the involvement of RVFV NSs in the ubiquitin-proteasome control of cellular components, no direct evidence of its ubiquitination and fate/function regulation has been shown.

Regarding TOSV, the involvement of the ubiquitin system in controlling its NSs activity was further demonstrated by a recent work, where an E3 ubiquitin ligase activity has been attributed to the viral protein. Similarly to RVFV, this E3 ligase activity was necessary to mediate RIG-I ubiquitination and proteasomal degradation and, consequently, impede IFN-β production [57]. The only evidence that Bunyaviridae NSs protein could be subjected to ubiquitination has been investigated in the Bunyamwera virus [62,63]. Indeed, analysis of recombinant virus carrying lysine knockdown NSs variant highlighted the increased stability of the mutated protein.

However, no significant advantage in virus growth and virulence in mice were reported, suggesting that NSs ubiquitination is not essential for the virus life cycle [62].

Here, we reported the first evidence of TOSV NSs ubiquitination. Mass spectrometry analysis allowed the identification of lysine residues 104, 109, 154, 180, 244, 294, and 298 on the NSs targeted for ubiquitination. The influence of these sites on protein stability was deeply investigated to evidence their role in protein function and stability, along with the effects of disordered regions located at the C- and N-terminus of the protein.

2. Materials and Methods

2.1. Cells and Viruses

Human embryonic kidney Lenti-X 293T cells (Clontech, Milan, Italy) were cultured in Dulbecco's modified Eagle's medium (DMEM) (Lonza, Milan, Italy) supplemented with 100 U/mL penicillin/streptomycin (Hyclone Europe, Milan, Italy) and 10% heat-inactivated fetal calf serum (FCS) (Lonza), at 37 °C. Toscana virus (TOSV) strain 1812 [64] was used as a template source for NSs cloning described where the N-terminal deleted (NSsΔN) NSs protein variant was generated.

2.2. Reagents and Antibodies

Transient transfections were performed with GeneJuice® Transfection reagent (Novagen, Milan, Italy), according to the manufacturer's instructions, or standard calcium phosphate method. The proteasome inhibitor MG-132 and cycloheximide (CHX) were purchased from Sigma-Aldrich (Milan, Italy). Mouse anti-6×His tag antibody (GE Healthcare, Milan, Italy), mouse monoclonal anti-HA tag antibody, and HRP-conjugated anti-mouse IgG were purchased from Sigma-Aldrich. Ni-NTA sepharose was from Novagen (Milan, Italy).

2.3. Plasmids

Six His-tagged full-length TOSV NSs expression vector was described elsewhere [58]. Amino-terminal-deleted (NSsΔN) and carboxy-terminal-deleted (NSsΔC) NSs protein variants were generated by cloning the nt: 217–948 and nt: 1–537 sequences on TOSV 1812 strain (GenBank: EU327772.1) in-frame into the pcDNA4HisMax (Life Technologies, Milan, Italy) expression plasmid. Having arginine instead of lysine 104, 108, 109, 150, 154, and 179, NSs mutant (NSs-6KR) was generated by using QuikChange II Site-Directed Mutagenesis Kit (Agilent Technologies, Milan, Italy) according to the manufacturer's instructions. NSs variants with lysine residues at the N-terminus (9, 17, 36, 57, 59, and 69) mutated to arginine (NSs-NKR and NSs-6KR-NKR) were generated substituting the N-terminal part with a mutated synthetic fragment (gBlocks, IDT Integrated DNA technologies, Leuven, Belgium). To measure NSs mutant proteins' stability, FireFly Luciferase (FFLuc) fused proteins were generated. FFLuc-NSs and FFLuc-NSsΔC were already described elsewhere [58]. A similar approach was used to obtain the FFLuc-NSs new variants. Briefly, the NSs recombinant plasmids were linearized with BamHI and the FFLuc coding gene was inserted upstream and in frame with the NSs gene by the InFusion system (Clontech, Milan, Italy) following the manufacturer's instructions. All the recombinant plasmids were verified by sequencing. The *Renilla* Luciferase reporter plasmid (pSV40-RL) was purchased by Promega (Promega, Milan, Italy). HA-tagged ubiquitin expressing plasmid was a kind gift of D. Arnoult (Inserm, France) while K48-only and K63-only ubiquitin plasmids were purchased from Addgene (Teddington, UK).

2.4. Cycloheximide Chase Analysis and NSs Protein Stability

Lenti-X 293T cells were seeded in 6-well plates and, after 24 h, transfected with the FFLuc-fused wt-; deleted or mutated NSs expressing plasmids along with 200 ng of pRL-SV40 (Promega) for normalization. Twenty-four hours later, transfected cells were split in a 24-well plate, in triplicate and, after additional 12 h, cells were treated with 25 μM MG-132 for 30 min or untreated. After the inhibitor treatment, in order to start protein expression quantification (T0), cell samples were collected, while the remaining samples were exposed to 100 μg/mL of CHX, or 25 μM MG-132 or 25 μM MG-132 along with 100 μg/mL of CHX. Samples were collected 1.5 and 3 h later for time course quantification. FFLuc-fusion protein amount, detected after translation inhibition by CHX, was quantified by measuring FFLuc activities. Lysates and assay set-up were prepared according to Dual-Luciferase reporter assay (Promega). Relative FFLuc values were normalized with respect to the corresponding RL activities (FFLuc/RL), then fold changes of each sample were calculated with regard to the corresponding T0,

mock-treated, sample. The deduced half-life of each protein was calculated with tools available on the web (https://www.calculator.net/half-life-calculator.html).

2.5. Pull-Down and Immunoblot Analysis

Lenti-X 293T cells, seeded in T25 flasks, were transfected with 4 µg of NSs expressing plasmid and, where indicated, with HA-tagged ubiquitin mutants by using standard calcium phosphate precipitation protocol [65]. Thirty-six hours later, cells were treated with 1 µM MG-132 for additional 12 h and collected 48 h post-transfection. Enrichment of the NSs protein was achieved by Immobilized Metal Affinity Chromatography (IMAC) under denaturing conditions [66]. Briefly, cell pellets were lysed in 5 M guanidine-HCl; 10 mM HEPES (pH 8.0) with sonication to share genomic DNA. His-tagged NSs was bound to Ni-NTA sepharose overnight (o/n) at 4 °C. Beads were collected and washed three times with 10 volumes of 10 mM HEPES (pH 8.0), 1 M NaCl, 0.3% w/v N-lauroylsarcosine (SRK), 20 mM imidazole. Bound proteins were eluted by washing buffer supplemented with 500 mM imidazole. An aliquot of eluted sample was loaded on SDS-PAGE, transferred to nitrocellulose membrane (Santa Cruz Biotechnology, Heidelberg, Germany) and processed for immunoblotting. Briefly, membrane blocking was accomplished with 5% non-fat dry milk, then filters were incubated o/n at 4 °C with anti-NSs (1:200 dilution) or mouse anti-HA monoclonal antibody (1:1000 dilution) (Sigma-Aldrich). After being washed with PBS 0.2% Tween-20 (PBS-T), membranes were incubated with a selected secondary antibody (1:5000 dilution). Immunocomplexes were detected with TMB Enhanced One Component HRP Membrane Substrate (Tebu-bio, Milan, Italy). Ubiquitin modification of the NSs was evidenced by a shift in its MW (10 kDa for mono-ubiquitination, 20 kDa for di-ubiquitination, 10.5 multiples for poly-ubiquitination).

2.6. Mass Spectrometry Detection of NSs Ubiquitination

NSs protein was enriched from Lenti-X 293T-transfected cells. Proteins were separated by SDS-PAGE and stained with Bio-safe Coomassie stain (Bio-Rad, Milan, Italy). Protein bands corresponding to potentially ubiquitinated NSs isoforms were manually cut from gel and prepared for mass-spectrometry analysis. Each band was first destained with 2.5 mM ammonium bicarbonate and 50% acetonitrile, and dehydrated in 100% acetonitrile. A reduction and alkylation procedure was then applied, using 10 mM DTE in 25 mM ammonium bicarbonate for 1 h at 56 °C, followed by incubation in 55 mM iodoacetamide and 25 mM ammonium bicarbonate at room temperature for 45 min, in dark room. Protein bands were rinsed for 10 min with 50 mM ammonium bicarbonate and dehydrated, again, with 100% acetonitrile. Dried gels were rehydrated in trypsin solution (Sigma Aldrich, Italy) and in-gel protein digestion was performed overnight at 37 °C. Protein identification was carried out by Peptide Mass Fingerprinting (PMF) on an ultrafleXtreme™ MALDI-TOF/TOF mass spectrometer (Brucker Corporation, Billerica, MA, USA). In total, 0.75 µL of each digested protein supernatant were spotted onto the MALDI target and allowed to dry. Then, 0.75 µL of matrix solution (5 mg/mL alpha-ciano 4-hydroxycynnamic acid in 50% *v/v* acetonitrile and 0.5% *v/v* trifluoroacetic acid) were added to the dried sample and air-dried again. A PMF search was performed in NCBInr databases using MASCOT search engine available on-line (Matrix Science Ltd., London, UK, http://www.matrixscience.com). The following parameters were used: taxonomy was limited to viruses, mass tolerance was 100 ppm, the acceptable number of missed cleavage sites was set to two, alkylation of cysteine by carbamidomethylation was assumed as a fixed modification, and oxidation of methionine was considered as a possible modification. The criteria used to accept identifications included the extent of sequence coverage (>15%), the number of matched peptides (>4), and the MASCOT algorithm assigned probabilistic score (>60 or *p* < 0.001). Confirmatory results were also obtained by analysis of the same samples, carried out by Cogentech Proteomics/MS (Cogentech S.c.a.r.l., Milan, Italy) and the mass spectrometry facility at the Toscana Life Sciences (TLS, Siena, Italy) by using the nLC-ESI-MS/MS QExactive-HF system.

3. Results

3.1. NSs Stability Is Influenced by Disordered Regions

Putative intrinsically disordered regions (IDRs) were identified in TOSV NSs by on-line tools (http://prdos.hgc.jp). Based on a predictive algorithm, two IDRs were mapped at aa 1–17 of the N-terminus and aa 295–316 of the C-terminus of the protein. Previous results already showed the important role of the C-terminus, since its deletion influenced protein stability [58]. Next, we assessed the role of the N-terminus on the NSs protein stability by deleting the first 72 aa (Figure 1).
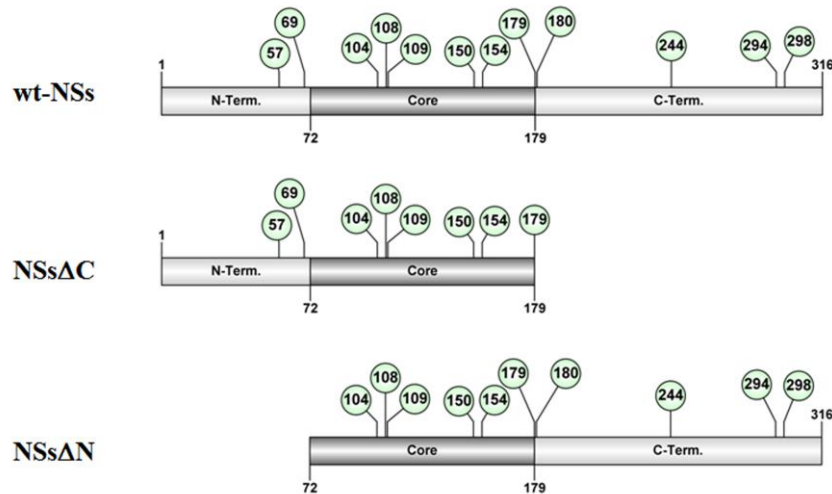
Figure 1. Schematic representation of the of TOSV NSs full-length (wt-NSs) sequence, N-(NSsΔN), or C-terminus deleted (NSsΔC) variants. Green dots indicate the lysine residues with a high predictive score for ubiquitination.

Immunoblotting and densitometric analysis of lysates of Lenti-X 293T cells transfected with NSs expressing plasmid showed a 9-fold increase of NSsΔN protein accumulation compared to the wt-NSs protein ($p \leq 0.0005$) (Figure 2A), confirming the presence of a disordered instable region at the N-terminus.

To better address the involvement of N-terminus IDR on the NSs stability, Firefly Luciferase (FFLuc) fusion proteins were generated. Afterwards, cycloheximide (CHX) chase experiments were performed to compare protein stability among the NSsΔN, NSsΔC, and wt-NSs. Luciferase activities were measured in transfected CHX-treated cells. After normalization with respect to the constitutively expressed *Renilla* luciferase (pSV40-RenLuc), a considerable reduction of the Luciferase activities, consistent with NSs degradation, was reported in wt-NSs lysates just 1.5 h after CHX treatment in comparison with the mock-treated sample. On the contrary, the detection of a higher Luciferase signal for NSsΔN and NSsΔC demonstrated a significant increased protein stability at both 1.5 and 3 h after CHX treatment (Figure 2B). Moreover, based on the CHX chase experiment datasets, the deduced half-lives of NSsΔN ($t_{1/2}$ 8.7 h) and NSsΔC ($t_{1/2}$ 4.8 h) were significantly longer ($p < 0.0001$) than those observed for wt-NSs ($t_{1/2}$ 1.6 h) (Data not shown). These data support the prediction of intrinsic disordered sequences located at the terminal ends of the NSs, thus the deleted variants of the protein acquired greater stability and cytoplasmic accumulation in transfected cells.
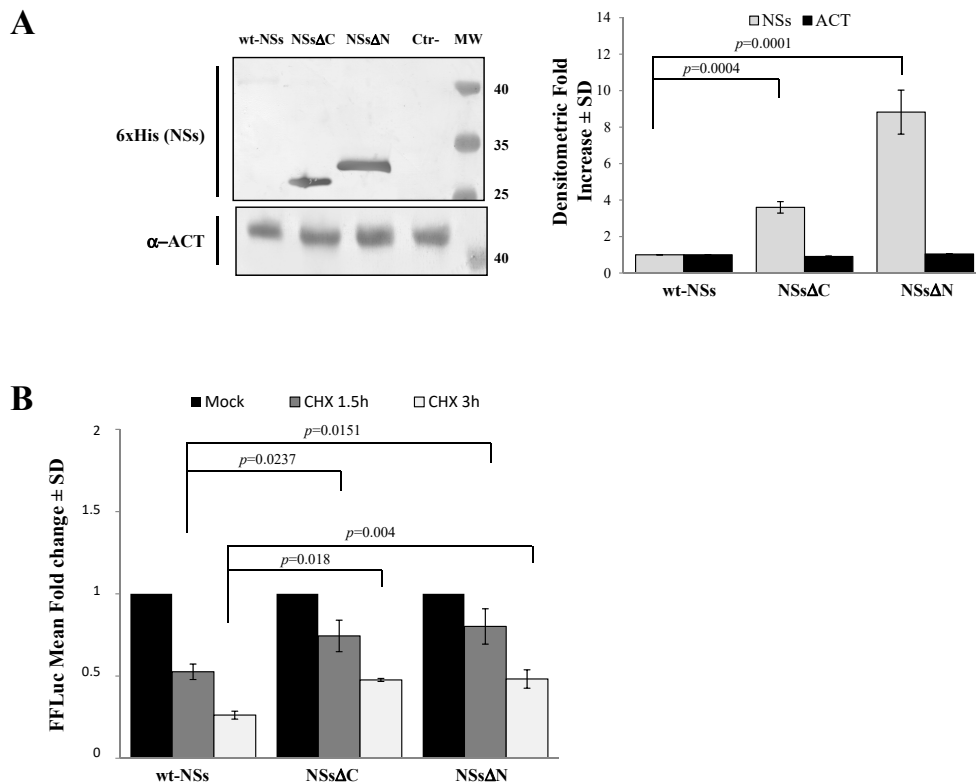
Figure 2. Domains affecting TOSV NSs stability. (**A**) The involvement of TOSV NSs C- and N-terminal regions on protein stability was demonstrated by generating deleted NSs proteins (NSsΔC and NSsΔN). The behavior of the deleted NSs variants was tested by immunoblotting on the whole-cell lysates (50 μg) of Lenti-X 293T-transfected cells. Specific proteins were detected by using anti-6×His (NSs) monoclonal antibody (left figure). Loading control was represented by actin (α-ACT) detection (left figure). Quantitative assessment of deleted NSs variants was determined by densitometric analysis (right figure). (**B**) Lenti-X 293T cells were transfected with FFLuc NSsΔN and NSsΔC fusion constructs and *Renilla* Luciferase as an internal control. Transfected cells were mock-treated or treated with cycloheximide (CHX) and collected at 1.5 and 3 h. Fold induction was obtained by luciferase activity normalization with respect to *Renilla* luciferase values and comparison to the relative mock-treated sample. Results were expressed as mean fold change values collected in at least three independent experiments ± standard deviation.

3.2. Ubiquitin-Dependent NSs Proteasomal Degradation

Previous results have shown that TOSV NSs retains antagonistic function on host innate immunity to viral infection [20,21,58] exhibiting an E3 ubiquitin ligase activity on RIG-I [57]. Therefore, we also investigated the effect of ubiquitination on the fate and function of the viral protein. Similarly to Bunyamwera virus, TOSV NSs protein stability was also evaluated analyzing its possible ubiquitination, since its accumulation into the cell cytoplasm was strongly enhanced by the exposure to the proteasome inhibitor MG-132 [20,21]. Indeed, a significant increase of protein stability ($p < 0.05$) was noticed when the inhibitor MG-132 was included during the CHX chase experiments, with a fold increase of protein accumulation at 3 h treatment of 2.3 for the wt-NSs, 6.1 for NSsΔC, and 3.9 for NSsΔN (Figure 3). Moreover, the immunoblotting confirmed the enhanced protein accumulation in the cell cytoplasm when the transfected cells were exposed only to MG-132 (Figure 3).
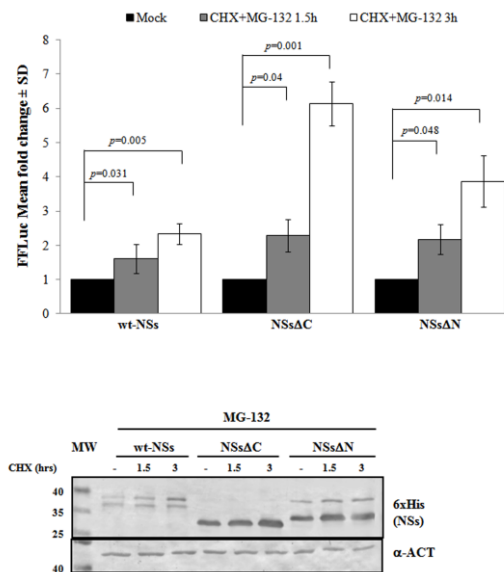
Figure 3. Effects of the proteasome inhibitor MG-132 on NSs deleted mutants were evaluated. (**Upper panel**) wt-NSs, NSsΔN, and NSsΔC expressing cells were treated with 25 µM of the inhibitors along with 100 µg/mL of CHX and collected at 1.5 and 3 h. Cell lysates were subjected to a dual-luciferase assay in order to estimate the stability of NSs protein variants. A significant increase of protein stability over time was noticed for wt-NSs, NSsΔC, and NSsΔN. (**Lower panel**) The immunoblotting with anti-6×His antibody or anti-ACT performed on MG-132 and CHX treated cells confirmed the stabilizing properties of the MG-132 on the NSs proteins tested. The error bars represent the standard deviation from the mean values obtained in independent experiments.

Furthermore, the positive effects of the proteasome inhibitor were evidenced by the deduced half-life of NSsΔC ($t_{1/2}$ 22 h) and NSsΔN ($t_{1/2}$ 26.4 h), which was significantly higher ($p < 0.05$) with respect to the untreated counterparts. This evidence confirmed the ubiquitinated status of TOSV NSs, suggesting that the stability of TOSV NSs was also controlled by ubiquitination and proteasomal degradation and that lysine residues target for ubiquitination were at least located in the central region of the protein, common to the three constructs.

3.3. Evidence of TOSV NSs Ubiquitination

To understand whether TOSV NSs was directly ubiquitinated, the presence of polyubiquitin chains linked to the viral protein was investigated. The denaturant pull-down assay performed on NSs and HA-Ub co-transfected cells allowed the efficient inactivation of de-ubiquitinating enzymes (DUBs), preserving NSs ubiquitinated forms [60]. The ubiquitination status of the affinity purified NSs was detected by immunoblotting using anti-6×His and anti-HA antibodies, demonstrating that NSs protein underwent a robust ubiquitination. Indeed, high-molecular-weight migrating bands with a constant increase were detected with anti-HA monoclonal antibody, corresponding to mono-, multi-, or poly-ubiquitinated forms of NSs (Figure 4A). Unfortunately, the anti-6×His monoclonal weakly detected these bands due to a lower sensitivity of the antibody.

As shown in Figure 4A, both the N- and C-terminal-truncated proteins underwent ubiquitination at a similar extent to that observed for the wt-NSs. On the basis on these results, it appears that lysine residues target for ubiquitination are located in the central region of the protein. We further investigated the ubiquitin-linkage type present on the NSs protein, particularly the K_{48}- or K_{63}-chain. These experiments demonstrated that both K_{48}- and K_{63}-ubiquitination moiety occurs in both wt- and the deleted NSs variants (Figure 4B). Indeed, anti-HA reactive bands corresponding to mono-, multi-, or poly-ubiquitinated forms of the NSs were detected in all the samples tested. These data supported

the idea that both K_{63} and K_{48} ubiquitin linkages take place, thus this type of post-translational modification does not only influence NSs stability, but it could also affect NSs protein activity.
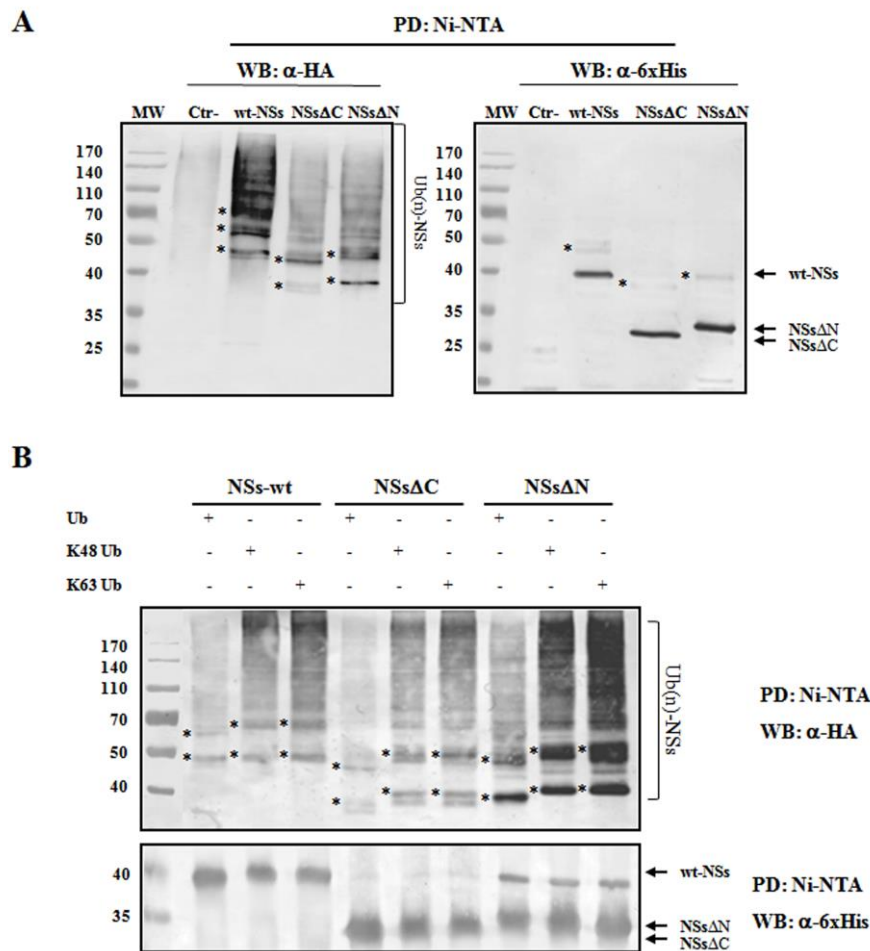

Figure 4. TOSV NSs undergoes ubiquitination. NSs ubiquitination was evaluated by immunoblotting. (**A**) Lenti-X 293T cells were transfected with wt-, ΔC-, or ΔN-expressing plasmids, along with the plasmid expressing HA-tagged wild-type ubiquitin (Ub). Cells treated with the proteasome inhibitor MG-132 were collected at 48 h post-transfection and NSs protein enrichment was performed on cell lysates by pull-down (PD) experiments using Ni-NTA agarose beads. 6×His-NSs-enriched samples were subjected to immunoblotting for Ub (α-HA) or NSs (α-6×His) detection. The ubiquitinated status of the three NSs forms was evaluated as a modification of the targeted substrate, causing a shift in MW of ~10 kDa (mono-ubiquitination) or multiples. Asterisk represents ubiquitinated NSs forms. (**B**) The rate on K_{48}-and K_{63}-moiety ubiquitination was assessed by PD assay and immunoblotting. Lenti-X 293T cells were transfected with wt-, ΔC, or ΔN NSs expressing plasmids, along with the plasmid expressing HA-tagged K_{48}-only or K_{63}-only ubiquitin mutants. Twenty-four hours later, cells were treated with MG-132 and collected after additional 24 h. Lysates were prepared and PD with Ni-NTA agarose beads. Isolated proteins were separated by SDS-PAGE and probed by immunoblotting for NSs (α-6×His) and Ub-K_{48} and Ub-K_{63} (α-HA) detection. Asterisk indicates ubiquitinated forms of the NSs proteins.

3.4. Specific NSs Lysine Residues Undergo Ubiquitination

The identification of specific NSs lysine residues targeted for ubiquitination was mapped by mass spectrometry analysis. NSs protein was enriched from transfected Lenti-X 293T cells under denaturing conditions. The recovered protein was resolved by SDS-PAGE and Coomassie staining. The gel portion of interest was processed for mass spectrometry analysis. NSs peptides generated by trypsin digestion

were subjected to mass spectrometry analysis. Some lysines carrying the Gly-Gly signature di-peptide were detected and assigned as being bound to ubiquitin [67]. Three lysine residues at position 104, 109, and 154, located in the central part of the NSs, were recognized as a target for ubiquitin on the recovered protein (Figure 5).
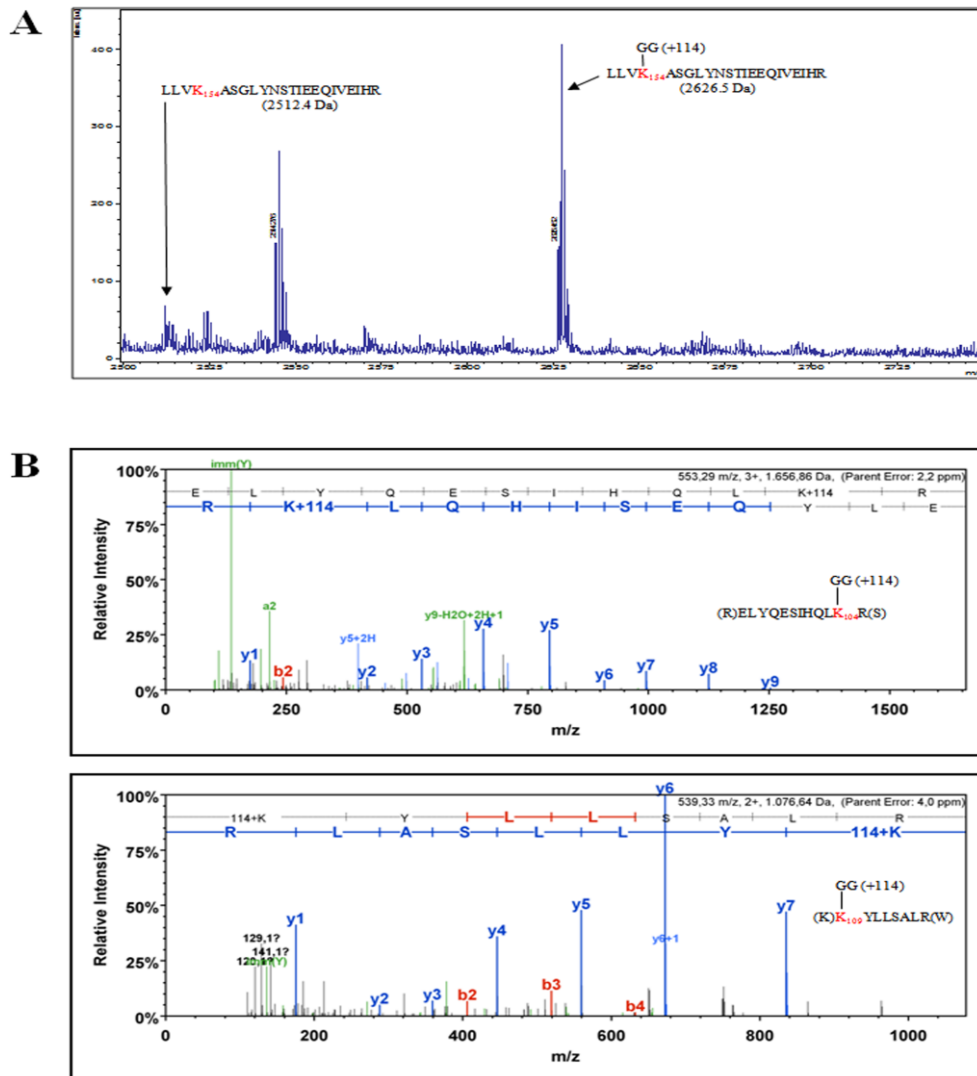

Figure 5. The NSs protein, enriched from cell lysate of transfected cells, was analyzed by mass spectrometry in an attempt to identify lysine residues targeted for specific ubiquitination. (**A**) MS1 mass spectrum (Department of Life Sciences, University of Siena, Siena) showing the identification of TOSV NSs peptide containing the ubiquitinated lysine residue at position 154 and (**B**) MS2 mass spectrum (Cogentech S.c.a.r.l., Milan, Italy) showing TOSV NSs peptides ubiquitinated on lysines at positions 109 and 104.

However, we could not exclude that other lysine residues subjected to ubiquitination were located in other regions of the NSs protein. Therefore, we expressed and tested the NSs-6KR protein variant, consisting of a full-length NSs protein with mutated lysine in the core region (K_{104}; K_{108}; K_{109}; K_{150}; K_{154}; and K_{179}), for the protein degradation rate. As evidenced by CHX chase, the 6KR mutant protein was highly stable compared to wt-NSs ($p = 0.003$), suggesting that lysine residues targeted for ubiquitination were located in the core region of the protein (Figure 6A).
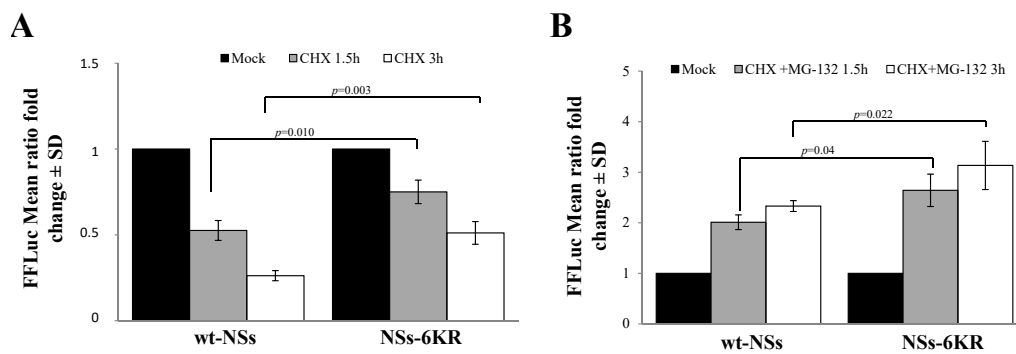
Figure 6. Effects of lysine residues in the core region on protein stability. (**A**) A new NSs mutant (NSs-6KR), consisting of arginine substitution at lysine 104, 108, 109, 150, 154, and 179 position, was generated and tested for protein stability. CHX chase experiments evidenced a significantly increased stability for the NSs mutant with respect to the wt-NSs protein. (**B**) The NSs-6KR mutant still responded to MG-132, as shown by the chase experiments. Transfected cells were treated with CHX in combination with 25 μM of MG-132 and then residual luciferase activities were measured. Graphs represent mean values ± standard deviations (SD) of three independent experiments.

Moreover, the estimated half-life of the NSs-6KR was double ($p = 0.0069$) than that of wt-NSs ($t_{1/2}$ 3.7 h vs. $t_{1/2}$ 1.6 h). Notwithstanding, MG-132 still affected NSs-6KR protein degradation by increasing its accumulation into the cells, leading to the conclusion that lysine residues other than those in the core region could undergo ubiquitination (Figure 6B).

We then evaluated the presence of specific lysines, which might undergo ubiquitination in the N- or C-terminal part of the NSs protein. Two NSs variants were generated, mutating the lysine residues 9, 17, 36, 57, 59, and 69 at the amino-terminus of the wt protein (NSs-NKR) or of the NSs-6KR mutant (NSs-6KR-NKR). The CHX chase assessed to determine variations in protein stability showed that lysine residues located at the N-terminus did not significantly influence the turnover of the protein. Indeed, compared to the relative counterpart NSsΔN (Figure 2B) and NSs-6KR (Figure 6), the new NSs proteins did not exhibit a remarkable increase ($p > 0.05$) of protein accumulation after exposure to CHX (Figure 7A), suggesting that those sites were not critical in determining the NSs protein fate.
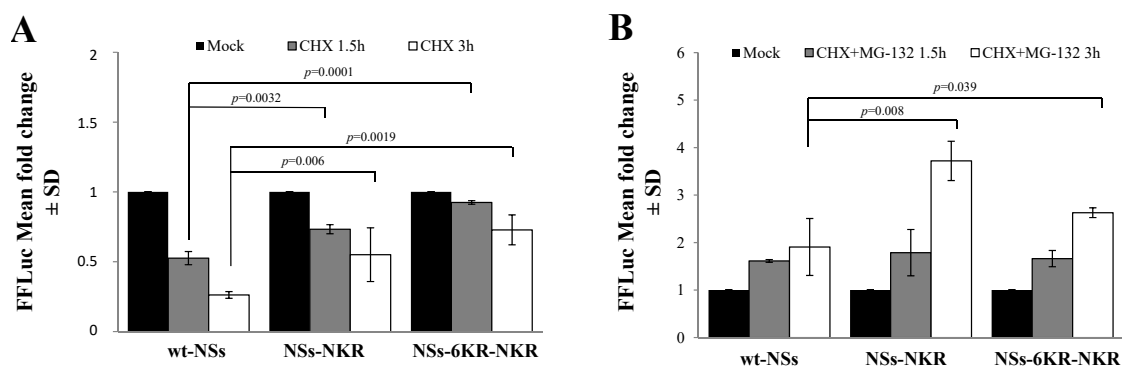

Figure 7. Effects of amino-terminal lysine residues on protein stability. (**A**) Lysates of NSs-NKR and NSs-6KR-NKR-transfected cells were collected at different time points after CHX exposure and subjected to the dual-luciferase assay in order to estimate the stability of NSs protein variants by measuring the FFLuc residual activities. (**B**) Cells expressing new NSs mutants, treated with 25 μM of MG-132, along with 100 μg/mL of CHX, evidenced the activity of the inhibitor on both NSs-NKR and NSs-6KR-NKR. Cells were collected at 1.5 and 3 h post-treatment and lysates were subjected to a dual-luciferase assay in order to estimate the stability of NSs protein variants. The error bars represent the standard deviation from the mean values obtained in independent experiments ± standard deviations (SD).

As expected, the chase experiments conducted in the presence of the proteasome inhibitor MG-132 and CHX evidenced that the NSs-NKR responded to inhibitor ($p = 0.008$), as lysines in the core region were maintained. However, even the NSs-6KR-NKR variant responded to the drug ($p = 0.039$) (Figure 7B), indicating that some lysine residues targeted for ubiquitination were still present in the protein besides these sequences. Furthermore, supporting the previous data, the inhibitor substantially ($p = 0.036$) augmented NSs-6KR-NKR protein mean half-life ($t_{1/2}$ 19.6 h) compared to the relative mock-treated sample ($t_{1/2}$ 9.8 h). A further investigation by mass-spectrometry revealed the presence of four more lysine residues, located in the C-terminal of the protein, which underwent ubiquitination. In particular, we found ubiquitinated lysines at the 180, 244, 294, and 298 position (Table 1).

Table 1. The enriched NSs protein was analyzed by mass spectrometry in an attempt to identify lysine residues targeted for specific ubiquitination. MS2 mass spectrometry results (TLS, Siena, Italy) are reported, showing the identification of TOSV NSs peptide containing the ubiquitinated lysine residues at position 180, 244, 294, and 298.

Lysine Position	Percentage Sequence Coverage	Peptide Sequence	Peptide Identification Probability	Mascot Ion Score	Mascot Identity Score	Mascot Delta Ion Score	Variable Modifications Identified by Spectrum
180	7.21%	VLIEGK*k*HGLTAFDLPGNDILGDICVVQAAR	99.70%	58.6	60.3	36.67597403	K7:GlyGly (+114.04)
180	7.21%	VLIEGK*k*HGLTAFDLPGNDILGDICVVQAAR	99.70%	45.9	33.3	32.14675325	K7:GlyGly (+114.04)
180	6.94%	*k*HGLTAFDLPGNDILGDICVVQAAR	99.70%	63.2	48.6	55.33246753	K1:GlyGly (+114.04)
244	3.80%	KED*k*	99.70%	55.4	60	21.31764706	K4:GlyGly (+114.04)
244	6.33%	KED*k*RAKAKGLm SmCAAR	99.70%	51.2	43.7	31.05	K4:GlyGly (+114.04)
244	6.33%	ED*k*RAKAKGLMSMCAAR	99.70%	48.7	50.4	30.65454545	K3:GlyGly (+114.04)
294–298	6.59%	TDLGFRETALSTFWAKDWPTPQETILSD*k*RcL*k*EDMR	99.70%	48.6	36	34.75324675	K29:GlyGly (+114.04) K33:GlyGly (+114.04)
294–298	6.33%	DWPTLQETILSD*k*RcL*k*EDmRVTK	99.70%	52.6	38	43.26406926	K13:GlyGly (+114.04) K17:GlyGly (+114.04)
294	6.33%	ETALSTFWAKDWPTPQETILSD*k*	99.70%	60.9	65.5	23.27176471	K23:GlyGly (+114.04)
298	6.33%	CL*k*EDMRVTKWLPSPPHYPPL	99.70%	45.8	38.3	27.21315789	K4:GlyGly (+114.04)
298	6.33%	CLKEDMRVTKWLPSPPHYPPL	99.70%	44.2	45.9	27.91753247	K23:GlyGly (+114.04)

4. Discussion

The non-structural NSs protein of many *Bunyaviridae* and *Phenuiviridae* family members has been shown to be an important virulence factor, able to counteract host innate immunity to viral infections [13–21,57,58].

An important factor affecting protein behavior resides in its stability and turnover. Indeed, a tight control of cell proteins' half-life is required in order to support an efficient cellular homeostasis, death/survival, and replication. Most of the viral proteins exert their activity by interfering in critical cellular processes, such as signal transduction and cell-cycle progression. Thus, their function is tightly controlled through several viral and cellular mechanisms.

One aspect that determines protein fate is the presence of unfolded domains, which confer a reduced stability and a rapid degradation via lysosome or proteasome systems [68–70]. The intrinsically disordered region (IDR) with an unfolded structure described for Bunyamwera virus (BUNV) NSs was associated with the reduced viral protein stability in infected cells [62,63].

Previously, we demonstrated that the C-terminus of TOSV NSs could retain an IDR with a negative effect on protein turnover [58]. In the present work, a deeper investigation of TOSV NSs protein properties was pursued. New data suggest that TOSV NSs shares similarities with BUNV NSs, since its stability is strongly influenced by IDR located at the N-terminus (NSsΔN), along with that at the C-terminal (NSsΔC) part of the protein. The increased stability of NSsΔN and NSsΔC, demonstrated by semi-quantitative immunoblotting, suggested that these domains are important in order to maintain protein stability. Indeed, the cycloheximide (CHX) chase assay allowed us to confirm that external NSs IDRs are strikingly related to protein half-life, and NSsΔN exhibited a longer half-life. Therefore, the unfolded NSs N-terminus drastically compromised protein stability, along with the C-terminus, which, in turn, had a minor effect.

Nevertheless, apart from protein IDRs, other mechanisms involved in protein stability were proposed. Based on Bunyamwera virus (BUNV) studies where the involvement of the ubiquitin-proteasome system in controlling NSs fate was described [62], post-translational modifications (PTMs) in TOSV NSs were considered. Contrary to RVFV and BUNV, TOSV NSs presented many lysine residues that could undergo ubiquitination.

Under specific experimental conditions, we provided direct evidence of TOSV NSs ubiquitination both by immunoblotting and mass spectrometry (MS). We identified the ubiquitin linkage at lysine residue 104, 109, and 154, as they were modified by the signature peptide 'Gly-Gly' derived from ubiquitin by MS. Surprisingly, identified PTM sites were located in the core region of the protein, suggesting an incisive role of this region in the protein fate.

However, TOSV NSs ubiquitination on other sites of the protein could be neither demonstrated nor excluded. Despite being more stable, the NSs mutant, lacking all the core lysine residues (NSs-6KR), was still susceptible to MG-132 treatment. This suggested the presence of additional lysine residues, located outside the core region, subjected to ubiquitination. In an attempt to better characterize the NSs post-translational modification by ubiquitination, a deeper investigation was conducted. The mutation of lysine residues located at the amino-terminal part of the protein (NSs-NKR) excluded the presence of ubiquitination targets in this region, since the mutation did not affect the protein degradation rate or half-life, as demonstrated by the CHX chase (Figure 7A).

Further experiments using the NSs-6KR-NKR, lacking all the lysines at the N-terminus and core regions, evidenced the presence of additional ubiquitination sites in the C-terminal part. The CHX chase in the presence of the proteasome inhibitor MG-132 revealed that the NSs-6KR-NKR mutant still responded to the inhibitor, thus ubiquitination still occurred on the protein. More comprehensive analysis by MS identified the ubiquitin-derived 'Gly-Gly' signature peptide linked at lysine residues 180, 244, 292, and 298, as they were modified by ubiquitin.

These data open the way to new cellular mechanisms responsible for TOSV NSs functions and to its role in TOSV pathogenicity. Indeed, during the first phases of viral replication, the rapid degradation of the NSs protein by the proteasome could be a regulatory mechanism of cell defense, thus inhibiting RIG-I degradation and allowing the expression of IFN-β in the infected host (Figure 8).
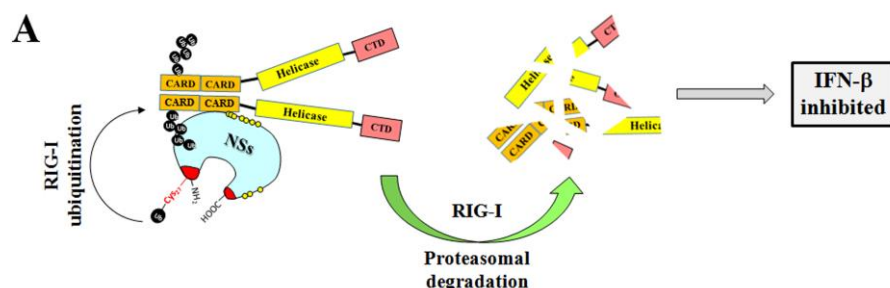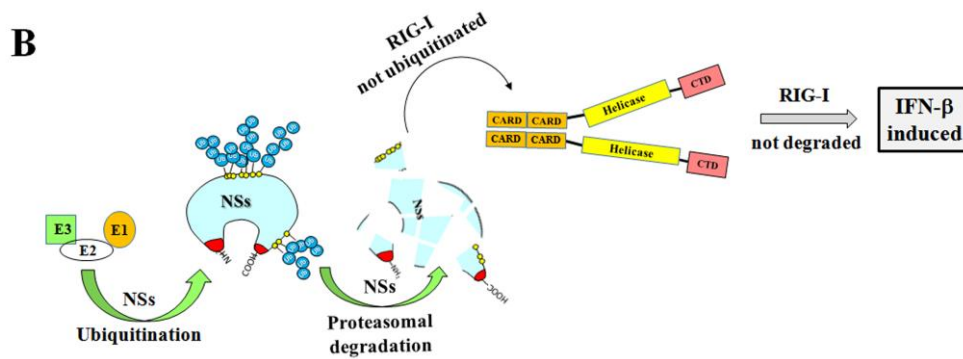

Figure 8. *Cont.*

Figure 8. Cartoon representation of the putative function of the TOSV NSs on RIG-I-mediated interferon beta production and the influence of ubiquitination on the viral protein function. (**A**) The TOSV NSs protein accumulated in the cell cytoplasm efficiently interacts with RIG-I and mediates its ubiquitination and subsequent degradation, counteracting IFN-β production. On the contrary (**B**), the high ubiquitination rate of the NSs negatively affects its stability, targeting the protein for proteasomal degradation. Consequently, RIG-I is not depleted and the physiological secretion of IFN-β occurs.

References

1. Braito, A.; Ciufolini, M.G.; Pippi, L.; Corbisiero, R.; Fiorentini, C.; Gistri, A.; Toscano, L. Phlebotomus-transmitted toscana virus infections of the central nervous system: A seven-year experience in Tuscany. *Scand. J. Infect. Dis.* **1998**, *30*, 505–508. [PubMed]

2. Verani, P.; Ciufolini, M.G.; Nicoletti, L.; Calducci, M.; Sabatinelli, G.; Coluzzi, M.; Paci, P.; Amaducci, L. Ecological and epidemiological studies of Toscana virus, an arbovirus isolated from Phlebotomus. *Ann. Ist. Super. Sanita* **1982**, *18*, 397–399. [PubMed]

3. Verani, P.; Lopes, M.C.; Nicoletti, L.; Balducci, M. Studies on Phlebotomus transmitted viruses in Italy: I. Isolation and characterization of a Sandfly fever Naples-like virus. Arboviruses in the Mediterranean Countries. *Zbl. Bakt. Suppl.* **1980**, *9*, 195–201.

4. Sanbonmatsu-Gámez, S.; Pérez-Ruiz, M.; Palop-Borrás, B.; Navarro-Marí, J.M. Unusual manifestation of Toscana virus infection, Spain. *Emerg. Infect. Dis.* **2009**, *15*, 347–348. [CrossRef]

5. Kuhn, J.; Bewermeyer, H.; Hartmann-Klosterkoetter, U.; Emmerich, P.; Schilling, S.; Valassina, M. Toscana virus causing severe meningoencephalitis in an elderly traveler. *J. Neurol. Neurosurg. Psychiatry* **2005**, *76*, 1605–1606. [CrossRef]

6. Bartels, S. Lethal encephalitis caused by Toscana virus in an elderly patient. *J. Neurol.* **2012**, *259*, 175–177. [CrossRef]

7. Sonderegger, B.; Hachler, H.; Dobler, G.; Frei, M. Imported aseptic meningitis due to Toscana virus acquired on the island of Elba, Italy, August 2008. *Euro Surveill.* **2009**, *14*, 19079.

8. Epelboin, L.; Hausfater, P.; Schuffenecker, I.; Riou, B.; Zeller, H.; Bricaire, F.; Bossi, P. Meningoencephalitis due to Toscana virus in a French traveler returning from central Italy. *J. Travel. Med.* **2008**, *15*, 361–363. [CrossRef]

9. Tschumi, F.; Schmutz, S.; Kufner, V.; Heider, M.; Pigny, F.; Schreiner, B.; Capaul, R.; Achermann, Y.; Huber, M. Meningitis and epididymitis caused by Toscana virus infection imported to Switzerland diagnosed by metagenomic sequencing: A case report. *BMC Infect. Dis.* **2019**, *19*, 591. [CrossRef]

10. Howell, B.A.; Azar, M.M.; Landry, M.L.; Shaw, A.C. Toscana virus encephalitis in a traveler returning to the United States. *J. Clin. Microbiol.* **2015**, *53*, 1445–1447. [CrossRef]

11. Dominati, A.; Sap, L.; Vora, S. Fever in a returning traveler from Tuscany. *Rev. Med. Suisse* **2018**, *14*, 294–296. [PubMed]

12. Sato, M.; Suemori, H.; Hata, N.; Asagiri, M.; Ogasawera, K.; Nakao, K.; Nakaya, T.; Katsuki, M.; Noguchi, S.; Tanaka, N.; et al. Distinct and essential roles of transcription factors IRF-3 and IRF-7 in response to viruses for IFN-alpha/beta gene induction. *Immunity* **2000**, *13*, 539–548. [CrossRef]

13. Weber, F.; Bridgen, A.; Fazakerley, J.K.; Streitenfeld, H.; Kessler, N.; Randall, R.E.; Elliott, R.M. Bunyamwera bunyavirus nonstructural protein NSs counteracts the induction of alpha/beta interferon. *J. Virol.* **2002**, *76*, 7949–7955. [CrossRef] [PubMed]

14. Jääskeläinen, K.M.; Kaukinen, P.; Minskaya, E.S.; Plyusnina, A.; Vapalahti, O.; Elliott, R.M.; Weber, F.; Vaheri, A.; Plyusnin, A. Tula and Puumala hantavirus NSs ORFs are functional and the products inhibit activation of the interferon-beta promoter. *J. Med. Virol.* **2007**, *79*, 1527–1536. [CrossRef] [PubMed]

15. Bridgen, A.M.; Weber, F.; Fazakerley, J.K.; Elliott, R.M. Bunyamvera bunyavirus non-structural protein NSs is nonessential gene product that contributes to the viral pathogenesis. *Proc. Natl. Acad. Sci. USA* **2001**, *98*, 664–669. [CrossRef]

16. Blakqori, G.; Delhaye, S.; Habjan, M.; Blair, C.D.; Sánchez-Vargas, I.; Olson, K.E.; Attarzadeh-Yazdi, G.; Fragkoudis, R.; Kohl, A.; Kalinke, U.; et al. La Crosse bunyavirus nonstructural protein NSs serves to suppress the type I interferon system of mammalian hosts. *J. Virol.* **2007**, *81*, 4991–4999. [CrossRef]

17. Léonard, V.H.; Kohl, A.; Hart, T.J.; Elliott, R.M. Interaction of Bunyamwera Orthobunyavirus NSs protein with mediator protein MED8: A mechanism for inhibiting the interferon response. *J. Virol.* **2006**, *80*, 9667–9675. [CrossRef]

18. Wuerth, J.D.; Weber, F. Phleboviruses and the Type I Interferon Response. *Viruses* **2016**, *8*, 174. [CrossRef]

19. Brisbarre, N.M.; Plumet, S.; de Micco, P.; Leparc-Goffart, I.; Emonet, S.F. Toscana virus inhibits the interferon beta response in cell cultures. *Virology* **2013**, *442*, 189–194. [CrossRef]

20. Savellini, G.G.; Weber, F.; Terrosi, C.; Habjan, M.; Martorelli, B.; Cusi, M.G. Toscana virus induces interferon although its NSs protein reveals antagonistic activity. *J. Gen. Virol.* **2011**, *92*, 71–79. [CrossRef]

21. Savellini, G.G.; Valentini, M.; Cusi, M.G. Toscana virus NSs protein inhibits the induction of type I interferon by interacting with RIG-I. *J. Virol.* **2013**, *87*, 6660–6667. [CrossRef] [PubMed]

22. Pickart, C.M. Mechanisms underlying ubiquitination. *Annu. Rev. Biochem.* **2001**, *70*, 503–533. [CrossRef] [PubMed]

23. Bernassola, F.; Karin, M.; Ciechanover, A.; Melino, G. The HECT family of E3 ubiquitin ligases: Multiple players in cancer development. *Cancer Cell* **2008**, *14*, 10–21. [CrossRef] [PubMed]

24. Jackson, P.K.; Eldridge, A.G.; Freed, E.; Furstenthal, L.; Hsu, J.Y.; Kaiser, B.K.; Reimann, J.D. The lore of the RINGs: Substrate recognition and catalysis by ubiquitin ligases. *Trends Cell. Biol.* **2000**, *10*, 429–439. [CrossRef]

25. Skaar, J.R.; Pagan, J.K.; Pagano, M. Mechanisms and function of substrate recruitment by F-box proteins. *Nat. Rev. Mol. Cell. Biol.* **2013**, *14*, 369–381. [CrossRef]

26. Bosu, D.R.; Kipreos, E.T. Cullin-RING ubiquitin ligases: Global regulation and activation cycles. *Cell Div.* **2008**, *3*, 7. [CrossRef]

27. Furukawa, M.; Andrews, P.S.; Xiong, Y. Assays for RING family ubiquitin ligases. *Methods Mol. Biol.* **2005**, *301*, 37–46.

28. Lee, E.K.; Diehl, J.A. SCFs in the new millennium. *Oncogene* **2014**, *33*, 2011–2018. [CrossRef]

29. Hatakeyama, S.; Nakayama, K.I. U-box proteins as a new family of ubiquitin ligases. *Biochem. Biophys. Res. Commun.* **2003**, *302*, 635–645. [CrossRef]

30. Scheffner, M.; Nuber, U.; Huibregtse, J.M. Protein ubiquitination involving an E1-E2-E3 enzyme ubiquitin thioester cascade. *Nature* **1995**, *373*, 81–83. [CrossRef]

31. Rotin, D.; Kumar, S. Physiological functions of the HECT family of ubiquitin ligases. *Nat. Rev. Mol. Cell. Biol.* **2009**, *10*, 398–409. [CrossRef] [PubMed]

32. Ardley, H.C.; Robinson, P.A. E3 ubiquitin ligases. *Essays Biochem.* **2005**, *41*, 15–30. [CrossRef] [PubMed]

33. Komander, D. The emerging complexity of protein ubiquitination. *Biochem. Soc. Trans.* **2009**, *37*, 937–953. [CrossRef] [PubMed]

34. Finley, D. Recognition and processing of ubiquitin-protein conjugates by the proteasome. *Annu. Rev. Biochem.* **2009**, *78*, 477–513. [CrossRef] [PubMed]

35. Akutsu, M.; Dikic, I.; Bremm, A. Ubiquitin chain diversity at a glance. *J. Cell. Sci.* **2016**, *129*, 875–880. [CrossRef]

36. Thrower, J.S.; Hoffman, L.; Rechsteiner, M.; Pickart, C.M. Recognition of the polyubiquitin proteolytic signal. *EMBO J.* **2000**, *19*, 94–102. [CrossRef]

37. Kawadler, H.; Yang, X. Lys63-linked polyubiquitin chains: Linking more than just ubiquitin. *Cancer Biol. Ther.* **2006**, *5*, 1273–1274. [CrossRef]

38. Chen, Z.J.; Sun, L.J. Nonproteolytic functions of ubiquitin in cell signaling. *Mol. Cell* **2009**, *33*, 275–286. [CrossRef]

39. Delboy, M.G.; Roller, D.G.; Nicola, A.V. Cellular proteasome activity facilitates Herpes simplex virus entry at a postpenetration step. *J. Virol.* **2008**, *82*, 3381–3390. [CrossRef]

40. Delboy, M.G.; Nicola, A.V. A pre-immediate-early role for tegument ICP0 in the proteasome-dependent entry of Herpes simplex virus. *J. Virol.* **2011**, *85*, 5910–5918. [CrossRef]

41. Greene, W.; Zhang, W.; He, M.; Witt, C.; Ye, F.; Gao, S.J. The ubiquitin/proteasome system mediates entry and endosomal trafficking of Kaposi's Sarcoma-associated herpesvirus in endothelial cells. *PLoS Pathog.* **2012**, *8*, e1002703. [CrossRef] [PubMed]

42. Chen, C.; Zhuang, X. Epsin 1 is a cargo-specific adaptor for the clathrin-mediated endocytosis of the influenza virus. *Proc. Natl. Acad. Sci. USA* **2008**, *105*, 11790–11795. [CrossRef] [PubMed]

43. Widjaja, I.; de Vries, E.; Tscherne, D.M.; García-Sastre, A.; Rottier, P.J.; de Haan, C.A. Inhibition of the ubiquitin-proteasome system affects influenza A virus infection at a postfusion step. *J. Virol.* **2010**, *84*, 9625–9631. [CrossRef] [PubMed]

44. Wodrich, H.; Henaff, D.; Jammar, B.; Segura-Morales, C.; Seelmeir, S.; Coux, O.; Ruzsics, Z.; Wiethoff, C.M.; Kremer, E.J. A capsid-encoded PPXY-motif facilitates adenovirus entry. *PLoS Pathog.* **2010**, *6*, e1000808. [CrossRef]

45. Nomaguchi, M.; Fujita, M.; Adachi, A. Role of HIV-1 Vpu protein for virus spread and pathogenesis. *Microbes Infect.* **2008**, *10*, 960–967. [CrossRef]

46. Ikeda, M.; Ikeda, A.; Longan, L.C.; Longnecker, R. The Epstein-Barr virus latent membrane protein 2A PY motif recruits WW domain-containing ubiquitin-protein ligases. *Virology* **2000**, *268*, 178–191. [CrossRef]

47. Ning, S.; Pagano, J.S. The A20 deubiquitinase activity negatively regulates LMP1 activation of IRF7. *J. Virol.* **2010**, *84*, 6130–6138. [CrossRef]

48. Beaudenon, S.; Huibregtse, J.M. HPV E6, E6AP and cervical cancer. *BMC Biochem.* **2008**, *9* (Suppl. 1), S4. [CrossRef]

49. Mammas, I.N.; Sourvinos, G.; Giannoudis, A.; Spandidos, D.A. Human papilloma virus (HPV) and host cellular interactions. *Pathol. Oncol. Res.* **2008**, *14*, 345–354. [CrossRef]

50. Huh, K.; Zhou, X.; Hayakawa, H.; Cho, J.Y.; Libermann, T.A.; Jin, J.; Harper, J.W.; Munger, K. Human papillomavirus type 16 E7 oncoprotein associates with the cullin 2 ubiquitin ligase complex, which contributes to degradation of the retinoblastoma tumor suppressor. *J. Virol.* **2007**, *81*, 9737–9747. [CrossRef]

51. Park, S.W.; Han, M.G.; Park, C.; Ju, Y.R.; Ahn, B.Y.; Ryou, J. Hantaan virus nucleocapsid protein stimulates MDM2-dependent p53 degradation. *J. Gen. Virol.* **2013**, *94*, 2424–2428. [CrossRef] [PubMed]

52. Garrus, J.E.; von Schwedler, U.K.; Pornillos, O.W.; Morham, S.G.; Zavitz, K.H.; Wang, H.E.; Wettstein, D.A.; Stray, K.M.; Côté, M.; Rich, R.L.; et al. Tsg101 and the vacuolar protein sorting pathway are essential for HIV-1 budding. *Cell* **2001**, *107*, 55–65. [CrossRef]

53. Demirov, D.G.; Ono, A.; Orenstein, J.M.; Freed, E.O. Overexpression of the N-terminal domain of TSG101 inhibits HIV-1 budding by blocking late domain function. *Proc. Natl. Acad. Sci. USA* **2002**, *99*, 955–960. [CrossRef] [PubMed]

54. Gack, M.U.; Albrecht, R.A.; Urano, T.; Inn, K.S.; Huang, I.C.; Carnero, E.; Farzan, M.; Inoue, S.; Jung, J.U.; García-Sastre, A. Influenza A virus NS1 targets the ubiquitin ligase TRIM25 to evade recognition by the host viral RNA sensor RIG-I. *Cell Host Microbe* **2009**, *5*, 439–449. [CrossRef]

55. Rajsbaum, R.; Albrecht, R.A.; Wang, M.K.; Maharaj, N.P.; Versteeg, G.A.; Nistal-Villán, E.; García-Sastre, A.; Gack, M.U. Species-specific inhibition of RIG-I ubiquitination and IFN induction by the influenza A virus NS1 protein. *PLoS Pathog.* **2012**, *8*, e1003059. [CrossRef]

56. Oshiumi, H.; Miyashita, M.; Matsumoto, M.; Seya, T. A distinct role of Riplet-mediated K63-Linked polyubiquitination of the RIG-I repressor domain in human antiviral innate immune responses. *PLoS Pathog.* **2013**, *9*, e1003533. [CrossRef]

57. Savellini, G.G.; Anichini, G.; Gandolfo, C.; Prathyumnan, S.; Cusi, M.G. Toscana virus non-structural protein NSs acts as E3 ubiquitin ligase promoting RIG-I degradation. *PLoS Pathog.* **2019**, *15*, e1008186. [CrossRef]

58. Savellini, G.G.; Gandolfo, C.; Cusi, M.G. Truncation of the C-terminal region of Toscana Virus NSs protein is critical for interferon-β antagonism and protein stability. *Virology* **2015**, *486*, 255–262. [CrossRef]

59. Kainulainen, M.; Lau, S.; Samuel, C.E.; Hornung, V.; Weber, F. NSs Virulence Factor of Rift Valley Fever Virus Engages the F-Box Proteins FBXW11 and β-TRCP1 To Degrade the Antiviral Protein Kinase PKR. *J. Virol.* **2016**, *90*, 6140–6147. [CrossRef]

60. Mudhasani, R.; Tran, J.P.; Retterer, C.; Kota, K.P.; Whitehouse, C.A.; Bavari, S. Protein Kinase R Degradation Is Essential for Rift Valley Fever Virus Infection and Is Regulated by SKP1-CUL1-F-box (SCF)FBXW11-NSs E3 Ligase. *PLoS Pathog.* **2016**, *12*, e1005437. [CrossRef]

61. Kainulainen, M.; Habjan, M.; Hubel, P.; Busch, L.; Lau, S.; Colinge, J.; Superti-Furga, G.; Pichlmair, A.; Weber, F. Virulence factor NSs of rift valley fever virus recruits the F-box protein FBXO3 to degrade subunit p62 of general transcription factor TFIIH. *J. Virol.* **2014**, *88*, 3464–3473. [CrossRef] [PubMed]

62. van Knippenberg, I.; Fragkoudis, R.; Elliott, R.M. The transient nature of Bunyamwera orthobunyavirus NSs protein expression: Effects of increased stability of NSs protein on virus replication. *PLoS ONE* **2013**, *8*, e64137. [CrossRef] [PubMed]

63. van Knippenberg, I.; Carlton-Smith, C.; Elliott, R.M. The N-terminus of Bunyamwera orthobunyavirus NSs protein is essential for interferon antagonism. *J. Gen. Virol.* **2010**, *91*, 2002–2006. [CrossRef] [PubMed]

64. Cusi, M.G.; Savellini, G.G.; Terrosi, C.; Di Genova, G.; Valassina, M.; Valentini, M.; Bartolommei, S.; Miracco, C. Development of a mouse model for the study of Toscana virus pathogenesis. *Virology* **2005**, *333*, 66–73. [CrossRef] [PubMed]

65. Kingstone, R.E.; Chen, C.A.; Rose, J.K. Calcium phosphate transfection. *Curr. Protoc. Mol. Biol.* **2003**, *63*, 9.1.1–9.1.11. [CrossRef] [PubMed]

66. Taylor, R.T.; Best, S.M. Assessing ubiquitination of viral proteins: Lessons from flavivirus NS5. *Methods* **2011**, *55*, 166–171. [CrossRef]

67. Xu, P.; Duong, D.M.; Seyfried, N.T.; Cheng, D.; Xie, Y.; Robert, J.; Rush, J.; Hochstrasser, M.; Finley, D.; Peng, J. Quantitative proteomics reveals the function of unconventional ubiquitin chains in proteasomal degradation. *Cell* **2009**, *137*, 133–145. [CrossRef]

68. van der Lee, R.; Lang, B.; Kruse, K.; Gsponer, J.; de Groot, N.S.; Huynen, M.A.; Matouschek, A.; Fuxreiter, M.; Babu, M.M. Intrinsically disordered segments affect protein half-life in the cell and during evolution. *Cell Rep.* **2014**, *8*, 1832–1844. [CrossRef]

69. Tompa, P.; Prilusky, J.; Silman, I.; Sussman, J.L. Structural disorder serves as a weak signal for intracellular protein degradation. *Proteins* **2008**, *71*, 903–909. [CrossRef]

70. Dice, J.F. Molecular determinants of protein half-lives in eukaryotic cells. *FASEB J.* **1987**, *1*, 349–357. [CrossRef]

![American Society for Microbiology | Microbiology Resource Announcements]

Whole-Genome Sequence of SARS-CoV-2 Isolate Siena-1/2020

Maria Grazia Cusi,[a,b] David Pinzauti,[a] Claudia Gandolfo,[a] Gabriele Anichini,[a] Gianni Pozzi,[a] ⓘ Francesco Santoro[a,b]

ᵃDepartment of Medical Biotechnologies, University of Siena, Siena, Italy
ᵇUOC Microbiologia e Virologia, Azienda Ospedaliera Universitaria Senese, Siena, Italy

ABSTRACT   The complete genome sequence of severe acute respiratory syndrome coronavirus 2 (SARS-CoV-2) isolate Siena-1/2020 was obtained by Nanopore sequencing, combining the direct RNA sequencing and amplicon sequencing approaches. The isolate belongs to the B1.1 lineage, which is prevalent in Europe, and contains a mutation in the spike protein coding sequence leading to the D614G amino acid change.

Here, we report the complete genome sequence of severe acute respiratory syndrome coronavirus 2 (SARS-CoV-2) isolate Siena-1/2020, belonging to the genus *Betacoronavirus* in the family *Coronaviridae*. The virus was isolated at the University Hospital of Siena (Tuscany, Italy) in April 2020, from a nasopharyngeal swab collected on 1 March 2020, and seeded on Vero E6 cells. This research was carried out according to the principles of the Helsinki Declaration, with reference to the document BIOBANK-MIU-2010, approved by the Siena University Hospital Ethics Committee with amendment no. 1, on 17 February 2020, regarding general data protection and regulation (GDPR).

After 3 days, cytopathic effect appeared on the cells, and the culture medium was collected and frozen at −80°C. Since this was the first SARS-CoV-2 viral isolate in our region, we decided to sequence it. Total RNA was isolated using the NucliSens easyMAG system (bioMérieux, Italy). Viral RNA was sequenced using both the direct RNA and amplicon sequencing approaches on a MinION instrument (Oxford Nanopore Technologies [ONT], UK).

Direct RNA sequencing was performed using the SQK-RNA002 kit (ONT). Briefly, about 300 ng of total RNA was ligated to the reverse transcriptase (RT) adapter, and the first strand was retrotranscribed using SuperScript III reverse transcriptase (Thermo Fisher); sequencing adapters were then ligated to the cDNA-RNA hybrid, and the library was loaded onto a flow cell (R9.4.1).

Amplicon sequencing was performed based on a modification of the Artic Network protocol (https://www.protocols.io/view/ncov-2019-sequencing-protocol-v2-bdp7i5rn); primers were designed using Primal Scheme (1) to generate 39 amplicons of about 900 bp with an overlap of about 50 bp (Table 1). About 100 ng of total RNA was reverse-transcribed using the SuperScript VILO reverse transcriptase kit (Thermo Fisher) following the manufacturer's instructions and then amplified in two multiplex PCRs using PrimeSTAR GXL polymerase (TaKaRa). The samples were barcoded, pooled, and adapter ligated following the ONT ligation-based sequencing protocol. The sequencing run was managed by MinKNOW v19.12.5, enabling live base calling. For data analysis, all tools were run with default parameters unless otherwise specified. Sequencing reads were demultiplexed using Guppy v3.6.1 and then filtered using the guppyplex command of the ARTIC environment to include only reads between 700 and 1,500 bases long (https://github.com/artic-network/artic-ncov2019). Amplicon reads were mapped to the reference genome Wuhan Hu-1 (GenBank accession no. MN908947) with minimap2 v2.17 (2) and indexed using SAMtools v1.9 (3). Primer sequences were trimmed

TABLE 1 Primers used for amplification of the SARS-CoV-2 genome

Primer	Nucleotide sequence	Pool	Length (no. of nucleotides)	Start[a]	End[a]
CoV-2_1_L	ACCAACCAACTTTCGATCTCTTGT	1	24	30	54
CoV-2_1_R	ATGCACTCAAGAGGGTAGCCAT	1	22	867	845
CoV-2_2_L	AGTGGTGTTACCCGTGAACTCA	2	22	763	785
CoV-2_2_R	ACCTTCGGAACCTTCTCCAACA	2	22	1600	1578
CoV-2_3_L_v2	GGCTGTGTGTTCTCTTATGTTGGT	1	24	1487	1510
CoV-2_3_R	ACAATCCCTTTGAGTGCGTGAC	1	22	2414	2392
CoV-2_4_L	TTTGGCTTTGTGTGCTGACTCT	2	22	2319	2341
CoV-2_4_R	AGCAGAAGTGGCACCAAATTCC	2	22	3166	3144
CoV-2_5_L	GATTGTGAAGAAGAAGAGTTTGAGCC	1	26	3067	3093
CoV-2_5_R	CAGCGATCTTTTGTTCAACTTGCT	1	24	3878	3854
CoV-2_6_L	TCGCACAAATGTCTACTTAGCTGT	2	24	3771	3795
CoV-2_6_R	ACCGAGCAGCTTCTTCCAAATT	2	22	4658	4636
CoV-2_7_L	ACAACTGTAGCGTCACTTATCAACA	1	25	4549	4574
CoV-2_7_R	AGCATCTTGTAGAGCAGGTGGA	1	22	5359	5337
CoV-2_8_L	ACTTCTATTAAATGGGCAGATAACAACTG	2	29	5257	5286
CoV-2_8_R	AGCCACCACATCACCATTTAAGT	2	23	6172	6149
CoV-2_9_L	CCATATCCAAACGCAAGCTTCG	1	22	6019	6041
CoV-2_9_R	GCCTCTAGACAAAATTTACCGACACT	1	26	6903	6877
CoV-2_10_L	AAACCGTGTTTGTACTAATTATATGCCTT	2	29	6747	6776
CoV-2_10_R	ACTGTAGTGACAAGTCTCTCGCA	2	23	7694	7671
CoV-2_11_L	GCTTTTGCAAACTACACAATTGGAAT	1	26	7592	7618
CoV-2_11_R	GCAGCACTACGTATTTGTTTTCGT	1	24	8463	8439
CoV-2_12_L	GCGCAGGTAGCAAAAAGTCACA	2	22	8365	8387
CoV-2_12_R	TGATCTTTCACAAGTGCCGTGC	2	22	9241	9219
CoV-2_13_L	TGCTCATGGATGGCTCTATTATTCAA	1	26	9128	9154
CoV-2_13_R	GAGCCTTTGCGAGATGACAACA	1	22	9977	9955
CoV-2_14_L	GTGATGTGCTATTACCTCTTACGCA	2	25	9848	9873
CoV-2_14_R	CAGCAGCGTACAACCAAGCTAA	2	22	10688	10666
CoV-2_15_L	CAACTGGAGTTCATGCTGGCAC	1	22	10556	10578
CoV-2_15_R	GTCCACACTCTCCTAGCACCAT	1	22	11394	11372
CoV-2_16_L	TGTCTGGTTTTAAGCTAAAAGACTGTGT	2	28	11285	11313
CoV-2_16_R	ATCACCATTAGCAACAGCCTGC	2	22	12181	12159
CoV-2_17_L	GGCAACCTTACAAGCTATAGCCT	1	23	12078	12101
CoV-2_17_R	CCTACAAGGTGGTTCCAGTTCTG	1	23	12907	12884
CoV-2_18_L	GGAGGTAGGTTTGTACTTGCACTG	2	24	12793	12817
CoV-2_18_R	CGTCCTTTTCTTGGAAGCGACA	2	22	13621	13599
CoV-2_19_L	ACAGGCACTAGTACTGATGTCGT	1	23	13509	13532
CoV-2_19_R	TGGGTGGTATGTCTGATCCCAA	1	22	14328	14306
CoV-2_20_L	CAAAGCCTTACATTAAGTGGGATTTGT	2	27	14224	14251
CoV-2_20_R	GGTGCGAGCTCTATTCTTTGCA	2	22	15108	15086
CoV-2_21_L	AGGATCAAGATGCACTTTTCGCA	1	23	15004	15027
CoV-2_21_R	AGTAAGGTCAGTCTCAGTCCAACA	1	24	15858	15834
CoV-2_22_L	TGCATCTCAAGGTCTAGTGGCT	2	22	15749	15771
CoV-2_22_R	GCGTTTCTGCTGCAAAAAGCTT	2	22	16648	16626
CoV-2_23_L	CGATAATGTTACTGACTTTAATGCAATTGC	1	30	16535	16565
CoV-2_23_R	GTGCAGGTAATTGAGCAGGGTC	1	22	17458	17436
CoV-2_24_L	TCTTTGATGAAATTTCAATGGCCACA	2	26	17350	17376
CoV-2_24_R	GCTTCTTCGCGGGTGATAAACA	2	22	18275	18253
CoV-2_25_L	TGGCATACCTAAGGACATGACCT	1	23	18167	18190
CoV-2_25_R	ACCAATGTCGTGAAGAACTGGG	1	22	19038	19016
CoV-2_26_L	TGATGAACTGAAGATTAATGCGGCT	2	25	18938	18963
CoV-2_26_R	GCAGCAATGTCCACACCCAAAT	2	22	19862	19840
CoV-2_27_L	ACACAAAAGTTGATGGTGTTGATGT	1	25	19714	19739
CoV-2_27_R	GGTTGCCACGCTTGACTAGATT	1	22	20678	20656
CoV-2_28_L	TCTGTAGTTTCTAAGGTTGTCAAAGTGA	2	28	20553	20581
CoV-2_28_R	AAAGACATAACAGCAGTACCCCTTAA	2	26	21443	21417
CoV-2_29_L_v2	CAAACCACGCGAACAAATAG	1	20	21297	21316
CoV-2_29_R_v2	CGAAAAACCCTGAGGGAGAT	1	20	22225	22206
CoV-2_30_L	AAACAGGGTAATTTCAAAAATCTTAGGGAA	2	30	22105	22135
CoV-2_30_R	TGTGCTACCGGCCTGATAGATT	2	22	22996	22974
CoV-2_31_L	AACAATCTTGATTCTAAGGTTGGTGGT	1	27	22876	22903
CoV-2_31_R	TGCTGCATTCAGTTGAATCACCA	1	23	23813	23790
CoV-2_32_L	ACCCACAAATTTTACTATTAGTGTTACCAC	2	30	23703	23733
CoV-2_32_R	TGCACTTCAGCCTCAACTTTGT	2	22	24537	24515

(Continued on next page)

TABLE 1 (Continued)

Primer	Nucleotide sequence	Pool	Length (no. of nucleotides)	Start[a]	End[a]
CoV-2_33_L	TGCACAAGCTTTAAACACGCTT	1	22	24426	24448
CoV-2_33_R	GCAGCAGGATCCACAAGAACAA	1	22	25324	25302
CoV-2_34_L	CTAGGTTTTATAGCTGGCTTGATTGC	2	26	25213	25239
CoV-2_34_R	ACATGTTCAACACCAGTGTCTGT	2	23	26075	26052
CoV-2_35_L	GGGAATCTGGAGTAAAAGACTGTGT	1	25	25969	25994
CoV-2_35_R	AATGACCACATGGAACGCGTAC	1	22	26857	26835
CoV-2_36_L	TGGATCACCGGTGGAATTGCTA	2	22	26744	26766
CoV-2_36_R	GTGTTTTACGCCGTCAGGACAA	2	22	27612	27590
CoV-2_37_L	ACGAGGGCAATTCACCATTTCA	1	22	27511	27533
CoV-2_37_R	ACTGCCAGTTGAATCTGAGGGT	1	22	28351	28329
CoV-2_38_L	AGAGTATCATGACGTTCGTGTTGT	2	24	28219	28243
CoV-2_38_R	GCTTCTTAGAAGCCTCAGCAGC	2	22	29045	29023
CoV-2_39_L	TGCTTGACAGATTGAACCAGCT	1	22	28940	28962
CoV-2_39_R	TTCTCCTAAGAAGCTATTAAAATCACATGG	1	30	29866	29836

[a] Nucleotide positions relative to the Wuhan Hu-1 reference genome.

from the aligned reads using BAMClipper v1.1.1 (4). Clipped reads were then merged with direct RNA sequencing reads with the – cat command of the Linux environment. Finally, Medaka v0.12.1 (https://github.com/nanoporetech/medaka) was used to build the consensus and call the single nucleotide variants. The reference genome Wuhan Hu-1 was edited using a Perl script, selecting variants with a quality score cutoff of 35 (https://github.com/CDCgov/SARS-CoV-2_Sequencing/tree/master/protocols/CDC-Comprehensive); nucleotide variations were also visually inspected using Tablet (5). We could not sequence the nucleotides corresponding to positions 1 and 2 of the Wuhan Hu-1 genome; therefore, we obtained a 29,901-bp viral genome with an average GC content of 37.97% and a mean depth of coverage of 1,153.64×, as calculated by the SAMtools – coverage function (3).
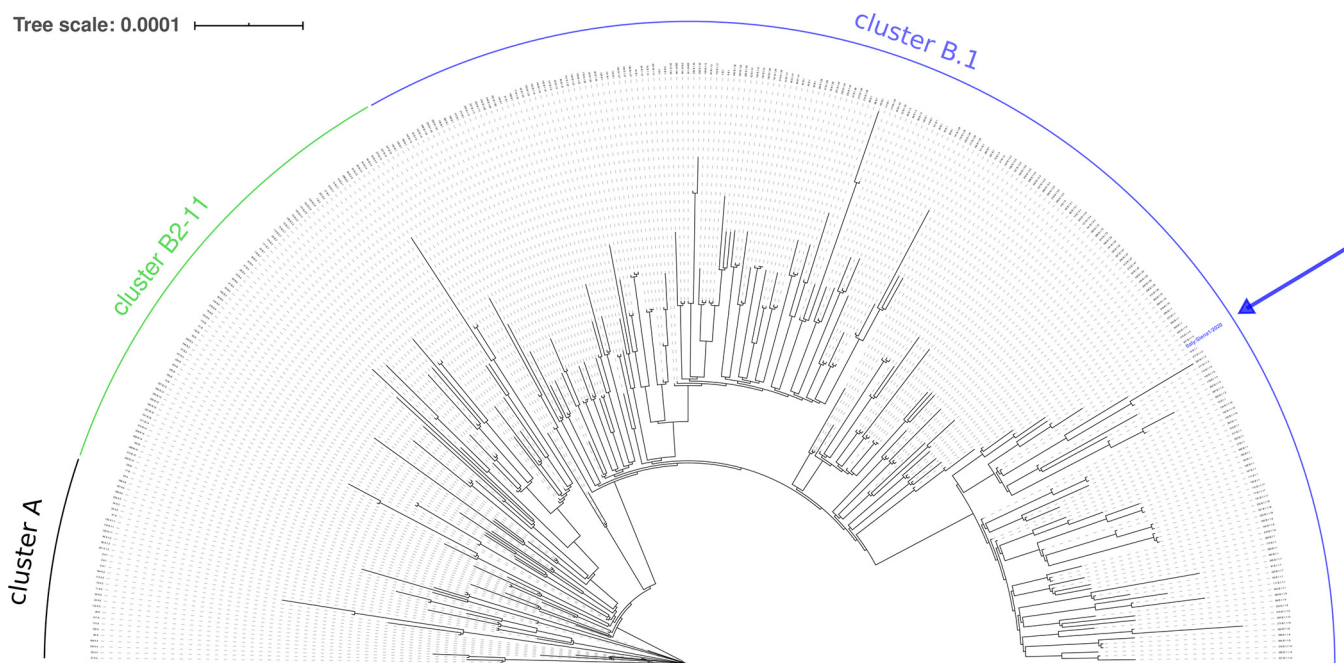

FIG 1 Phylogenetic tree of SARS-CoV-2 genomes. The tree was generated with Pangolin v1.14 and visualized using Interactive Tree Of Life (iTOL) (8). A total of 322 viral genomes are displayed, including the genomes selected by Pangolin software as representatives for the genetic diversity of SARS-CoV-2. As of 30 July 2020, two major clusters (A and B) were identified. Cluster B was subdivided into 11 clusters (B1 to B11); of those, the most represented is cluster B1 (covered by the blue arch), which comprises most of the lineages identified and sequenced in Europe. Cluster B1.1 is a large subcluster characterized by the mutation of three consecutive nucleotides at position 28881. The blue arrow indicates the position of the Siena-1/2020 isolate in the phylogenetic tree.

Phylogenetic analysis performed with Pangolin v1.14 (6) assigned strain Siena-1/2020 to the B1.1 lineage, which is associated with the Italian SARS-CoV-2 outbreak and includes isolates circulating in Europe (Fig. 1). Compared to the reference genome Wuhan Hu-1, Siena-1/2020 harbors 5 single nucleotide changes (at positions 241, 3037, 14408, 19839, and 23403) and mutations of 3 consecutive nucleotides (GGG→AAC) at position 28881. Among the 5 single nucleotide changes, the one at position 23403 causes a change in the predicted amino acid sequence of the spike (S) protein (D614G), which is now the most common variant worldwide (7).

Data availability. The genome sequence of SARS-CoV-2 Siena-1/2020 has been deposited in GenBank under the accession no. MT531537. The version described in this paper is the second version. The raw Nanopore reads were deposited in the Sequence Read Archive under BioProject accession no. PRJNA658490 with accession no. SRX8982904 (direct RNA sequencing) and SRX8982905 (amplicon sequencing).

ACKNOWLEDGMENTS

We thank all the laboratory personnel involved in SARS-CoV-2 diagnostics at the University Hospital of Siena for their tireless commitment during the coronavirus disease 2019 (COVID-19) pandemic.

REFERENCES

1. Quick J, Grubaugh ND, Pullan ST, Claro IM, Smith AD, Gangavarapu K, Oliveira G, Robles-Sikisaka R, Rogers TF, Beutler NA, Burton DR, Lewis-Ximenez LL, de Jesus JG, Giovanetti M, Hill SC, Black A, Bedford T, Carroll MW, Nunes M, Alcantara LC, Jr, Sabino EC, Baylis SA, Faria NR, Loose M, Simpson JT, Pybus OG, Andersen KG, Loman NJ. 2017. Multiplex PCR method for MinION and Illumina sequencing of Zika and other virus genomes directly from clinical samples. Nat Protoc 12:1261–1276. https://doi.org/10.1038/nprot.2017.066.
2. Li H. 2018. minimap2: pairwise alignment for nucleotide sequences. Bioinformatics 34:3094–3100. https://doi.org/10.1093/bioinformatics/bty191.
3. Li H, Handsaker B, Wysoker A, Fennell T, Ruan J, Homer N, Marth G, Abecasis G, Durbin R, 1000 Genome Project Data Processing Subgroup. 2009. The Sequence Alignment/Map format and SAMtools. Bioinformatics 25:2078–2079. https://doi.org/10.1093/bioinformatics/btp352.
4. Au CH, Ho DN, Kwong A, Chan TL, Ma ESK. 2017. BAMClipper: removing primers from alignments to minimize false-negative mutations in amplicon next-generation sequencing. Sci Rep 7:1567. https://doi.org/10.1038/s41598-017-01703-6.
5. Milne I, Stephen G, Bayer M, Cock PJA, Pritchard L, Cardle L, Shaw PD, Marshall D. 2013. Using Tablet for visual exploration of second-generation sequencing data. Brief Bioinform 14:193–202. https://doi.org/10.1093/bib/bbs012.
6. Rambaut A, Holmes EC, Hill V, O'Toole Á, McCrone JT, Ruis C, Du Plessis L, Pybus OG. 2020. A dynamic nomenclature proposal for SARS-CoV-2 to assist genomic epidemiology. bioRxiv https://doi.org/10.1101/2020.04.17.046086.
7. Korber B, Fischer WM, Gnanakaran S, Yoon H, Theiler J, Abfalterer W, Hengartner N, Giorgi EE, Bhattacharya T, Foley B, Hastie KM, Parker MD, Partridge DG, Evans CM, Freeman TM, de Silva TI, McDanal C, Perez LG, Tang H, Moon-Walker A, Whelan SP, LaBranche CC, Saphire EO, Montefiori DC, Sheffield COVID-19 Genomics Group. 2020. Tracking changes in SARS-CoV-2 spike: evidence that D614G increases infectivity of the COVID-19 virus. Cell 182:812–827.e19. https://doi.org/10.1016/j.cell.2020.06.043.
8. Letunic I, Bork P. 2019. Interactive Tree Of Life (iTOL) v4: recent updates and new developments. Nucleic Acids Res 47:W256–W259. https://doi.org/10.1093/nar/gkz239.

Seroprevalence to Measles Virus after Vaccination or Natural Infection in an Adult Population, in Italy

Gabriele Anichini [1] , **Claudia Gandolfo** [1], **Simonetta Fabrizi** [2], **Giovan Battista Miceli** [2], **Chiara Terrosi** [1], **Gianni Gori Savellini** [1] , **Shibily Prathyumnan** [1], **Daniela Orsi** [2], **Giuseppe Battista** [2] and **Maria Grazia Cusi** [2,*]

[1] Department of Medical Biotechnologies, University of Siena, Santa Maria delle Scotte Hospital, V.le Bracci, 1 53100 Siena, Italy; gabriele.anichini@student.unisi.it (G.A.); claudia.gandolfo@unisi.it (C.G.); chiara.terrosi@unisi.it (C.T.); gianni.gori@unisi.it (G.G.S.); shibilyps@gmail.com (S.P.)

[2] Preventive Medicine and Health Surveillance Unit, Santa Maria delle Scotte Hospital, V.le Bracci, 1 53100 Siena, Italy; s.fabrizi@ao-siena.toscana.it (S.F.); giovanni.miceli@ao-siena.toscana.it (G.B.M.); daniela.orsi@unisi.it (D.O.); giuseppe.battista@unisi.it (G.B.)

* Correspondence: mariagrazia.cusi@unisi.it; Tel.: +39-0577-233871

Abstract: An increase in measles cases worldwide, with outbreaks, has been registered in the last few years, despite the availability of a safe and highly efficacious vaccine. In addition to an inadequate vaccination coverage, even in high-income European countries studies proved that some vaccinated people were also found seronegative years after vaccination, thus increasing the number of people susceptible to measles infection. In this study, we evaluated the immunization status and the seroprevalence of measles antibodies among 1092 healthy adults, either vaccinated or naturally infected, in order to investigate the persistence of anti-measles IgG. Among subjects who received two doses of measles vaccine, the neutralizing antibody titer tended to decline over time. In addition, data collected from a neutralization assay performed on 110 healthy vaccinated subjects suggested an inverse correlation between neutralizing antibody titers and the time elapsed between the two vaccinations, with a significant decline in the neutralizing titer when the interval between the two doses was ≥11 years. On the basis of these results, monitoring the serological status of the population 10–12 years after vaccination could be important both to limit the number of people who are potentially susceptible to measles, despite the high efficacy of MMR vaccine, and to recommend a booster vaccine for the seronegatives.

Keywords: measles virus; vaccine; neutralizing antibodies; seroprevalence

1. Introduction

Measles virus (MV) is a negative single-stranded RNA virus belonging to the Morbillivirus genus, *Paramixoviridae* family [1]. It is the causative agent of a highly contagious acute infectious disease, typical of infancy, characterized by fever, skin rash, cough, coryza, conjunctivitis and a generalized immune suppression [1]. The virus is transmitted by large respiratory droplets, it spreads in the respiratory route and in regional lymph nodes, thus resulting in lymphatic and hematic dissemination with appearance of first clinical signs after 9–19 days [2]. Recovery is followed by lifelong immunity to measles. In rare cases, severe measles-associated central nervous system (CNS) complications may develop [3]. MV infection is also responsible for a transient immune suppression that may last longer than two years after infection and it leads to opportunistic infections [4] and to life-threatening complications, such as pneumonia and/or gastrointestinal disease [5,6]. Nevertheless, this disease is associated with the induction of a strong and specific life-long immune response to the virus [7].

There is no specific antiviral treatment against measles, thus the prophylactic vaccine is considered the best strategy to prevent this virus infection [8]. Furthermore, the monotypic nature of the virus and the lack of an animal reservoir make measles a considerable candidate for eradication [9]. In Italy, a single-antigen measles vaccine became commercially available in 1976 and its administration has been recommended by the Ministry of Health since 1979, with one dose for children aged 15 months. In the early 1990s, the trivalent measles-mumps-rubella (MMR) vaccine containing a live attenuated Edmonston B strain was recommended for administration at 12 months of age. Since 2003, the national vaccination schedule has recommended two doses of MMR vaccine in all Italian regions: The first at 12–15 months and the second at six years or older, only for those who had already received one dose and were older than six years at that date [10,11]. Subsequently, due to the lower MMR vaccination coverage (<90%) in Italy, especially among infants and adolescents [12], and the occurrence of a large measles outbreak in January 2017, a new law was passed and adopted in July 2017. This law extended the number of mandatory vaccines from four to ten, including MMR, administered at 13–15 months and six years [13]. Since then, the attenuated varicella strain has been included in the formulation of the vaccine. This can be administered at the same session as trivalent anti-measles-mumps-rubella plus the monovalent anti-varicella vaccine or as quadrivalent MMRV combined vaccine [14].

In spite of this, according to the latest update on measles circulation by ECDC, 29 EU/EEA Member States reported 13,331 cases of measles, from October 2018 to September 2019, 10,541 (79%) of which were laboratory-confirmed. No countries reported zero cases during the 12-month period. The highest number of cases were reported by France (2699), Italy (1845), Poland (1811), and Romania (1485), accounting for 20%, 14%, 12%, and 11% of all cases, respectively [15]. Measles outbreaks mostly occurred in unvaccinated individuals, thus a high vaccination coverage is the most important goal to prevent the disease. Epidemiologic studies have shown that the level of functional neutralizing antibodies at the time of exposure to the wild-type (WT) virus during a measles outbreak is a good correlate of protection from infection, with higher titers needed to prevent infection rather than to prevent the disease [16]. According to literature, levels of anti-measles antibodies tend to decline over the life course, as demonstrated by measuring the level of measles neutralizing antibodies in the subjects' sera at different times after vaccination [17–20]. Moreover, this phenomenon appears to occur faster following vaccination rather than after naturally acquired infection [21,22]. Thus, it is important to better understand vaccine-induced antibody persistence and how persistence patterns may influence the risk of vaccine failure. In this study, we report data concerning the seroprevalence of a healthy population sample, analyzing 1092 sera among healthy adults, the immunogenicity of the vaccine and the protective antibody levels to measles virus after vaccination or natural exposure to the virus.

2. Materials and Methods

2.1. Study Population

The participants in this observational study were students, postgraduates, medical doctorsand health care workers subjected to routine analysis for the biological risk assessment at the Center of Preventive Medicine and Health Surveillance of the University Hospital 'Santa Maria alle Scotte' in Siena between January 2018 and May 2019. Among the participants, some subjects presented their history of vaccination against measles, some had never been vaccinated and others had a history of measles infection. This research was carried out according to the principles of Helsinki declaration. Ethical approval was obtained from the local Ethical Committee for clinical trials (approval n° 11466_2017) (Comitato Etico Regione Toscana-Area Vasta Sud Est) in terms of General Data Protection and Regulation (GDPR) upon written informed consent signed by all subjects prior to participating in this study [23,24]. A total of 1092 subjects, 361 males and 731 females, (mean age 27.1 years; CI 95% 26.6–27.6) were screened for anti-measles IgG. All subjects born before 1977 declared to have contracted measles infection; the others, born later, were distinguished into three groups, according to their vaccination records: vaccinated with one or two doses and nonvaccinated (Figure 1). Lastly, among

those born after 1977, 110 sera of subjects (mean age 24.9 years; CI 95% 24.1–25.7) vaccinated with two doses of measles vaccine, either monovalent (Moraten, Istituto sieroterapico e vaccinogeno svizzero, Berna, Switzerland) or trivalent (measles, mumps and rubella (MMR) Priorix (GlaxoSmithKline, Verona, Italy) were analyzed for the titer of specific neutralizing antibodies. These titers were compared with 100 samples of subjects (mean age 48.6 years; CI 95% 46.2–51.1), who had been exposed to natural infection.
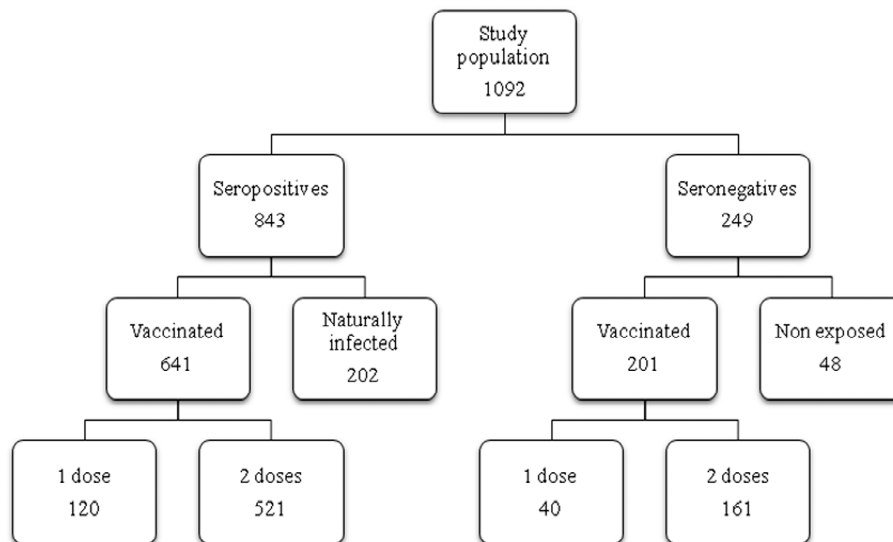

Figure 1. Flow diagram of the study population. Schematic representation of the study population enrolled in the study with the relative number of subjects in each group.

2.2. Cells and Viruses

Vero cells (ATCC CCL-81) were grown as a monolayer in Dulbecco's modified Eagle's medium (DMEM) (Euroclone, Milan, Italy) supplemented with 100 U/mL penicillin/streptomycin (Euroclone) and 5% heat-inactivated fetal calf serum (FCS) (Euroclone) at 37 °C in a humidified 5% CO_2 atmosphere. Measles virus Edmonston B strain (ATCC VR-24) was propagated on Vero cells until a cytopathic effect (CPE) appeared. Viral stocks were prepared, titrated on Vero cells, and stored at −80 °C for long term.

2.3. Measles IgM/IgG Antibody Detection

Sera obtained from subjects were analyzed for the presence of measles specific IgM/IgG antibodies to the recombinant MV nucleoprotein, by LIAISON XL (Liaison Measles IgG/IgM, DiaSorin, Saluggia, Italy), a chemiluminescence analyzer using paramagnetic solid phase microparticles. Threshold IgG values regarded as positive immune status were >16.5 AU (Arbitrary Unit)/mL, with detection limit of 13.5 AU/mL; while IgM threshold for the presence of measles infection was >1.1 AU/mL, with detection limit at 0.9 AU/mL.

2.4. Measles Microneutralization Test

The measles virus neutralization assay was carried out on Vero cells in a 96-well microplate. Twenty-five microliters of 2-fold serial dilutions (1:8 to 1:1024) of vaccinated or naturally infected people sera were added to an equal volume of the Edmonston B strain MV containing 250 $TCID_{50}$ and incubated for 90 min at 37 °C. Finally, 50 μL of Vero cells suspension (2×10^5 cells/mL) prepared in a complete DMEM (Euroclone) medium were added to each well. Five days after incubation at 37 °C, the cultures were microscopically examined for the presence of CPE. The 50% end point titer of the serum neutralizing titer was calculated using the Reed and Muench method [25]. Serum samples with neutralizing titers of less than eight were considered negative [26]. A positive and negative control serum (Liaison Measles IgG Ctr) were included in each assay.

2.5. Statistical Analysis

Seroprevalence was calculated as the ratio between the number of positive test results and the number of performed tests. Geometric mean titers (GMTs), obtained by the neutralization assay, were calculated as log-transformed reciprocal titers and reported as back-transformed for each subclass. Differences between vaccination status, sex, time elapsed between dose one and two of the vaccine and time elapsed since the second dose of vaccine, and the last serological measles investigation, were evaluated. Furthermore, statistical significances were assessed with the two-tailed chi-squared test. Results were considered statistically significant at $p < 0.05$. Spearman's rank correlation coefficient was used to assess correlations of log-transformed continuous variables by the group.

3. Results

3.1. Study Group

We enrolled 1092 subjects, who were screened for specific anti-measles IgG. Out of 1092 subjects, 843 (77.2%) were seropositive and 249 (22.8%) seronegative to the measles virus (Figure 1). The mean age of vaccinated subjects was 24.9 years (CI 95% CI 24.1–25.7). Among the nonvaccinated subjects, seropositives (naturally infected) and seronegatives (never exposed to the virus) had, respectively, a mean age of 39.0 years (95% CI 37.1–40.9) and 26.1 years (95% CI 24.6–27.4) ($p < 0.00001$). Vaccination coverage with one or two doses of vaccine of this population sample was estimated 77.1% (842/1092), lower than the 90%–95% threshold required for achieving herd immunity. The enrolled people were lately divided according to their vaccination history (one or two doses) or nonvaccinated (naturally infected or nonexposed to the virus) (Figure 1). Surprisingly, among those who received two doses of vaccine (as recommended by the Italian Ministry of Health since 2003), 161 out of 682 subjects (23.6%) were seronegative after vaccination. Except for one subject, who had not responded to the trivalent vaccine, the others were seropositive to mumps and rubella viruses, indicating that these individuals had responded to the vaccine. Surprisingly, this percentage was similar to that observed for vaccines with only one dose (40/160, 25%) (Figure 1). No significant differences in the seroprevalence rates were found in all the groups with respect to gender ($p > 0.05$).

3.2. Age-Specific IgG prevalence

In order to analyze the IgG prevalence trend, the enrolled subjects have also been divided into groups according to their age, regardless of their vaccination status. There was no significant difference in the percentage of seronegatives ($p > 0.05$) among the groups aged 19–42 (Figure 2). On the contrary, a consistent increase of seropositives, up to almost 100%, was observed in subjects over 43 years old, therefore born before the introduction of measles vaccine in Italy. As far as seronegativity rates are concerned, some differences among the age groups are also worthy of being mentioned. All negative subjects in the 37–42 age group had never been exposed to the virus; most of the subjects aged 31–36 had been vaccinated with just one dose, while the majority of the 19–24 age group had been vaccinated with two doses. Regarding the group aged 25–30, the percentage of seronegatives was equally distributed between those vaccinated with one or two doses of vaccine.
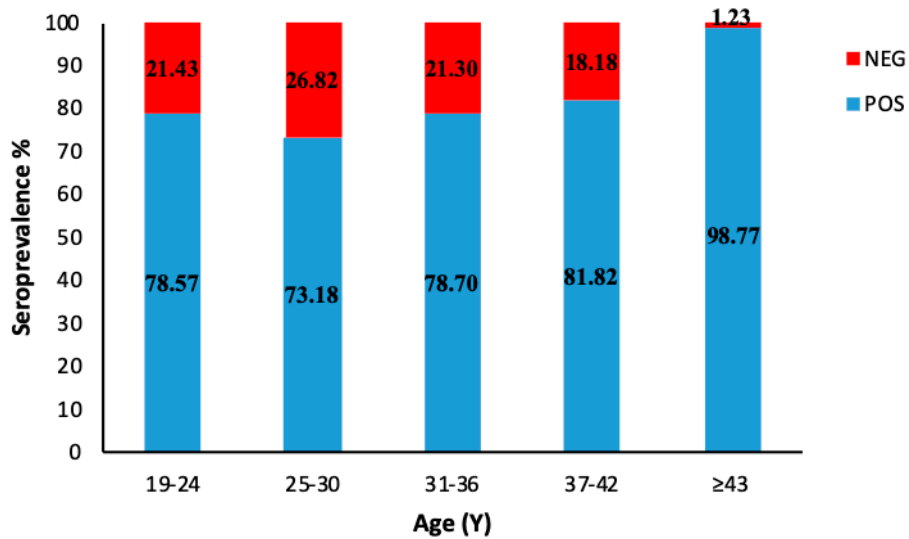
Figure 2. Age-specific measles IgG prevalence categorized into different age groups. Subjects over 43 years old were included into the same group.

3.3. Decline of Humoral Response to Measles after Vaccination

Figure 3 reports the seroprevalence analyzed during the period of 8–18 years after two doses of vaccination in 562 subjects within the same range of age (mean age 24.4 years; CI 95% 24.2–24.6). Although the number of tested subjects decreased over time, it was evident that an increasing number of vaccinees became seronegative in parallel with the increase of time post-vaccination. We noticed a higher percentage of seronegative subjects between 13 and 16 years after vaccination, suggesting that the decrease of the humoral response could be due to a measles-specific antibody titer after vaccination lower than after natural infection. However, this hypothesis could not be endorsed since the antibody titers after vaccine administration were not available. Extending the monitoring time, the trend was similar, although the serological profile appeared variable, probably due to the limited number of tested samples. No specific IgM were detected in any tested sample.
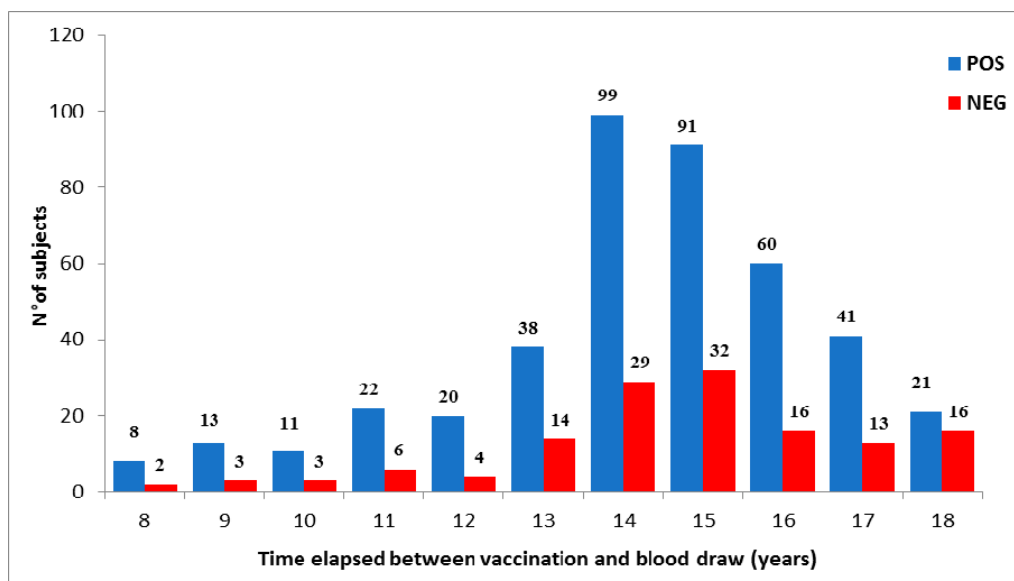

Figure 3. Seroprevalence of measles antibodies after vaccination over-time. Antibody response in vaccinees was analyzed 8–18 years after complete vaccination. The number of seropositive and seronegative subjects was plotted.

3.4. Evaluation of Neutralizing Ab Titers

One hundred and ten sera of seropositive subjects who had received two doses of the measles vaccine and 100 sera of randomly selected subjects who had contracted a natural infection were tested for the presence of neutralizing antibodies against the virus. With regard to naturally infected subjects, the GMT of the tested samples was 570.6 and no substantial differences were found between males and females ($p = 0.46$). Among those vaccinated with two doses of measles vaccine, the GMT was 172.1, which was considerably lower than that recorded in naturally infected subjects ($p < 0.00001$). Moreover, no gender related significant differences in GMT were found during this analysis ($p = 0.38$) (Figure 4).
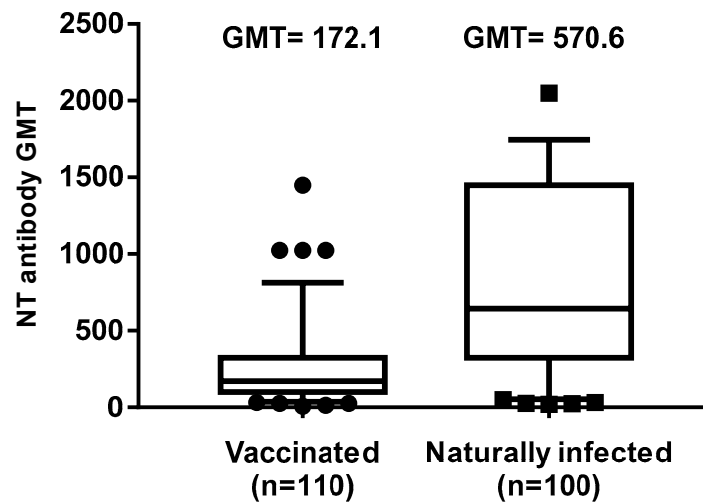

Figure 4. Differences in neutralizing antibody titers between subjects vaccinated with two doses of measles vaccine and naturally infected subjects are shown. The whiskers represent the values from the 5th to the 95th percentiles; the median, the 25th and 75th percentiles are depicted by the horizontal lines in the boxes. Individual data points are shown; outlier values are shown as black circles or squares. GMTs are shown above the population columns. *p*-value of the GMT between the two groups is ≤0.00001.

3.5. Decline of Neutralizing Ab Titers

Since previous studies reported that the measles protective antibody titer was decreasing over time after the administration of the second dose of MMR vaccine [17–21], our aim was to evaluate this phenomenon in our cohort. The vaccinated subjects (110) were divided into three groups, on the basis of the time elapsed since the administration of the second dose of vaccine: eleven years (35 subjects), 12–14 years (39 subjects) and ≥15 years (36 subjects). Results showed a significant decrease in GMT between the groups tested at 1–11 and 12–14 years after vaccination (232.4 vs. 147.4; *p* < 0.05) (Figure 5), thus confirming a possible decline of the protective antibody response against measles during their lifetime. No further difference was evidenced after ≥15 years since vaccination.
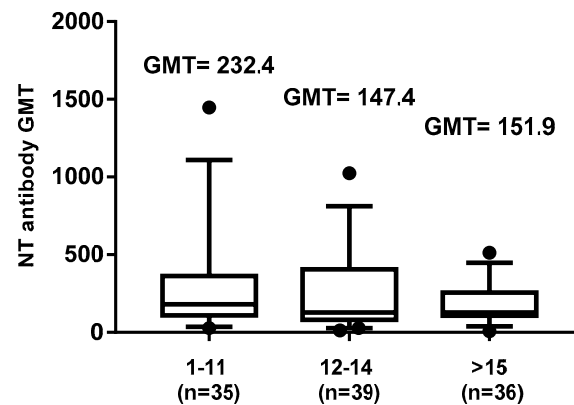
Figure 5. Time elapsed between the second dose of vaccine and the serological test (years). Effects of negative correlation based on the time elapsed between the second dose of measles vaccine and the last measles investigation test on neutralizing antibody response. The whiskers represent the values from the 5th to the 95th percentiles; the median, the 25th and 75th percentiles are depicted by the horizontal lines in the boxes. Individual data points are shown; outlier values are shown as black circles. GMTs are shown above the population columns. *P*-value of the GMT between the first (1–11) and second (12–14) group is <0.05.

Subjects vaccinated with two doses were further studied on the basis of the time elapsed between the first and second dose of vaccine: 1–6 y (49 subjects), 7–10 y (34 subjects), and ≥11y (27 subjects). Spearman's rank correlation analysis showed a statistically significant ($p = 0.004$) inverse correlation (r = −0.270), between neutralization titers of subject sera and time elapsed between the two-dose vaccination. Indeed, the GMT comparison among the three groups evidenced a decrease of neutralizing GMTs, 215.5 in the 1–6 y, 165.6 in the 7–10 y, and 120.1 in the ≥11 y groups ($p < 0.05$) (Figure 6), particularly relevant in subjects receiving the second dose of vaccine over 10–11 years since the first vaccination ($p < 0.05$). No significant differences related to the gender were found in this analysis either.
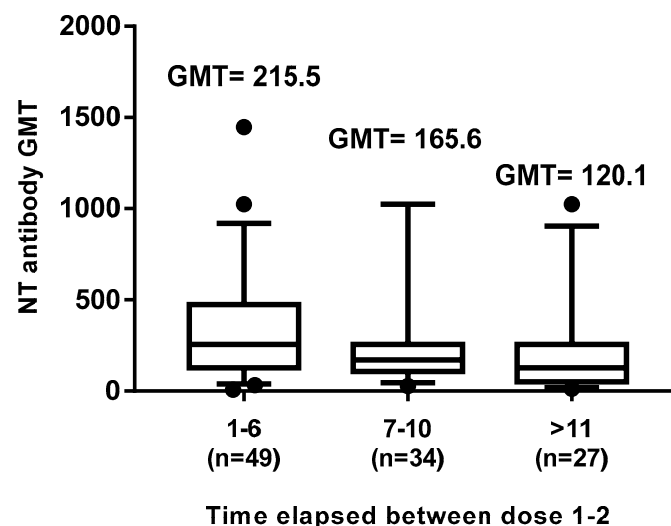
Figure 6. Effect of time elapsed between the two doses of measles vaccine on the neutralizing antibody response. The whiskers represent the values from the 5th to the 95th percentiles; the median, the 25th and 75th percentiles are depicted by the horizontal lines in the boxes. Individual data points are shown; outlier values are shown as black circles or squares. GMTs are shown above the population columns. The difference in GMTs between the first (1–6) and the third (≥11) group is statistically significant ($p \leq 0.05$).

3.6. Neutralizing Antibody GMT in Natural Infected Subjects

No GMT differences were found in serum samples of naturally infected subjects during their childhood, either in those born before (GMT 571.7; mean age 54.8) or after (GMT 552.9; mean age 31.0) the introduction of measles vaccine (Figure 7). These data confirmed a more pronounced tendency of the protective immune response to wane in vaccinated people than in naturally infected people.
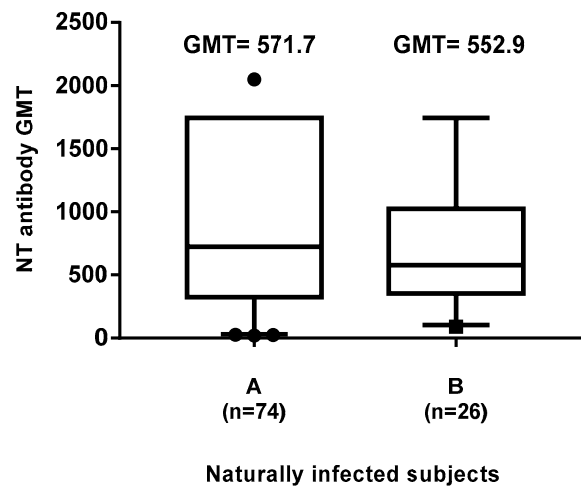

Figure 7. Differences in neutralizing antibody titers in naturally infected subjects born before (A) and after (B) 1977 (one year after the introduction of measles vaccine in Italy). The whiskers represent the values from the 5th to the 95th percentiles; the median, the 25th and 75th percentiles are depicted by the horizontal lines in the boxes. Individual data points are shown; outlier values are shown as black circles or squares. GMTs are shown above the population columns. Difference in GMT between the two groups is not significant (*p* > 0.05).

4. Discussion

Measles morbidity and mortality have been reduced since the implementation of enhanced vaccination strategies [27], and in several countries the interruption of indigenous transmission of measles disease has been reported [28]. Unfortunately, the measles disease continues to be difficult to eradicate, especially in European countries where recurrent outbreaks have been described [29]. In Italy, although a significant reduction of measles infection has been obtained since the introduction of the measles vaccine in 1976, the goal of measles eradication fixed by WHO Europe has still not been met. A new law, adopted in Italy in July 2017 [13], extended the number of mandatory vaccines from four to 10 vaccines for those aged 0–16. This law allowed the vaccine coverage for MMR vaccine to increase up to 94.1% (range 82.2–97.5) but still with geographical variations throughout the country [30]. This program aimed at preventing widespread measles transmission [31], by inducing a specific humoral response in the community, which is a good indicator of protection from infection.

In this study, we evaluated the immunization status and the seroprevalence of measles antibodies among a healthy adult population after vaccination or natural infection. In particular, the aim of this study was to investigate the persistence of anti-measles IgG among vaccinated and naturally infected people. Collected data showed that, out of the 1092 enrolled subjects, 682 (62.45%) had received two doses of measles vaccine (monovalent and/or MMR) and among these, only 24 subjects received as first dose the monovalent vaccine, since this was replaced in the early 1990s by the combined measles–mumps–rubella (MMR). We noted that 23% of the subjects who received two doses of measles vaccine did not show IgG response, similarly to those receiving only one dose of vaccine (25%) (Figure 1). This percentage appeared higher than that reported by other authors [17,20,32,33], thus, it is advisable to monitor the immune status of vaccines 10–15 years since vaccination, in order to evaluate the immune protection against measles and, eventually, implement a possible prophylactic

measure. On the other hand, a long-term high rate of seropositivity persisted after natural infection; indeed, subjects enrolled in this study who reported measles infection history were all seropositive. Therefore, we evaluated the presence of the neutralizing antibody response to the virus in naturally infected subjects and in those vaccinated with two doses. The geometric mean titer to measles was high (GMT 552.9) in naturally infected people, versus a GMT of 172.1 in vaccines of the same age cohort, indicating that the antibody titer decline was more evident in the vaccinated people, probably because the starting antibody titer after vaccination was lower than that induced after natural infection [34]. This finding is also supported by the observation that a measles virus antibody titer decrease has been revealed in source plasma donors after the introduction of measles vaccination in the United States [35], resulting in a high level of immunity and limited spread of the virus, but lower antibody level in the population. Indeed, in this study, the neutralizing antibody titer inversely correlated with the time elapsed between the second dose of vaccine and the blood drawn. This trend was confirmed (r = −0.11) by a gradual decrease of GMT titers (Figure 4), concomitant with the increase of years spent since vaccination, particularly over 12–14 years (GMT 232.4 vs. 147.4). Finally, a new interesting factor considered in this analysis was that most of the subjects had been vaccinated at different lifetimes with two doses, because of the change of the national vaccination schedule in 2003. Therefore, this parameter was analyzed to understand whether the interval of time elapsed between the two doses of vaccine could influence the immune response. It is known that schedules which have longer intervals between vaccine doses usually lead to higher immune responses [36–38]. On the contrary, our results, obtained by the neutralization assay on serum samples of subjects vaccinated with two doses (Figure 5), showed a different picture. An inverse correlation between neutralizing titer and time elapsed between the two vaccinations was evidenced (r = −0.27) with a significant decline of the GMT when the interval was ≥11 years in comparison to that observed within the 1–6 years interval (*p* = 0.02). The result could be very useful for the formulation of the vaccination schedule, because this finding is not valid for all vaccinations and represents a further variable factor to be considered when new vaccinations are requested. We did not find the gender factor as a variable for the immune response to measles vaccination, since no significant difference was recorded. Nowadays, measles can be easily prevented through a two-dose vaccination; however, the estimated rate of antibody decline along the time upon vaccination might represent a factor to be taken into account to limit the number of people susceptible to measles infection in the future. In this work, we only based our study on the humoral response to measles, without considering the role of cell-mediated immunity for the induction of protective immunity [39], which might be present and re-stimulated in a subject who does not apparently reveal a specific antibody response. The above discussed data suggest that there is still a small nonimmunized portion of adults, thus it is necessary to continue the monitoring of the level of protection in the population in order to limit the endemic circulation and outbreaks of measles. Finally, it is interesting to examine the immune response in depth and in its entirety and evaluate the possibility of a booster vaccination, reassessing the multiple factors that can affect and improve the immunogenicity and efficacy of the vaccine.

5. Conclusions

Although MMR vaccine is very efficacious to induce a protective response against measles, considering that a physiological decline of the humoral response has been revealed in some studies [35], it could be important to monitor the population 10–15 years after vaccination, in order to revaccinate the seronegatives. However, since booster revaccination might not induce a sustainable increase of MV antibodies [40], it could be advisable to implement the prophylaxis with alternative vaccines that could obviate this possibility.

References

1. Griffin, D.E. Measles virus. In *Fields Virology*; Knipe, D.M., Howley, P.M., Eds.; Wolters Kluwer | Lippincott Williams & Wilkins: Philadelphia, PA, USA, 2013; Volume 6, pp. 1042–1069.

2. de Vries, R.D.; Duprex, W.P.; de Swart, R.L. Morbillivirus infections: An introduction. *Viruses* **2015**, *7*, 699–706. [CrossRef] [PubMed]

3. Buchanan, R.; Bonthius, D.J. Measles virus and associated central nervous system sequelae. *Semin. Pediatr. Neurol.* **2012**, *19*, 107–114. [CrossRef] [PubMed]

4. Mina, M.J.; Metcalf, C.J.; de Swart, R.L.; Osterhaus, A.D.; Grenfell, B.T. Long-term measles-induced immunomodulation increases overall childhood infectious disease mortality. *Science* **2015**, *348*, 694–699. [CrossRef] [PubMed]

5. de Vries, R.D.; McQuaid, S.; van Amerongen, G.; Yüksel, S.; Verburgh, R.J.; Osterhaus, A.D.; Duprex, W.P.; de Swart, R.L. Measles Immune Suppression: Lessons from the Macaque Model. *PLoS Pathog.* **2012**, *8*. [CrossRef] [PubMed]

6. de Vries, R.D.; de Swart, R.L.; Lamouille, B.; Astier, A.; Rabourdin-Combe, C. Measles Immune Suppression: Functional Impairment or Numbers Game? *PLoS Pathog.* **2014**, *10*, e1004482. [CrossRef] [PubMed]

7. Laksono, B.M.; de Vries, R.D.; McQuaid, S.; Duprex, W.P.; de Swart, R.L. Measles Virus Host Invasion and Pathogenesis. *Viruses* **2016**, *8*. [CrossRef] [PubMed]

8. Uzicanin, A.; Zimmerman, L. Field effectiveness of live attenuated measles-containing vaccines: A review of published literature. *J. Infect. Dis.* **2011**, *204*, 133–148. [CrossRef]

9. Rota, P.A.; Moss, W.J.; Takeda, M.; de Swart, R.L.; Thompson, K.M.; Goodson, J.L. Measles. *Nat. Rev. Dis. Primers* **2016**, *2*. [CrossRef]

10. Italian Ministry of Health. Circolare n.12 del 13 luglio 1999. Controllo ed eliminazione di morbillo, rosolia e parotite attraverso la vaccinazione. Available online: http://www.salute.gov.it/imgs/C_17_normativa_86_allegato.pdf (accessed on 13 July 1999).

11. Italian Ministry of Health. Piano nazionale per l'eliminazione del morbillo e della rosolia congenita. 2003. Available online: http://www.salute.gov.it/imgs/C_17_pubblicazioni_730_allegato.pdf (accessed on 13 November 2003).

12. Andrianou, X.D.; Del Manso, M.; Bella, A.; Vescio, M.F.; Baggieri, M.; Rota, M.C.; Pezzotti, P.; Filia, A. Spatiotemporal distribution and determinants of measles incidence during a large outbreak, Italy, September 2016 to July 2018. *Euro. Surveill.* **2019**, *24*. [CrossRef]

13. Italian Ministry of Health. Decree Law 7 June 2017, n. 73, Urgent Provisions on Vaccination Prevention, as Amended by the Conversion Law. Available online: http://www.trovanorme.salute.gov.it/norme/dettaglioAtto?id=60201 (accessed on 31 July 2017).

14. Cocchio, S.; Zanoni, G.; Opri, R.; Russo, F.; Baldo, V.; Collaborative group. A postmarket safety comparison of 2 vaccination strategies for measles, mumps, rubella and varicella in Italy. *Hum. Vaccin. Immunother.* **2016**, *12*, 651–654. [CrossRef]

15. European Centre for Disease Prevention and Control. *Monthly Measles and Rubella Monitoring Report*; ECDC: Stockholm, Sweden, 2019; Available online: https://www.ecdc.europa.eu/en/publications-data/monthly-measles-and-rubella-monitoring-report-september-2019 (accessed on 13 September 2019).

16. Yeung, L.F.; Lurie, P.; Dayan, G.; Eduardo, E.; Britz, P.H.; Redd, S.B.; Papania, M.J.; Seward, J.F. A limited measles outbreak in a highly vaccinated US boarding school. *Pediatrics* **2005**, *116*, 1287–1291. [CrossRef] [PubMed]

17. Kennedy, R.B.; Ovsyannikova, I.G.; Thomas, A.; Larrabee, B.R.; Rubin, S.; Poland, G.A. Differential durability of immune responses to measles and mumps following MMR vaccination. *Vaccine* **2019**, *37*, 1775–1784. [CrossRef] [PubMed]

18. Carryn, S.; Feyssaguet, M.; Povey, M.; Di Paolo, E. Long-term immunogenicity of measles, mumps and rubella-containing vaccines in healthy young children: A 10-year follow-up. *Vaccine* **2019**, *37*, 5323–5331. [CrossRef] [PubMed]

19. Davidkin, I.; Jokinen, S.; Broman, M.; Leinikki, P.; Peltola, H. Persistence of measles, mumps, and rubella antibodies in an MMR-vaccinated cohort: A 20-year follow-up. *J. Infect. Dis.* **2008**, *197*, 950–956. [CrossRef] [PubMed]

20. Seagle, E.E.; Bednarczyk, R.A.; Hill, T.; Fiebelkorn, A.P.; Hickman, C.J.; Icenogle, J.P.; Belongia, E.A.; McLean, H.Q. Measles, mumps, and rubella antibody patterns of persistence and rate of decline following the second dose of the MMR vaccine. *Vaccine* **2018**, *36*, 818–826. [CrossRef] [PubMed]

21. Gonçalves, G.; Frade, J.; Nunes, C.; Mesquita, J.R.; Nascimento, M.S. Persistence of measles antibodies, following changes in the recommended age for the second dose of MMR-vaccine in Portugal. *Vaccine* **2015**, *33*, 5057–5063. [CrossRef]

22. LeBaron, C.W.; Beeler, J.; Sullivan, B.J.; Forghani, B.; Bi, D.; Beck, C.; Audet, S.; Gargiullo, P. Persistence of measles antibodies after 2 doses of measles vaccine in a post-elimination environment. *Arch. Pediatr. Adolesc. Med.* **2007**, *161*, 294–301. [CrossRef]

23. Authorisation no. 9/2014—General Authorisation to Process Personal Data for Scientific Research Purposes. Available online: https://www.gazzettaufficiale.it/atto/serie_generale/caricaDettaglioAtto/originario?atto. dataPbblicazioneGazzetta=2014-12-30&atto.codiceRedazionale=14A09916&elenco30giorni=true (accessed on 30 December 2014).

24. Law Decree 22 December 2017, No. 219, published in the Official Gazette No. 12 of 16 January 2018. Available online: https://www.gazzettaufficiale.it/eli/gu/2018/01/16/12/sg/pdf (accessed on 16 January 2016).

25. Reed, L.J.; Muench, H. A simple method of estimating fifty per cent endpoints. *Am. J. Hyg.* **1938**, *27*, 493–497.

26. Pacenti, M.; Maione, N.; Lavezzo, E.; Franchin, E.; Dal Bello, F.; Gottardello, L.; Barzon, L. Measles Virus Infection and Immunity in a Suboptimal Vaccination Coverage Setting. *Vaccines* **2019**, *7*, 199. [CrossRef]

27. Patel, M.K.; Dumolard, L.; Nedelec, Y.; Sodha, S.V.; Steulet, C.; Gacic-Dobo, M.; Kretsinger, K.; McFarland, J.; Rota, P.A.; Goodson, J.L. Progress Toward Regional Measles Elimination—Worldwide, 2000–2018. *MMWR Morb. Mortal. Wkly. Rep.* **2019**, *68*, 1105–1111. [CrossRef]

28. World Health Organization. Measles Cases Hit Record High in the European Region. 2018. Available online: http://www.euro.who.int/en/media-centre/sections/press-releases/2018/measles-cases-hit-record-high-in-the-european-region (accessed on 20 August 2018).

29. World Health Organization. 8th Meeting of the European Regional Verification Commission for Measles and Rubella Elimination (RVC). Available online: http://www.euro.who.int/en/health-topics/communicable-diseases/measles-and-rubella/publications/2019/8th-meeting-of-the-european-regional-verification-commission-for-measles-and-rubella-elimination-rvc-2019 (accessed on 12 June 2019).

30. D'Ancona, F.; D'Amario, C.; Maraglino, F.; Rezza, G.; Iannazzo, S. The law on compulsory vaccination in Italy: An update 2 years after the introduction. *Euro. Surveill.* **2019**, *24*. [CrossRef] [PubMed]

31. McLean, H.Q.; Fiebelkorn, A.P.; Temte, J.L.; Wallace, G.S. Centers for Disease Control and Prevention. Prevention of measles, rubella, congenital rubella syndrome, and mumps, 2013: Summary recommendations of the Advisory Committee on Immunization Practices (ACIP). *MMWR Recomm. Rep.* **2013**, *62*, 1–34. [PubMed]

32. Bianchi, F.P.; Stefanizzi, P.; De Nitto, S.; Larocca, A.M.V.; Germinario, C.; Tafuri, S. Long-term immunogenicity of Measles vaccine: An Italian retrospective cohort study. *J. Infect. Dis.* **2019**. [CrossRef] [PubMed]

33. Smetana, J.; Chlibek, R.; Hanovcova, I.; Sosovickova, R.; Smetanova, L.; Gal, P.; Dite, P. Decreasing Seroprevalence of Measles Antibodies after Vaccination—Possible Gap in Measles Protection in Adults in the Czech Republic. *PLoS ONE* **2017**, *12*, e0170257. [CrossRef]

34. Christenson, B.; Böttiger, M. Measles antibody: Comparison of long-term vaccination titres, early vaccination titres and naturally acquired immunity to and booster effects on the measles virus. *Vaccine* **1994**, *12*, 129–133. [CrossRef]

35. Modrof, J.; Tille, B.; Farcet, M.R.; McVey, J.; Schreiner, J.A.; Borders, C.M.; Gudino, M.; Fitzgerald, P.; Simon, T.L.; Kreil, T.R. Measles Virus Neutralizing Antibodies in Intravenous Immunoglobulins: Is an Increase by Revaccination of Plasma Donors Possible? *J. Infect. Dis.* **2017**, *216*, 977–980. [CrossRef]

36. Rümke, H.C.; Loch, H.P.; Hoppenbrouwers, K.; Vandermeulen, C.; Malfroot, A.; Helm, K.; Douha, M.; Willems, P. Immunogenicity and safety of a measles-mumps-rubella-varicella vaccine following a 4-week or a 12-month interval between two doses. *Vaccine* **2011**, *29*, 3842–3849. [CrossRef]

37.　Middleman, A.B.; Kozinetz, C.A.; Robertson, L.M.; DuRant, R.H.; Emans, S.J. The effect of late doses on the achievement of seroprotection and antibody titer levels with hepatitis b immunization among adolescents. *Pediatrics* **2001**, *107*, 1065–1069. [CrossRef]

38.　Sabidó, M.; Gavaldà, L.; Olona, N.; Ramon, J.M. Timing of hepatitis B vaccination: Its effect on vaccine response in health care workers. *Vaccine* **2007**, *25*, 7568–7572. [CrossRef]

39.　Griffin, D.E. The Immune Response in Measles: Virus Control, Clearance and Protective Immunity. *Viruses* **2016**, *8*, 282. [CrossRef]

40.　Fiebelkorn, A.P.; Coleman, L.A.; Belongia, E.A.; Freeman, S.K.; York, D.; Bi, D.; Kulkarni, A.; Audet, S.; Mercader, S.; McGrew, M.; et al. Measles Virus Neutralizing Antibody Response, Cell-Mediated Immunity, and Immunoglobulin G Antibody Avidity Before and After Receipt of a Third Dose of Measles, Mumps, and Rubella Vaccine in Young Adults. *J. Infect. Dis.* **2016**, *213*, 1115–1123. [CrossRef]
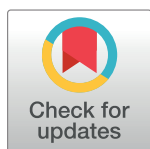
Toscana virus non-structural protein NSs acts as E3 ubiquitin ligase promoting RIG-I degradation

Gianni Gori Savellini [ID], **Gabriele Anichini, Claudia Gandolfo** [ID]**, Shibily Prathyumnan** [ID]**, Maria Grazia Cusi** [ID]*

Department of Medical Biotechnologies, University of Siena, Siena, Italy

* mariagrazia.cusi@unisi.it

Abstract

It is known that the non-structural protein (NSs) of Toscana virus (TOSV), an emergent sandfly-borne virus causing meningitis or more severe central nervous system injuries in humans, exerts its function triggering RIG-I for degradation in a proteasome-dependent manner, thus breaking off the IFN-β production. The non-structural protein of different members of Bunyavirales has recently appeared as a fundamental protagonist in immunity evasion through ubiquitination-mediated protein degradation targets. We showed that TOSV NSs has an E3 ubiquitin ligase activity, mapping at the carboxy-terminal domain and also involving the amino-terminal of the protein. Indeed, neither the amino- (NSsΔN) nor the carboxy- (NSsΔC) terminal-deleted mutants of TOSV NSs were able to cause ubiquitin-mediated proteasome degradation of RIG-I. Moreover, the addition of the C-terminus of TOSV NSs to the homologous protein of the Sandfly Fever Naples Virus, belonging to the same genus and unable to inhibit IFN-β activity, conferred new properties to this protein, favoring RIG-I ubiquitination and its degradation. NSs lost its antagonistic activity to IFN when one of the terminal residues was missing. Therefore, we showed that NSs could behave as an atypical RING between RING (RBR) E3 ubiquitin ligases. This is the first report which identified the E3 ubiquitin ligase activity in a viral protein among negative strand RNA viruses.

Author summary

Toscana virus is an emergent sandfly-borne virus mainly transmitted to humans by phlebotomine sandflies, which can cause meningitis or more severe central nervous system injuries in some subjects. As many other RNA viruses, it counteracts IFN-β expression by its non-structural protein. Our results expanded our knowledge about the molecular mechanisms by which TOSV exerts its activity as an E3 ubiquitin ligase. This is the first example of a viral protein presenting this activity among negative-strand RNA viruses. Thus, the recognition of this activity and its substrates among viruses are of primary importance to understand how viruses can alter their fitness by the ubiquitin pathway and provide an attractive target for the development of antiviral therapies.

Introduction

Toscana virus (TOSV; *Phenuiviridae* family, Phlebovirus genus) is an emergent sandfly-borne virus mainly transmitted to humans by phlebotomine sandflies [1–3]. A large number of infections is asymptomatic, however, TOSV infection is the leading cause of meningitis or more severe central nervous system (CNS) injuries, such as encephalitis and ischemia during the summer season in southern Europe [4–5]. The viral genome is composed of the large (L), medium (M) and small (S) segments [6]. The L segment encodes an RNA-dependent RNA-polymerase, the M segment encodes the envelope glycoproteins (Gn and Gc) and a non-structural protein (NSm) and the S segment encodes a nucleocapsid (N) protein and a non-structural (NSs) protein [6, 7, 8, 9]. The NSs protein of some members of the *Phenuiviridae* family represents an important virulence factor being a potent antagonist of type I interferons (IFN-α/β), the main protagonists of the host innate immunity against viral infections. The signaling pathway leading to the secretion of IFN-β and the establishment of an antiviral state are achieved by the induction of the cytoplasmic viral sensors RIG-I (Retinoic-acid Inducible Gene I) and MDA-5 (Melanoma Differentiation Associated gene-5) able to recognize dsRNA molecules generated during viral replication [10]. In order to overcome this first-line defense implemented by the host, viruses have evolved protein(s) able to block IFN-β production and its downstream activity at different steps in the signaling cascade. Among Bunyavirales, Toscana virus (TOSV), the Bunyamwera Virus (BUNV), La Crosse Virus (LACV), Sin Nombre (SNV), Tula (TULV) and Puumala (PUUV) Hantaviruses, Rift Valley Fever Virus (RVFV) and Severe Fever with Thrombocytopenia Syndrome Virus (SFTSV), express the NSs protein acting as a suppressor of IFNs [11–21]. Along with this evidence, previous studies have shown that TOSV NSs could exert its function by triggering RIG-I for degradation in a proteasome-dependent manner, thus breaking off the IFN-β production and blocking the establishment of an efficient antiviral state [21, 22]. The proteasomal degradation of proteins by ubiquitination is a process consisting of a covalent attachment of ubiquitin to target proteins. The molecular machinery which leads to the assembly and linkage of poly-Ub chains to the target protein consists of three enzymes defined as ubiquitin-activating enzymes (E1), ubiquitin-conjugating enzymes (E2) and ubiquitin-ligases (E3), which work sequentially in a cascade. In this context, the E3 ubiquitin ligase is the only enzyme which confers specificity to this system by recognizing a selected target protein [23, 24, 25]. E3 ligases are distinguished in RING (Really Interesting New Gene), HECT (Homologous to the E6-AP Carboxy Terminus) and RBR (RING Between RING). A notable distinction in the mechanism among the classes is that RING E3 catalyzes a direct transfer of ubiquitin from E2 to the target protein, whereas a transfer of ubiquitin by HECT E3 involves an intermediate step where the ubiquitin is first transferred from E2 to an active cysteine residue on HECT E3 ligase, then it is conjugated to the target protein [26–35]. RBR combines properties of RING and HECT E3s to conjugate Ub to target proteins. [32]. Based on the linkage generated between ubiquitin moieties, the cognate proteins undergo regulation of their physiological functions, although the role of some chains is still elusive [36–41]. The non-structural protein of different members of Bunyavirales has recently appeared as a fundamental protagonist in virus replication and immunity evasion through ubiquitination-mediated protein degradation [22, 42–45]. To better understand the interaction between the ubiquitin system and TOSV NSs, we investigated whether this viral protein could be responsible for ubiquitin modifications of specific targets. In this study, we showed that TOSV NSs has an E3 ubiquitin ligase activity mapping at the carboxy- and the amino-terminal domains of the protein. Indeed, it appears to promote the transfer of ubiquitin to RIG-I, thus favoring its proteasome-dependent proteolysis. During the course of evolution and adaptation, many of the large DNA viruses have shown to encode their own Ub modifying machinery to facilitate viral

replication through regulating immune responses. Here, we present the first report which identifies the E3 ubiquitin ligase activity in a viral protein among negative-strand RNA viruses, to mediate host–virus interactions.

Results

NSs and RIG-I expression in Toscana virus infected cells

Previous results have shown that TOSV was able to induce a RIG-I-mediated IFN-β expression in infected cells, likely because NSs was expressed at a low level and relatively late during the viral replication cycle [18]. Therefore, only the *in vitro* over-expression of NSs could evidence its properties mediating a decrease of RIG-I, due to the ubiquitination and proteasomal degradation of RIG-I after their interaction [21]. To better characterize the role of NSs during TOSV infection, the IFN-β competent cell line, Lenti-X 293T, was infected and analysed. The immunoblotting evaluating the expression of endogenous RIG-I performed on cell lysates of mock-infected, TOSV infected, or poly(I:C) stimulated cells showed that RIG-I was induced as revealed at 24h and 48h post-infection (p.i.), alongside with the NSs protein. To better address whether the lack of endogenous RIG-I degradation in TOSV infected cells was due to the low amount of the non structural protein in the early phase of replication, an over-expression of NSs was performed by transient transfection in infected cells. The immunoblotting of these cell lysates confirmed that the level of endogenous RIG-I was reduced in the presence of a higher amount of NSs (S1 Fig, S1 Dataset). Therefore, as previously reported [18], we might hypothesize that the fast replication of TOSV was able to trigger an early innate immune response by inducing IFNs, and that the NSs protein could not counteract this effect, as it was produced later during the virus replication cycle. (S1 Fig, S1 Dataset). As expected, stimulation with poly(I:C) strongly induced cellular accumulation of RIG-I in the selected cell line and the over-expression of TOSV NSs was able to contrast poly(I:C) effects (S1 Fig, S1 Dataset).

NSs contains an E3 ubiquitin ligase activity *in vitro*

Previous results [18, 21, 22] have shown that TOSV NSs presented inhibitory properties versus the IFN-β mediated immune response. In particular, RIG-I was targeted for proteasomal-degradation through the action of NSs, and its functional activity was related to the carboxyl-terminus of the protein itself [22], however, assuming that other domains could also be involved. Therefore, we also tested the activity of the amino-terminus (71 aa.) deleted NSs protein (NSsΔN) (S2 Fig) towards RIG-I. Surprisingly, we found a behavior similar to the one observed for the carboxy-terminus deleted NSs (NSsΔC). NSsΔN significantly lost its degrading activity on RIG-I upon co-transfection of cells with the respective plasmids (Fig 1A, S2 Dataset). Moreover, RIG-I-mediated IFN-β promoter activation was not affected by NSsΔN, as shown by the luciferase reporter assay ($p = 0.638$) (Fig 1A, S2 Dataset). Since the treatment with the proteasome inhibitor MG-132 reversed RIG-I degradation by NSs [21], the possibility of a ubiquitin-mediated proteasomal degradation was evaluated. A growing number of viruses was found to weaponize the ubiquitin modification system to suppress IFN [11–21]. Thus, looking for a tool to identify a functional site of the protein, we submitted the NSs protein sequence to the Phyre2 prediction software (www.sbg.bio.ic.ac.uk/phyre2/html/page.cgi) [46], which provided an alignment of 15 residues (aa. 277–292) and a confidence of 30.7% between NSs and RNF31, the E3 ubiquitin-protein ligase. Considering the potentiality of NSs both to act as an E3 ligase and its ability to induce proteasome degradation of RIG-I, we investigated whether TOSV NSs could have this activity *in vitro*. The His-tagged recombinant NSs protein was produced in bacteria, purified and tested for the E3 ubiquitin ligase activity, as described in Materials and Methods. In such reactions, the ability of a protein to promote a ubiquitin-
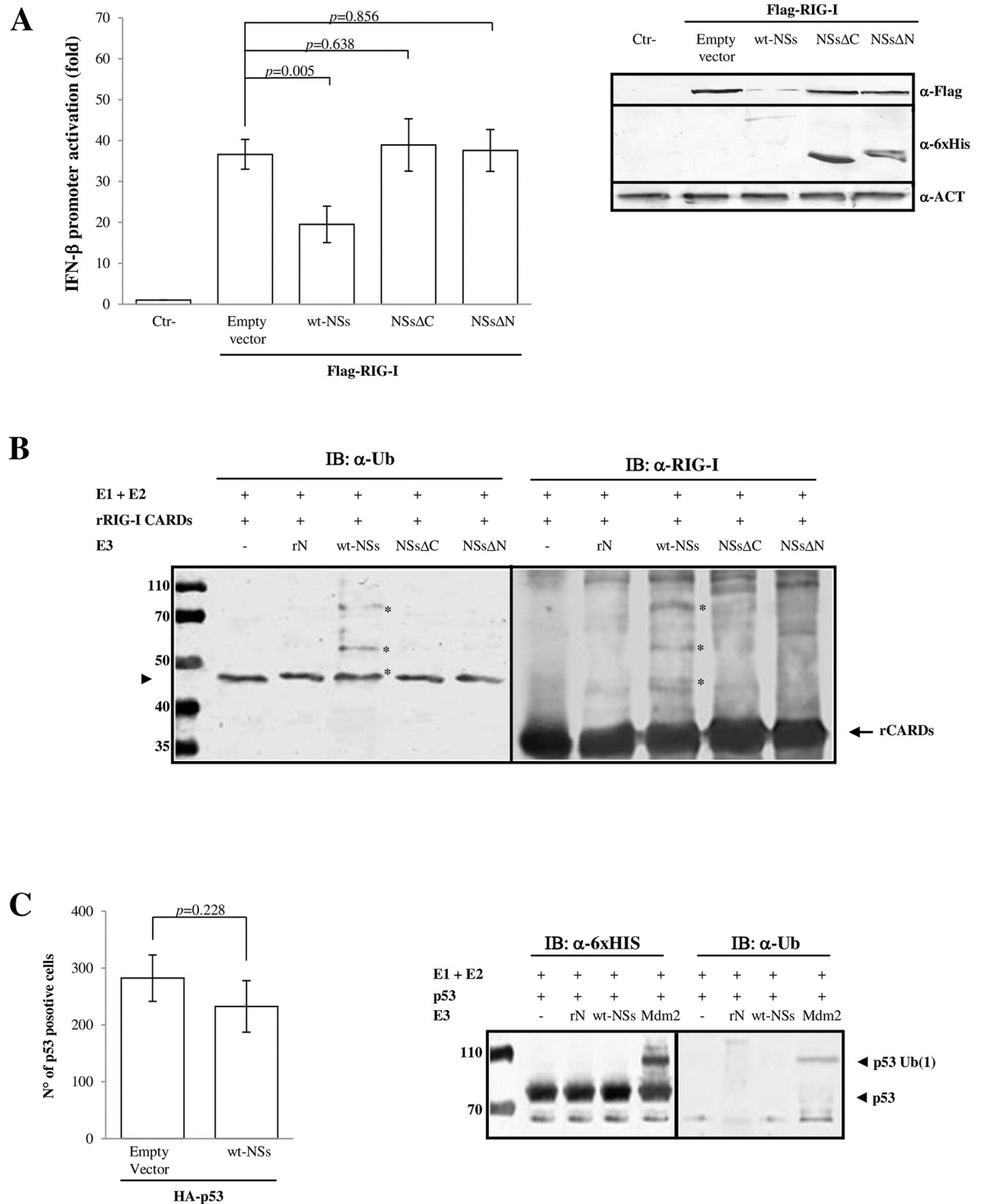
Fig 1. NSs acts as E3 ubiquitin ligase on RIG-I CARDs. Toscana virus NSs inhibits the IFN-β promoter activation through the RIG-I signalling pathway mediating its degradation. Lenti-X 293T cells were transfected (A) with IFN-β promoter-driven FireFly Luciferase (p125-FFLuc) reporter plasmid, expression plasmid encoding FLAG-RIG-I and wild-type (wt-) NSs, as well as deleted NSs expression plasmids, as indicated. In addition, pSV40-RenLuc plasmid was added as internal control. Luciferase activity was analyzed at 48h post-transfection by the Dual-Luciferase Reporter assay as described by the manufacturer (Promega). Relative luciferase activities were measured as fold induction (relative to the basal level of reporter genes in the presence of empty vector after normalization with co-transfected RenLuc activities). Values represent means of triplicate independent experiments ± standard deviations (SD). Representative western blot showing the protein expression levels in the reporter gene assay samples was done on whole cell extracts, resolved by sodium dodecyl sulfate

(SDS)-polyacrylamide gel electrophoresis (PAGE) and analyzed by immunoblotting with the FLAG-RIG-I, 6xHis-NSs and β-Actin specific antibodies and densitometric analysis (Supplement data 2). (B) Recombinant proteins were used in the *in vitro* ubiquitination assay using UbcH5b/c as E2 and wt-rNSs, rNSsΔC or rNSsΔN as source of E3 ubiquitin ligase. The negative controls were represented by rRIG-I CARDs tested with the ubiquitination reagents except for E3 Ub ligase or TOSV nucleoprotein (rN) in place of E3 Ub ligase. The ubiquitinated rRIG-I CARDs were detected with anti-ubiquitin (left panel) or anti-RIG-I (right panel) antibodies. The ubiquitinated forms of rCARDS (indicated by asterisk) are present only in the samples containing wt-rNSs, as demonstrated by mass-spectrometry (S4 Fig). The band indicated by arrowhead (left panel) corresponding to the ubiquitinated-E2 (Ub-E2) intermediate present in all the tested samples, comigrates with the monoubiquitinated-rRIG-I CARDs in presence of rNSs. (C) NSs does not affect p53 expression in cells transfected with HA-p53 and 6xHis-NSs expressing plasmids (left panel). Immunofluorescence was performed with indicated specific antibodies; positive cells were counted. The bars depict the average number of p53 positive cells in the presence or absence of wt-NSs. The mean ± SD of three independent experiments is shown. The specificity of the E3 ubiquitin ligase activity of wt-NSs was evaluated in the *in vitro* ubiquitination assay using UbcH5b/c as E2 and recombinant p53 protein as acceptor target for ubiquitination (right panel). Poly-ubiquitinated forms were detected by anti-6xHis tag and anti-ubiquitin antibodies. Higher molecular weight bands corresponding to ubiquitinated p53 were detected only in the reaction supplemented with Mdm2 E3 ubiquitin ligase, but not in the samples containing wt-rNSs or rN.

https://doi.org/10.1371/journal.ppat.1008186.g001

protein ligation was indicative of an E3 ligase activity. For this purpose, an *in vitro* biochemical assay was performed with E1, E2, rNSs and recombinant full-length RIG-I (FL-rRIG-I). When the wt-NSs was used as a source of E3 Ub ligase in the assay, a shift in RIG-I molecular weight, corresponding to its ubiquitinated form, was revealed by immunoblotting using anti-Ub or anti-RIG-I antibodies (S3 Fig). In subsequent experiments, the recombinant N-terminus of RIG-I containing two tandem-repeated CAspase Recruitment Domains (CARDs), necessary and sufficient to activate RIG-I and induce the recruitment of downstream signaling molecules, were tested. Likewise, when the E3 Ub ligase was substituted by the wt-NSs in the assay, higher molecular weight ubiquitinated bands were revealed by immunoblotting on rRIG-I CARDs, using anti-Ub or anti-RIG-I antibodies (Fig 1B). In order to better evaluate which domain of NSs could have a role in the ubiquitination process, the His-tagged recombinant NSs protein, NSsΔC and NSsΔN deleted proteins were produced in bacteria, purified and tested for the E3 ubiquitin ligase activity. Ubiquitinated rRIG-I CARDs bands were not present when NSsΔC, NSsΔN or TOSV nucleocapsid (N) proteins were added in place of NSs (Fig 1B), indicating that NSs possessed an E3 Ub ligase activity directed to RIG-I. Furthermore, as this activity was not observed in deletion mutants, it was likely located in the amino- and carboxy-terminus regions. In the attempt to investigate the potential substrate specificity of TOSV NSs protein, we tested NSs with the recombinant human p53 protein, known to be ubiquitinated by many different E3 ligases. The co-expression of NSs and p53 plasmids in cells did not reveal any decrease of the p53 protein, in comparison with the control represented by cells transfected with p53 plasmid alone, as evidenced by immunoblotting and immunofluorescence (Fig 1C). Moreover, in biochemical assays, p53 was ubiquitinated by Mdm2 E3 Ub ligase, and not by NSs (Fig 1C), indicating that its activity appeared to be target specific. Finally, ubiquitinated products were not detected in the negative controls, when E3 ubiquitin ligase was omitted or substituted by TOSV N protein in the reaction (Fig 1C).

E3 ubiquitin ligase activity is associated with the C-terminus of NSs

In order to confirm whether NSs E3 ubiquitin ligase activity, required for targeting RIG-I to proteasomal degradation, mapped to the C-terminal sequence of the NSs, we adopted a 'twist' strategy and constructed a TOSV-Sandfly Fever Naples Virus (SFNV) NSs chimeric protein. Toscana virus and Sandfly Fever Naples virus (SFNV) belong to the same viral genus and share a high sequence homology in the non-structural protein (54%) (S4 Fig). However, SFNV NSs lacks the last 78 aa, present in TOSV NSs. Since this domain was proved to be strikingly associated to TOSV NSs degrading activity on RIG-I [22], we generated a chimeric SFNV NSs (cSFNV) protein by fusing the C-terminus of TOSV NSs onto the NSs of the related SFNV. In comparison with TOSV NSs, SFNV NSs was well expressed in transfected cells and did not

show any RIG-I-mediated IFN-β inhibition, since unable to mediate RIG-I degradation ($p = 0.166$) (Fig 2A and 2B). Thus, we supposed that the addition of TOSV C-terminus to SFNV NSs could confer new properties to this protein. Analysing the cSFNV NSs expression by immunofluorescence and immunoblotting, no significant difference was evidenced with the wild-type counterpart ($p = 0.255$) (Fig 2A). On the other hand, the addition of a partial TOSV sequence completely altered the SFNV NSs function. Indeed, an evident decrease of RIG-I was revealed in cSFNV and FLAG-RIG-I plasmids transfected cells, showing few RIG-I positive cells by immunofluorescence ($p = 0.00006$) and a faint band of RIG-I by immunoblotting (Fig 2A, S3 Dataset). Furthermore, the newly acquired IFN-β antagonistic property of cSFNV NSs was confirmed by luciferase reporter assay, demonstrating a strong inhibition of RIG-I-mediated IFN-β promoter activation (Fig 2B) and endorsing the hypothesis of an E3 ubiquitin ligase activity related to the C-terminal domain of TOSV NSs. This data was also supported by the *in vitro* ubiquitination assay of rRIG-I CARDs in the presence of the recombinant cSFNV NSs protein. As shown in Fig 2C, rRIG-I CARDs were ubiquitinated when the chimeric protein was added in the reaction, in place of the E3 Ub ligase. On the contrary, SFNV NSs protein did not have any effect on rRIG-I CARDs (Fig 2C). Moreover, the mass spectrometry, performed on the products of the *in vitro* ubiquitination reactions, identified RIG-I CARDs ubiquitinated at the lysine residues 115 and 172 (S5 Fig). Since Ub-CARDs specific peptides were only identified in the wt-NSs and cSFNV containing samples, the E3 ubiquitin ligase activity of TOSV NSs and the incisive role of its C-terminal domain were further confirmed.

Cysteine $_{27}$ at the N-terminus of NSs is also involved in the ubiquitination process

Since we have demonstrated that NSsΔC and NSsΔN did not have any inhibitory activity to RIG-I mediated IFN-β promoter activation (Fig 1A), we hypothesized that both the C- and N-terminus of NSs might be involved in the ubiquitination of RIG-I. We suspected that NSs could behave such as an RBR E3 Ub ligase, which transfers ubiquitin to a catalytic cysteine on the E3 ligase and then to the substrate. Therefore, a mass spectrometry analysis was performed on the wt-NSs protein, recovered from transfected Lenti-X 293T cells, to see whether a cysteine of NSs was ubiquitinated. The analysis revealed a ubiquitinated cysteine at position 27, in the N-terminal of TOSV protein (S6 Fig). In the recent years, several new modes of ubiquitin chain attachment have emerged and even the thiol groups of cysteine residues could be employed as sites of ubiquitination [47]. However, the potential importance of this 'non-canonical ubiquitination' and its roles still need to be elucidated [48]. Therefore, in order to understand the role of this cysteine in the ubiquitination process, we mutated Cys_{27} to Gly in the wt-NSs and tested the new construct in the *in vitro* ubiquitination assay of rRIG-I CARDs. rNSs-C_{27}G was unable to ubiquitinate rRIG-I CARDs (S7 Fig) and the result was supported by immunofluorescence, immunoblotting (Fig 3A, S4 Dataset) and luciferase assays (Fig 3B), which revealed a behaviour of rNSs-C_{27}G similar to the one observed for NSsΔN and NSsΔC, and indicated the fundamental role elicited by this amino-acid, interfering with cell signaling. Therefore, this result also validated the involvement of the NSs N-terminus in the ubiquitination process.

Discussion

Innate immunity is fundamental to protect host cells against pathogens. In turn, viruses have developed different strategies to counteract host innate immune response [11–21, 42–45]. New mechanisms of viral evasion of host immune response, exploiting the ubiquitin system,
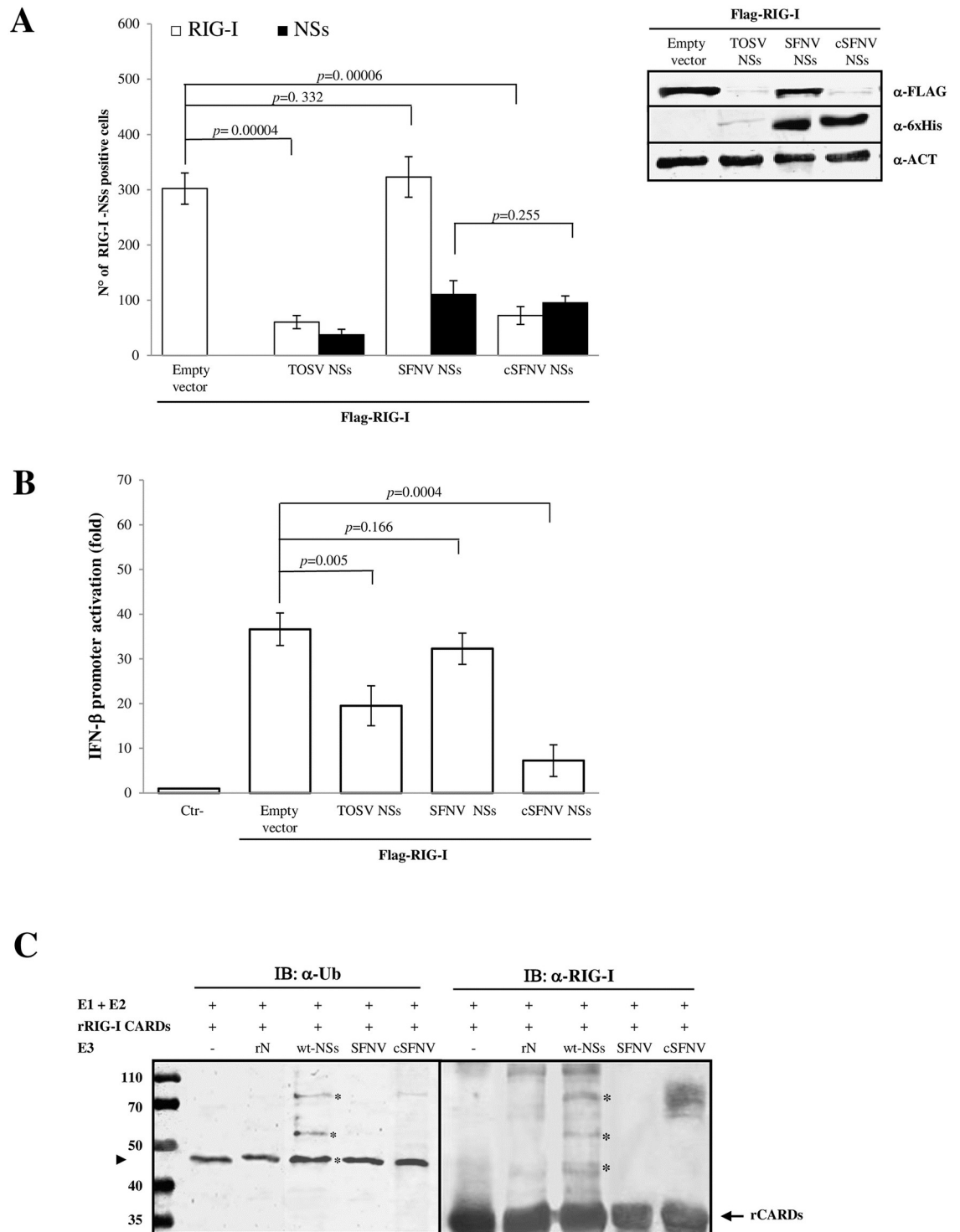
Fig 2. C-terminus of TOSV NSs is linked to E3 ubiquitin ligase activity. The fusion of TOSV NSs C-terminus to Sandfly Fever Naples Virus (SFNV) NSs conferred it a different behaviour. (A, left panel) The chimeric protein cSFNV NSs was tested for its degrading activity on RIG-I co-transfected cells, by immunofluorescence, using specific antibodies [RIG-I (□), NSs (■)]. Graphs are based on the mean values of three independent experiments ± SD. (A, right panel) A more accurate analysis of cellular RIG-I degradation was performed in co-transfected cells by immunoblotting on the whole cell lysates using anti-FLAG or anti-6xHis antibodies. The intensity of the RIG-I band was quantified by densitometry (Supplement data 3). (B) Lenti-X 293T cells were transfected with IFN-β reporter plasmid, FLAG-RIG-I expression plasmid along with TOSV wt-NSs, SFNV wt-NSs or chimeric cSFNV NSs expressing plasmids. Luciferase activities were measured after poly(I:C) treatment. Fold induction was calculated for

each sample with respect to the basal empty plasmid transfected sample, after normalization of the signal with the pSV40-RenLuc internal control. The mean values of at least three sets of experiments ± SD are presented. C) cSFNV NSs showed E3 ubiquitin ligase activity in the biochemical reaction, in association with UbcH5b/c as E2. Poly-ubiquitinated bands of rRIG-I CARDs were detected by immunoblotting using anti-RIG-I or anti-Ub antibodies when cSFNV or TOSV NSs was used in the reaction in place of E3 Ub ligase. No ubiquitination activity was shown when SFNV NSs was used.
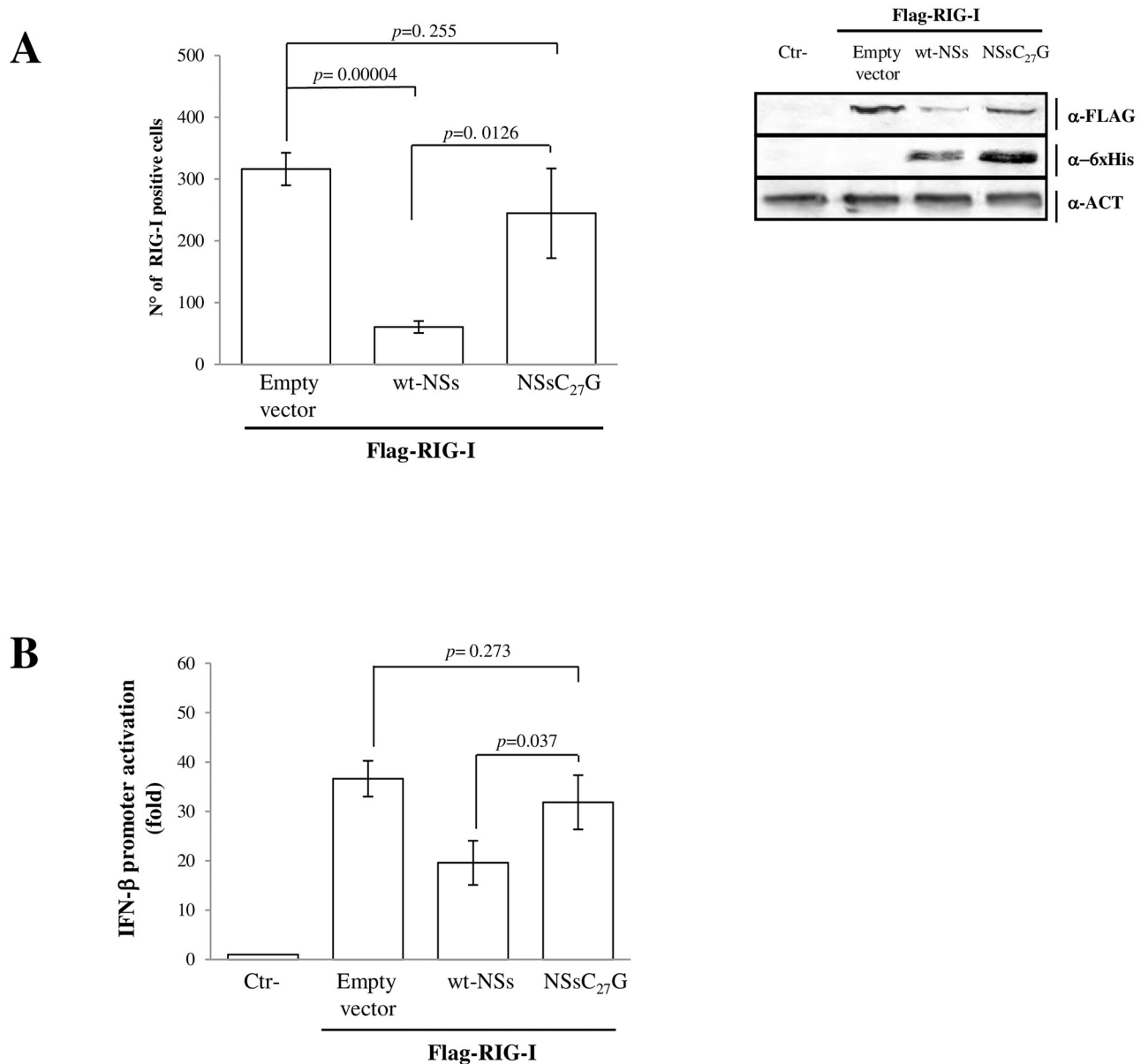
Fig 3. Effects of TOSV NSs N-terminal domain on E3 ubiquitin ligase activity. (A) The involvement of NSs Cystein$_{27}$ in the ubiquitination of RIG-I was evaluated by immunofluorescence on cells co-transfected with RIG-I and NSs plasmids. Cells were stained with anti-FLAG antibody and RIG-I positive cells were counted on different fields. Mean values ± SD of more than three independent experiments were plotted (left panel). Results were validated by immunoblotting (right panel) using total cell lysates of co-transfected cells and semi-quantitative analysis was done by densitometry (supplement data 4). (B) Lenti-X 293T cells were transfected with IFN-β reporter plasmid (p125-FFLuc) along with RIG-I and pSV40-RenLuc plasmids in addition with the wild type-NSs, or C$_{27}$G-NSs mutant or empty plasmids. After stimulation with poly(I:C), luciferase activity was analyzed. For each sample, luciferase was normalized to the RenLuc reporter activity. Data are representative of three independent experiments and are expressed as mean ± SD of normalized luciferase activity.

have recently been described. Indeed, some viruses encode proteins that manipulate the ubiquitin pathway, inhibiting the immune signaling and forwarding the degradation of host proteins [49–53]. Examples are provided by members of the *Herpesviridae* family; Varicella Zoster virus (VZV) encodes ORF61 containing a RING domain, which inhibits the IFN expression, by targeting IRF3 degradation [54]. Similarly, Herpes virus type 1 (HSV-1) has a RING domain in the ICP0 protein that confers E3Ub ligase activity for the degradation of host proteins involved in the innate immunity [55]. Poxviruses behave in a similar way [56]. Thus, ubiquitination has an important role in regulating signal transduction during the immune response [53, 57, 58]. Although viral E3 Ub ligases have been identified in large DNA viruses, some RNA viruses have developed mechanisms to interact with host molecules involved in the ubiquitination pathway. Influenza NS1 protein binds and inactivates the TRIM-25 and Riplet E3 ubiquitin ligase, preventing the downstream activation by K_{63} poly-Ub chain moiety of RIG-I [59, 60, 61]. Likewise, the Paramyxovirus V protein interacts with RIG-I/TRIM-25 regulatory complex by inhibiting RIG-I signaling [62]. Hepatitis C virus NS3-4A protein targets Riplet for degradation [57]; Rotavirus NSP1 triggers the degradation of targets by hijacking a subset of E3 Ub ligases, the cullin-RING ligases [63]. Among *Phenuiviridae* members, Rift Valley fever virus (RVFV) is the most investigated virus for the antagonistic effects of its NSs protein on the innate immune response and recently, the involvement of ubiquitin system, particularly the SCF E3 ubiquitin ligase complex, has been elucidated [44, 58]. Ubiquitin-proteasomal degradation of p62 subunit of the transcription factor TFIIH is a consequence of the interaction between RVFV NSs and the F-box protein FBXO3-SKP1-Cullin1/7 SCF multi-protein complex [43]. Furthermore, RVFV NSs is able to recruit the F-box protein FBXW11 and induce ubiquitination and proteasomal degradation of the antiviral protein PKR [44, 58]. In this study, we have shown how TOSV NSs protein was inducing RIG-I degradation upon their binding [21]. In particular, TOSV NSs revealed an E3 ubiquitin ligase activity related to both the carboxy- and amino-terminal domains of the protein, promoting the transfer of ubiquitin to RIG-I and favoring its proteasome-dependent proteolysis. Indeed, TOSV NSs mutants, such as those deleted at the amino- or carboxy-terminal (NSsΔN, NSsΔC), unlike wt-NSs, were not able to activate IFN induction. This data conferred a new role to the protein terminal sequences and suggested an involvement of these protein regions in the E3 ligase activity. Initially, an E3 ubiquitin ligase activity appeared to be localized at the NSs carboxy-terminal; thus, in order to demonstrate it, the amino-acid stretch 248–316 was fused to the carboxy-terminus of the SFNV NSs, sharing a homology of 54% with TOSV NSs, and lacking this sequence (S4 Fig). SFNV NSs did not show any degrading activity to RIG-I; on the contrary, the obtained chimeric protein acquired the features of TOSV NSs, becoming capable to degrade RIG-I. Then, we demonstrated that neither NSsΔC nor NSsΔN were able to ubiquitinate RIG-I *in vitro*. Thus, it appeared that both the amino-acid ends of TOSV NSs could be involved in an E3 ubiquitin ligase activity. Indeed, NSs, but not NSsΔC or NSsΔN, could transfer ubiquitin to the RIG-I substrate, as shown in the *in vitro* reaction in which ubiquitination process only occurred in the presence of E1, E2 and wt-NSs in place of the E3 Ub ligase. The results were also confirmed by mass spectrometry analysis, which revealed the presence of ubiquitin at positions 115 and 172 of rRIG-I CARDS after the *in vitro* reaction, in the presence of NSs. Moreover, this reaction was specific for RIG-I CARDs, since NSs did not show this activity with a different target, such as the onco-suppressor protein p53. Therefore, it was interesting to understand which type of E3 ubiquitin ligase could be ascribed to TOSV NSs. While some RING or HECT E3 ligases appear to interact directly with the substrate and E2 [25, 26, 29, 31, 64], others require additional components and interact with the substrate only indirectly, as part of a multi-subunit CRL complex [26–35]. Both RING and HECT E3 ligases transfer ubiquitin to a lysine residue on the substrate, RING E3s act as a platform to allow a
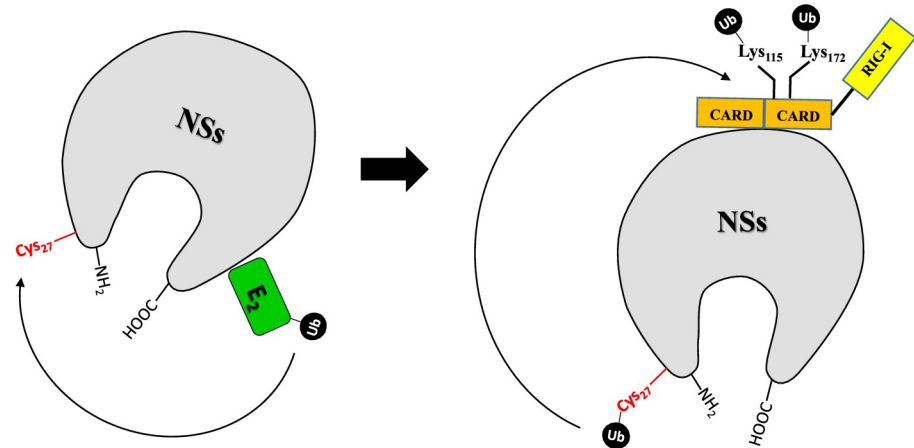
Fig 4. Model for NSs E3 Ub ligase function. Schematic model for TOSV NSs which carries out an unconventional E3 Ub ligase activity (RING between RING; RBR) by a RING-HECT-hybrid mechanism. The model proposes the transfer of ubiquitin from the charged E2 Ub conjugating enzyme, bound to the C-terminal of NSs, to Cysteine $_{27}$ located at the N-terminal of the protein. Then, ubiquitin is transferred to the lysine residues of RIG-I target protein, interacting with the central region of TOSV NSs, and leading to its proteasome-dependent degradation.

direct transfer of ubiquitin from the E2 to the substrate [64]. On the other hand, HECT E3s accept ubiquitin from E2 to form a ubiquitin-thioester intermediate with an active cysteine, then transfer ubiquitin to both the ε-amino groups of lysine side chains of the substrate [25, 31]. Thus, cysteine may play a significant role, particularly in the ubiquitin modification for signaling. In our study, the finding of a ubiquitinated cysteine, a non-canonical site [47, 48], at position 27 of TOSV NSs, led us to suppose that this residue could also be involved in the E3 ubiquitin ligase activity, in addition to the C-terminal sequence of the same protein. Indeed, even the $C_{27}G$ mutant of NSs was no more able to degrade RIG-I and could induce an IFN promoter in transfected cells, although at a lower level, in comparison to the NSsΔN. Therefore, we hypothesized that NSs could behave as an atypical RBR that has elements of both HECT and RING ligases: one RING domain binds the charged E2, while the other domain accepts the ubiquitin molecule before transferring it onto the substrate [32]. We hypothesized that ubiquitin-conjugated E2, bound to the carboxyl-terminus of NSs, transferred the ubiquitin to Cys_{27} (thioester intermediate), in the amino-terminal, as demonstrated by mass spectrometry, and, from there, to RIG-I, linked to NSs (Fig 4). This model might explain why NSs was losing its antagonistic activity to IFN, when one of the two amino-acid ends was lost. At present, we do not know why cSFNV NSs showed a ubiquitin E3 ligase activity, despite not having a cysteine at position 27, but it is possible that cysteine at position 39 of SNFV NSs was processed in the same way. Further investigations are ongoing in order to better determine the dynamics of the steps in this ubiquitination process; however, this is the first study showing a viral protein with an E3 ubiquitin ligase activity among negative strand RNA viruses. Although viruses have acquired tactics to minimize host antiviral responses by co-evolving with their hosts, RING E3s, encoded or hijacked by viruses for evading immune responses, are largely undiscovered and can clarify how viruses play this game with their host.

Materials and methods

Cells and viruses

Vero cells (ATCC CCL-81) and human embryonic kidney Lenti-X 293T cells (Clontech, Milan, Italy) were cultured in Dulbecco's modified Eagle's medium (DMEM) (Lonza, Milan,

Italy) supplemented with 100 U/mL penicillin/streptomycin (Hyclone Europe, Milan, Italy) and 10% heat-inactivated foetal calf serum (FCS) (Lonza), respectively, at 37 ˚C. Toscana virus (TOSV) strain 1812 [18] was used for all the experiments described.

Reagents and antibodies

Transient transfections were performed with GeneJuice Transfection reagent (Novagen, Milan, Italy), according to the manufacturer's instruction, or standard calcium phosphate method [65]. Chemicals were all purchased from AppliChem GmbH (Germany). The proteasome inhibitor MG-132 was purchased from Sigma-Aldrich (Milan, Italy). Mouse anti-6xHis tag antibody (GE Healthcare, Milan, Italy), anti-RIG-I (DDX58) polyclonal antibody (OriGene, Rockville, MD, USA), mouse anti-FLAG M2 monoclonal antibody (Agilent Technologies, Milan, Italy), mouse monoclonal anti-HA tag antibody, fluorescein (FITC)-labeled anti-mouse IgG and anti-mouse IgG HRP-conjugated were purchased from Sigma-Aldrich. Anti-rabbit IgG HRP-conjugated was supplied by Santa Cruz Biotechnology Inc. (Heidelberg,Germany) Ni-NTA sepharose was purchased from Novagen (Milan, Italy) and anti-Ub FK2 clone from Enzo Life Sciences (New York, USA).

RIG-I expression in TOSV infected cells

Lenti-X 293T cells were grown in a 24-wells plate ($5x10^5$/ml). After 24h, cell monolayers were infected with TOSV 1812, by using a multiplicity of infection (MOI) of 1. After 1h adsorption at 37 ˚C, viral inoculum was removed and replaced by complete growth medium. Cells were collected at 24h and 48h post-infection (p.i.). Where indicated, infected cells were transfected with 1 μg of NSs expression plasmid or empty plasmid, 5h after infection. Positive control was obtained by stimulating cell with poly(I:C) for 18h. Cell lysates were collected in RIPA buffer; 50 μg of total proteins were resolved by SDS-PAGE and then transferred to nitrocellulose (NC) membrane (Santa Cruz Biotechnology, Heidelberg, Germany). After blocking with 5% non-fat dry milk, filters were incubated O/N at room temperature with anti-RIG-I (1:5000 dilution), anti-NSs (1:200 dilution) or anti-N (1:200 dilution) mouse sera. After being washed with PBS 0.2% Tween-20 (PBS-T), membranes were incubated with anti-mouse HRP-conjugated secondary antibody (1:5000 dilution) and proteins were detected with TMB Enhanced One Component HRP Membrane Substrate (Tebu-bio, Milan, Italy).

Plasmids

Toscana virus full-length, NSsΔC (nt: 1–861) expressing plasmids were cloned in pcDNA4His-Max (Life Technologies, Milan, Italy) as described elsewhere [22]. Similarly, NSsΔN (nt: 217–537) expressing plasmid was generated by PCR with NSsΔN BamHI sense (nt 217–231) 5'-CGCGGATCCCCATGGCTGTACTGGGGCCT-3' and NSs EcoRI antisense (nt 948–931) 5'-CCGGAATTCTAAGGGTGGGTAGTGGGG -3' primers (Sigma-Aldrich). The gene was cloned in pcDNA4HisMax-A plasmid (Invitrogen) at the BamHI-EcoRI unique sites of the polylinker in frame with the 6xHis tag. The Cysteine$_{27}$ mutant was obtained by using Quik-Change II Site-Directed Mutagenesis Kit (Agilent Technologies, Milan, Italy), according to the manufacture's instruction. Sandfly Fever Naples Virus (SFNV), strain Sabin (GenBank Accession N˚ EF201829) chimeric NSs gene carrying the TOSV C-terminal domain (cSFNV) was generated by PCR using, as reverse primer, a synthetic DNA fragment (gBlock: Integrated DNA Technologies) consisting of the C-terminus of TOSV NSs gene (nt: 739–951) partially overlapping to the 3'-end of SFNV NSs ORF, and a SFNV-NSs sense primer (primers sequences available upon request). The chimeric gene was cloned in the pcDNA4HisMax plasmid (Life Technologies) by standard procedure. Full-length Toscana virus NSs gene was also

cloned in the bacterial expression plasmid pET15b (Novagen), while ORFs coding for all the NSs mutants and RIG-I RIG-I CARDs were cloned in pRSET plasmid (Life Technologies). All the recombinant plasmids were confirmed by sequencing. The reporter plasmid encoding Firefly Luciferase downstream the complete interferon-beta promoter (p125-Luc) was kindly provided by Takashi Fujita (Tokyo Metropolitan Institute of Medical Science, Tokyo, Japan) [66], while the *Renilla* Luciferase reporter plasmid (pSV40-RL) was purchased from Promega (Promega, Milan, Italy). Plasmids for FLAG-tagged human RIG-I, RIG-I N-terminal RIG-I CARDs domain (RIG-IN), HA- human p53 and the HA-tagged human ubiquitin were kindly provided by A. García-Sastre (Mount Sinai School of Medicine, New York), T. Fujita (Tokyo Metropolitan Institute of Medical Science, Tokyo, Japan), M. Tommasino (International Agency for Research on Cancer, Lyon, France) and D. Arnoult (Inserm, France), respectively.

Recombinant proteins expression and purification

Recombinant proteins production was achieved by induction of transformed BL21(DE3)-pLys (Novagen) cells with 1 mM IPTG for 3h at 37 ˚C. TOSV NSs was recovered from inclusion bodies via solubilisation with 50 mM Tris-HCl [pH 7.5]; 300 mM NaCl; 0.3% w/v N-laurylsarcosine (SRK) and 6xHis tagged fusion proteins were purified by using Ni-NTA sepharose following manufacturer's instruction. 6xHis-RIG-I CARDs were purified from IPTG induced BL21(DE3)-pLys (Novagen) bacterial culture as described above, with SRK omission. Purified protein fractions were analysed by SDS-PAGE and pure protein containing fractions were pooled, diluted ten-folds with 10 mM Tris-HCl [pH 8.0] and dialysed against the same buffer O/N at room temperature. Recovered proteins were concentrated by using ultrafiltration devices, quantified by BCA reagent (Pierce, Milan, Italy) and stored at -80 ˚C in aliquots. TOSV recombinant nucleoprotein N was produced and purified as described elsewhere [67]. Recombinant human full-length RIG-I was purchased by BPS Bioscience Inc. (San Diego, CA, USA).

Immunofluorescence

Lenti-X 293T cells, seeded in 24-wells culture plate, were transfected with 0.5 μg of wt-, deleted- or mutated-NSs expressing plasmids, alone or in combination with 0.05 μg of FLAG-RIG-I or HA-p53 expressing plasmids. Cells were collected and stained with anti-6xHis antibody (1:2000 dilution), anti-HA antibody (1:500 dilution) or with anti-FLAG M2 antibody (1:500 dilution). FITC-labeled anti-mouse IgG (1:320 dilution) was used as secondary antibody. Immunofluorescence was visualized by a Diaplan microscope (Leica Microsystems, Milan, Italy). RIG-I and NSs positive cells were counted in three different fields of the same slide. The mean value of positive cells was calculated with respect to the total number of spotted cells (3.5×10^5/well).

Luciferase reporter gene assay

2×10^5 Lenti-X 293T cells were seeded in 24-well plates and transfected with indicated plasmids as previously described. Briefly, 0.2 μg of p125-FFLuc, 0.05 μg of RIG-I and, where indicated, 0.5 μg of wt-NSs or NSs mutants expressing plasmids were co-transfected. Empty plasmid was used to normalize total DNA amount. Twenty ng of pSV40-RL were co-transfected as internal control. Thirty-six hours post-transfection, cells were stimulated with 2 μg/ml of poly(I:C). After additional 12h, cells were collected and luciferase activities were measured on lysates by using dual Luciferase reporter assay reagent (Promega), according to the manufacturer's instructions. Cell lysates were stored at -20 ˚C for further analysis by immunoblotting. Results are given as mean values of several experiments ± standard deviations (SD).

Immunoblot analysis

Fifty μg of total cell lysates of co-transfected cells were resolved by SDS-PAGE and then transferred to nitrocellulose membrane. Immunoblotting was performed as described above, by using anti-HA (1:1000 dilution), anti-FLAG (1:2000 dilution) or anti-6xHis (1:1000 dilution). Quantitative comparison among samples was performed by densitometric analysis using the ImageJ software as reported in Supplement data.

In vitro ubiquitination assay

To evaluate TOSV NSs E3 ubiquitin ligase activity, purified recombinant wt-NSs or its mutants were used in the *in vitro* protein Ubiquitination assay (Enzo Life Science). Experimental reactions and controls were added as suggested by the manufacturer. Briefly, 100 nM ubiquitin activating enzyme (E1); 2.5 μM of ubiquitin conjugating enzyme (E2) UbcH5b/c; 1 μM of rNSs protein or its mutants as source of E3 ligase, 2.5 μM of biotinylated ubiquitin and 1 μM of recombinant purified RIG-I, RIG-I CARDs or p53 were incubated at 37 ˚C for 4-6h. Negative control reactions lacking rNSs or containing 1 μM of TOSV rN in place of E3 ubiquitin ligase were included in the experiment set. Reactions were quenched by adding 5X gel loading buffer and analysed by western blotting for ubiquitinated RIG-I CARDs by anti-DDX58 polyclonal antibody (1:500 dilution) or anti-Ub FK2 clone (1:1000 dilution).

Mass spectrometry detection of ubiquitinated protein residues

Lenti-X 293T seeded in T25 flasks were transfected with 3 μg of wt-NSs plasmid in combination with 1 μg of plasmid encoding for HA-tagged ubiquitin. At 36h post-transfection, cells were treated with MG-132 to a final concentration of 1 μM for additional 12h and collected at 48 h post-transfection. Pull-down for NSs was achieved by Immobilized Metal Affinity Chromatography (IMAC) under denaturing conditions. Briefly, cell pellets were lysed in 5 M guanidine-HCl; 10 mM HEPES [pH 8.0] with sonication. His-tagged NSs was bound to Ni-NTA sepharose for 3h at room-temperature. Beads were collected and extensively washed with 10 mM HEPES [pH 8.0], 1 M NaCl, 0.3% w/v SRK, 50 mM imidazole. Bound proteins were eluted with Laemmli denaturing sample buffer, loaded on SDS-PAGE and stained with Bio-safe Coomassie stain (Bio-Rad, Milan, Italy). Protein bands were cut from gel and prepared for mass-spectrometry analysis as carried out by Cogentech Proteomics/MS (Cogentech S.c.a.r.l., Milan, Italy), by using the nLC-ESI-MS/MS QExactive-HF system. Similarly, the rRIG-I CARDs ubiquitination was confirmed by mass-spectrometry performed on the *in vitro* ubiquitination reaction products.

Statistical analysis

The mean differences were statistically analyzed using Stat View statistical software (Abacus Concepts, Berkeley, CA). Immunofluorescence and luciferase reporter gene assay results were expressed as the mean ± SD of determinations made in three different experiments. Probability (p) values were calculated by t-test. A p value of less than 0.05 was considered statistically significant.

Supporting information

S1 Fig. Toscana virus infection leads to RIG-I production. Endogenous RIG-I protein level was observed by western blotting. Lenti-X 293T cells were stimulated with polyI:C transfection for 18h, mock-infected or infected with TOSV (MOI = 1). Where indicated, stimulated or infected cells were either transfected with empty plasmid or plasmid

expressing wt-NSs. Cell lysates were prepared at indicated times post-infections and 50 μg of total proteins were resolved by SDS-PAGE and assessed for RIG-I expression by specific antibody. TOSV NSs expression, along with nucleoprotein N, was determined on the same lysates to confirm viral infection and replication. Band intensity was determined by densitometric analysis performed on at least three independent experiments. Results are given in Supplement data 1.
(TIF)

S2 Fig. TOSV NSs amino-acid sequence. Full-length NSs amino-acidic sequence showing the amino-terminal (NSsΔN) and the carboxy-terminal (NSsΔC) deleted mutants of the protein. The functional active Cysteine residue at position 27 is shown in bold.
(TIF)

S3 Fig. Toscana virus NSs protein retains E3 ubiquitin ligase activity on RIG-I. Recombinant NSs and RIG-I proteins were used in combination with E1 ubiquitin activating enzyme, UbcH5b/c E2 ubiquitin conjugating enzyme and wt-rNSs, as source of E3 ubiquitin ligase, in the ubiquitination assay *in vitro*. Target protein for ubiquitination was represented by the full-length human rRIG-I. Negative controls, including the recombinant TOSV viral nucleoprotein (rN) or the omission of ATP energy source, were included. The presence of poly-ubiquitinated rRIG-I was revealed with anti-ubiquitin or anti-RIG-I antibodies represented by an increase of the specific molecular weight.
(TIF)

S4 Fig. Sequence alignment of TOSV and SFNV NSs proteins. Comparison of the amino acid sequences of Toscana virus (TOSV; strain 1812, GenBank Accession N˚ ABY19522.1) and Sandfly Fever Naples virus (SFNV; strain Sabin, GenBank Accession N˚ EF201829) NSs showing the homology (54%) between the two related viral proteins and the lack of TOSV C-terminal domain in SFNV NSs.
(TIF)

S5 Fig. Tracking of RIG-I CARDs ubiquitination by mass spectrometry. Confirmatory results of RIG-I CARDs ubiquitination by TOSV NSs were obtained by the mass spectrometry analysis. The ≥ 40 KDa fraction of the biochemical reaction products revealed the presence of ubiquitinated RIG-I peptides only in samples supplemented with wt-rNSs or cSFNV NSs. Moreover, this approach allowed the identification of RIG-I CARDs lysine residues 115 and 172 as target for ubiquitination by the NSs.
(TIF)

S6 Fig. Mass spectrum of Toscana virus NSs protein. A cell line derived from Lenti-X 293T cells stably expressing Toscana virus NSs protein was used for purification under denaturing conditions of the viral protein. The enriched substrate protein was subjected to mass spectrum showing the identification of TOSV NSs peptide containing the ubiquitinated Cysteine residue at position 27 (Cys_{27}).
(TIF)

S7 Fig. C_{27}G-NSs mutant is unable to mediate RIG-I rCARDs ubiquitination. The key role of C_{27} in the N-terminus of TOSV NSs was further investigated by *in vitro* ubiquitination of RIG-I rCARDs. Higher molecular weight bands corresponding to rCARDs ubiquitinated forms were detected by both anti-RIG-I and anti-Ub antibodies only when the wt-NSs was used in the biochemical reaction. On the contrary, C_{27}G-NSs mutant was unable to mediate RIG-I rCARDs ubiquitination, confirming a direct involvement of the C_{27} in the ubiquitination process. Asterisk in the sample containing wt-NSs indicates ubiquitinated rRIG-I CARDs,

as reported by mass spectrometry (S5 Fig). On the contrary, the corresponding immune-reactive bands evidenced in other samples were identified as the E2-Ub intermediate.
(TIF)

S1 Dataset. Evaluation of TOSV effects on endogenous RIG-I expression. Immunoblotting for detection of endogenous RIG-I expression in TOSV infected, poly(I:C) and NSs transfected Lenti-X 293T cells were subjected to densitometric analysis. Raw dataset of RIG-I, TOSV NSs and actin band intensity was reported from three independent experiments. After normalization with respect to relative actin values, a comparison was performed and protein expression levels ± standard deviation (SD) were calculated as fold induction. A p value of less than 0.05 was considered statistically significant.
(XLS)

S2 Dataset. Ubiquitination activity of wt NSs and NSs deleted variants. Lenti-X 293T cells were transfected with RIG-I or p53 expressing plasmids, alone or in combination to wt-NSs or its deleted mutants. Quantification of RIG-I or p53 expression levels was performed by densitometric analysis on immunoblotting and raw dataset of RIG-I, p53, NSs and actin band intensity were reported from three independent experiments. After normalization with respect to relative actin values, a comparison was performed and protein expression levels ± standard deviation (SD) were calculated as fold induction. Moreover, specificity of wt-NSs was assessed by immunofluorescence in p53 plasmid co-transfected cells. Both p53 or NSs positive cells were counted and percentage was calculated ± standard deviation (SD). The influence of NSs deleted mutants on RIG-I-mediated IFN-β promoter activation was assessed by Luciferase reporter gene assay. Fold induction of IFN-β promoter activation was reported from three independent experiments ± standard deviation (SD). A p value of less than 0.05 was considered statistically significant.
(XLS)

S3 Dataset. C-terminal domain of TOSV NSs is associated to its ubiquitination function. Quantification of RIG-I cellular accumulation was performed by densitometric analysis on immunoblotting from Fig 2. Raw dataset of RIG-I, TOSV or SFNV NSs, chimeric cSFNV NSs and actin band intensity was listed from three independent experiments. After normalization with respect to relative actin values, fold induction/decrease in protein expression levels ± standard deviation (SD) was calculated. Immunofluorescence data referring to RIG-I or NSs positive cells were given and final results were expressed as percentage of positive cells with respect to the total number of spotted cell. A more accurate analysis was performed by Luciferase reporter gene assay by which the effects of different NSs variants on RIG-I-mediated IFN-β promoter activation was evaluated. Fold induction was calculated for each sample with respect to the basal empty plasmid transfected sample, after normalization of the signal with the pSV40-RenLuc internal control. The mean values of at least three sets of experiments ± SD were presented. For all the experimental procedures a p value of less than 0.05 was considered statistically significant.
(XLS)

S4 Dataset. C_{27} residue at the TOSV NSs N-terminal domain is critical for its E3 ubiquitin ligase activity. RIG-I expression levels were quantified by densitometric analysis on immunoblotting performed on cell lysates of RIG-I and NSs, wild-type or cystein mutant, co-transfected cells. Raw dataset represented the band intensity for RIG-I, wt-NSs, NSsC$_{27}$G and actin. Fold induction/decrease in protein expression levels was calculated after actin normalization. Immunofluorescence results performed for RIG-I or NSs immune-staining were given. Positive cells for both RIG-I or NSs were counted; results were expressed as percentage of positive

cells with respect to the total number of tested cells. Reporter gene assay was used to determine the effects of cysteine mutated NSs on RIG-I-mediated IFN-β promoter activation. Luciferase reporter gene assay was performed and fold induction in IFN-β promoter activation was calculated for each sample after normalization of the signal with the pSV40-RenLuc internal control. For all the experimental procedures, results were collected from three independent experiments and expressed as mean values ± standard deviations (SD). A p value of less than 0.05 was considered statistically significant.
(XLS)

Author Contributions

Conceptualization: Gianni Gori Savellini, Maria Grazia Cusi.

Data curation: Gianni Gori Savellini, Maria Grazia Cusi.

Investigation: Gianni Gori Savellini.

Methodology: Gianni Gori Savellini, Gabriele Anichini, Claudia Gandolfo, Shibily Prathyumnan.

Resources: Maria Grazia Cusi.

Supervision: Maria Grazia Cusi.

Writing – original draft: Gianni Gori Savellini, Maria Grazia Cusi.

Writing – review & editing: Maria Grazia Cusi.

References

1. Braito A, Ciufolini MG, Pippi L, Corbisiero R, Fiorentini C, Gistri A, et al. Phlebotomus-transmitted Toscana virus infections of the central nervous system: a seven-year experience in Tuscany. Scand J Infect Dis. 1998; 30: 505–508. https://doi.org/10.1080/00365549850161539 PMID: 10066054

2. Verani P, Ciufolini MG, Nicoletti L, Calducci M, Sabatinelli G, Coluzzi M, Paci P, et al. Ecological and epidemiological studies of Toscana virus, an arbovirus isolated from Phlebotomus. Ann Ist Super Sanità. 1982; 18: 397–399. PMID: 7187828

3. Kuhn J, Bewermeyer H, Hartmann-Klosterkoetter U, Emmerich P, Schilling S, Valassina M. Toscana virus causing severe meningoencephalitis in an elderly traveler. J Neurol Neurosurg Psychiatry. 2005; 76: 1605–1606.

4. Bartels S, Heckmann JG. Lethal encephalitis caused by Toscana virus in an elderly patient. J Neurol. 2012; 259: 175–177. https://doi.org/10.1007/s00415-011-6121-y PMID: 21656341

5. Sanbonmatsu-Gámez S, Pérez-Ruiz M, Palop-Borrás B, Navarro-Marí JM. Unusual manifestation of Toscana virus infection, Spain. Emerg Infect Dis. 2009; 15: 347–348 https://doi.org/10.3201/eid1502.081001 PMID: 19193294

6. Bouloy M. Bunyaviridae: genome organization and replication strategies. Adv Virus Res. 1991; 40: 235–75 https://doi.org/10.1016/s0065-3527(08)60281-x PMID: 1957720

7. Di Bonito P, Mochi S, Grò MC, Fortini D, Giorgi C. Organization of the M genomic segment of Toscana phlebovirus. J Gen Virol. 1997; 76: 77–81.

8. Accardi L, Gro MC, Di Bonito P, Giorgi C. Toscana virus genomic L segment: molecular cloning, coding strategy and amino acid sequence in comparison with other negative strand RNA viruses. Virus Res. 1993; 27: 119–131. https://doi.org/10.1016/0168-1702(93)90076-y PMID: 8460526

9. Grò MC, Di Bonito P, Fortini D, Mochi S, Giorgi C. Completion of molecular characterization of Toscana phlebovirus genome: nucleotide sequence, coding strategy of M genomic segment and its amino acid sequence comparison to other phleboviruses. Virus Res. 1997; 51: 81–91. https://doi.org/10.1016/s0168-1702(97)00076-2 PMID: 9381797

10. Reikine S, Nguyen JB, Modis Y. Pattern Recognition and Signaling Mechanisms of RIG-I and MDA5. Front Immunol. 2014; 5: 342. https://doi.org/10.3389/fimmu.2014.00342 PMID: 25101084

11. Weber F, Bridgen A, Fazakerley JK, Streitenfeld H, Kessler N, Randall RE, et al. Bunyamwera bunyavirus nonstructural protein NSs counteracts the induction of alpha/beta interferon. J Virol. 2002; 76: 7949–7955. https://doi.org/10.1128/JVI.76.16.7949-7955.2002 PMID: 12133999

12. Jääskeläinen KM, Kaukinen P, Minskaya ES, Plyusnina A, Vapalahti O, Elliott RM, et al. Tula and Puumala hantavirus NSs ORFs are functional and the products inhibit activation of the interferon-beta promoter. J Med Virol. 2007; 79: 1527–1536. https://doi.org/10.1002/jmv.20948 PMID: 17705180

13. Bridgen AM, Weber F, Fazakerley JK, Elliott RM. Bunyamvera bunyavirus non-structural protein NSs is nonessential gene product that contributes to the viral pathogenesis. Proc Natl Acad Sci. 2001; 98: 664–669. https://doi.org/10.1073/pnas.98.2.664 PMID: 11209062

14. Blakqori G, Delhaye S, Habjan M, Blair CD, Sánchez-Vargas I, Olson KE, et al. La Crosse bunyavirus nonstructural protein NSs serves to suppress the type I interferon system of mammalian hosts. J Virol. 2007; 81: 4991–4999. https://doi.org/10.1128/JVI.01933-06 PMID: 17344298

15. Léonard VH, Kohl A, Hart TJ, Elliott RM. Interaction of Bunyamwera Orthobunyavirus NSs protein with mediator protein MED8: a mechanism for inhibiting the interferon response. J Virol. 2006; 80: 9667–9675. https://doi.org/10.1128/JVI.00822-06 PMID: 16973571

16. Wuerth JD, Weber F. Phleboviruses and the Type I Interferon Response. Viruses. 2016; 8:pii: E174.

17. Brisbarre NM, Plumet S, de Micco P, Leparc-Goffart I, Emonet SF. Toscana virus inhibits the interferon beta response in cell cultures. Virology. 2013; 442: 189–194. https://doi.org/10.1016/j.virol.2013.04.016 PMID: 23684418

18. Gori Savellini G, Weber F, Terrosi C, Habjan M, Martorelli B, Cusi MG. Toscana virus induces interferon although its NSs protein reveals antagonistic activity. J Gen Virol. 2011; 92: 71–79. https://doi.org/10.1099/vir.0.025999-0 PMID: 20861320

19. Chen X, Ye H, Li S, Jiao B, Wu J, Zeng P, et al. Severe fever with thrombocytopenia syndrome virus inhibits exogenous Type I IFN signaling pathway through its NSs in vitro. PLoS One. 2017; 12: e0172744. https://doi.org/10.1371/journal.pone.0172744 PMID: 28234991

20. Zhang S, Zheng B, Wang T, Li A, Wan J, Qu J, et al. NSs protein of severe fever with thrombocytopenia syndrome virus suppresses interferon production through different mechanism than Rift Valley fever virus. Acta Virol. 2017; 61: 289–298. https://doi.org/10.4149/av_2017_307 PMID: 28854793

21. Gori Savellini G, Valentini M, Cusi MG. Toscana virus NSs protein inhibits the induction of type I interferon by interacting with RIG-I. J Virol. 2013; 87: 6660–6667. https://doi.org/10.1128/JVI.03129-12 PMID: 23552410

22. Gori Savellini G, Gandolfo C, Cusi MG. Truncation of the C-terminal region of Toscana Virus NSs protein is critical for interferon-β antagonism and protein stability. Virology. 2015; 486: 255–262. https://doi.org/10.1016/j.virol.2015.09.021 PMID: 26474372

23. Pickart CM. Mechanisms underlying ubiquitination. Annu Rev Biochem. 2001; 70: 503–533. https://doi.org/10.1146/annurev.biochem.70.1.503 PMID: 11395416

24. Scheffner M, Nuber U, Huibregtse JM. Protein ubiquitination involving an E1-E2-E3 enzyme ubiquitin thioester cascade. Nature. 1995; 373: 81–83. https://doi.org/10.1038/373081a0 PMID: 7800044

25. Ardley HC, Robinson PA. E3 ubiquitin ligases. Essays Biochem. 2005; 41: 15–30. PMID: 16250895

26. Bernassola F, Karin M, Ciechanover A, Melino G. The HECT family of E3 ubiquitin ligases: multiple players in cancer development. Cancer Cell. 2008; 14: 10–21. https://doi.org/10.1016/j.ccr.2008.06.001 PMID: 18598940

27. Bosu DR, Kipreos ET. Cullin-RING ubiquitin ligases: global regulation and activation cycles. Cell Div. 2008; 3: 7. https://doi.org/10.1186/1747-1028-3-7 PMID: 18282298

28. Zheng N, Shabek N. Ubiquitin Ligases: Structure, Function, and Regulation. Annu Rev Biochem. 2017; 86: 129–157. https://doi.org/10.1146/annurev-biochem-060815-014922 PMID: 28375744

29. Jackson PK, Eldridge AG, Freed E, Furstenthal L, Hsu JY, Kaiser BK, et al. The lore of the RINGs: substrate recognition and catalysis by ubiquitin ligases. Trends Cell Biol. 2000; 10: 429–439. https://doi.org/10.1016/s0962-8924(00)01834-1 PMID: 10998601

30. Weber J, Polo S, Maspero E. HECT E3 Ligases: A Tale With Multiple Facets. Front Physiol. 2019; 10: 370. https://doi.org/10.3389/fphys.2019.00370 PMID: 31001145

31. Rotin D, Kumar S. Physiological functions of the HECT family of ubiquitin ligases. Nat Rev Mol Cell Biol. 2009; 10: 398–409. https://doi.org/10.1038/nrm2690 PMID: 19436320

32. Spratt DE, Walden H, Shaw GS. RBR E3 ubiquitin ligases: new structures, new insights, new questions. Biochem J. 2014; 458: 421–437. https://doi.org/10.1042/BJ20140006 PMID: 24576094

33. Sluimer J, Distel B. Regulating the human HECT E3 ligases. Cell Mol Life Sci. 2018; 75: 3121–3141. https://doi.org/10.1007/s00018-018-2848-2 PMID: 29858610

34. Metzger MB, Pruneda JN, Klevit RE, Weissman AM. RING-type E3 ligases: master manipulators of E2 ubiquitin-conjugating enzymes and ubiquitination. Biochim Biophys Acta. 2013; 1843: 47–60. https://doi.org/10.1016/j.bbamcr.2013.05.026 PMID: 23747565

35. Deshaies RJ, Joazeiro CA. RING domain E3 ubiquitin ligases. Annu Rev Biochem. 2009; 78: 399–434. https://doi.org/10.1146/annurev.biochem.78.101807.093809 PMID: 19489725

36. Finley D. Recognition and processing of ubiquitin-protein conjugates by the proteasome. Annu Rev Biochem. 2009; 78: 477–513. https://doi.org/10.1146/annurev.biochem.78.081507.101607 PMID: 19489727

37. Thrower JS, Hoffman L, Rechsteiner M, Pickart CM. Recognition of the polyubiquitin proteolytic signal. EMBO J. 2000; 19: 94–102. https://doi.org/10.1093/emboj/19.1.94 PMID: 10619848

38. Akutsu M, Dikic I, Bremm A. Ubiquitin chain diversity at a glance. J Cell Sci. 2016; 129: 875–880. https://doi.org/10.1242/jcs.183954 PMID: 26906419

39. Komander D. The emerging complexity of protein ubiquitination. Biochem Soc Trans. 2009; 37: 937–953. https://doi.org/10.1042/BST0370937 PMID: 19754430

40. Chen ZJ, Sun LJ. Nonproteolytic functions of ubiquitin in cell signaling. Mol Cell. 2009; 33: 275–286. https://doi.org/10.1016/j.molcel.2009.01.014 PMID: 19217402

41. Kawadler H, Yang X. Lys63-linked polyubiquitin chains: linking more than just ubiquitin. Cancer Biol Ther. 2006; 5: 1273–1274. https://doi.org/10.4161/cbt.5.10.3289 PMID: 16969079

42. Park SW, Han MG, Park C, Ju YR, Ahn BY, Ryou J. Hantaan virus nucleocapsid protein stimulates MDM2-dependent p53 degradation. J Gen Virol. 2013; 94: 2424–2428. https://doi.org/10.1099/vir.0.054312-0 PMID: 23994832

43. Kainulainen M, Habjan M, Hubel P, Busch L, Lau S, Colinge J, et al. Virulence factor NSs of rift valley fever virus recruits the F-box protein FBXO3 to degrade subunit p62 of general transcription factor TFIIH. J Virol. 2014; 88: 3464–3473. https://doi.org/10.1128/JVI.02914-13 PMID: 24403578

44. Kainulainen M, Lau S, Samuel CE, Hornung V, Weber F. NSs Virulence Factor of Rift Valley Fever Virus Engages the F-Box Proteins FBXW11 and β-TRCP1 To Degrade the Antiviral Protein Kinase PKR. J Virol. 2016; 90: 6140–6147. https://doi.org/10.1128/JVI.00016-16 PMID: 27122577

45. van Knippenberg I, Carlton-Smith C, Elliott RM. The N-terminus of Bunyamwera orthobunyavirus NSs protein is essential for interferon antagonism. J Gen Virol. 2010; 91: 2002–2006. https://doi.org/10.1099/vir.0.021774-0 PMID: 20427562

46. Kelley LA, Mezulis S, Yates CM, Wass MN, Sternberg MJ. The Phyre2 web portal for protein modeling, prediction and analysis. Nat Protoc. 2015; 10: 845–858. https://doi.org/10.1038/nprot.2015.053 PMID: 25950237

47. Vosper JM, McDowel GS, Hindley CJ, Fiore-Heriche CS,Kucerova R, Horan I, Philpott A. Ubiquitylation on canonical and non-canonical sites targets the transcription factor neurogenin for ubiquitin-mediated proteolysis. J Biol Chem. 2009; 284: 15458–15468 https://doi.org/10.1074/jbc.M809366200 PMID: 19336407

48. Kravtsova-Ivantsiv Y, Ciechanover A. Non-canonical ubiquitin-based signals for proteasomal degradation. J Cell Sci. 2012; 125: 539–548 https://doi.org/10.1242/jcs.093567 PMID: 22389393

49. Viswanathan K, Früh K, DeFilippis V. Viral hijacking of the host ubiquitin system to evade interferon responses. Curr Opin Microbiol. 2010; 13: 517–523. https://doi.org/10.1016/j.mib.2010.05.012 PMID: 20699190

50. Rahman MM, McFadden G. Modulation of NF-κB signalling by microbial pathogens. Nat Rev Microbiol. 2011; 9: 291–306. https://doi.org/10.1038/nrmicro2539 PMID: 21383764

51. Lindner HA. Deubiquitination in virus infection. Virology. 2007; 362: 245–256. https://doi.org/10.1016/j.virol.2006.12.035 PMID: 17291557

52. Maelfait J, Beyaert R. Emerging role of ubiquitination in antiviral RIG-I signaling. Microbiol Mol Biol Rev. 2012; 76: 33–45. https://doi.org/10.1128/MMBR.05012-11 PMID: 22390971

53. Heaton SM, Borg NA, Dixit VM. Ubiquitin in the activation and attenuation of innate antiviral immunity. J Exp Med. 2016; 213: 1–13. https://doi.org/10.1084/jem.20151531 PMID: 26712804

54. Zhu H, Zheng C, Xing J, Wang S, Li S, Lin R, et al. Varicella-zoster virus immediate-early protein ORF61 abrogates the IRF3-mediated innate immune response through degradation of activated IRF3. J Virol. 2011; 85: 11079–11089. https://doi.org/10.1128/JVI.05098-11 PMID: 21835786

55. Lanfranca MP, Mostafa HH, Davido DJ. HSV-1 ICP0: An E3 Ubiquitin Ligase That Counteracts Host Intrinsic and Innate Immunity. Cells. 2014; 3: 438–454. https://doi.org/10.3390/cells3020438 PMID: 24852129

56. Zhang L, Villa NY, McFadden G. Interplay between poxviruses and the cellular ubiquitin/ubiquitin-like pathways. FEBS Lett. 2009; 583: 607–614. https://doi.org/10.1016/j.febslet.2009.01.023 PMID: 19174161

57. Oshiumi H, Miyashita M, Matsumoto M, Seya T. A distinct role of Riplet-mediated K63-Linked polyubi-quitination of the RIG-I repressor domain in human antiviral innate immune responses. PLoS Pathog. 2013; 9: e1003533. https://doi.org/10.1371/journal.ppat.1003533 PMID: 23950712

58. Mudhasani R, Tran JP, Retterer C, Kota KP, Whitehouse CA, Bavari S. Protein Kinase R Degradation Is Essential for Rift Valley Fever Virus Infection and Is Regulated by SKP1-CUL1-F-box (SCF) FBXW11-NSs E3 Ligase. PLoS Pathog. 2016; 12: e1005437. https://doi.org/10.1371/journal.ppat.1005437 PMID: 26837067

59. Koliopoulos MG, Lethier M, van der Veen AG, et al. Molecular mechanism of influenza A NS1-mediated TRIM25 recognition and inhibition. Nat Commun. 2018; 9: 1820. https://doi.org/10.1038/s41467-018-04214-8 PMID: 29739942

60. Rajsbaum R, Albrecht RA, Wang MK, Maharaj NP, Versteeg GA, Nistal-Villán E, et al. Species-specific inhibition of RIG-I ubiquitination and IFN induction by the influenza A virus NS1 protein. PLoS Pathog. 2012; 8: e1003059. https://doi.org/10.1371/journal.ppat.1003059 PMID: 23209422

61. Gack MU, Albrecht RA, Urano T, Inn KS, Huang IC, Carnero E, et al. Influenza A virus NS1 targets the ubiquitin ligase TRIM25 to evade recognition by the host viral RNA sensor RIG-I. Cell Host Microbe. 2006; 5: 439–449.

62. Sánchez-Aparicio MT, Feinman LJ, García-Sastre A, Shaw ML. Paramyxovirus V Proteins Interact with the RIG-I/TRIM25 Regulatory Complex and Inhibit RIG-I Signaling. J Virol. 2018; 92: e01960–17. https://doi.org/10.1128/JVI.01960-17 PMID: 29321315

63. Ding S, Mooney N, Li B, et al. Comparative Proteomics Reveals Strain-Specific β-TrCP Degradation via Rotavirus NSP1 Hijacking a Host Cullin-3-Rbx1 Complex. PLoS Pathog. 2016; 12: e1005929. https://doi.org/10.1371/journal.ppat.1005929 PMID: 27706223

64. Riley BE, Lougheed JC, Callaway K, Velasquez M, Brecht E, Nguyen L, et al. Structure and function of Parkin E3 ubiquitin ligase reveals aspects of RING and HECT ligases. Nat Commun. 2013; 4: 1982. https://doi.org/10.1038/ncomms2982 PMID: 23770887

65. Kingstone RE, Chen CA, Rose JK. Calcium phosphate transfection. In: Ausubel F, Brent R, Kingston R, Moore D, Seidman J, Smith J, Struhl K, editors. Curr Protoc Mol Biol. New York: 63; 2003. 1–9.

66. Yoneyama M, Suhara W, Fukuhara Y, Sato M, Ozato K, Fujita T. Autocrine amplification of type I inter-feron gene expression mediated by interferon stimulated gene factor 3 (ISGF3). J Biochem. 1996; 120: 160–169. https://doi.org/10.1093/oxfordjournals.jbchem.a021379 PMID: 8864859

67. Valassina M, Soldateschi D, dal Maso GM, Santini L, Bianchi S, Valensin PE, Cusi MG. Diagnostic Potential of Toscana Virus N Protein Expressed in Escherichia coli. J Clin Microbiol. 1999; 37: 1237.